

# **NONDESTRUCTIVE EVALUATION OF THE STRUCTURAL CONDITION OF TIMBER PILES**

**Project: HWY 98-5**

**Volume 1 of 2**

A Final Report Submitted to the  
North Carolina Department of Transportation  
*(FHWA/NC/2000-004)*

by

Y. Richard Kim, Ph.D., P.E.  
S. Ranji Ranjithan, Ph.D.  
Paul J. Donato  
Chris M. Murphy

Department of Civil Engineering  
North Carolina State University

May 2000

**Technical Report Documentation Page**

<b>1. Report No.</b> FHWA/NC/2000-004	<b>2. Government Accession No.</b>	<b>3. Recipient's Catalog No.</b>	
<b>4. Title and Subtitle</b> Nondestructive Evaluation of the Structural Condition of Timber Piles (Volume 1 of 2)		<b>5. Report Date</b> May 2000	
		<b>6. Performing Organization Code</b>	
<b>7. Author(s)</b> Y. Richard Kim, S. Ranji Ranjithan, Paul J. Donato, Chris M. Murphy		<b>8. Performing Organization Report No.</b>	
<b>9. Performing Organization Name and Address</b> Center for Transportation Engineering Studies Box 7908 Mann Hall North Carolina State University Raleigh, NC 27695-7908		<b>10. Work Unit No. (TRAIS)</b>	
		<b>11. Contract or Grant No.</b>	
<b>12. Sponsoring Agency Name and Address</b> North Carolina Department of Transportation Raleigh, NC 27699-1549  Federal Highway Administration 400 Seventh Street, SW Washington, DC 20590		<b>13. Type of Report and Period Covered</b> Final Report July 1998 – December 1999	
		<b>14. Sponsoring Agency Code</b> HWY-98-5	
<b>15. Supplementary Notes</b>			
<b>16. Abstract</b> <p>Condition evaluation of timber piles is currently based on traditional methods of visual inspection and sounding. Unfortunately, this method is vague and in many cases relies on interpretation of information and not on measurable parameters. Because nondestructive evaluation (NDE) using stress waves provides a fast and relatively inexpensive way of predicting the condition of in-service structural systems, these techniques have become an increasingly common tool for field evaluation of structural components. In this research, the bending wave technique has been used to measure wave propagation parameters for installed timber piles. Both laboratory and in-situ piles were tested in various conditions (i.e., liquid content and damage degree). The results were used to formulate analysis and testing procedures for quantitatively determining the condition of timber piles.</p> <p>In this research, a high correlation between stress wave parameters and the condition of timber was found. Stress wave properties measured in the time domain, more specifically the phase velocities, are effective indicators of the remaining sound cross-sectional area of timber pilings. Properties of stress wave propagation obtained from the frequency domain are unreliable and are sensitive to natural structural variations of timber. A strong relationship was observed between the phase velocities and liquid contents for intact sections. Controlled laboratory data from damaged pile sections were used in conjunction with information obtained from field specimens to develop a condition prediction model. In predicting the remaining cross-sectional area of field specimens, the prediction model yielded conservative results in 30% of the cases. A qualitative reject/accept criterion was also developed that distinguishes between intact and damaged pile sections.</p> <p>A field testing procedure evolved during the course of this research. The testing methods (that are utilized to obtain appropriate stress wave properties used to predict pile condition) as well as analysis procedures are presented. Additional testing of installed timber piles will allow for the improvement of the current analysis procedures and methods.</p>			
<b>17. Key Words</b> Timber pile Nondestructive evaluation Bending wave Remaining sound area		<b>18. Distribution Statement</b> No restrictions.	
<b>19. Security Classif. (of this report)</b> Unclassified	<b>20. Security Classif. (of this page)</b> Unclassified	<b>21. No. of Pages</b> 160	<b>22. Price</b>

## **DISCLAIMER**

The contents of this report reflect the views of the author(s) and not necessarily the views of the University. The authors are responsible for the facts and the accuracy of the data presented herein. The contents do not necessarily reflect the official views or policies of the North Carolina Department of Transportation nor the Federal Highway Administration at the time of publication. This report does not constitute a standard, specification, or regulation.

## **Abstract**

Condition evaluation of timber piles is currently based on traditional methods of visual inspection and sounding. Unfortunately, this method is vague and in many cases relies on interpretation of information and not on measurable parameters. Because nondestructive evaluation (NDE) using stress waves provides a fast and relatively inexpensive way of predicting the condition of in-service structural systems, these techniques have become an increasingly common tool for field evaluation of structural components. In this research, the bending wave technique has been used to measure wave propagation parameters for installed timber piles. Both laboratory and in-situ piles were tested in various conditions (i.e., liquid content and damage degree). The results were used to formulate analysis and testing procedures for quantitatively determining the condition of timber piles.

In this research, a high correlation between stress wave parameters and the condition of timber was found. Stress wave properties measured in the time domain, more specifically the phase velocities, are effective indicators of the remaining sound cross-sectional area of timber pilings. Properties of stress wave propagation obtained from the frequency domain are unreliable and are sensitive to natural structural variations of timber. A strong relationship was observed between the phase velocities and liquid contents for intact sections. Controlled laboratory data from damaged pile sections were used in conjunction with information obtained from field specimens to develop a condition prediction model. In predicting the remaining cross-sectional area of field specimens, the prediction model yielded conservative results in 30% of the cases. A qualitative reject/accept criterion was also developed that distinguishes between intact and damaged pile sections.

A field testing procedure evolved during the course of this research. The testing methods (that are utilized to obtain appropriate stress wave properties used to predict pile condition) as well as analysis procedures are presented. Additional testing of installed timber piles will allow for the improvement of the current analysis procedures and methods.

# Table of Contents

<b>List of Tables.....</b>	<b>vii</b>
<b>List of Figures.....</b>	<b>viii</b>
<b>1. Introduction.....</b>	<b>1</b>
1.1 Motives for Research.....	2
1.2 Scope of Research.....	3
1.3 Literature Review.....	4
1.3.1 Wave Propagation Theory.....	4
1.3.2 Condition Assessment Using Stress Waves.....	4
1.4 Organization of Report.....	6
<b>2. Background and Theory of NDE.....</b>	<b>7</b>
2.1 Overview.....	7
2.1.1 Visual and Optical Inspection Methods.....	7
2.1.2 Radiographic Methods.....	8
2.1.3 Ultrasonic Technology.....	9
2.1.4 Stress Wave Testing.....	9
2.2 Fundamental Stress Wave Theory.....	10
2.2.1 Body Waves.....	10
2.2.2 Surface Waves.....	11
2.2.3 Flexural Waves.....	11
2.3 Development of Wave Equations.....	12
2.3.1 Wave propagation in an Elastic Half-Space.....	12
2.3.2 Longitudinal Wave Propagation in Thin Rods.....	17

2.3.3	Torsional (Shear) Wave Propagation in Thin Rods.....	19
2.3.4	Flexural Wave Propagation in Thin Rods.....	20
2.4	Dispersion.....	23
2.5	The Discrete and Fast Fourier Transforms.....	23
2.5.1	The Fourier Phase Method.....	27
2.6	The Short Kernel Method.....	27
<b>3.</b>	<b>The Bending Wave Testing Procedure.....</b>	<b>30</b>
3.1	Overview.....	30
3.1.1	The Bending Wave Testing Procedure.....	31
3.1.2	Energy Source (Impact Device).....	31
3.1.3	Sensors.....	33
3.1.4	Signal Acquisition.....	34
3.1.5	Signal Processing Tools.....	35
3.2	Stress Wave Parameters Used for Condition Assessment.....	36
3.2.1	Wave Speed and Phase Velocity.....	36
3.2.2	Attenuation Ratio.....	36
3.2.3	Dominant Frequency and Centroid Frequency.....	38
3.3	Determining the Wave Speed.....	38
<b>4.</b>	<b>Development of a Standard Impact Device.....</b>	<b>44</b>
4.1	Importance of Impact Device Selection.....	44
4.2	Creating an Effective Impact.....	45
4.3	Evaluation of Various Impact Devices.....	45
4.3.1	Experimental Setup.....	46
4.3.2	Comparison of Wave Propagation Properties.....	47
4.3.2.1	Impact-to-Impact Variations.....	49

4.3.2.2	Operator-to-Operator Variations.....	55
4.4	Summary.....	58
<b>5.</b>	<b>Laboratory Investigation of the Influence of Natural Wood</b>	
	<b>Variation on Wave Properties.....</b>	<b>60</b>
5.1	Anatomical Variations in Wood.....	60
5.2	Internal Discontinuities.....	60
5.2.1	Experimental Setup.....	61
5.2.2	Analysis in the Frequency Domain.....	61
5.2.3	Analysis in the Time Domain.....	65
5.3	Surface Variations.....	67
5.3.1	Experimental Setup.....	68
5.3.2	Analysis in the Time Domain.....	69
5.4	Effect of Diameter Variation on Phase Velocity.....	69
5.4.1	Experimental Setup.....	70
5.4.2	Effect of Diameter Variation on Phase Velocity.....	70
5.5	Summary.....	71
<b>6.</b>	<b>Determination of the Moisture Content .....</b>	<b>73</b>
6.1	Moisture Content of Wood.....	73
6.1.1	Determination of Moisture Content.....	73
6.1.1.1	Conventional Oven Drying.....	74
6.1.1.2	Moisture Content Determination Using a Centrifuge.....	75
6.1.1.3	The Halogen Moisture Analyzer (HMA).....	75
6.2	Effect of Treatment on Moisture Content Determination.....	77
6.2.1	Moisture Content as a Function of Liquid Composition.....	77

6.2.1.1 Determination of Volatile Component Removal Using the HMA.....	78
6.2.2 Wave Propagation Properties as a Function of Liquid Content....	79
6.3 Development of a Relationship Between Liquid Content and Wave Speed.....	81
6.3.1 Experimental Setup.....	82
6.3.2 Phase Velocity as a Function of Liquid Content.....	82
6.4 Summary.....	83
<b>7. Laboratory Evaluation of Simulated Internal Defects.....</b>	<b>85</b>
7.1 Damage and Decay in Timber.....	85
7.2 Decay Mechanisms in Wood.....	86
7.2.1 Fungal Decay.....	86
7.2.1.1 Brown Rot.....	87
7.2.1.2 White Rot.....	87
7.2.1.3 Soft Rot.....	87
7.2.2 Bacterial Decay.....	88
7.2.3 Marine Borer Attack of Wood.....	88
7.2.3.1 Teredinids (Shipworms).....	88
7.2.3.2 Limnoria.....	89
7.3 Simulation and Evaluation of Internal Defects.....	89
7.3.1 Experimental Setup and Drilling Process.....	89
7.3.2 Condition Assessment Using the Frequency Domain.....	91
7.3.2.1 Effect of Damage on Centroid and Dominant Frequency.....	92
7.3.2.2 Effect of Damage on the Attenuation Ratio.....	94
7.3.3 Condition Assessment Using the Time Domain.....	96
7.4 Summary.....	100

<b>8.</b>	<b>Investigation of Installed Timber Piles.....</b>	<b>101</b>
	8.1 Experimental Design.....	101
	8.1.1 In-situ Testing.....	102
	8.1.2 Extracted-wet Testing.....	102
	8.1.3 Extracted-dry Testing.....	104
	8.1.3.1 Kiln Drying.....	105
	8.2 Cutting of Pile Sections.....	108
	8.3 Determination of Remaining Cross-sectional Area.....	109
	8.4 Test Results.....	113
	8.4.1 Frequency Information.....	114
	8.4.2 Phase Velocity Information.....	117
	8.4.2.1 Impact Device.....	117
	8.4.2.2 Selection of Standard Kernel.....	118
	8.4.2.3 In-situ Results.....	119
	8.4.2.4 Extracted-wet Results.....	119
	8.4.2.5 Extracted-dry Results.....	119
	8.4.2.6 Effect of Boundary Conditions.....	121
	8.4.2.7 Number of Lines and Data Files to be Considered for Each Test Location.....	123
	8.4.2.8 Relationship between Phase Velocity and Liquid Content.....	125
	8.4.2.9 Formation of Condition Analysis Charts.....	128
<b>9.</b>	<b>Conclusions.....</b>	<b>136</b>
	<b>List of References.....</b>	<b>139</b>

## List of Tables

4.1	Average standard deviation for the phase velocity measured using the modified hammer and wood spring mechanism.....	58
6.1	Moisture content determination using the centrifuge and by oven-drying...	75
6.2	Moisture content determination using the HMA and oven-drying methods...	76
6.3	Liquid Content at various drying temperatures for treated wood core samples.....	78
6.4	Liquid content results of southern yellow pine specimen before and after treatment.....	79
6.5	Stress wave velocity measured along the length of specimens in Table 6.4.....	80
8.1	Comparison of liquid content for kiln dried piles.....	108
8.2	Remaining cross-sectional area of damaged extracted field piles.....	110
8.3	Summary of errors associated with condition evaluation relationships.....	135

## List of Figures

2.1	A thin prismatic rod with coordinate $x$ and displacement $u$ of a section.....	17
2.2	Differential element of a rod subjected to end torques.....	19
2.3	A differential element of a thin rod undergoing transverse motion due to a vertical impact.....	21
3.1	Laboratory bending wave testing configuration.....	32
3.2	Field bending wave testing configuration.....	33
3.3	Typical raw signal obtained from the bending wave test.....	35
3.4	Dominant and centroid frequency in the magnitude vs. frequency plot (FFT plot).....	37
3.5	Typical raw signal obtained from the bending wave testing procedure.....	39
3.6	FFT plot for typical measured raw signal using the bending wave technique.....	40
3.7	SKM plot for typical raw signal shown in Figure 3.5 using the SWAP... ..	41
4.1	Comparison of frequency spectra plots for the impact devices tested.....	46
4.2	Average phase velocities measured using the bending wave technique for various impact devices.....	47
4.3	Average centroid frequencies measured using the bending wave technique for various impact devices.....	48

4.4	Average phase velocities measured using the bending wave technique for the steel ball mechanism with corresponding one standard deviation bars.....	50
4.5	Average phase velocities measured using the bending wave technique for the wood spring mechanism with corresponding one standard deviation bars.....	51
4.6	Average phase velocities measured using the bending wave technique for the modified hammer with corresponding one standard deviation bars.....	52
4.7	Average centroid frequencies measured using the bending wave technique for the steel ball mechanism with corresponding one standard deviation bars.....	53
4.8	Average centroid frequencies measured using the bending wave technique for the wood spring mechanism with corresponding one standard deviation bars.....	54
4.9	Average centroid frequencies measured using the bending wave technique for the modified hammer with corresponding one standard deviation bars.....	55
4.10	Comparison of phase velocities measured using the modified hammer for selected versus non-selected impacts with corresponding one standard deviation bars.....	56
4.11	Comparison of phase velocities measured using the wooden spring mechanism for selected versus non-selected impacts with corresponding one standard deviation bars.....	57
4.12	Wood spring mechanism (WSM-1999) used for imparting impact to the pile surfaces .....	59

5.1	Average dominant frequencies measured from various pile sections of a similar diameter using the bending wave technique with corresponding one standard deviation bars (pile 4).....	62
5.2	Average dominant frequencies measured from various pile sections of a similar diameter using the bending wave technique with corresponding one standard deviation bars (pile 4c).....	63
5.3	Average centroid frequencies measured from various pile sections of a similar diameter using the bending wave technique with corresponding one standard deviation bars (pile 3).....	64
5.4	Average centroid frequencies measured from various pile sections of a similar diameter using the bending wave technique with corresponding one standard deviation bars (pile 4c).....	65
5.5	Average phase velocities measured from various pile sections of a similar diameter using the bending wave technique with corresponding one standard deviation bars (pile 3c).....	66
5.6	Average phase velocities measured from various pile sections of a similar diameter using the bending wave technique with corresponding one standard deviation bars (pile 4).....	67
5.7	Profile of the pile cross-section showing measurement points along the pile circumference at each test location.....	68
5.8	Repeatability study to determine the effect of structural variations on wave properties using the bending wave technique.....	69
5.9	Phase velocity as diameter varies for three different piles.....	71
6.1	Comparison of phase velocities for specimens with varying liquid composition.....	81
6.2	Phase velocity as a function of liquid content for various laboratory and field specimens.....	83
7.1	Drill press with timber pile for laboratory damage simulation.....	90

7.2	The centroid frequency measured using the bending wave technique for wave propagation through a timber pile section with varying degrees of damage.....	93
7.3	The dominant frequency measured using the bending wave technique for wave propagation through a timber pile section with varying degrees of damage.....	94
7.4	Attenuation ratio versus damage for a typical pile section obtained using the bending wave technique.....	95
7.5	Phase velocity as damage increases for pile sections with varying liquid content values.....	96
7.6	Damage trends shown in Figure 7.5 as liquid contents of specimens vary.....	98
7.7	Average measured RCSA versus predicted value based on Eq. 7.4.....	99
7.8	Condition Evaluation Chart Developed Using Laboratory Data.....	100
8.1	Extraction of installed timber piles.....	103
8.2	Field testing of piles in the extracted-wet condition.....	104
8.3	Extracted-dry testing with the wood spring mechanism.....	105
8.4	Piles loaded in kiln for drying.....	107
8.5	Cutting of extracted piles.....	109
8.6	Damaged portion of pile CC.....	111
8.7	Damaged section of pile EE.....	112
8.8	Damaged section of pile O.....	113
8.9	Attenuation ratio vs. liquid content for intact field piles.....	114
8.10	Centroid Frequency vs. liquid content for intact field piles.....	115
8.11	Dominant frequency vs. liquid content for intact field piles.....	116
8.12	Phase velocity vs. liquid content for intact sections in the in-situ condition.....	118

8.13	Phase velocity vs. liquid content for intact sections in the extracted-wet condition.....	120
8.14	Phase velocity vs. liquid content for intact sections in the extracted-dry condition.....	121
8.15	Phase velocity vs. liquid content for in-situ and extracted-dry conditions using the modified hammer.....	122
8.16	Average phase velocity of 5 files vs. 2 files.....	124
8.17	Predicted RCSA for 5 files and 3 lines vs. 2 files and 1 line.....	125
8.18	Phase velocity vs. liquid content for WSM data.....	126
8.19	Phase Velocity vs. Liquid Content with Intact Relationship 95 % Confidence Intervals.....	127
8.20	Plot of $R^2$ versus A.....	130
8.21	$\text{LN}((V_{ph}-A)/\text{RCSA})$ versus LC.....	131
8.22	The condition evaluation chart.....	132
8.23	Predicted RCSA versus Measured RCSA.....	133
8.24	Predicted RCSA versus Measured RCSA using the relationship developed in the laboratory.....	134

# Chapter 1

## Introduction

For many years, an overwhelming proportion of rural highway bridges were on roads that serve low volumes of traffic. Timber was the material of choice in many of these bridges due to ease of installation and the low cost. Unfortunately, the life span of many of these structures is coming to an end due to deterioration, while the service lives of many bridges have also been exceeded due to rapid population growth in rural areas. In its Seventh Annual Report to Congress on the status of the nations bridges, the U.S. Department of Transportation reported that 574,729 highway bridges were inventoried in the United States at the end of 1985 that were 20 ft. or more in length (Brungraber et al., 1987). Based on the data furnished by the states, the FHWA estimates that about 42 percent of these bridges are deficient for either structural or functional reasons. On a local scale, of the 17,262 maintained bridges in North Carolina, 2,964 are supported, at least in part, by timber (Wiggins, 1999).

Because of the transition of train and rail based transport to more commonly available truck transportation in rural areas (where many of these timber bridges are located), many of today's rural bridges have seen a dramatic increase in traffic as well as a demand for much larger carrying capacities. Therefore, it is of particular interest to state departments of transportation to be able to easily assess the condition of in-place structures thereby ensuring public safety. As a result, it is necessary to develop analysis and testing procedures that can accurately predict the structural integrity of these systems.

## 1.1 Motives for Research

While there are a number of techniques used to prevent deterioration and decay (from a combination of insects, marine organisms, fungi, and waves) of timber piles, a widespread practice is to simply replace all the piles at regular intervals. This criterion for replacement is currently based on traditional methods of determining a timber piles condition by visual inspection and sounding. Unfortunately, this method is vague and in many cases relies on interpretation of information and not measurable parameters.

Because Nondestructive Evaluation (NDE) using stress waves provides a fast and relatively inexpensive way of predicting the condition of in-service structural systems, these techniques have become an increasingly common tool for field evaluation of structural components. An NDE technique that is commonly used to evaluate mechanical properties of wood products is known as the longitudinal stress wave propagation technique. This method is based on the measurement of vibrational characteristics while using stress waves to measure two fundamental properties: elastic wave energy transmission and the resulting particle motion. The test involves striking the pile head to create longitudinal stress waves which travel to the pile's butt and return. The waves are detected by accelerometers attached to the side of the pile as they pass and are recorded on a digital oscilloscope. The phase velocity is used as an indicator of the structural soundness of the pile.

Previous research (Qian, 1997) has shown a strong correlation between stress wave properties and the mechanical properties of wood; the phase velocity being the strongest indicator of the remaining effective area of a wood member. Ross and Pellerin (Ross and Pellerin, 1991), using the longitudinal stress wave technique, have also shown that strong relationships between stress wave parameters and static mechanical properties of dry wood-based materials exist. Unfortunately, because the superstructure covers the primary point of impact for the longitudinal technique (the pile top), this method has limited applications for on-site testing. As a result of these limitations, an alternative

method was developed. It is known as the bending wave technique. The method involves striking the pile on its side to induce a stress pulse perpendicular to the longitudinal axis of the pile. This alleviates the problem of striking the piles head, which in most cases is not accessible to the operator.

The purpose of this research is to further investigate the work performed by Qian (1997) in correlating wave propagation properties and the internal condition of wood to accurately predict the remaining cross-sectional area of timber pilings. Laboratory and field databases are used to develop an in-situ field testing procedure for quantitatively determining the condition of installed timber piles.

## **1.2 Scope of Research**

To ensure the structural integrity of timber, it is essential to develop an accurate testing procedure that predicts the internal condition and identifies locations of deterioration. One such method currently being investigated is the bending stress wave propagation technique. Such effort requires the determination of explicit relationships between stress wave properties and the structural condition of timber pilings that could provide the basis for a testing and analysis procedure. In this study, nondestructive testing techniques were used to determine properties of laboratory and field specimens.

Laboratory experiments were designed to evaluate the effects that moisture content, anatomical variations of wood, and environmental conditions (such as changing moisture content) have on stress wave properties. The effect of internal damage on wave propagation properties was evaluated by simulating damage in a laboratory controlled environment. Effects of moisture content variations were determined using both results from field specimens and laboratory specimens. Anatomical variations and their effects on wave properties were determined using laboratory specimens. All stress wave properties were determined using the bending wave technique.

A series of bending wave tests have been conducted on twenty-two field piles of various conditions. The results of these tests along with controlled data from laboratory specimens were used to develop the necessary relationships for a standard condition evaluation procedure.

## **1.3 Literature Review**

### **1.3.1 Wave Propagation Theory**

Wave propagation theory has been investigated by many mechanists throughout history. Kolsky (1963) describes the basic theory of stress wave propagation in infinite and semi-infinite elastic media. Furthermore, Kolsky discusses the dispersive wave propagation phenomena inherent in bounded media and considers three types of waves that can be propagated along thin rods: longitudinal, torsional, and flexural. Kolsky gives the solution for the velocity of longitudinal and torsional wave propagation while Graff (1975) develops the exact solution to flexural wave propagation in thin rods of infinite length.

### **1.3.2 Condition Assessment Using Stress Waves**

Significant effort has been devoted to developing relationships between stress wave parameters and material properties of wood for use in a nondestructive evaluation procedure. The following is a brief synopsis of various literature devoted to the subject of nondestructive evaluation of wood structures using stress waves.

Ross et al. (1997) investigated the use of a longitudinal stress wave technique to assess the strength of wood members exposed to biological attack. Wave speed and attenuation properties were correlated with the parallel-to-grain compressive strength of the specimen. Predicted values based on information from stress wave testing agreed well with the values obtained from actual compressive strength values measured in the laboratory.

Ross and Pellerin (1991) used the longitudinal stress wave technique to evaluate the effect changes in wood moisture content (MC) have on wave propagation speeds. The study also examined the relationship between stress wave characteristics and the static modulus of elasticity of green Douglas-fir dimension lumber. Results showed a strong correlation between the moisture content and wave propagation speeds. As the moisture content of the specimen increased, the corresponding wave speed decreased. Results also revealed a useful relationship between the wave propagation speed and the modulus of elasticity (MOE) of the specimens. Lower wave speeds corresponded to a lower MOE.

Qian (1997) used the bending stress wave technique to identify the condition and material properties of timber. Results indicated a strong correlation between properties of stress wave propagation and moisture content of the timber. Furthermore, material properties such as the modulus of elasticity had a strong influence on wave properties.

Ross and Pellerin (1988) used the longitudinal stress wave technique to predict mechanical properties of wood-based composites. Findings indicated that stress wave speed and attenuation are excellent indicators of the mechanical properties of wood specimens.

Pellerin et al. (1985) showed that stress wave velocity is a good indicator of wood decomposition when caused by brown-rot fungi. A reduction in stress wave speed indicated locations of brown-rot fungi in specimens.

Ross et al. (1996) used stress waves techniques to evaluate the condition of the USS Constitution (the oldest ship in the U.S. Navy) and locate decayed sections of the hull. Variations in stress wave propagation properties successfully indicated the location of deteriorated wood. Significantly lower wave velocities were observed in deteriorated wood.

Ross et al. (1994) used stress wave techniques to evaluate the condition of wetwood (bacterially infected wood), thereby allowing separation of bacterially infected wood from good quality lumber before kiln-drying. Time-of-transmission measurements were utilized to detect the presence of wetwood. On average, the NDE technique correctly

identified 84 percent of the bacterially infected red oak while identifying an average of 45 percent of the infected white oak.

Kim et al. (1997) used stress wave testing methods to locate deteriorated wood in a submerged timber gate. The stress wave testing program identified the location of damage in individual members based on the time of transit of wave propagation. Based on the resulting information, components of the timber gate whose structural integrity was suspect were then replaced.

## **1.4 Organization of Report**

Specific topics investigated herein are divided in the following manner. Chapter 2 presents the theoretical background for stress wave propagation and an explanation of the signal processing tools used to evaluate properties of stress wave propagation. Chapter 3 outlines the bending wave testing procedure and parameters used to quantify stress wave propagation in a medium. Chapter 4 discusses the development of a standard impact device used for the bending stress wave technique. The influence of the anatomical variations in wood and their effect on stress wave propagation properties is discussed in Chapter 5. Chapter 6 examines the effect the moisture content and treatment types have on stress wave propagation in timber. Chapter 7 includes an evaluation of the bending wave testing procedure's ability to predict the remaining cross-sectional area of timber piles with simulated laboratory damage. An investigation of installed timber pilings was conducted and the results are presented in chapter 8. A summary of the major findings of this research is presented in chapter 9.

## **Chapter 2**

# **Background and Theory of NDE**

### **2.1 Overview**

Non-destructive evaluation is the science of identifying the physical and mechanical properties of a piece of material without altering its end-use capabilities and using this information to make decisions regarding appropriate applications (Ross et al., 1998). Today, applications of NDE go much further than the detection of gross defects. They concern all aspects of the characterization of solids, their microstructure, texture, morphology, chemical constituents, physical and chemical properties, as well as their methods of preparation (Cartz, 1996). Traditionally, NDE had been used for quality assessment of new materials and plays an important role in the prediction of failure and analysis of many structural systems. Inherently, NDE is a tedious and typically monotonous task, but vigilance is required order to conduct inspection skillfully and to recognize signs of the defects.

#### **2.1.1 Visual and Optical Inspection Methods**

Visual inspection is still the oldest and most widely used form of nondestructive evaluation. Traditionally, the unaided human eye has been used to inspect engineering systems and detect various abnormalities. In 1948, Dr. Dennis Gabor of the Imperial College of London introduced the concept of holography. He demonstrated that amplitude and phase information contained within the image of an illuminated object could be recorded, stored, and retrieved. He termed this recording a hologram. In the

early 1960's, dramatic progress in the science of holography was made with the advent of the laser, making the use of off-axis holography possible (Bray et al., 1992).

The advancement of video technology over the past 15 years has dramatically changed the way in which visual quality control is utilized. Improved video camera resolution has made remote monitoring practical while a new source detection system utilizing video output permits visual imaging of heat, sonic, ultrasonic, and X-ray patterns. These improvements in addition to advancement in computer visual related technologies have permitted the visual study and evaluation of information not detected by the human eye.

### **2.1.2 Radiographic Methods**

Radiography is the technique of obtaining a shadow image of a solid using penetrating radiation such as x-rays or gamma rays (Cartz, 1996). Images obtained on film are known as radiographs and are obtained as a projection, lacking any detail of depth within the solid. A radiographic image is essentially a two-dimensional shadow display or picture of the intensity distribution of X-rays or gamma rays that have passed through a material object (Bray et al., 1992). Differences in contrast are due to different degrees of absorption of X-rays in the specimen and can also be attributed to a variation of specimen thickness, different chemical constituents, non-uniform densities, flaws, discontinuities, or to scattering processes within the specimen.

Traditionally, this technology has been utilized in the medical field. Today however, correct use of radiography provides manufacturers in all areas of engineering the ability to observe defects before these parts are installed in systems. Defects and flaws are detectable during the early stages of the manufacturing process, increasing productivity while decreasing necessity for post-assembly quality control. Gamma-ray inspection is utilized for inspecting earth-bound structures like aerospace ground equipment, pipelines, storage tanks, and other heavy structures.

### **2.1.3 Ultrasonic Technology**

Ultrasonic inspection is accomplished by using electronically controlled pulses introduced into a material from an outer surface. High-frequency sound in the non-audible range is transmitted with a certain velocity through a medium by the vibrations of atoms and molecules. The velocity at which the sound travels is dependent on the mechanical properties of the medium. Imperfections and inclusions in the medium cause sound waves to dampen and scatter resulting in a decrease in velocity across the object. Various testing arrangements using ultrasonic technology have evolved, including pulse echo, transmission method, reflection method, and the transmission-reflection crack tip diffraction technique.

The pulse echo method is used extensively in various civil engineering non-destructive testing applications. A transducer is attached to the surface of a specimen through a coupling agent. A pulse of ultrasonic waves are sent through the medium by the transducer probe. The waves travel to another surface of the material and then are reflected back to a transducer that may or may not be the transmitting transducer, depending on the testing setup. When the reflecting surface is parallel to the probe contact surface, the same probe may act as the transmitter and receiver. The time of flight for the pulse to travel out and back can be calculated. Knowing the geometry of the specimen, the position of possible flaws or inclusions can be determined.

### **2.1.4 Stress Wave Testing**

Stress wave testing has found many applications in the engineering field beginning in the early 1960's. Stress wave testing has been used to evaluate concrete conditions, delaminations of asphalt, length of installed bridge pilings, as well as the prediction of material condition. The most widely used application is to measure the time of transit of

stress waves through the specimen. Stress wave transit times will vary depending on the properties of the medium through which they are traveling.

When a disturbance is caused on the surface of an elastic specimen, body waves, surface waves and flexural waves result. Body waves propagate radially outward from the source along a hemispherical wavefront while surface and flexural waves propagate radially outward along the surface of the specimen. The frequency at which these waves are generated can be varied. In the case of the bending wave technique, the frequencies generated are normally in the inaudible range. The sources of the disturbance can be either mechanical, such as a hammer, or electronic. A digital oscilloscope is utilized along with various detection devices to measure stress wave propagation through the specimen. Strong relationships have been developed between stress wave properties and properties of various materials such as wood, concrete, and asphalt.

## **2.2 Fundamental Stress Wave Theory**

When a force is applied to any one point on a body, the resulting stresses set every other point in motion instantaneously, and the force can be considered as producing a linear acceleration in the whole body, together with an angular acceleration about its center of gravity (Kolsky, 1963). The resulting particle motion (in an ideal half space) can be described by two kinds of wave propagation: body and surface waves. Body waves consist of shear (also known as dilatational waves, primary waves, or P-waves) and compression (also known as longitudinal, distortional, secondary, or S-waves). In bounded media, flexural wave propagation also occurs.

### **2.2.1 Body Waves**

Body waves can be distinguished from one another by considering the direction of particle motion relative to the direction of wave propagation. Compression wave propagation and particle motion are in the same direction. This results in a push-pull

phenomena. These waves are the fastest of all waves but carry the least amount of energy and are therefore quite difficult to detect. Shear waves have particle motion perpendicular to the direction of wave propagation and travel much slower than compression waves.

### **2.2.2 Surface Waves**

As stated previously, if the solid is unbounded, only two types of waves can propagate through the medium: compression and shear waves. In a solid half-space with a boundary surface (as in the case of timber piles), an elastic surface (Rayleigh) wave may also be propagated. Surface waves were first investigated by Lord Rayleigh in (1885). While compression and shear waves propagate radially outward from the source, surface waves propagate along a cylindrical wavefront near the surface and the particle motion is both in the vertical and horizontal directions and varies with depth (Richart, 1970). Although surface waves travel much slower (approximately 60% of the compression wave speed) than body waves, they contain 67% of the total energy created from a vertical impact to the body surface.

By nature, surface waves are non-dispersive in a homogeneous, isotropic linear elastic, solid-half space. Because timber is a non-homogenous material, surface waves will tend to be dispersive; that is, the phase velocity depends on the frequency.

### **2.2.3 Flexural Waves**

Bounded media, such as cylinders and plates, will also allow the transmission of stress disturbances (i.e., wave propagation). The only difference between the propagation of elastic stress disturbances in unbounded and bounded media is due to the geometry of the specimen (Kolsky, 1963). When a vertical impact is made to a bounded surface, transverse motion resulting from bending action occurs. This creates flexural wave propagation in the bounded media. Flexural waves are dispersive by nature, meaning

that the phase velocity of flexural waves depends on their frequency. In the most elementary theory of flexural vibrations, it is assumed that the motion of each element of the specimen's cross-section is purely of translation in a direction perpendicular to the axis of a specimen of uniform cross-section.

## 2.3 Development of Wave Equations

The major contributors to the theory of the propagation of elastic waves in solids in the last century included; Stokes, Poisson, Rayleigh, and Kelvin. The theory was derived as an extension of the theory of elasticity to the problem of vibrating bodies, and also to assist in their studies of the transmission of light considered as vibrations of an elastic ether (Kolsky, 1963). During the first quarter of this century further development of the theory stalled due to the rival attractions of new theory such as atomic physics and partly because of the complexity in examining stress waves in the laboratory. There was no way to measure stress wave propagation experimentally. As a result of the advancement in technology, more specifically high speed computer processors, and development of measurement devices to observe wave transmission, interest in the topic has again peaked. In the subsequent sections, the fundamental principles of elastic wave propagation theory are summarized while keeping the mathematical complexity of the theory to a minimum.

### 2.3.1 Wave propagation in an Elastic Half-Space

For any point  $P$  in a three-dimensional body, six independent components of stress can be identified relative to planes passing through point  $P$  which are parallel to the coordinate planes of a Cartesian coordinate system  $x, y, z$ . The components  $\sigma_x, \sigma_y, \sigma_z, \tau_{yz}, \tau_{xy}, \tau_{xz}$  determine the state of stress at the point  $P$  and can be represented through the stress-strain relations (constitutive equations) for the material. For a linearly elastic

isotropic solid, two elastic constants,  $\lambda$  and  $\mu$  are required to relate stress to strain. For convenience, normally four elastic constants are used. These are Young's modulus  $E$ , Poisson's ratio  $\nu$ , the bulk modulus  $k$ , and the rigidity modulus which is identical to Lamé's constant  $\mu$ .  $E$  is then defined as the ratio between the applied stress and the fractional extension that results when a cylindrical or prismatic specimen is subjected to a uniform stress over its plane ends and its lateral surfaces are free from constraint (Kolsky, 1963). The six components of stress acting on an infinitesimal rectangular parallelepiped (simplifying assumption) can be expressed in the form of Hooke's Law as follows:

$$\begin{aligned} \tau_{xy} &= \mu\gamma_{xy}, & \tau_{zx} &= \mu\gamma_{zx}, & \sigma_x &= \lambda\Delta + 2\mu\epsilon_x, \\ \tau_{yz} &= \mu\gamma_{yz}, & \sigma_y &= \lambda\Delta + 2\mu\epsilon_y, & \sigma_z &= \lambda\Delta + 2\mu\epsilon_z, \end{aligned} \quad (2.1)$$

where,

$$\begin{aligned} \lambda, \mu &= \text{Lame's} \\ \Delta &= \epsilon_x + \epsilon_y + \epsilon_z. \end{aligned}$$

If the x-axis is taken parallel to the axis of the cylinder,  $\sigma_x$  equals the applied stress and the other five components are zero. Thus, the first three equations can be simplified and expressed as:

$$\begin{aligned} \sigma_x &= (\lambda + 2\mu)\epsilon_x + \lambda(\epsilon_y + \epsilon_z), \\ 0 &= (\lambda + 2\mu)\epsilon_z + \lambda(\epsilon_x + \epsilon_y), \\ 0 &= (\lambda + 2\mu)\epsilon_y + \lambda(\epsilon_x + \epsilon_z). \end{aligned} \quad (2.2)$$

By solving equation (2.2) for  $\varepsilon_x$ ,  $\varepsilon_y$ ,  $\varepsilon_z$ ,

$$\varepsilon_y = \varepsilon_z = -\frac{\lambda}{2\mu(3\lambda + 2\mu)}\sigma_x \quad \text{and} \quad \varepsilon_x = \frac{\lambda + \mu}{\mu(3\lambda + 2\mu)}\sigma_x, \quad (2.3)$$

the expression for Young's modulus  $E$  (given by  $\sigma_x/\varepsilon_x$ ), can be written in the following form:

$$E = \frac{\mu(3\lambda + 2\mu)}{\lambda + \mu}. \quad (2.4)$$

Poisson's ratio  $\nu$  is the ratio between the lateral contraction and longitudinal extension of the specimen (Kolsky, 1963), the lateral surfaces being free, i.e.,  $\nu = -\varepsilon_y/\varepsilon_x$ . From eqn. (2.3), Poisson's ratio can be expressed in terms of Lamé's constants in the form:

$$\nu = \frac{\lambda}{2(\lambda + \mu)}. \quad (2.5)$$

The shear modulus or rigidity,  $\mu$ , corresponds to the ratio between the shear stress and the shear strain. The shear modulus is given by eqn. (2.6):

$$\mu = G = \frac{\lambda(1 - 2\nu)}{2\nu}. \quad (2.6)$$

The dynamic equilibrium equations in a Cartesian coordinate system for an infinitesimal element are expressed as:

$$\frac{\partial \sigma_x}{\partial x} + \frac{\partial \tau_{xy}}{\partial y} + \frac{\partial \tau_{xz}}{\partial z} = \rho \frac{\partial^2 u}{\partial t^2},$$

$$\begin{aligned}\frac{\partial \tau_{zx}}{\partial x} + \frac{\partial \tau_{yz}}{\partial y} + \frac{\partial \sigma_z}{\partial z} &= \rho \frac{\partial^2 w}{\partial t^2}, \\ \frac{\partial \tau_{xy}}{\partial x} + \frac{\partial \sigma_y}{\partial y} + \frac{\partial \tau_{yz}}{\partial z} &= \rho \frac{\partial^2 v}{\partial t^2},\end{aligned}\quad (2.7)$$

where  $\sigma$  and  $\tau$  represent the normal and shear stresses on the surface identified by the corresponding suffixes: the first of which represents the plane on which the stress is acting while the latter represents the direction. The components of the displacement in the  $x$ ,  $y$ , and  $z$  directions are denoted by  $u$ ,  $v$ , and  $w$  while  $\rho$  represents the mass density of the material. Next, by substituting the stress components from eqn. (2.1) into eqn. (2.7), one obtains:

$$\begin{aligned}\frac{\partial}{\partial x}(\mu\lambda_{zx}) + \frac{\partial}{\partial y}(\mu\gamma_{yz}) + \frac{\partial}{\partial z}(\lambda\Delta + 2\mu\epsilon_z) &= \rho \frac{\partial^2 w}{\partial t^2}, \\ \frac{\partial}{\partial x}(\mu\gamma_{xy}) + \frac{\partial}{\partial y}(\lambda\Delta + 2\epsilon_y) + \frac{\partial}{\partial z}(\mu\gamma_{yz}) &= \rho \frac{\partial^2 v}{\partial t^2}, \\ \frac{\partial}{\partial x}(\lambda\Delta + 2\mu\epsilon_x) + \frac{\partial}{\partial y}(\mu\gamma_{xy}) + \frac{\partial}{\partial z}(\mu\gamma_{xz}) &= \rho \frac{\partial^2 u}{\partial t^2}.\end{aligned}\quad (2.8)$$

By definition,

$$\gamma_{xy} = \frac{\partial u}{\partial y} + \frac{\partial v}{\partial x}, \quad \gamma_{xz} = \frac{\partial u}{\partial z} + \frac{\partial w}{\partial x}, \quad \epsilon_x = \frac{\partial u}{\partial x}.$$

Replacing  $\epsilon_x$ ,  $\gamma_{xz}$ , and  $\gamma_{xy}$  in eqn. (2.8) with the above definitions yields:

$$(\lambda + \mu) \frac{\partial \Delta}{\partial x} + \mu \nabla^2 u = \rho \frac{\partial^2 u}{\partial t^2}, \quad (2.9)$$

$$(\lambda + \mu) \frac{\partial \Delta}{\partial z} + \mu \nabla^2 w = \rho \frac{\partial^2 w}{\partial t^2}, \quad (2.10)$$

$$(\lambda + \mu) \frac{\partial \Delta}{\partial y} + \mu \nabla^2 v = \rho \frac{\partial^2 v}{\partial t^2}, \quad (2.11)$$

where the Laplacian Operator is given by:

$$\nabla^2 = \frac{\partial^2}{\partial x^2} + \frac{\partial^2}{\partial y^2} + \frac{\partial^2}{\partial z^2}.$$

These are the equations of motion of an isotropic elastic solid in which body forces are absent (Kolsky, 1963). Differentiating the dynamic equations of equilibrium with respect to the dilatation ( $\Delta$ ) and rotation ( $\Omega$ ) yields the wave equations for longitudinal and shear waves respectively (Kolsky, 1963):

$$V_c = \sqrt{\frac{(\lambda + 2\mu)}{\rho}}, \quad (2.12)$$

$$V_s = \sqrt{\frac{\mu}{\rho}}. \quad (2.13)$$

where,

$V_c$  = compression wave velocity

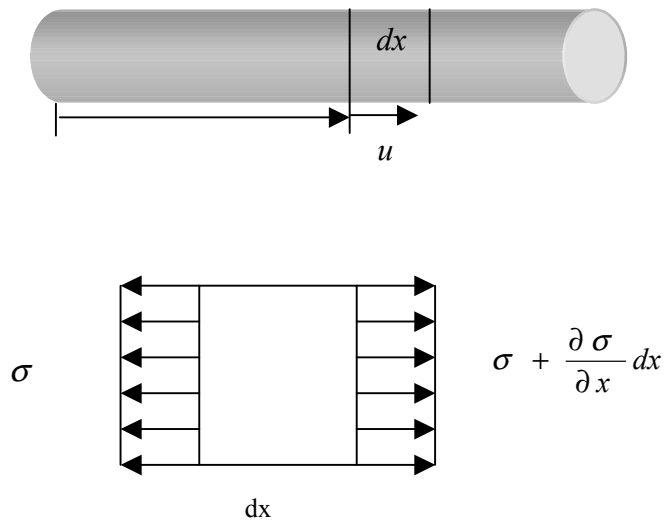
$\lambda, \mu$  = Lamé's constants

$\rho$  = mass density

### 2.3.2 Longitudinal Wave Propagation in Thin Rods

The wave equation which, governs the motion of compression waves in an elastic-half space, also governs the longitudinal rod motion. Consider a straight, prismatic rod shown in Figure 2.1 and the corresponding differential element.

**Figure 2.1** A thin prismatic rod with coordinate  $x$  and displacement  $u$  of a section.



Referring to Figure 2.1, the coordinate  $x$  refers to a cross-section of the rod, while the longitudinal displacement of that section is given by  $u(x, t)$ . According to Graff (1975), if we presume the rod to be under a dynamically-varying stress field  $\sigma(x, t)$  such that adjacent sections are subjected to varying stress, the equation of motion in the  $x$  direction then (considering the differential element shown in Figure 2.1) becomes:

$$-\sigma A + \left(\sigma + \frac{\partial \sigma}{\partial x} dx\right) A + q A dx = \rho A dx \frac{\partial^2 u}{\partial t^2}, \quad (2.14)$$

where  $A$  represents the cross-sectional area of the rod. If we assume the tensile stress to be positive, eqn. (2.14) reduces to:

$$\frac{\partial \sigma}{\partial x} + q = \rho \frac{\partial^2 u}{\partial t^2}. \quad (2.15)$$

Assuming the material behaves elastically, Hooke's law is given by:

$$\sigma = E\varepsilon,$$

where,

$$\varepsilon = \frac{\partial u}{\partial x}.$$

It is assumed that all parallel cross-sections remain plane and that a uniform distribution of stress exists. Assuming the rod is homogeneous, that is the mass density and Young's modulus do not vary with  $x$ , the equation of motion reduces to:

$$E \frac{\partial^2 u}{\partial x^2} + q = \rho \frac{\partial^2 u}{\partial t^2}. \quad (2.16)$$

It is also important to note that there are lateral expansions and contractions arising for the axial stress. At this point, the lateral inertia effect associated with these contraction-expansions has been neglected (Graff, 1975). In the absence of body forces ( $q$ ), eqn. (2.16) reduces to:

$$E \frac{\partial^2 u}{\partial x^2} = \rho \frac{\partial^2 u}{\partial t^2}$$

or,

$$\frac{\partial^2 u}{\partial x^2} = \frac{1}{c_o^2} \frac{\partial^2 u}{\partial t^2}. \quad (2.17)$$

Hence, the longitudinal wave propagation speed is given by:

$$c_o = V_c = \sqrt{\frac{E}{\rho}}. \quad (2.18)$$

### 2.3.3 Torsional (Shear) Wave Propagation in Thin Rods

The torsional (shear wave velocity) is identical to that of longitudinal motion; that is, the familiar form of the wave equation results. Consider a differential element of a straight rod subjected to end torques in Figure 2.2.

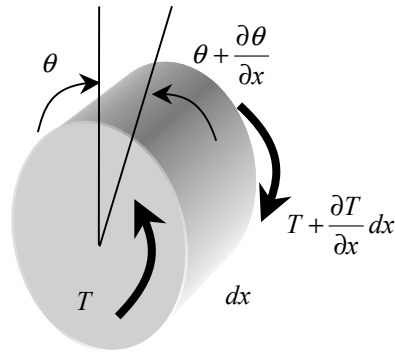


**Figure 2.2** Differential element of a rod subjected to end torques.

Neglecting the body forces and noting clockwise as the positive direction, the equation of motion of the element is given by:

$$-T + \left(T + \frac{\partial T}{\partial x} dx\right) = \rho J dx \frac{\partial^2 \theta}{\partial x^2}, \quad (2.19)$$

where  $J$  is the polar moment of inertia or otherwise known as the torsional constant of the bar. This then reduces to:

$$\frac{\partial T}{\partial x} = \rho J \frac{\partial^2 \theta}{\partial x^2}. \quad (2.20)$$

The torque is related to the angle of twist by the torsional rigidity or torsional stiffness of the bar  $C$  by:

$$T = C \frac{\partial \theta}{\partial x}. \quad (2.21)$$

The torsional rigidity is defined as the product of  $G$ , the shear modulus, and the torsional constant,  $J$ . By, inserting the relation of torque to the angle of twist into eqn. (2.20), one obtains:

$$\frac{\partial^2 \theta}{\partial x^2} = \frac{\rho J}{C} \frac{\partial^2 \theta}{\partial t^2}. \quad (2.22)$$

The torsional rigidity will vary as the complexity of the cross-section varies and is the product of  $GJ$ . By substituting this relationship into eqn. (2.22), we obtain the governing equation for the rod:

$$\frac{\partial^2 \theta}{\partial x^2} = \frac{1}{c_s^2} \frac{\partial^2 \theta}{\partial t^2} \quad (2.23)$$

where,

$$c_s = \sqrt{\frac{G}{\rho}}. \quad (2.24)$$

### 2.3.4 Flexural Wave Propagation in Thin Rods

The theory which governs the transverse motion in thin rods is based on the Bernoulli-Euler theory of beams. The first assumption made is that plane cross-sections initially perpendicular to the axis of the beam remain planar and perpendicular to the neutral axis during bending. This assumption implies that the longitudinal strains vary linearly across the depth of the beam and that, for elastic behavior, the neutral axis of the

beam passes through the centroid of the cross-section (Graff, 1975). Consider a differential element of a thin rod undergoing transverse motion, as shown in Figure 2.3.

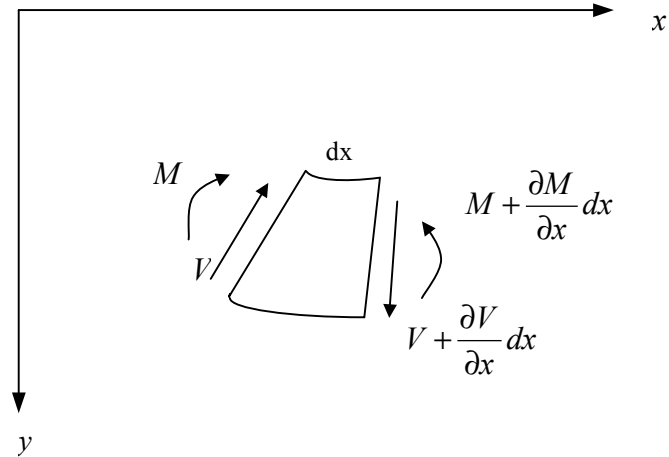


**Figure 2.3** A differential element of a thin rod undergoing transverse motion due to a vertical impact.

As the beam begins to bend, a variation of bending moments  $M$  and shear forces  $V$  are on the element. The relationship between curvature and the bending moment is given by:

$$\frac{\partial^2 y}{\partial x^2} = -\frac{M}{EI} \quad (2.25)$$

where  $x$  is the direction along the axis of the bar and  $y$  is the coordinate of the neutral surface of the beam. Knowing that the theory holds for small deflection of beams and neglecting any loading on the element, the equation of motion in the vertical direction can be written as:

$$-V + \left(V + \frac{\partial V}{\partial x} dx\right) = \rho A dx \frac{\partial^2 y}{\partial t^2} \quad (2.26)$$

where,

$A$  = cross-sectional area of the beam

$\rho$  = mass density per unit volume

Next, upon summation of moments while neglecting the rotational-inertia effects of the element (Graff, 1975), and knowing that the shear and moment are related in the following manner,

$$V = \frac{\partial M}{\partial x}, \quad (2.27)$$

one can show that:

$$\frac{\partial^2 M}{\partial x^2} = \rho A \frac{\partial^2 y}{\partial t^2}. \quad (2.28)$$

Substituting eqn. (2.25) into eqn. (2.28) will yield the following governing equation for the transverse motion of a thin rod or beam:

$$\frac{\partial^2}{\partial x^2} (EI \frac{\partial^2 y}{\partial x^2}) + \rho A \frac{\partial^2 y}{\partial t^2} = 0. \quad (2.29)$$

Furthermore, if the material is homogeneous ( $E$  is constant) and the cross-section is constant so that  $I$  is constant, the equation for transverse motion reduces to:

$$\frac{\partial^4 y}{\partial x^4} = \frac{1}{c^2} \frac{\partial^2 y}{\partial t^2}, \quad (2.30)$$

yielding a velocity such that:

$$c^2 = \frac{EI}{\rho A}. \quad (2.31)$$

It should be noted that  $c$  does not have the dimensions of velocity and that the restrictions for the development of this relationship were accounted for; that is, material homogeneity and constant-cross section. Beams not having these properties can be analyzed using this theorized framework based on eqn. (2.29), with only the cost of increased mathematical complexity (Graff, 1975).

## 2.4 Dispersion

As previously mentioned, all waves defined in the previous section are dispersive by nature in a bounded solid such as a timber pile. Elementary theory has shown that wave velocity of bending (or flexural) waves depends on its frequency. Because waveforms created upon impact from a transverse blow to the piles surface contain many frequencies, a single frequency embedded in a bending wave will travel at its own separate velocity. If several are added together, each traveling at their own individual velocity, the waves shape will continuously change over time. This phenomenon is known as dispersion. As a result, determining the velocity at which the wave is traveling is theoretically quite difficult. But with the use of signal processing tools, we can effectively determine the velocity of individual frequencies in a waveform. To do this, we utilize a mathematical technique known as the Fourier Transform.

## 2.5 The Discrete and Fast Fourier Transforms

In 1807 Jean Baptiste Joseph Fourier began work on *Theorie analytique de la chaleur* (English translation, 1878, The Analytical Theory of Heat), the Fourier series, which was the first systematic application of a trigonometric series to a problem solution. This was the prelude to the mathematical tools that we now refer to as Fourier Analysis. Both the

Fourier series and the Fourier integral allow transformation of physically realizable time-domain waveforms to the frequency domain and vice versa (Ramirez, 1985).

A typical signal obtained from the bending wave test is non-periodic by nature. To transform these waveforms, which are obtained as a function of time, to a function of frequency, the Fourier transform can be utilized. The continuous Fourier transform (or integral) of  $x(t)$  is defined as:

$$X(f) = \int_{-\infty}^{\infty} x(t) e^{-j2\pi(f)(t)dt} \quad (2.32)$$

This formulation is used to define a waveform in the frequency domain for a continuous time interval. Because waveform signals obtained in practice are obtained in digitized form (data is only obtained at discrete intervals in the time domain), a variation of the Fourier transform was developed for use in digital signal processing (Ramirez, 1985). The discrete Fourier transform (DFT) of  $x(n\Delta t)$  is defined as:

$$X(k\Delta f) = \Delta t \sum_{n=0}^{N-1} x(n\Delta t) e^{-j2\pi(k\Delta f)(n\Delta t)} \quad (2.33)$$

where,

$x(n\Delta t)$  = the discrete set of time samples that defines the waveform to be transformed.

$X(k\Delta f)$  = the set of Fourier coefficients obtained by the DFT of  $x(n\Delta t)$ .

$\Delta t$  = time increment between data points, sec.

$\Delta f$  = frequency interval in the frequency domain ( $1/N\Delta t$ ), Hz.

$k$  = the index for the computed set of discrete frequency components,

$k = 0, 1, 2, \dots, N-1$ .

$n$  = the time sample index,  $n = 0, 1, 2, \dots, N-1$ .

$N$  = total number of data points being considered from the digitized signal.

$X(f)$  is a complex number with a real component  $X_{\text{Re}}(f)$  and an imaginary component  $X_{\text{Im}}(f)$ , and therefore can be represented as a vector in a complex coordinate system (Katzke, 1997). By Euler's identity,  $e^{\pm j\theta} = \cos \theta \pm j \sin \theta$ , which yields:

$$X(k\Delta f) = X_{\text{Re}}(k\Delta f) - jX_{\text{Im}}(k\Delta f), \quad (2.34)$$

while,

$$X_{\text{Im}}(k\Delta f) = \Delta t \sum_{n=0}^{N-1} x(n\Delta t) \sin[2\pi(k\Delta f)(n\Delta t)] \quad (2.35)$$

and,

$$X_{\text{Re}}(k\Delta f) = \Delta t \sum_{n=0}^{N-1} x(n\Delta t) \cos[2\pi(k\Delta f)(n\Delta t)] \quad (2.36)$$

where,

$x(n\Delta t)$  = the discrete set of time samples that defines the waveform to be transformed.

$X(k\Delta f)$  = the set of Fourier coefficients obtained by the DFT of  $x(n\Delta t)$ .

$\Delta t$  = time increment between data points, sec.

$\Delta f$  = frequency interval in the frequency domain ( $1/N\Delta t$ ), Hz.

$k$  = the index for the computed set of discrete frequency components,  
 $k = 0, 1, 2, \dots, N-1$ .

$n$  = the time sample index. Its values are  $n = 0, 1, 2, \dots, N-1$ .

$N$  = total number of data points being considered from the digitized signal.

$X_{\text{Re}}(k\Delta f)$  = the real part of the frequency domain.

$X_{\text{Im}}(k\Delta f)$  = the imaginary part of the frequency domain.

By letting  $f = k(\Delta f) = k/N\Delta t$ , the magnitude of the discrete Fourier transform is defined as:

$$A(f) = |X(f)| = \sqrt{(X_{\text{Re}}(f))^2 + (X_{\text{Im}}(f))^2}, \quad (2.37)$$

while the phase angle of the Discrete Fourier transform is defined as:

$$\phi(f) = \tan^{-1} \left( \frac{X_{\text{Im}}(f)}{X_{\text{Re}}(f)} \right). \quad (2.38)$$

In a more general sense, the idea of the FFT is to transform a digitized signal in the time domain to the frequency domain by placing a sine and cosine curves next to the digitized waveform so the data points in the curves line up with the sample points (at a specific time interval) in the signal. Points which are adjacent between the sine and cosine curves and the points representing the digitized waveform are then multiplied (eqns. 2.35-36). The resulting cross-products, one corresponding to the cosine curve and one corresponding to the sine curve (the latter representing the imaginary part  $X_{\text{Im}}(k\Delta f)$ , while the former represents the real part  $X_{\text{Re}}(k\Delta f)$ ), are summed. It is important to note that all algebraic signs are maintained in eqn. (2.34). This summation,  $X(k\Delta f)$ , is the form of the complex vector representing the set of Fourier transform coefficients (specific frequencies).

Using this set of frequencies obtained from the Fourier transform of the digitized waveform, a plot of amplitude versus frequency can be made, which will identify the most prominent frequency contained within the waveform, known more commonly as a dispersion curve. Due to the lengthy calculations performed during the discrete Fourier transform, a fast Fourier transform (FFT) algorithm is commonly used. The FFT

requires that the number of input data points must be a power of 2. This creates mathematical symmetries which will tend to speed up the calculations when the sampling rates are high.

### **2.5.1 The Fourier Phase Method**

A technique known as the Fourier Phase Method is commonly used to determine appropriate frequencies for determining phase velocities of real waveforms. The technique utilizes the resulting frequencies obtained from the FFT to construct a plot of amplitude versus frequency known as a dispersion curve. This is then used to identify the frequency components of the waveform (a typical dispersion curve obtained from a stress wave can be seen in Figure 3.4).

However, there is a drawback to this method. In a non-homogeneous medium, there will be multiple limbs of the dispersion curve, meaning that there is more than one wave speed solution for each frequency (Douglas et al., 1989). The Fourier phase method is incapable of determining multiple limbs of the dispersion curve. The curve constructed from the coefficients (frequencies) obtained from the FFT represent an average of the multiple limbs. Another problem which results from this method is that the exact value of the phase angle  $\theta$  is unknown since it can be the angle computed or that angle plus some multiple of 360 degrees (Douglas et al., 1989).

## **2.6 The Short Kernel Method**

The Short Kernel Method (SKM) is a digital signal processing technique that was developed at North Carolina State University by Dr. R.A. Douglas (Holt, 1994). This frequency-dependent scanning operation is based upon the cross-correlation procedure described by Bendat and Piersol (1980) and is used to aid in determining the velocity of wave propagation.

During the bending wave test, a digitized signal is obtained and stored. Because of the dispersive nature of flexural waves, there exist numerous frequencies within a typical signal that correspond to a specific phase velocity. The purpose of the SKM is to amplify a given frequency within the time domain to aid in determining the most prominent frequency within the waveform. The process involves a piecewise examination of the signal by use of an SKM kernel. The kernel, which must have the same time step as the recorded data, can be a sine, cosine, or any other function. Mathematically, a single value of the SKM at a particular frequency can be stated by the following:

$$SKM(j, k) = \sum_{i=1}^{N_2-N_1} f(\tau_i) \cdot g[(\tau_i + j \cdot \Delta t), k] \cdot \Delta t \quad (2.39)$$

where,

$SKM(j, k)$  = the  $j$ th term of the cross-correlation currently being performed at the  $k$ th frequency.

$f$  = the time record from one accelerometer.

$g$  = the fragment of kernel used to perform the cross-correlation.

$N_2$  = the number of data points in  $f$ .

$N_1$  = the number of data points in  $g$ .

The SKM utilizes the kernel (a user-determined frequency) and aligns it with the signal so that the first points of the original signal and kernel are adjacent. The amplitudes corresponding to the raw signal are then cross-multiplied by the amplitude of the kernel at each data point at corresponding time intervals. The number of data points in the raw signal is determined by the sampling rate and time window on the oscilloscope while those of the kernel are user-determined. The products of the multiplication are then summed while maintaining the algebraic sign of each individual multiplication. The summation represents the first point on the SKM plot. Next, the kernel is shifted by

a pre-selected number of data points and the cross-products are again formed. The process continues until the end of the data set or a user-defined maximum is reached.

The resulting SKM values (amplitudes) indicate the amount of correlation between the kernel and the raw signal; that is, the frequency of the kernel is the most prominent frequency in the raw signal. If the amplitude of the raw signal matches that of the kernel, the corresponding SKM value will be greater. The SKM essentially acts as a filter. It magnifies the frequency of interest within the waveform and filters out those that are not. If the values of the SKM are positive, the kernel and raw signal are in phase. Conversely, if the SKM value obtained is negative, they are out of phase, meaning they lie on opposite sides of the amplitude scale. Upon completion of the SKM plot, the peaks and troughs can be used to determine wave speed and travel time of individual frequencies within the waveform.

## **Chapter 3**

# **The Bending Wave Testing Procedure**

### **3.1 Overview**

The bending stress wave technique is similar to the longitudinal technique described by Ross et al. (1997). A stress wave is induced by an impact made on the pile's surface, which creates a stress wave field consisting of, but not limited to: shear, compression (longitudinal), surface (Rayleigh), and flexural waves. Wave propagation is detected by sensors attached in a linear array along the longitudinal axis of the pile. The particle displacements detected by the sensors are then converted to voltages and displayed as digitized signals on an oscilloscope. Signal processing tools are then used to determine information necessary to evaluate the condition of the medium.

Using this technique, one does not distinguish between types of waves. Although bending waves are thought to contain the most energy, raw data from a stress wave test contains information from a combination of several mechanical inputs to the accelerometers by the various branches of the structure (Douglas et al., 1989). Although this statement might seem discouraging, it cannot negate the many studies, which have determined relationships between material properties and stress wave parameters using similar test methods. This has led to the belief that at least one wave, most likely the flexural component, is dominant in the signal.

### **3.1.1 The Bending Wave Testing Procedure**

An impact is made perpendicular to the surface of the pile, inducing a stress field which propagates radially outward from the point of origin. The impact is made with various impact mechanisms, depending on the frequency composition required for evaluation. In this research, devices were utilized with varying material properties. Through experimentation, it was found that wood was the most desirable material for creating an impact, most likely due to the matching impedance of the materials.

Sensors were attached to the timber pile through a magnetic head that is coupled to one-inch roofing nails. In this research, piezoelectric accelerometers were used to measure the particle accelerations along the wave front. Four accelerometers were attached in a linear fashion at one-foot intervals along the longitudinal axis of the pile. As the disturbance propagates through the medium (induced by the impact device), the resulting particle motion is captured using a digital oscilloscope. The sensors measure the particle acceleration. The oscilloscope reads the voltage changes from each sensor as the wave front passes and plots them as a function of time. The raw signal is transferred and stored on a computer. Signal processing tools developed at North Carolina State University are then used to determine spectral information and wave propagation speeds. A diagram of the testing procedure in both the laboratory and field can be seen in Figures 3.1 and 3.2.

### **3.1.2 Energy Source (Impact Device)**

One of the most important aspects in successfully using the bending wave technique for condition assessment is creating a proper impact. Most importantly, the impact must create a signal containing the frequency range of interest. For this research, the frequency range used was approximately 2000 to 3000 Hz. Operators using this technique rarely have any formal training in the use and interpretation of stress wave

information. Therefore, it is particularly important to provide an impact that not only provides adequate spectral information but also relies minimally on user discretion. In this case, random errors due to the impact-to-impact variations and operator-to-operator variations can be reduced.

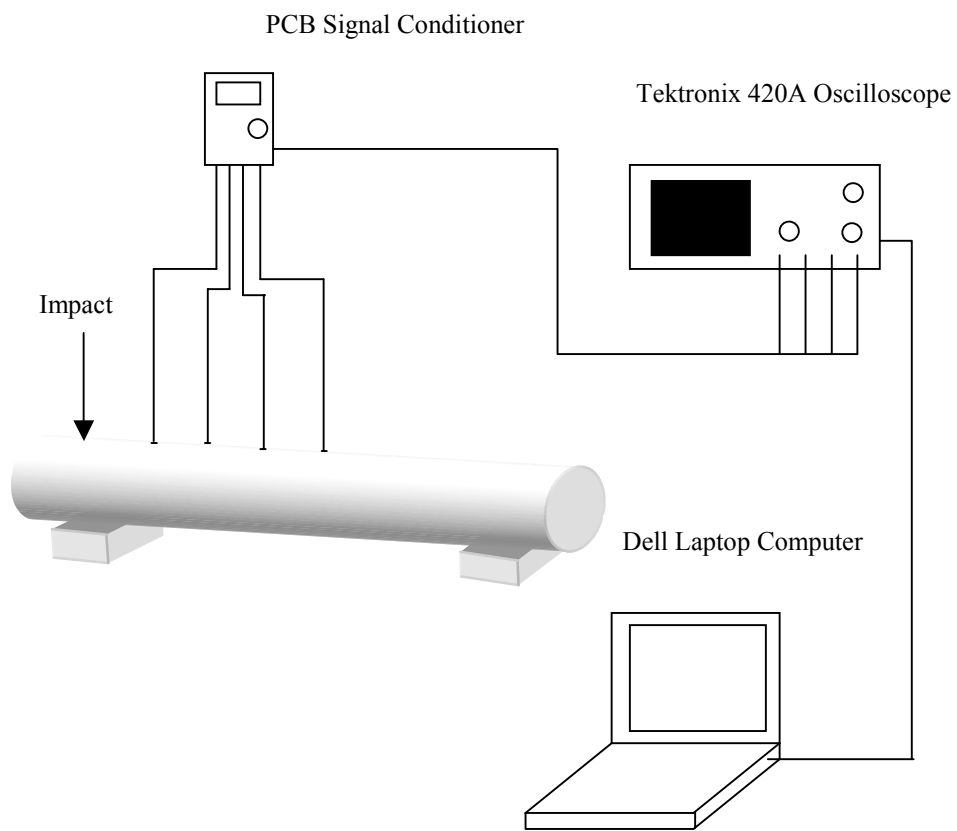


**Figure 3.1** Laboratory bending wave testing configuration.

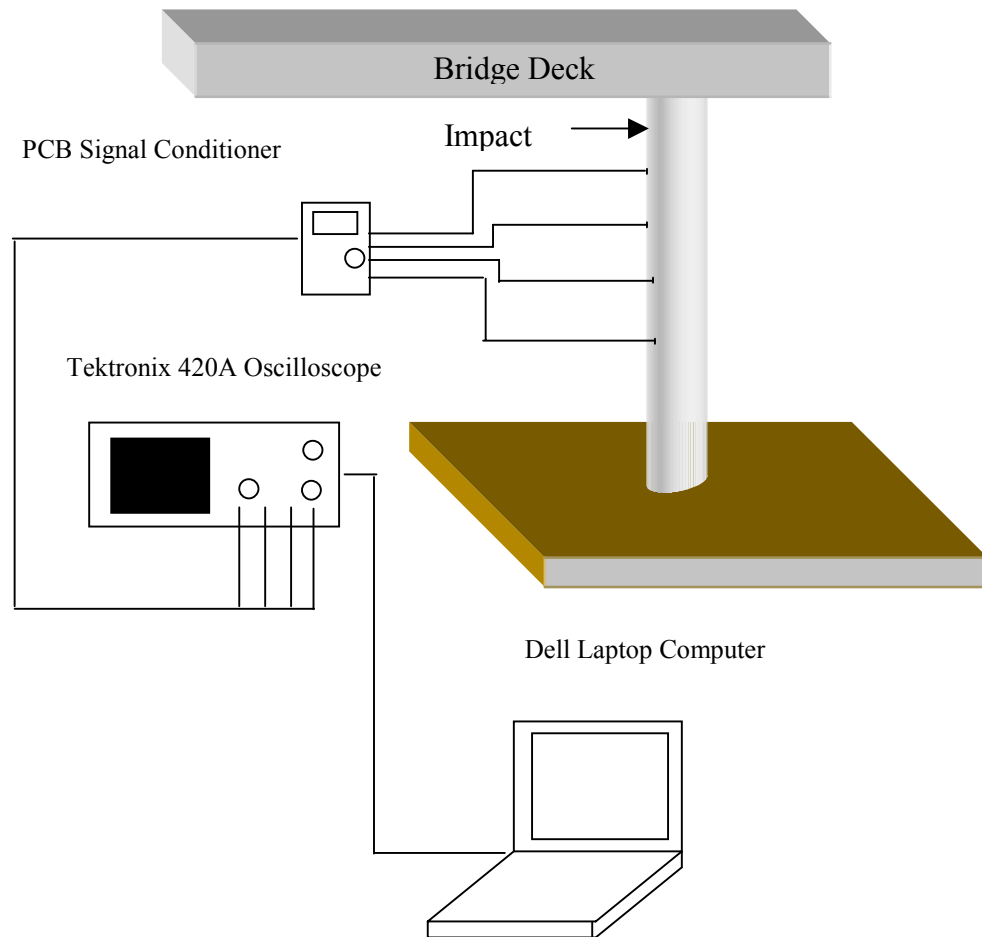


**Figure 3.2** Field bending wave testing configuration

### 3.1.3 Sensors

Upon disturbing the medium by an impact to its surface, a wavefront will propagate radially outward in all directions, inducing particle motion. The particle motion results from shearing action of adjacent particles as the wavefront passes. For this research, PCB model 303A02 piezoelectric accelerometers were used to measure the particle

accelerations at the pile surface. The measured particle acceleration is then converted to voltage and stored on a digital oscilloscope.

Sensors are attached in a linear fashion along the longitudinal axis of the pile. The accelerometers have magnetic heads that allow coupling to the pile surface with the use of standard roofing nails. Roofing nails have a large diameter head that provides sufficient area to mount the gages. The nails should be driven in such a manner that the head does not touch the surface of the pile. The accelerometers were connected to a PCB Piezotronics ICP power supply, model 482A05. The power supply was then connected to an oscilloscope using standard coaxial cable.

### **3.1.4 Signal Acquisition**

When measuring particle displacements, the time base is used to generate a time axis for an amplitude history that will completely describe the waveform. The oscilloscope uses a ramp voltage to drive an electron beam at a constant rate across the face of a CRT (cathode ray tube). The measurement of the signal drives the pen or CRT trace in a direction normal to the time-base drive which results in a time history of amplitude variation (Ramirez, 1985). The time base is partitioned into equal intervals, normally reported in milliseconds. A typical bending wave can be seen in Figure 3.3.

It is of particular importance to collect enough points to fully describe the waveform. If the time window is too short, an incomplete picture of the waveform will be displayed from which few conclusions regarding wave shape and type can be discerned. The sampling rate can be adjusted to vary the time window using the horizontal scaling function. Vertical scaling of the waveform can also be performed to enhance signal clarity. For this research, a Tektronix 420 digital oscilloscope was used.

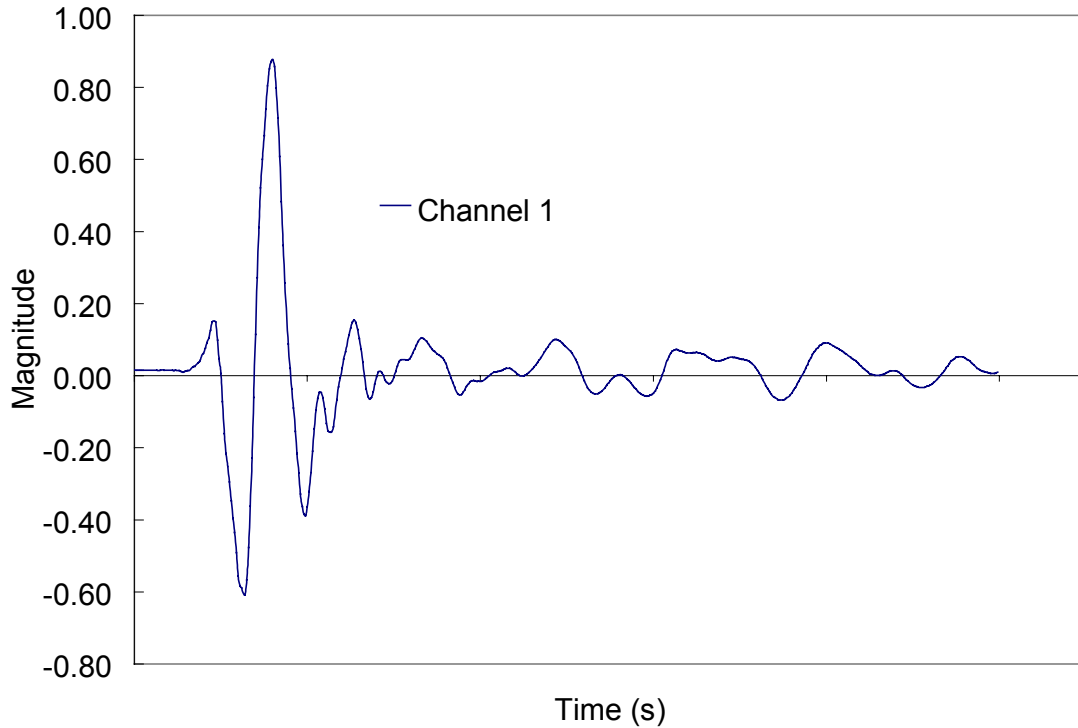


**Figure 3.3** Typical raw signal obtained from the bending wave test.

### 3.1.5 Signal Processing Tools

Once a signal is obtained, it must undergo signal processing to determine spectral information that characterizes the waveform. The Stress Wave Analysis Program contains features that can be utilized to determine necessary wave propagation parameters. SWAP is a program written in Visual Basic that has the capability of data acquisition and signal processing. SWAP has built-in utilities that perform frequency-domain analysis using the FFT for the calculation of frequency parameters and time-domain analysis for the construction of the dispersion field using either SKM or Fourier

Phase Methods. SWAP also has the capability of graphically presenting the information to ensure that data is presented in a convenient and organized manner.

## **3.2 Stress Wave Parameters Used for Condition Assessment**

As stress waves propagate through the medium, their characteristics reflect the material properties of the medium through which they are passing. These parameters are used as evaluation tools in non-destructive testing procedures. Knowledge of the following terms is necessary to characterize medium properties.

### **3.2.1 Wave Speed and Phase Velocity**

Throughout this document, the terms wave speed and phase velocity have been used to describe the speed of transmission of elastic wave propagation through a specific medium. It is important to distinguish the difference between them. The wave speed is the speed of the elastic wave propagating through the medium. As discussed previously, a stress wave is composed of many frequencies, traveling at their own specific velocities. Using signal processing techniques, an attempt is made to isolate frequencies that are the greatest in magnitude using the FFT and SKM. The phase velocity is the speed at which a specific frequency contained within the stress wave travels. Therefore, for a single stress wave there exists one wave speed, while there are many phase velocities depending upon the frequency of interest.

### **3.2.2 Attenuation Ratio**

Because of their dispersive nature, stress waves are composed of many frequencies traveling at their own individual velocities. Frequencies composing a stress wave and their corresponding magnitudes are illustrated by the frequency spectrum plot. The wave

is detected as it passes the location of each sensor. As a result, there exists a frequency spectrum plot for each channel used in the bending wave technique. The attenuation ratio is the ratio of the area under the magnitude-frequency plot of one channel to the area under the magnitude-frequency plot of another channel. The area under the frequency spectrum plot is calculated by integrating the curve within a given frequency range. Normally the attenuation ratio is determined using the first two channels where the greatest attenuation occurs.

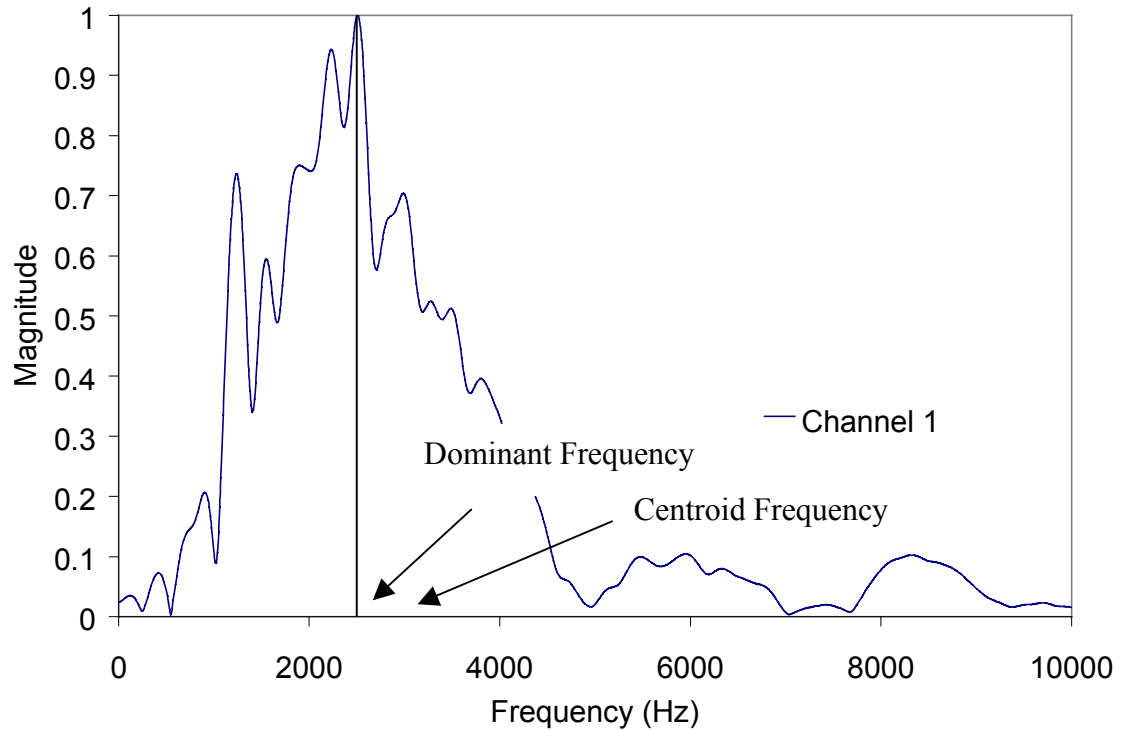


**Figure 3.4** Dominant and centroid frequency in the magnitude vs. frequency plot.

### 3.2.3 Dominant Frequency and Centroid Frequency

The dominant frequency of a stress wave is the frequency with the highest magnitude, calculated using the FFT. This value is obtained from the frequency spectrum plot for a specific waveform. The centroid frequency, also obtained from the frequency spectrum plot, is the frequency that divides the area under the magnitude-frequency curve in half. An illustration of the centroid frequency for a waveform and the dominant frequency can be seen in Figure 3.4.

## 3.3 Determining the Wave Speed

Because many frequencies are embedded in a single waveform, it is difficult to obtain a theoretical value for the wave speed. Inclusions and discontinuities in the timber also inhibit the path of the waveform, influencing wave propagation speeds. Therefore, assumptions governing the theoretical development of the wave propagation speeds shown in Chapter 2 are no longer valid. The wave speed must be determined experimentally.

A typical waveform is measured using the bending wave technique described in Section 3.1.1. The resulting waveform is then stored on a computer as a time versus amplitude record and awaits signal processing using the SWAP. Figure 3.5 shows a typical raw waveform displayed using the SWAP.

CH-A through CH-D represent the corresponding measured waveform detected at each sensor location. Figure 3.6 is the FFT plot for the signal obtained in Figure 3.5. The plot illustrates the frequencies that compose the waveform and the corresponding magnitudes. The information necessary to create this plot is obtained from the FFT method described in Chapter 2. From Figure 3.6, the dominant frequency, i.e., the frequency with the greatest magnitude embedded in the waveform, is approximately 2500 Hz. This is the frequency that is used as the “kernel” when using the SKM.

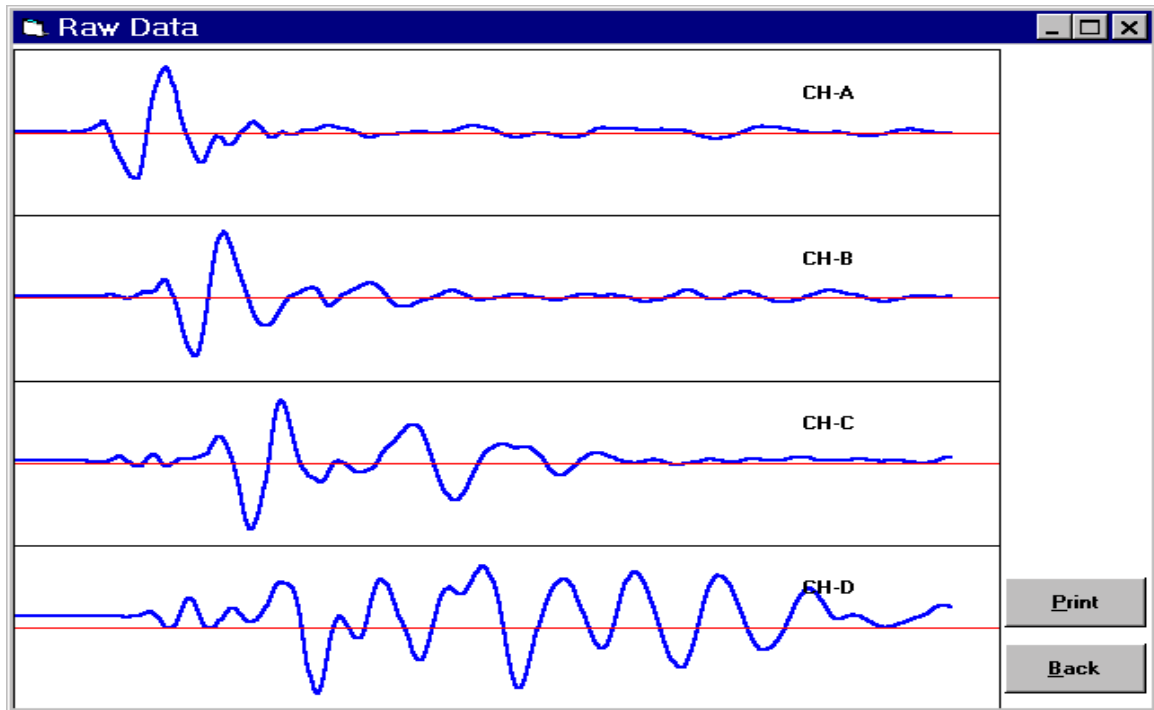


**Figure 3.5** Typical raw signal obtained from the bending wave testing procedure.

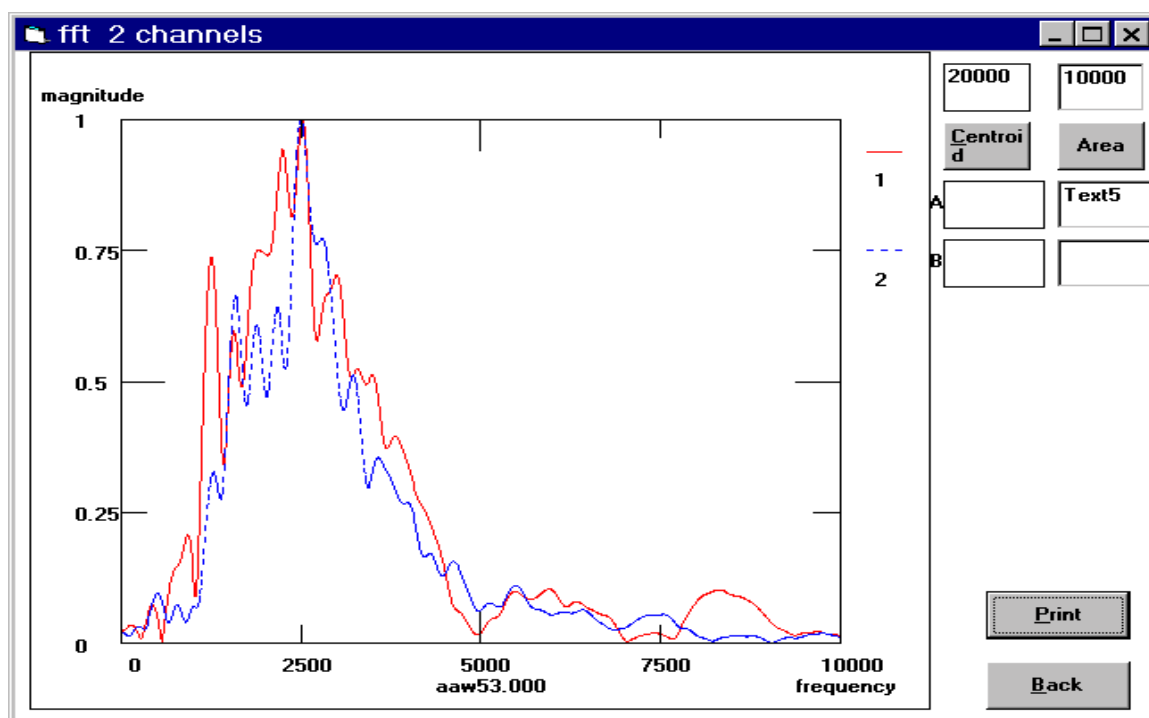


**Figure 3.6** FFT plot for typical measured raw signal using the bending wave technique.

Figure 3.7 is the SKM plot of the time records obtained for the signal measured in Figure 3.5 using 1 cycle of the 2500 Hz kernel for each channel. The SKM has acted as a “sieve” in that it extracted the 2500 Hz component from the signal and displayed its approximate location inside the time records of each channel. A large amplitude in each channel corresponds to how well the kernel is aligned with the raw signal. For further description of the SKM, see Chapter 2.

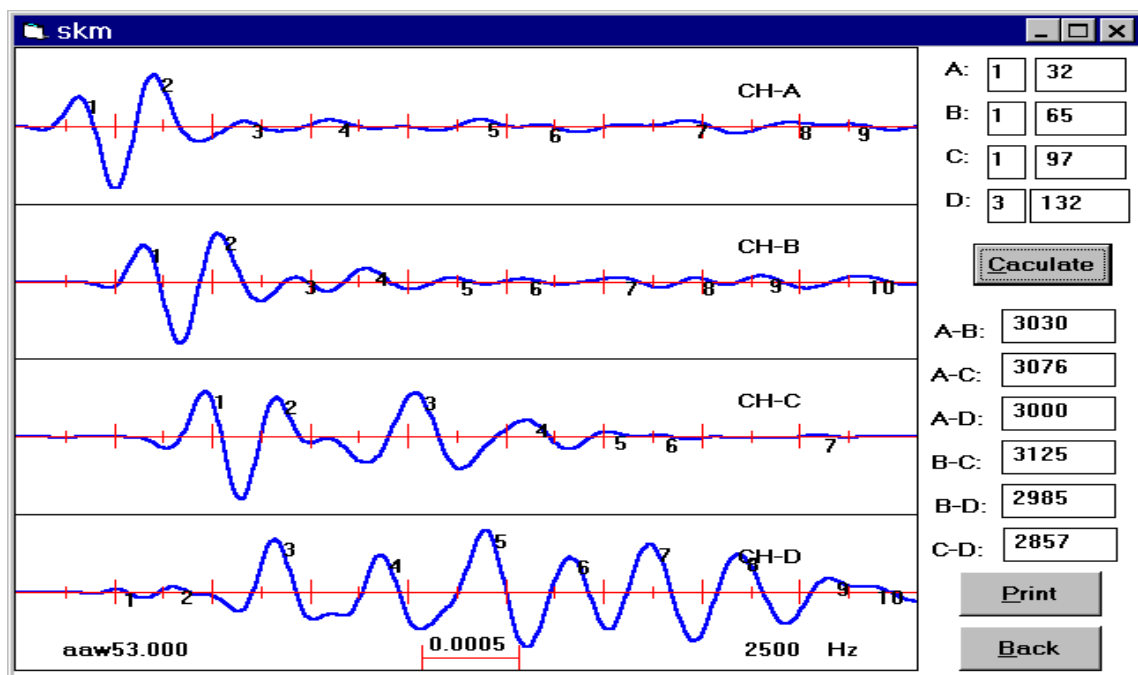


**Figure 3.7** SKM plot for typical raw signal shown in Figure 3.5 using the SWAP.

To calculate the phase velocity, one can use the first positive peak labeled 1 in Figure 3.7. In theory, the raw signal will maintain its form while appearing at each sensor location at a different time: appearing at the sensor location nearest the impact first; the next furthest sensor second; and continue in a similar manner until sampling is terminated. Therefore, corresponding peaks in each channel indicate when the

waveform passed that location. In the raw signal (shown in Figure 3.5), corresponding peaks are difficult to detect in CH-C and CH-D. However, with the use of the SKM, the corresponding peaks can be determined. In Figure 3.7, after signal processing using the SKM, one can see the peak labeled 1 in CH-C corresponds to the peak labeled 3 in CH-D. Finally, knowing the distance between sensors, and the time (as recorded in the amplitude-time record for each channel), the wave speed can be determined by the following:

$$V_{ph} = \frac{D}{n \times \Delta t}$$

where,

$V_{ph}$  = phase velocity of a specific frequency contained within the waveform (ft/s).

$D$  = distance between accelerometers (ft).

$n$  = the number of data points between peaks.

$\Delta t$  = the time interval between data points obtained from the oscilloscope (s).

For the waveform shown in Figure 3.5, the phase velocity determined using a 2500 Hz kernel is 3030 ft/s. In comparison, using the eqn. (2.31) developed for the wave propagation speed of a flexural wave in Chapter 2, the wave speed is given by:

$$V = \sqrt{\frac{EI}{\rho A}} \quad (2.31)$$

where,

$E$  = Young' modulus (psi).

$I$  = moment of inertia (in<sup>4</sup>).

$\rho$  = density of timber (lbs/in<sup>3</sup>).

$A$  = cross-sectional area (in<sup>2</sup>).

From ASTM D143, Young's modulus for southern yellow pine is 1,500,000 psi. The density  $\rho$  is approximately 35 lbs/ft<sup>3</sup> (this varies from species to species) while the moment of inertia  $I$  is given by:

$$I = \frac{\pi r^4}{4},$$

where,

$r$  = radius (*in*).

For a pile with a diameter of 8 in., the resulting moment of inertia  $I$  is 201 in<sup>4</sup>. The cross-sectional area  $A$  is 50.3 in<sup>2</sup>. The resulting velocity from eqn. (2.31) is 1433.7 ft/s. The difference between the theoretical value and the experimental value should be noted. Because wood is neither homogeneous nor isotropic, the basic assumptions made in the development of the velocity obtained in eqn. (2.31) are invalid; therefore, the values obtained using one-dimensional wave theory in wood are inaccurate.

## **Chapter 4**

# **Development of a Standard Impact Device**

### **4.1 Importance of Impact Device Selection**

One of the most important aspects of successfully utilizing the bending wave technique for condition assessment is creating a proper impact. A major problem that arises when using stress wave techniques is the inability to control and reproduce the desired impact that produces a frequency spectrum that provides us with adequate information to assess wave properties. Currently, a wooden mallet is used to create an impact known as the modified hammer. The information obtained from this device provided adequate spectral information which could be used for condition assessment (Qian, 1997).

Because the user manually deploys the mallet, the energy imparted by the impact and the measured wave properties are dependent on the operator. To improve the reliability of our results, it was necessary to develop a standard impact device that relies less on user discretion. The objective of the laboratory testing was to machine a device that would accomplish the following:

- Minimize the impact-to-impact and operator-to-operator variations.
- Produce an impact replicating the frequency spectra produced by the modified hammer.
- Detect variations in the remaining cross-section of a timber pile.

In doing so, more accurate relationships could be developed between wave propagation properties and various environmental and physical conditions while increasing the efficiency of testing by reducing the amount of replications necessary to produce accurate results.

## **4.2 Creating an Effective Impact**

To create bending waves in a timber pile, the pile must be struck in a transverse direction to its longitudinal axis. The impact must be controlled to reduce local crushing of the contact interface between the pile and the impact mechanism. The surface of the pile and impact device must be free of any debris that might inhibit the energy exchange between the device and pile surface. The geometry of the impact device must be able to conform to the small angular irregularities that occur between the pile surface and the impact device. The energy upon impact must be sufficient to create signals with frequency content ranges of 2000 to 3000 Hz. Impact variations due to the operator must be controlled and minimized. Contact time must be kept at a minimum to prevent damping and reduce noise. It is essential that the impact device itself also is able to withstand multiple impacts without crushing or damage.

## **4.3 Evaluation of Various Impact Devices**

Because the modified hammer used in previous research was proven to provide wave properties able to predict variations in a cross-section, an attempt was made to model its behavior. A spring-loaded mechanism using a one-inch steel ball for impact and a wooden spring device were machined at the precision machine shop at North Carolina State University. Ten feet intact timber piles were used as the propagation medium.

### 4.3.1 Experimental Setup

Southern yellow pine piles (CCA treated) were simply supported in the laboratory during the course of testing. Wave properties were measured at one-foot intervals along the longitudinal axis of the pile using each impact device. A record of the wave propagation properties was obtained using the bending wave technique. The primary wave properties used for consideration in comparing the devices were: the frequency spectra plots, average centroid frequency, and the average phase velocity. Signal processing was performed using the stress wave analysis program (SWAP).

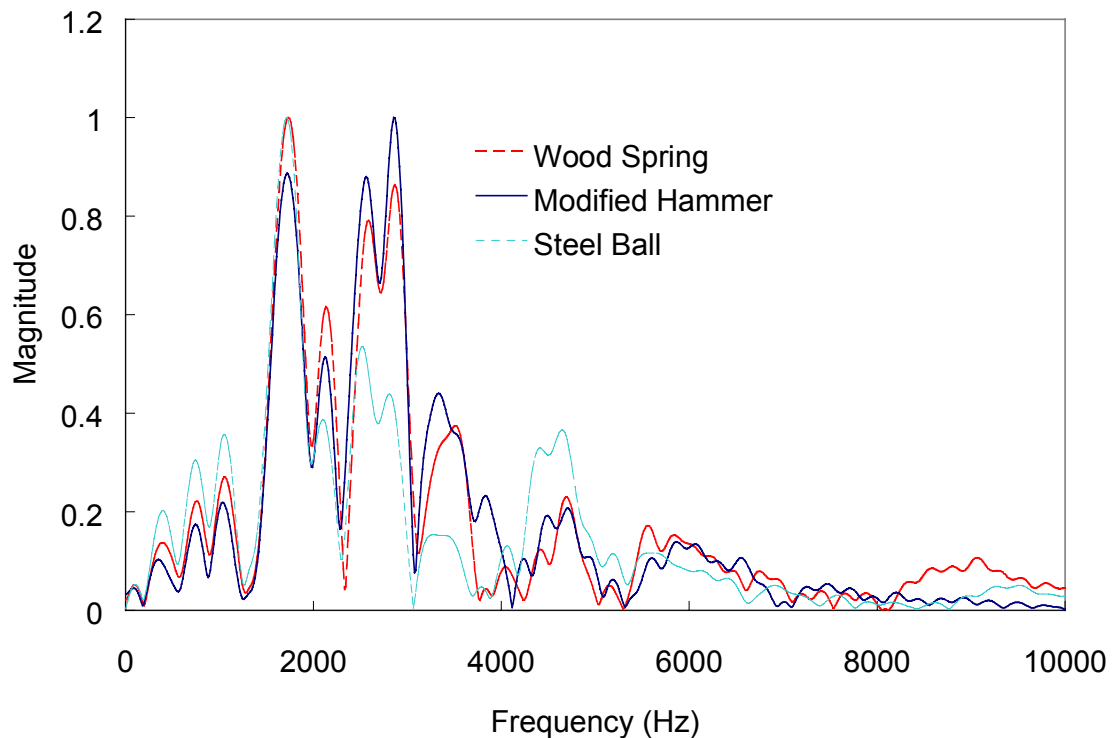


**Figure 4.1** Comparison of frequency spectra plots for the impact devices tested.

### 4.3.2 Comparison of Wave Propagation Properties

As seen in Figure 4.1, the frequency spectral plots obtained from impacts made with the steel ball and the wood spring mechanism closely resembled those produced by the modified hammer. This indicates the waveforms and corresponding magnitudes would show a strong correlation between devices.

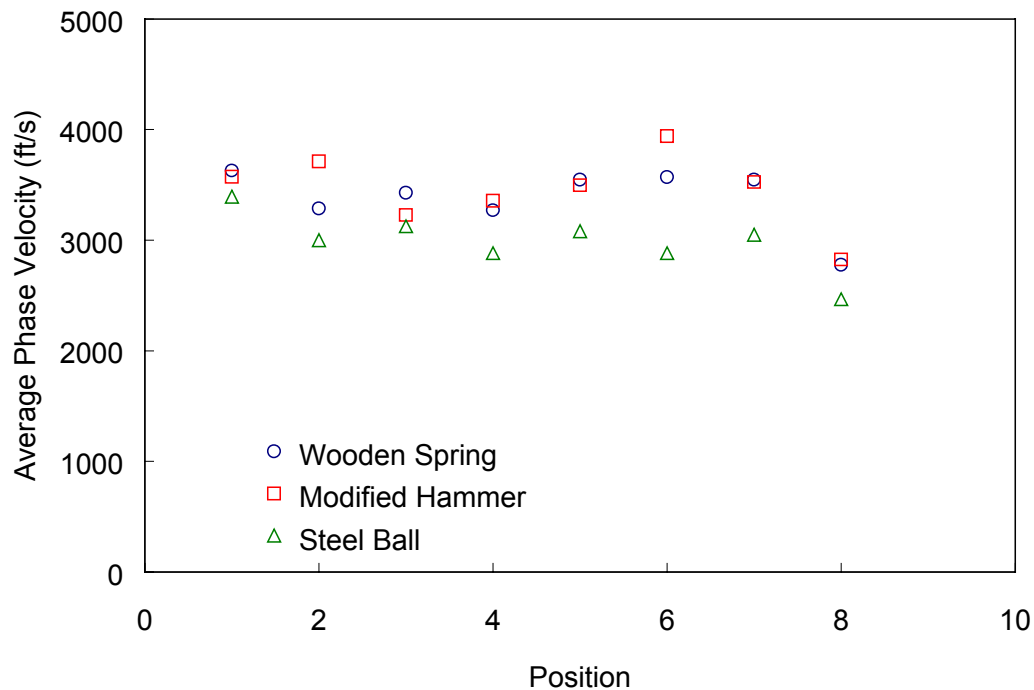


**Figure 4.2** Average phase velocities measured using the bending wave technique for various impact devices.

The waveforms created from each device were then compared by considering the wave speed and specific properties of the frequency content of the waveform. Figure 4.2 illustrates the average phase velocity obtained (recall that during the bending wave testing procedure the average of 5 records is obtained to reduce random error inherent in

experimentation) at locations along the axis of a timber pile for each impact device. The velocities obtained using the wooden spring mechanism correspond well with those obtained using the modified hammer while the values measured using the steel ball are lower. The actual value of the phase velocity is inconsequential. It is only important that the values obtained from the new device correspond well with those values measured when using the modified hammer for impact.

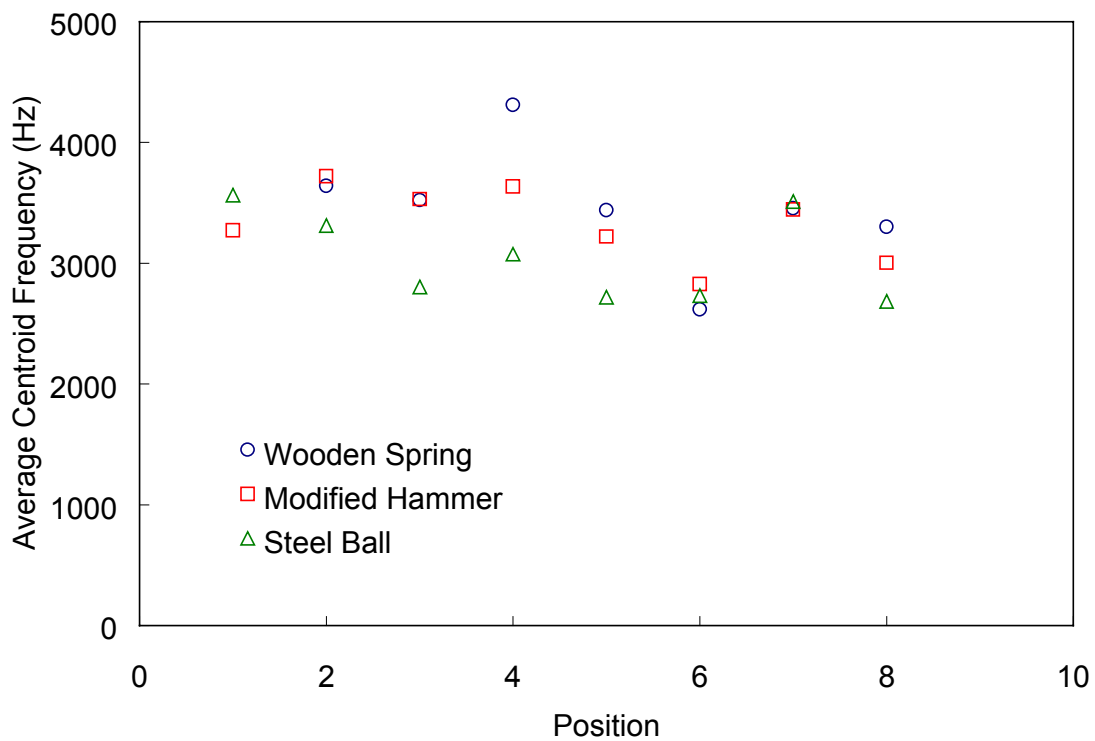


**Figure 4.3** Average centroid frequencies measured using the bending wave technique for various impact devices.

Figure 4.3 shows the average centroid frequency measured using each device for impact. In general, the frequencies measured using the wood spring mechanism

correspond well with the values measured using the modified hammer. Again, those values measured using the steel ball mechanism are lower than those obtained when using the modified hammer and wooden spring device.

#### **4.3.2.1 Impact-to Impact Variations**

To eliminate impact-to-impact variations in wave propagation properties, consistency between impacts is essential. This can be quantified by comparing the standard deviations of each impact device (for a data set at each position along the pile length). At specific locations along the pile, five records were obtained for each device using the bending wave technique. A record consists of wave propagation and particle motion recorded upon impact from the device.

Figures 4.4 through 4.6 show the average phase velocities for each device with corresponding one standard deviation error bars. Comparing standard deviations of the average phase velocities obtained using the steel ball mechanism (see Figure 4.4) with those obtained using the modified hammer (see Figure 4.6), the steel ball is much less consistent. Furthermore, results indicated that a more consistent signal could be obtained using an impact device that has material properties matching those of the pile (more specifically, matching impedance). The standard deviations produced by impacts made with the steel ball are much larger than those of the modified hammer. As seen in Figure 4.5, the standard deviations of the average phase velocity obtained using the wooden spring mechanism are on the same order as that of the modified hammer (see Figure 4.6).

Furthermore, Figures 4.7 through 4.9 show the average centroid frequency measured along the longitudinal axis of a timber pile using the bending wave technique. Examining the values obtained for each device and their corresponding standard deviations, the wood spring mechanism was more precise. The standard deviations of the measured centroid frequency created from impacts made with the wooden spring (see Figure 4.8) are quite low, comparable to those values obtained from impacts made with

the modified hammer (see Figure 4.9). In Figure 4.7, the standard deviations obtained using the steel ball mechanism are shown. The precision of the steel ball mechanism is much lower than that of both the modified hammer and wooden spring devices, which is indicated by the larger standard deviations.

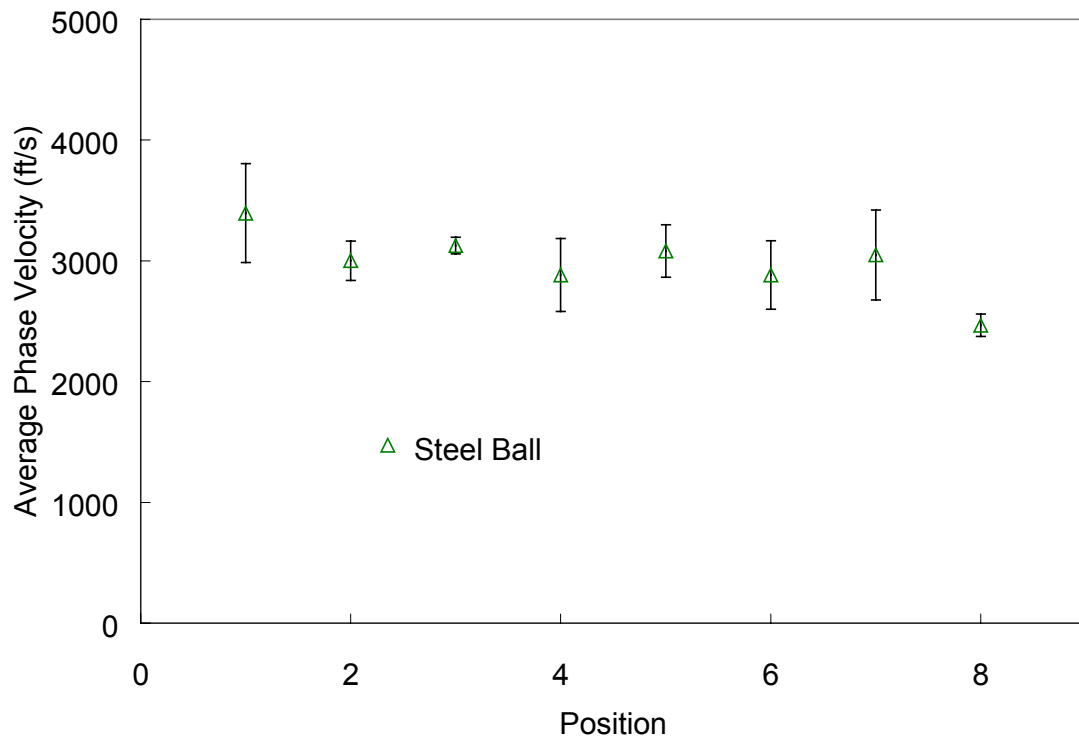


**Figure 4.4** Average phase velocities measured using the bending wave technique for the steel ball mechanism with corresponding one standard deviation bars.

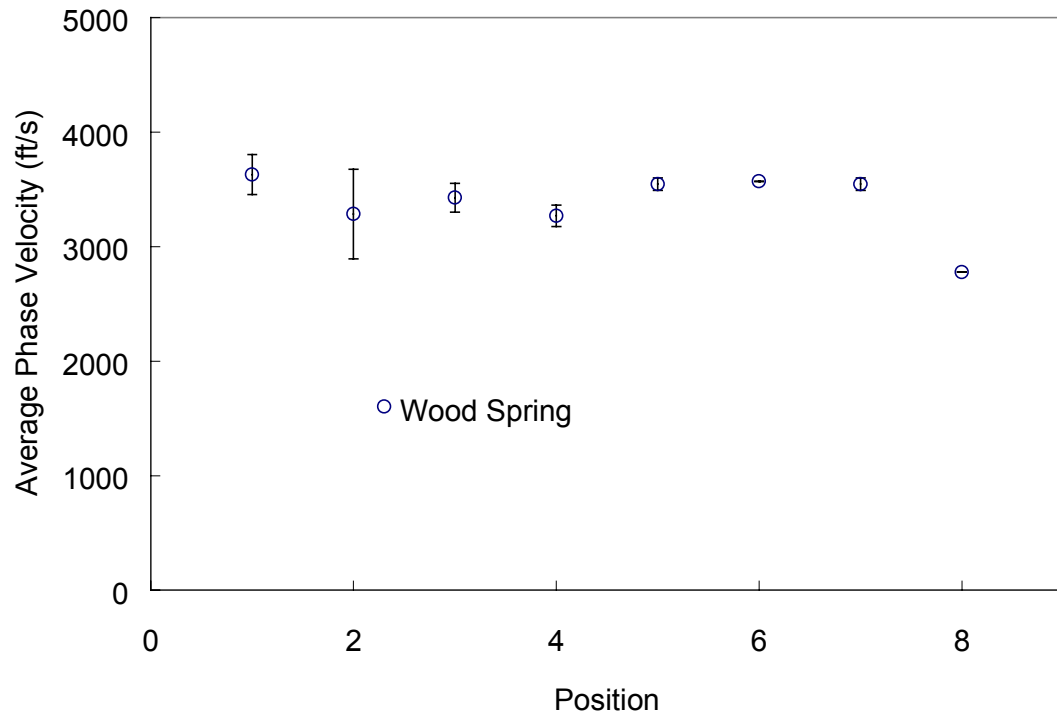


**Figure 4.5** Average phase velocities measured using the bending wave technique for the wood spring mechanism with corresponding one standard deviation bars.

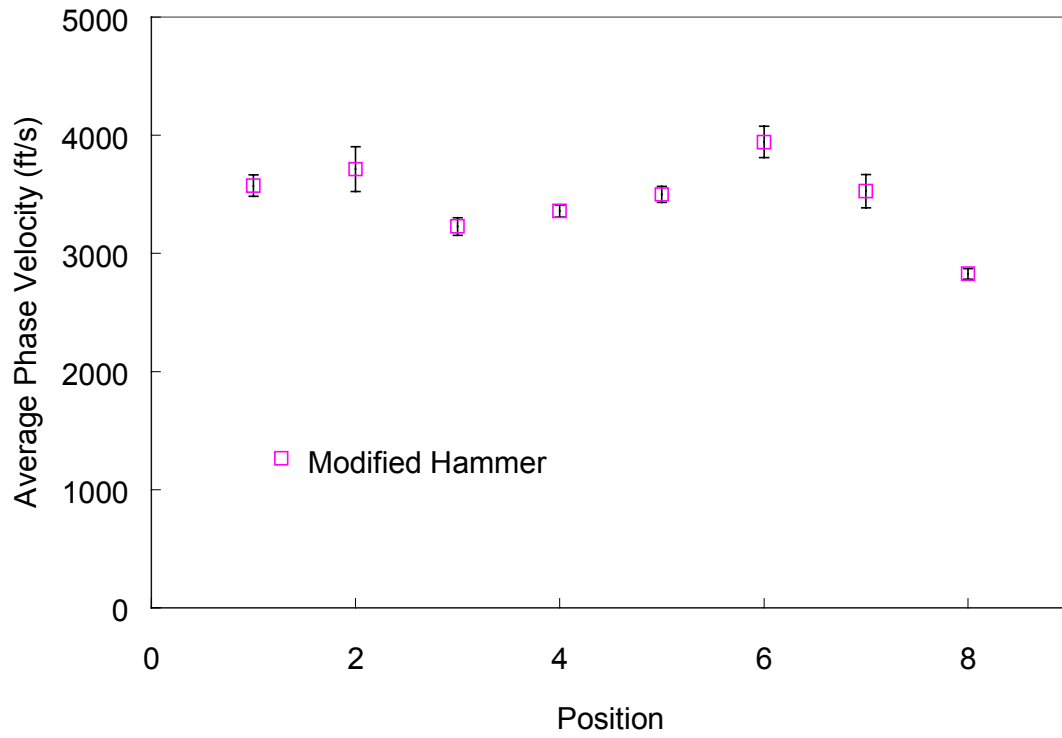


**Figure 4.6** Average phase velocities measured using the bending wave technique for the modified hammer with corresponding one standard deviation bars.

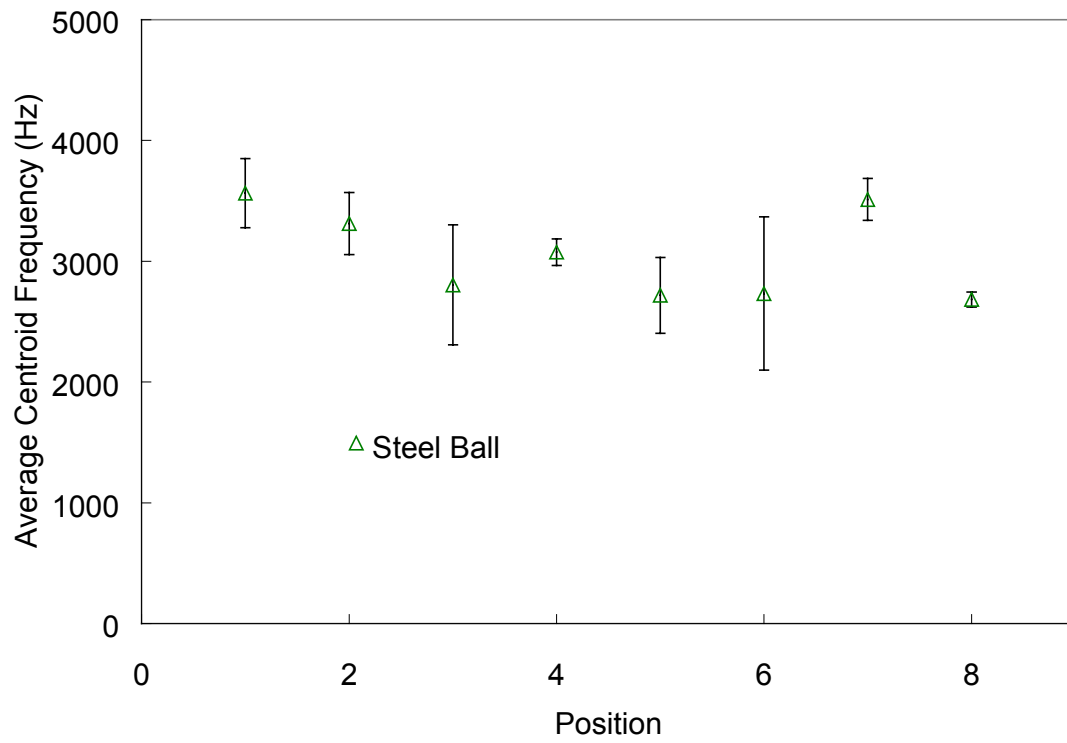


**Figure 4.7** Average centroid frequencies measured using the bending wave technique for the steel ball mechanism with corresponding one standard deviation bars.

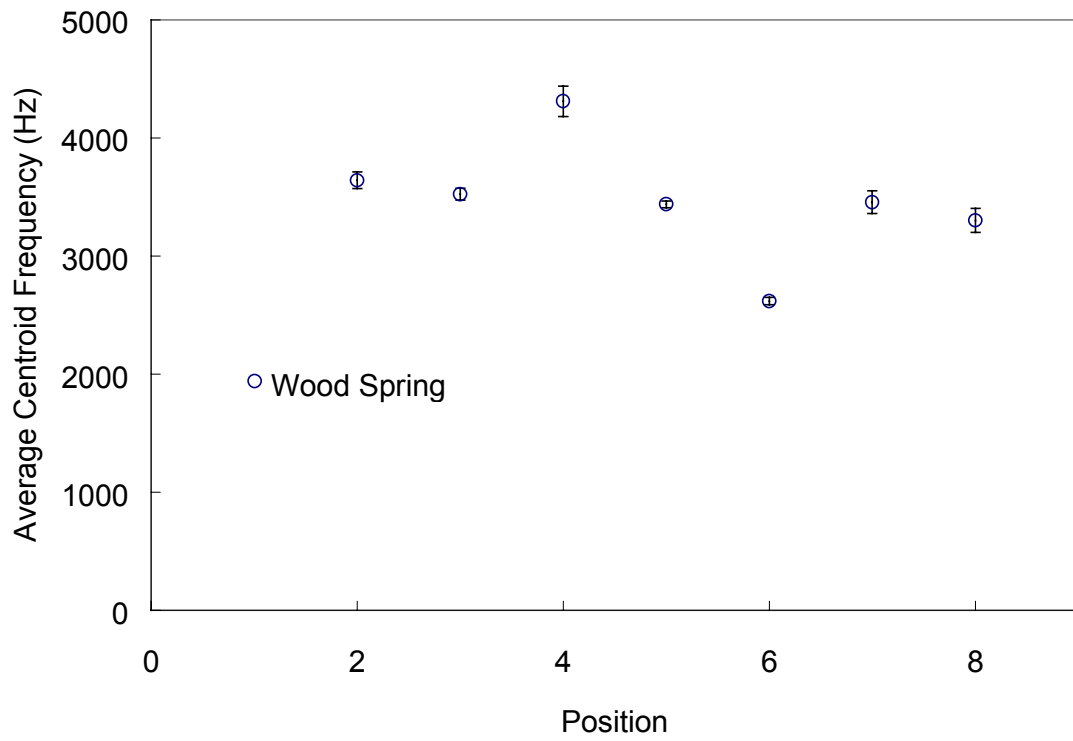


**Figure 4.8** Average centroid frequencies measured using the bending wave technique for the wood spring mechanism with corresponding one standard deviation bars.

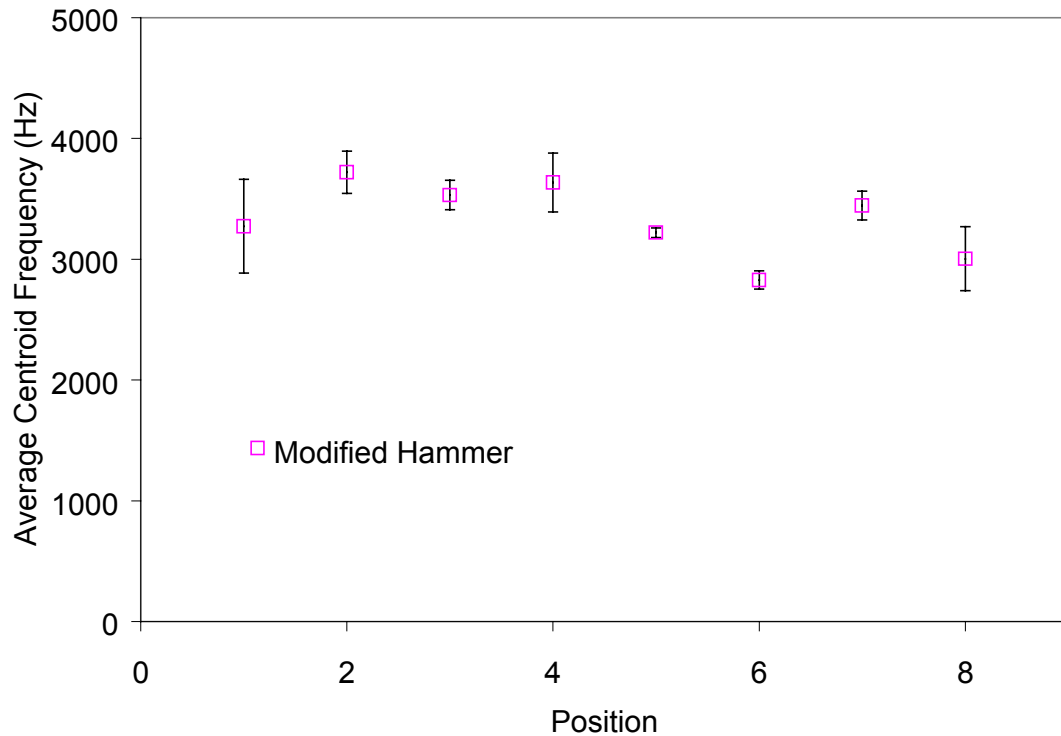


**Figure 4.9** Average centroid frequencies measured using the bending wave technique for the modified hammer with corresponding one standard deviation bars.

#### 4.3.2.2 Operator-to-Operator Variations

The shape and clarity of a waveform are dependent on the medium condition. As a result, a knowledgeable technician is often needed to discern whether variations in the waveform are due to pile condition alone, or possibly due to an improper impact. Because the operators employing the bending wave technique may vary from day to day, i.e., the person determining whether the signals are adequate (by reading the the oscilloscope) may differ, the quality of data is dependent on the discretion of the oscilloscope operator. If variations due to the impact device can be minimized, the

quality of data will rely less on the skill and technical knowledge of the individual using the oscilloscope.

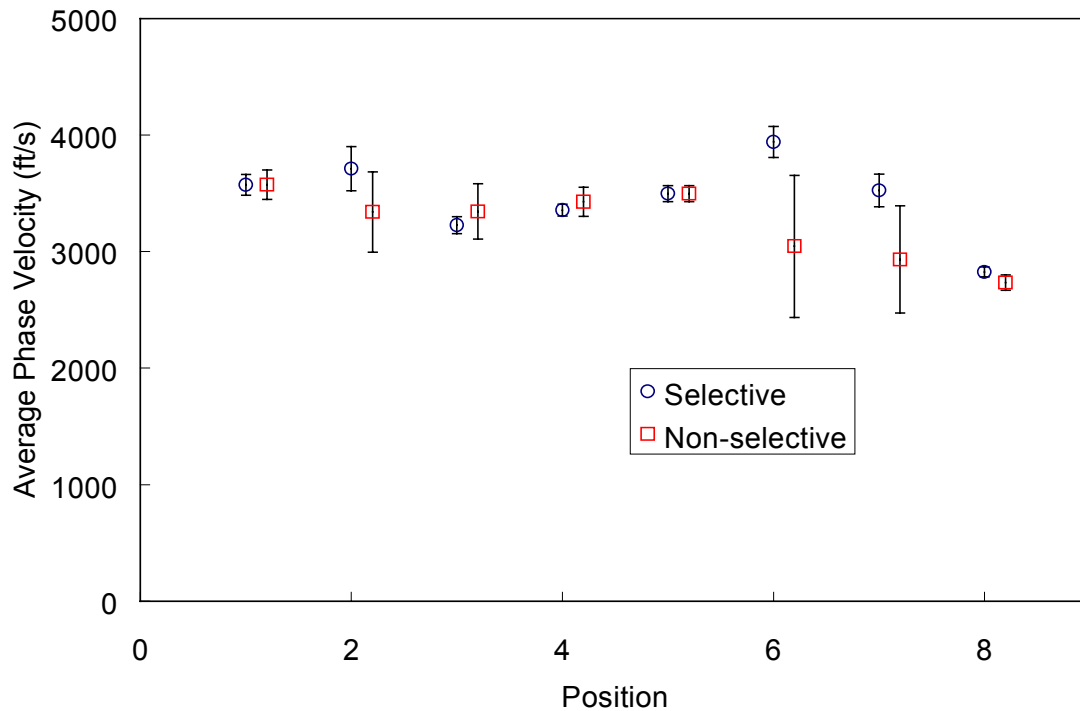


**Figure 4.10** Comparison of phase velocity measured using the modified hammer for selected versus non-selected impacts with corresponding one standard deviation bars.

Two sets of files, each containing five records, were obtained at each position along the pile. In the first portion of experimentation, a skilled operator selected records at each location along the longitudinal axis of the pile (selection was based on signal quality seen on the oscilloscope). The wave properties were measured using the bending wave technique while wave properties were determined using SWAP. Next, five random measurements (non-selective signals) were taken at each location (locations corresponding to the same position as those selected by the skilled operator) and the wave

properties were again measured. The bending wave technique was also utilized to obtain wave properties. Figure 4.10 illustrates the average phase velocities measured using the modified hammer for a data set using both non-selective and selected impacts (skilled operator).

Figure 4.11 is the same plot for the wood spring mechanism. Both plots indicate that repetition is attainable using both the wooden spring device and modified hammer. However, the average standard deviation obtained when an unskilled operator interprets the signal quality (discerned from clarity and shape of the waveform as seen on the oscilloscope) is much greater when using the modified hammer.

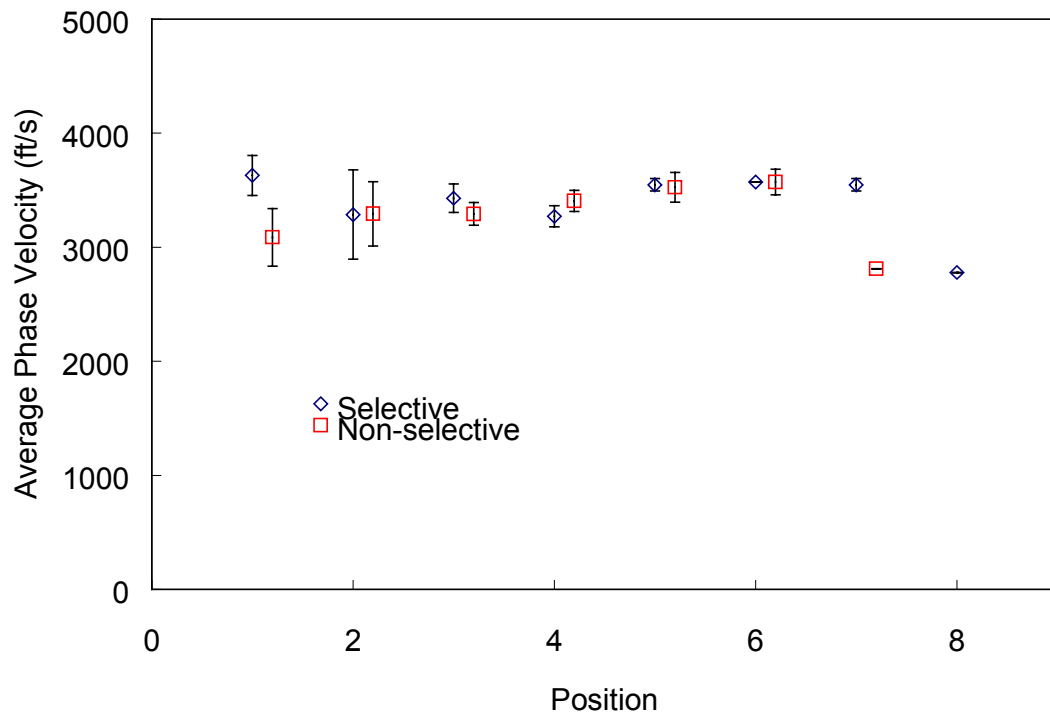


**Figure 4.11** Comparison of phase velocities measured using the wood spring mechanism for selected impact (skilled operator) versus non-selected impacts.

Because the properties measured using the steel ball mechanism did not correlate well with those of the modified hammer, further analysis using the steel ball was not necessary. Table 4.1 indicates the average standard deviation of the data shown in Figures 4.10 and 4.11. The wood spring mechanism reduces the errors occurring from operator-to-operator to a minimum.

**Table 4.1** Average Standard Deviation for the phase velocity measured using the modified hammer and the wood spring mechanism.

Device	Selective Impacts	Non-selective Impacts
Wood spring Mechanism	103	109
Modified Hammer	100	273

## 4.4 Summary

The development of a standard impact device is essential in measuring accurate and repeatable stress wave propagation properties in timber. The wood spring mechanism (WSM-99) reduces operator-to-operator variations as well as impact-to-impact variations while producing waveforms containing frequencies necessary for the prediction of wave propagation properties in timber. Operation and use of the WSM-99 requires minimal training and technical expertise. As a result, the wood spring mechanism was adopted for the remaining portion of experimentation and used to develop specific relationships between stress wave propagation properties and timber.

The WSM-99 is a spring-loaded device that utilizes the most basic principles of physics and dynamics. A wooden mallet is driven by a small coil spring. The impact mallet is made of hickory and resembles the shape of a normal carpenter's hammer handle. Two cylindrical footpads allow the hammer to adhere to various surface irregularities seen in timber pilings. The hammer is manually deployed by the operator to

allow for variation in impact energy as a result of varying pile surface conditions. A picture of the WSM-99 can be seen in Figure 4.12.

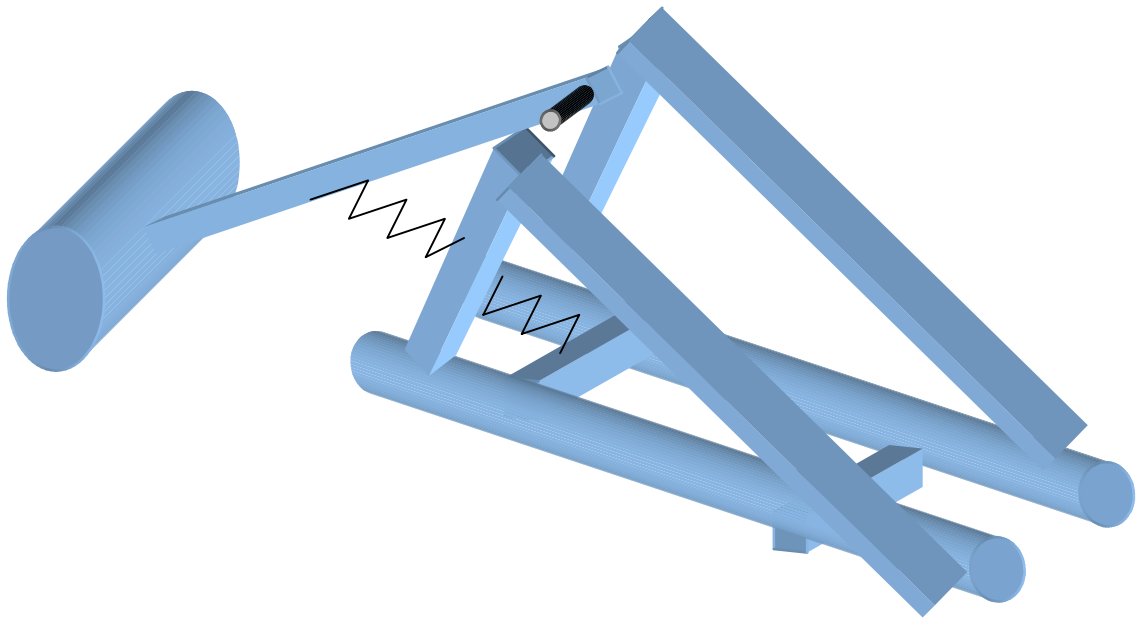


**Figure 4.12** Wood spring mechanism (WSM-1999) used for imparting impact to the pile surface.

## **Chapter 5**

# **Laboratory Investigation of the Influence of Natural Wood Variation on Wave Properties**

### **5.1 Anatomical Variations in Wood**

To ensure precision of the testing procedure, the same one-foot section (which was previously tested) was tested on more than one occasion. Though the same longitudinal position was used, the sensors were not necessarily attached at the same radial location along the circumference. Because wood is a biological material, it is subject to variations in structure resulting from anatomical factors related to growth and environmental factors encountered in service. Because these anomalies affect wave propagation properties, it was necessary to qualify the influence these variations have on wave propagation properties.

### **5.2 Internal Discontinuities**

Anatomical factors are variations in wood structure resulting from natural processes or growth influence. These include slope of grain, knots, growth abnormality, and shake and pitch pockets. Variations in wood structure are also caused by environmental conditions. In bridge construction, wood is exposed to wetting and drying cycles. As moisture content fluctuates, wood shrinkage and swelling occurs, producing internal stresses that lead to crack formation and propagation. These anomalies interrupt the

continuity and direction of the wood fibers. The orientation of these discontinuities in relation to the direction of propagation has a significant effect on wave properties.

### **5.2.1 Experimental Setup**

CCA treated, southern yellow pine intact timber piles were simply supported in the laboratory. The liquid content of the piles was approximately 15%. Wave properties were measured at one-foot intervals along the longitudinal axis of the pile using the bending wave technique. The SWAP was then used to determine specific properties of wave propagation.

### **5.2.2 Analysis in the Frequency Domain**

Evaluating properties of materials in the frequency domain provides a much more sensitive measure of wave propagation properties than those obtained from the time domain (more specifically, phase velocity). When stress waves encounter a boundary or discontinuity in the medium, variations in the frequency components of the waveform will occur. Waves become dispersive which leads to propagation of individual frequency components within the waveform at different speeds.

Previous research (Qian, 1997) had shown a strong correlation between properties obtained from the frequency domain and material properties. Because timber is a non-homogenous material with a vast number of discontinuities due to cracking and growth, it is difficult to support relationships developed from the frequency domain. Properties such as the centroid frequency and dominant frequency are sensitive to small variations in the frequency spectra of the waveform due to discontinuities present in timber piles. Figures 5.1 through 5.4 illustrate the variations in the centroid and dominant frequencies measured for intact pile sections with similar diameters.

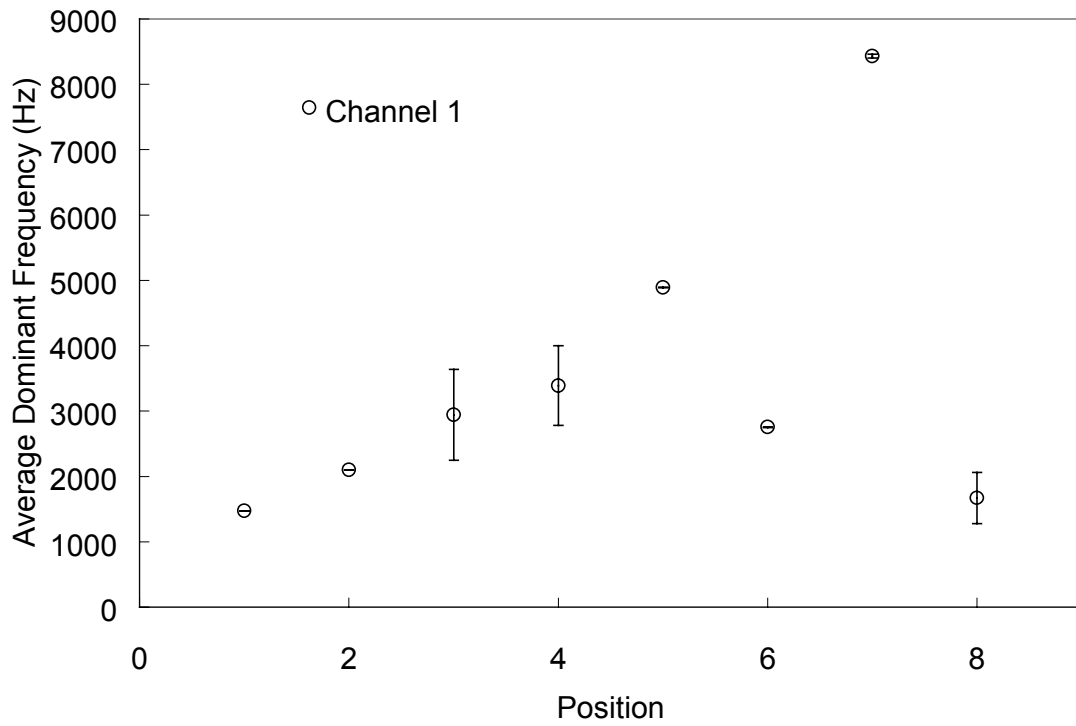


**Figure 5.1** Average dominant frequencies measured from various pile sections of a similar diameter using the bending wave technique with corresponding one standard deviation bars (pile 4).

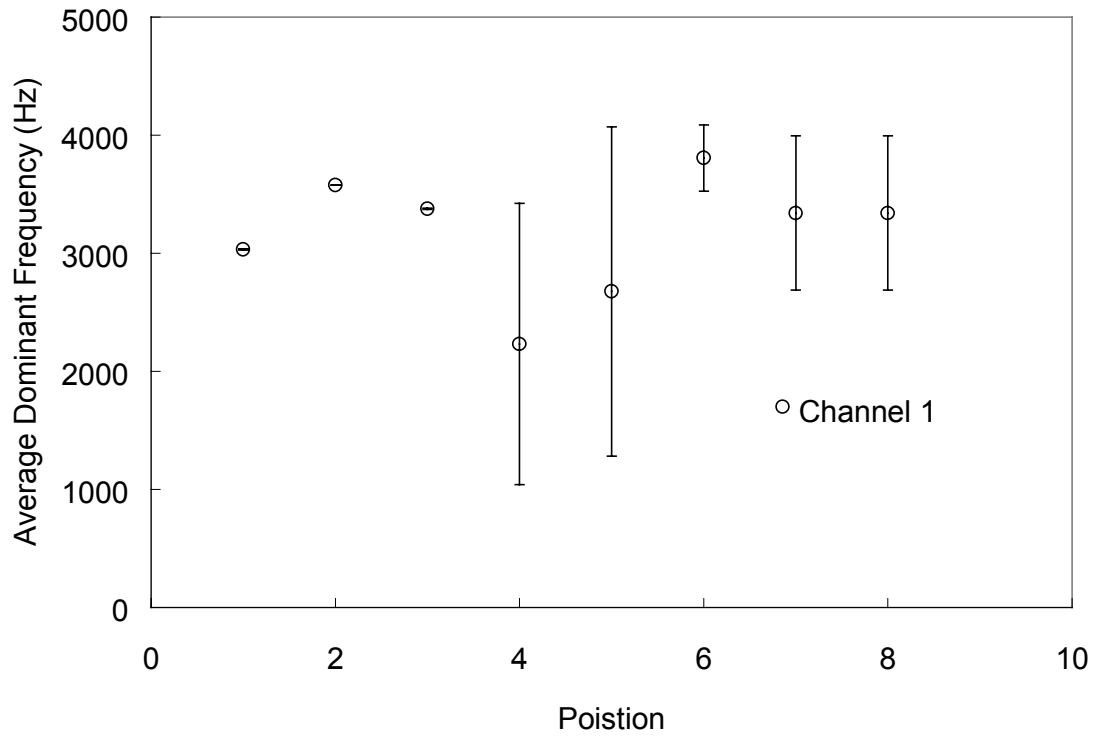


**Figure 5.2** Average dominant frequencies measured from various pile sections of a similar diameter using the bending wave technique with corresponding one standard deviation bars (pile 4c).

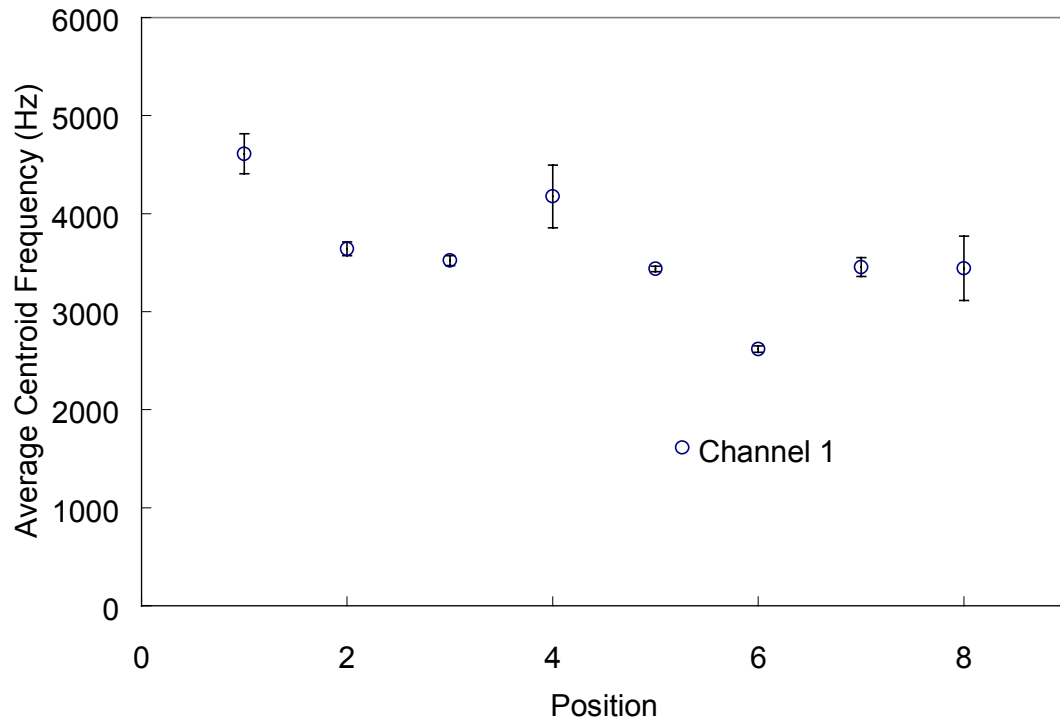


**Figure 5.3** Average centroid frequencies measured from various pile sections of a similar diameter using the bending wave technique with corresponding one standard deviation bars (pile 3).

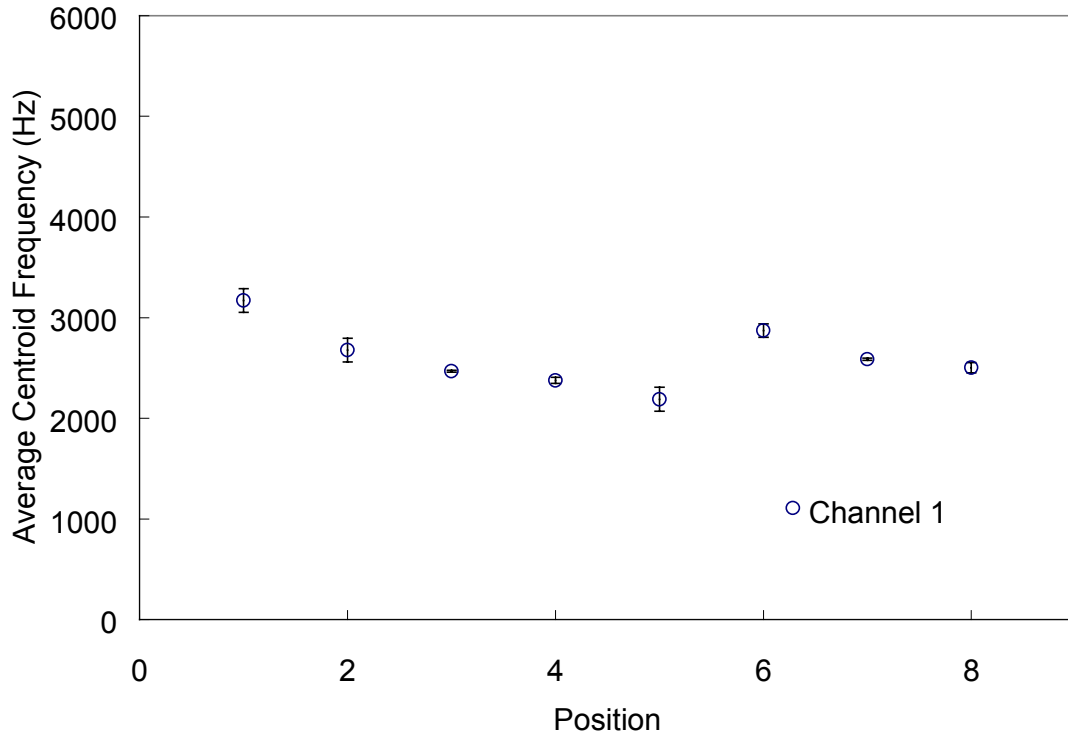


**Figure 5.4** Average centroid frequencies measured from various pile sections of a similar diameter using the bending wave technique with corresponding one standard deviation bars (pile 4c).

### 5.2.3 Analysis in the Time Domain

Wave propagation properties determined from the time domain are less dependent on the structural variations inherent in timber piles. Velocity measurements (obtained from the time domain) provide the necessary sensitivity to detect internal damage due to deterioration, while not being considerably influenced by the internal structural variations of wood. Figures 5.5 and 5.6 illustrate the phase velocity measured using the bending wave technique for pile sections of similar diameter. As propagation occurs in different directions relative to the inclusions and discontinuities in the wood, propagation speed

and direction will tend to vary. Though there is a slight variation in phase velocity at different locations along the length of the pile, the measured phase velocities of intact sections of the piling are fairly consistent.

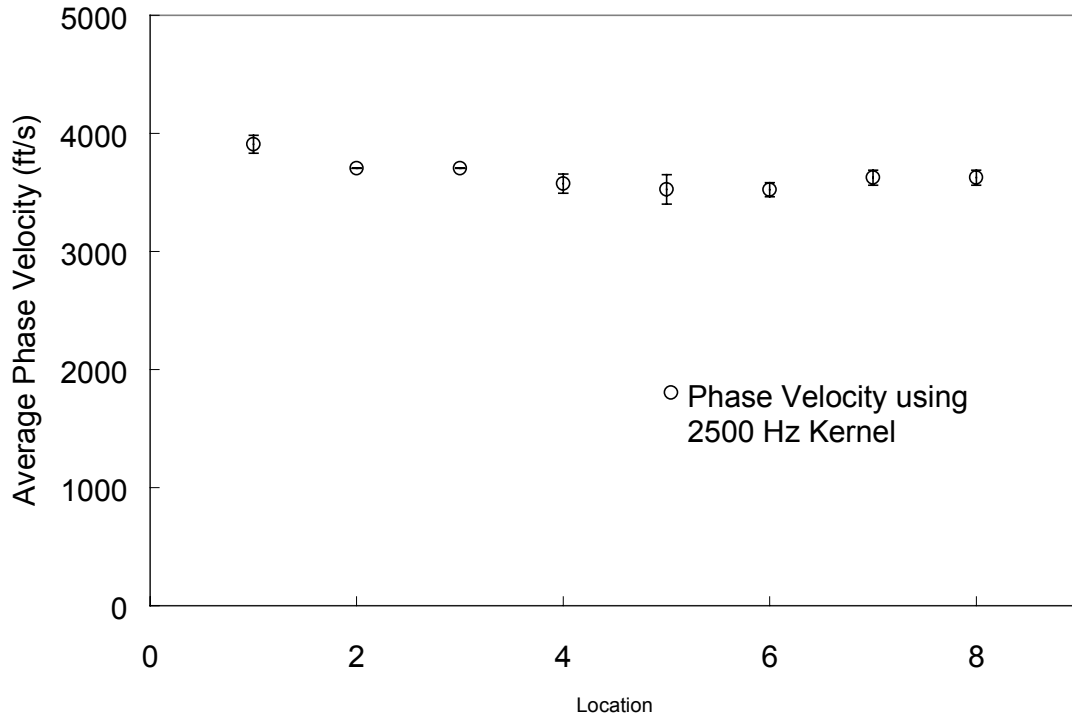


**Figure 5.5** Average phase velocities measured from various pile sections of a similar diameter using the bending wave technique with corresponding one standard deviation bars (pile 3c).

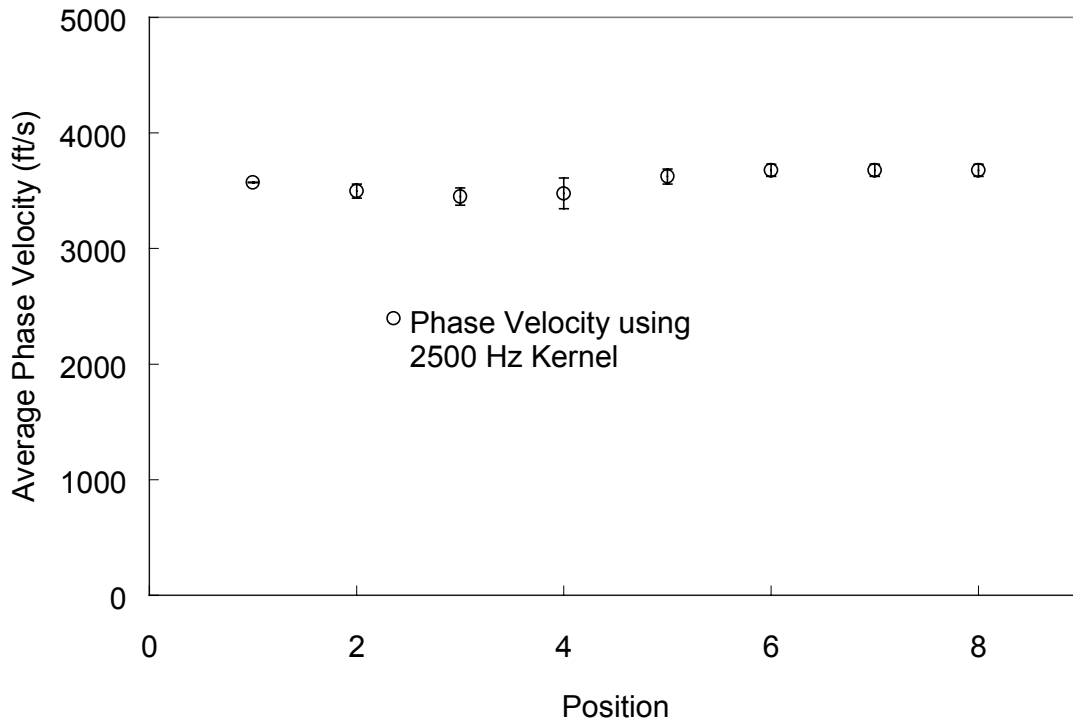


**Figure 5.6** Average phase velocities measured from various pile sections of a similar diameter using the bending wave technique with corresponding one standard deviation bars (pile 4).

### 5.3 Surface Variations

When performing the bending wave test, it is not always possible to obtain a good contact surface between the impact device and pile. If piles have been treated with creosote tar, the pile most often lacks a smooth surface necessary to ensure appropriate energy transfer from the impact device to the pile. Also in many cases, because wood is subject to wetting and drying cycles, flaking and cracking occur along the pile surface due to expansion and shrinkage. As a result, the properties associated with the frequency domain will vary correspondingly. Because of the lack of repeatability in measuring the properties associated with the frequency domain, and the variability in values associated

with intact pile sections from previous testing, investigation leading to development of relationships associated with properties in the frequency domain were not evaluated. Waveforms and corresponding properties were analyzed in the time domain.

### 5.3.1 Experimental Setup

A CCA treated southern yellow pine timber pile was used to determine the effect surface variations have on wave properties. The liquid content of the piles being tested was approximately 15%. Piles were simply supported in the laboratory. Sensors were placed at one-foot intervals along the longitudinal axis of the pile. The wave propagation properties were measured using the bending wave technique. Each position was tested at three locations along the circumference of the pile, at an interval of approximately 120°. A diagram of a pile cross-section with corresponding testing position can be seen in Figure 5.7. The wave properties were measured using the bending wave technique.

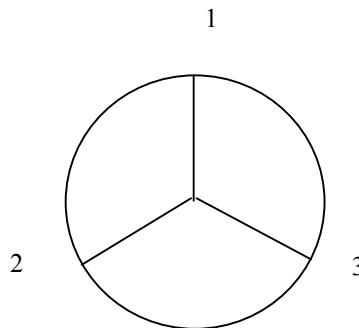


**Figure 5.7** Profile of the pile cross-section showing measurement points along the pile circumference at each test location.

### 5.3.2 Analysis in the Time Domain

The results shown in Figure 5.8 indicate that surface variations along the axis of the pile can cause differences in measured wave properties. The measured phase velocity, determined using the WSM-99 (using the bending wave technique), varied at each location, depending on the radial position of the measurement.

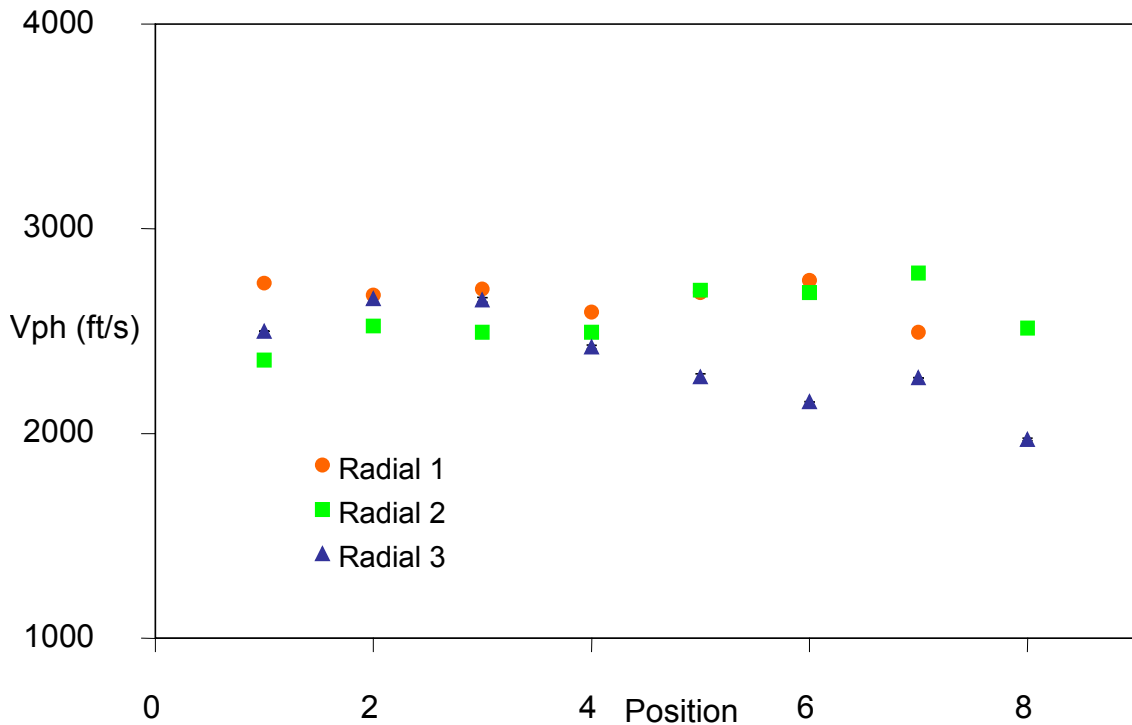


**Figure 5.8** Repeatability study to determine the effect of structural variations on wave properties using the bending wave technique.

## 5.4 Effect of Diameter Variation on Phase Velocity

As the diameter of the cross-section varies, the measured phase velocity will vary correspondingly. To develop an accurate relationship between the phase velocity and

diameter, however, one must be able to isolate that specific parameter. When testing pilings, the liquid content along the longitudinal axis of the pile varies as does the internal structural alignment of various discontinuities inherent in the timber. These anomalies and variations disturb the propagation of stress waves, influencing the phase velocity. As a result, it is difficult to obtain a relationship solely for phase velocity as a function of diameter. Because variations in a pile's diameter are small for each individual pile, its effect on the phase velocity is negligible when considering the effect of other physical properties of the medium on wave propagation.

#### **5.4.1 Experimental Setup**

Intact southern yellow pine timber piles (CCA treated) were tested using the bending wave technique. Piles were simply supported in the laboratory. Wave speeds were measured at one foot intervals along the length of the pile. The liquid content of the pile sections was maintained between 15% and 20%, though varying slightly from position to position. The circumference of pile sections varied from approximately 2.75 to 3.25 ft.

#### **5.4.2 Effect of Diameter Variation on Phase Velocity**

Figure 5.9 shows the phase velocity variation as the diameter changes for three different piles. Differences in the measured phase velocity occur due to internal structural variations and liquid content (LC) variations along the pile length. As a result, a single trend can not be isolated. In Figure 5.9, the LC varied along the length considerably for pile 3. The resulting trend shown is a function of LC, not pile diameter. Previous research (Chen, 1995) shows that the phase velocity decreases correspondingly as diameter decreases. Further investigation needs to be completed before a conclusive relationship can be developed.

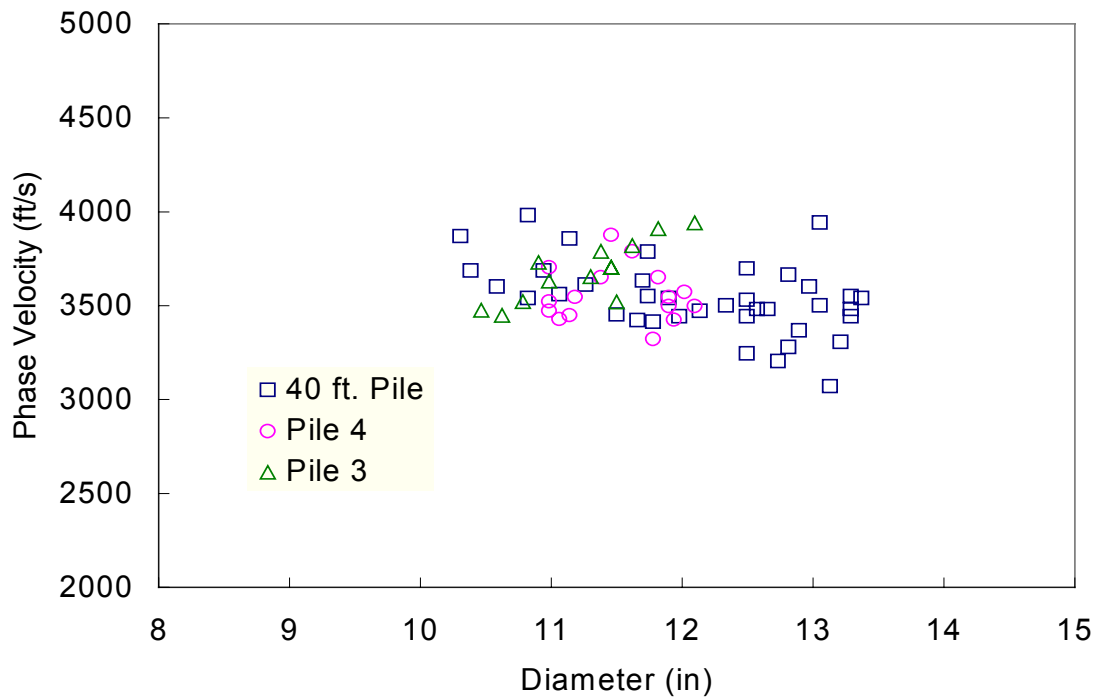


**Figure 5.9** Phase velocity as diameter varies for 3 different piles.

## 5.5 Summary

Structural discontinuities in timber influence wave propagation properties. Properties obtained from the frequency domain are very sensitive to anomalies present in the internal structure of wood. As a result, prediction of wave properties using the frequency domain is unreliable. Properties of wave propagation obtained from the time domain are less sensitive than those obtained from the frequency domain. As a result, the phase velocity measured using the bending wave technique can be obtained consistently. While variations in phase velocity occur due to structural irregularities, they can be reduced with increased sampling of locations. Measurement of phase velocities at a minimum three radial locations along the circumference at each position should be considered to

reduce random errors. The average phase velocity can then be computed providing a more accurate representation of sectional structural integrity. The number of circumferential locations will be considered in more detail using field data in Chapter 8. The diameter affects the wave propagation speed. Further investigation needs to be performed to quantify this phenomenon.

## Chapter 6

### Determination of the Moisture Content

#### 6.1 Moisture Content of Wood

The moisture content of wood (MC) is defined as the weight of water in wood given as a percentage of oven-dry weight:

$$MC = \frac{\text{Moist weight} - \text{Ovendry weight}}{\text{Ovendry weight}} \quad (6.1)$$

The moisture content of living wood ranges from approximately 30 percent to more than 250 percent, varying from species to species. Because wood is a hygroscopic material, moisture content will vary as humidity fluctuates. The moisture content depends on the environmental conditions, relative humidity and temperature of the surrounding air. In conditions such as those experienced in bridge applications, wood moisture content is almost always undergoing gradual changes as the temperature and humidity conditions vary. Eventually the wood moisture content will reach an equilibrium moisture condition relative to the surrounding environment. This is the value obtained from the timber pilings gathered from the field conditions.

##### 6.1.1 Determination of Moisture Content

Determination of the moisture content of wood is an important consideration associated with the bending wave technique. Variations in moisture content affect the

transmission of elastic waves in solids and their properties. More specifically, the addition of moisture to wood increases the internal friction between particles. Because elastic wave propagation is a function of such properties (of the medium), it is of particular interest to accurately determine the moisture content of timber piles and qualify the effect of the moisture content on elastic wave propagation.

#### **6.1.1.1 Conventional Oven-drying**

Conventional oven-drying is the standard method for determining the moisture content and is designed to provide the most precise values consistent with the needs of the user. A forced-convection oven maintained at  $103 \pm 2^{\circ}\text{C}$  is used to dry the specimen. The oven is ventilated to allow for the evaporating moisture to escape. Sample size and material type are independent of the testing procedure. Drying is terminated once the mass in a three hour interval is equal to or less than twice the selected balance sensitivity. Balance sensitivity is prescribed by the user and is dependent on the precision necessary in determining the moisture content. Once the specimen has dried, the samples are stored in a dessicator until they reached room temperature to ensure that no additional moisture from the air is absorbed. For a further description of the process, see ASTM D4442-84. The moisture content is then calculated from Equation 6.1.

This process is very precise for research purposes, but in many instances requires significant time to obtain reportable results. Sample drying times are on the order of hours. Because the results herein are the basis for establishing a field testing procedure, it is essential that a method for determining the moisture content be developed which is conducive to on-site testing of specimens. The moisture content of timber at the precise time of testing is important for determining accurate relationships between wave propagation properties and the moisture content. Various alternatives were investigated that would reduce the man-hours necessary to perform this operation and provide a procedure which would have better application for field testing of specimens.

### 6.1.1.2 Moisture Content Determination Using a Centrifuge

An alternative method was used to determine the moisture content using a centrifuge. Wood core samples were obtained from various field piles (obtained from actual in-situ pilings) using a standard one foot wood coring device. The weight of each sample was then recorded (1-5 grams). Samples were then placed in a centrifuge vial that was separated into two chambers by a 21 mm glass microfibre filter. In theory, the sample placed in the top chamber would be isolated from the moisture which would be allowed to pass through the filter. The samples were placed in the centrifuge and spun approximately 3500 rpms for 20 minutes. This was the maximum speed of the centrifuge available at the NCSU Department of Civil Engineering. After the cycle had been completed, samples were removed and the weight of each was again recorded.

It was found that only a minute portion of the liquid in the sample was removed. As stated previously, the moisture content of wood is greatly affected by the humidity conditions in the air. Because these samples were enclosed in a centrifuge vial, the high moisture present in the vial was reabsorbed by the specimen. Also, the cycle speed was not high enough to remove the trapped water present in the cells (that portion below the fiber saturation point). The results of representative core samples are shown in Table 6.1.

**Table 6.1** MC determination using the centrifuge and by oven-drying.

Pile	MC by Centrifuge	MC by Oven-drying
G	4.4%	26%
V	0.0%	28%

### 6.1.1.3 The Halogen Moisture Analyzer (HMA)

A sample was obtained using a standard one foot wood-coring device. The sample weight was then recorded (1-5 grams). The sample was then placed in a device known as the Halogen Moisture Analyzer (HMA), which was obtained for use from Metlar-Toledo,

Inc. This instrument operates on the thermogravimetric principle. A halogen radiator dries the test sample under investigation while the precision balance integrated into the instrument continuously measures the sample weight. Once the weight has stabilized; i.e., the weight is no longer decreasing with time, the moisture content can be determined. The moisture content is based on weight loss of the sample during the drying period. Drying temperature can be varied depending on the liquid content of the samples. Determination of the correct drying temperature will be discussed in Section 6.5.

The major advantage of this method is the shorter measurement time compared to the traditional oven-drying method as defined by the ASTM Manual. The drying time is on the order of minutes using the HMA, while oven-drying takes on the order of hours. The reduced man-hours necessary to complete moisture content determination using this method is more applicable for use in determining the moisture content in field conditions where time is of the essence. The HMA is also a portable device which is powered by a standard 110 mV power source. The results show that those values obtained from the HMA correspond well with the oven-drying results as shown in Table 6.2.

**Table 6.2** Moisture content using HMA and oven-drying methods.

Pile	MC by HMA	MC by Oven-drying
G	24%	26%
V	24%	28%

The samples' MC values obtained are lower using the HMA. This is due to the drying termination setting in the HMA. The drying process was automatically terminated once the weight change percentage was less than a prescribed value within a certain time interval. This setting can be adjusted depending on material properties. In instances when moisture in the specimen is trapped within the material itself (i.e., wood cells), the

drying time can be increased to account for this phenomena. Upon increased drying of the samples, an additional 1 to 2% moisture was removed. Including this additional percent, these results correlate well with the moisture content values obtained using the conventional oven-drying method.

This method was used during the remaining portion of experimentation due to reduction of sample processing time and accuracy. Drying temperatures will be varied depending on the desired results. Drying times will vary depending on the amount of trapped moisture in each specimen.

## **6.2 Effect of Treatment on Moisture Content Determination**

During the timber treatment process, additional liquids are added (creosote or Chromated Copper Arsenate (CCA)) which increase the moisture content and density. This is of particular importance because previous research (Qian, 1997) reported that an increase in water content will decrease the wave propagation speed. This relationship is specifically based on water, and not liquid addition. The primary goal of this research task was to determine if the relationship between wave propagation properties and MC may be developed from any liquid (independent of the nature and form), or as a function of the liquid composition (i.e., chemicals) as well as density.

### **6.2.1 Moisture Content as a Function of Liquid Composition**

To separate the MC from the LC values (those values representing water and volatile components), advanced measurement techniques such as the distillation method described in ASTM D4442-84 are necessary. Not only is this method time consuming, but also requires advanced knowledge of laboratory testing equipment and procedures which is not conducive to the development of a field testing procedure. Therefore, it was

of particular interest to develop a relationship based on liquid addition, independent of type (chemical composition) and density using the Halogen Moisture Analyzer.

### 6.2.1.1 Determination of Volatile Component Removal Using the HMA

Before determining whether liquid type is of significance, it had to be determined that moisture content obtained from the Halogen Moisture Analyzer is a function of all liquid present in the pile (treatment and water). During previous experimentation, an implementable procedure to determine the liquid content using the HMA was developed as outlined in Section 6.1.1.3.

Using the specified temperature for drying wood samples in ASTM D4442-84, the MC was determined for a southern yellow pine 4 in. x 4 in. treated timber post at a drying temperature of 103° C using the HMA. To ensure all moisture was being removed, the samples were again tested at higher temperatures, ranging from 110-150° C. Various components of the treatment will volatilize due to the heating process. The moisture content rose correspondingly as the drying temperature was increased. Results of the drying process using the HMA can be seen in Table 6.3.

**Table 6.3** Liquid Content at various drying temperatures for treated wood core samples.

Sample	CCA		Creosote	
	LC @ 103°C	LC @ 150°C	LC @ 103°C	LC @ 150°C
1	12.0%	12.8%	16.2%	17.3%
2	11.3%	12.3%	19.5%	20.4%
3	12.7%	13.6%	21.0%	21.8%
4	13.7%	14.9%	21.3%	22.5%

At temperatures greater than 103° C, the HMA not only removes the moisture from the sample, but also a percentage of the volatile liquids present in the sample whose boiling point is below 150° C. Volatile matter is emitted as vapor when the treated sample is heated. Because at temperatures greater than 150° C scorching was noticed on the specimens (i.e., the surface of the wood samples began to burn), the drying temperature was not increased further. The noticeable secretion of odor of creosote during the drying process confirmed this hypothesis; that volatile liquids were escaping from the specimen. In conclusion, the measurements obtained from the HMA are based on “liquid content” (LC) which represents the true MC plus any additional volatile liquid (creosote) removal attributed to the heating process.

### 6.2.2 Wave Propagation Properties as a Function of Liquid Content

The LC’s of two 10 ft. x 4 in. x 4 in. southern yellow pine untreated timber specimens were measured. An initial fingerprint of the wave propagation properties was obtained at various locations along the length of the specimen using the bending wave technique. Using this information, specific wave properties were determined by means of SWAP. One specimen was then treated with CCA and the other with creosote by a local wood treatment company. Upon completion of the treatment process, each sample was returned to the laboratory and wave properties and LC were again measured. The liquid content values are shown in Table 6.4 for each specimen before and after the treatment process.

**Table 6.4** Liquid content results of southern yellow pine specimen before and after treatment.

Sample	Ave. Air-Dry LC	Post-treatment LC
1-CCA	15%	22.6%
2-Creosote	15%	31.7%

Because the LC increases due to the treatment process, the wave speed will decrease correspondingly. This phenomena is shown in Table 6.5. After the treatment, the phase velocities measured from each specimen decreased on the order of 100 to 150 ft/s. Therefore, it was of particular importance to determine if the treatment (i.e., chemicals) itself causes a variation in the wave properties, or if the decrease in wave speed is due only to the increased LC (MC plus any volatile liquid addition).

**Table 6.5** Stress wave velocity measured along the length of specimens in Table 6.4.

Specimen/Position	Before Treatment	w/ CCA	w/ Creosote
1.1	2940 ft/s	2825 ft/s	
1.2	2835	2675	
1.3	2850	2690	
2.1	2850		2700 ft/s
2.2	2850		2645
2.3	2815		2765

Two untreated specimens were saturated to LC values that reflect those of the treated specimen. After saturation was achieved, wave propagation speeds were measured using the bending wave technique as the moisture content decreased. A trend was developed over the range of corresponding liquid contents obtained from the treated timber posts. The decrease in phase velocity of the untreated specimens (due to purely moisture increase as a function of water) was then compared to the specimens which had been treated. This data, using both the modified and wood spring impact devices, is shown in Figure 6.1.

Comparing the phase velocity of treated specimens to those that were untreated, the measured phase velocities for treated specimens are lower at corresponding LC. Initial

results also indicate CCA treatment has a larger effect on the measured phase velocity (i.e., a larger decrease in the phase velocity).

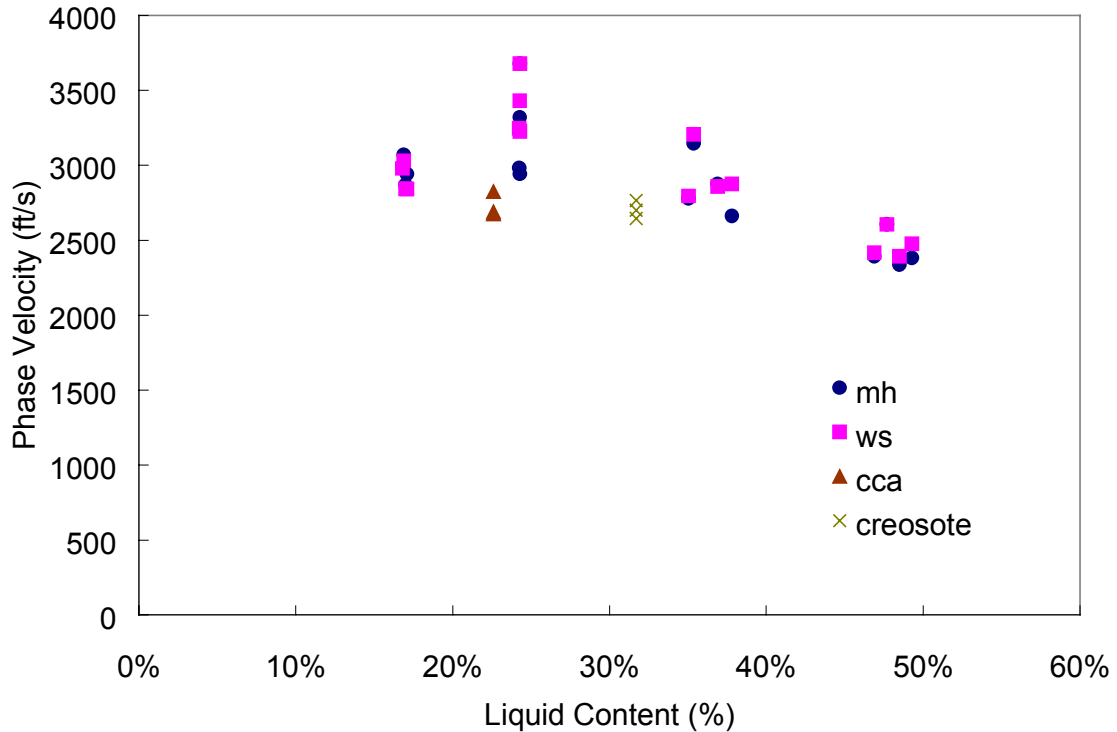


**Figure 6.1** Comparison of phase velocity for specimens with varying liquid composition.

### 6.3 Development of a Relationship between Liquid Content and Wave Speed

Research by Qian (1997) and Ross et al. (1991) has shown a strong correlation between wave propagation speeds and the liquid content (LC) of timber. As the LC increases the wave velocity tends to decrease proportionally. A major portion of the laboratory experimentation was devoted to determining the effect of LC on wave properties, specifically the phase velocity.

### 6.3.1 Experimental Setup.

Initial wave properties were measured for two CCA treated 10 foot piles which were then submerged in a creek in Wake County for approximately 8 to 10 months. Upon removal from the creek, the wave properties were again measured using the bending wave technique. Piles were simply supported in the laboratory. The LC values were obtained at a maximum of 46% upon first removal from the creek. Piles were returned to the laboratory, allowing them to dry, and monitored during the proceeding months. At specific LC levels, the wave propagation speeds were measured using the bending wave technique.

### 6.3.2 Phase Velocity as a Function of Liquid Content

Because of the difficulty associated with obtaining the LC over a wide range of values in the laboratory, the LC of several field piles (treated with creosote) were obtained and corresponding phase velocities determined (Donato, 1999). Figure 6.2 shows the phase velocity measured for various creosote and CCA treated pile sections as a function of LC. The CCA treated specimens tend to show a lower phase velocity than the creosote treated specimens at the same LC. Therefore, two trends were developed, one for CCA piles and the other for creosote treated specimens.

The phase velocity as a function of liquid content is given by the following relationships:

$$V_{ph} = 6002(LC)^{-0.209} \quad (\text{CCA})$$

and

$$V_{ph} = 5804(LC)^{-0.165} \quad (\text{Creosote}) \quad (6.2)$$

where,

$V_{ph}$  = phase velocity (ft/s) and

LC = liquid content (%).

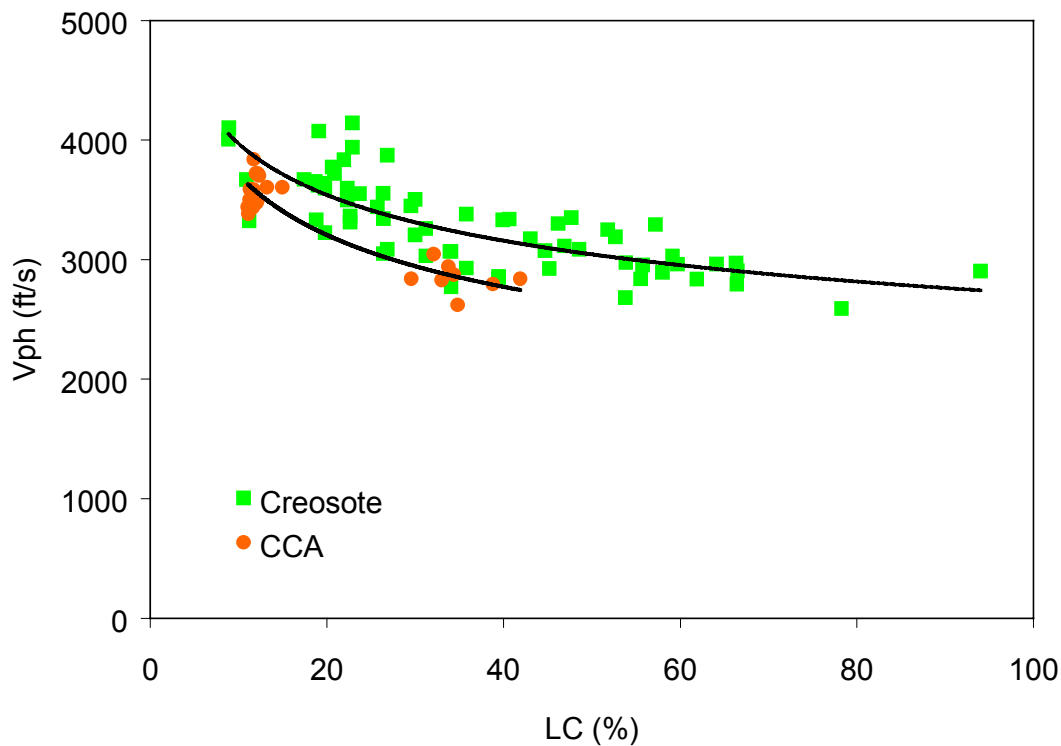


**Figure 6.2** Phase velocity as a function of liquid content for various laboratory and field specimens.

## 6.4 Summary

As the liquid content of timber increases, the phase velocity of waves propagating through the medium decreases. The measured phase velocity at a specific LC varies depending on the treatment type. Relationships are shown between the LC and the measured phase velocity for piles treated with creosote and CCA. Further investigation is necessary to determine the effect treatment has on wave properties. These preliminary

findings serve as a basis for a relationship between LC and phase velocity that can be utilized in a field testing procedure.

## **Chapter 7**

# **Laboratory Evaluation of Internal Defects**

### **7.1 Damage and Decay in Timber**

In many structural systems, timber is subject to a wide variety of environmental conditions that affect its mechanical properties. One of the most commonly used applications of timber piles is as sub-structures in bridge construction. In such instances, deterioration by various biological mechanisms is enhanced due to the abundant moisture and environmental conditions which lead to the progression of decay. Decay is the most common condition contributing to a loss of structural integrity in timber pilings.

A reduction in strength characteristics affects the overall load bearing capacity of installed timber pilings. Therefore, it is essential that one have evaluation techniques to quantitatively identify and assess these conditions as they occur in timber pilings. One such method currently being investigated is to use the bending stress wave propagation technique. Such effort would require the determination of explicit relationships between stress wave properties and the structural condition of timber pilings and the development of testing and analysis systems based on these relationships. Because of the difficulty of obtaining field specimens with precise amounts of damage (due to the complexity of the geometry of the damage within the cross-section), damage was simulated in the laboratory. In this manner, specific remaining sound areas could be correlated to specific stress wave parameters from which a relationship could be developed.

## **7.2 Decay Mechanisms in Wood**

Because wood piles are subjected to a wide variety of environment conditions, they are often susceptible to deterioration. Biological mechanisms are the most common agents of decay while wood-boring insects contribute significantly to deterioration in marine environments. Wood decay results in a loss of strength which could prove catastrophic when timber is used as sub-structures in bridge construction. It is essential that these damage mechanisms are recognizable to ensure that any loss in structural integrity of timber can be identified.

### **7.2.1 Fungal Decay**

Fungi are chemo-organotrophic organisms meaning that they derive both their energy and carbon requirement from organic materials. The two most important factors affecting fungal growth in natural habitats are the presence of a food source (carbon) and moisture. Fungal decay in wood results from the fungi requirements for organic compounds found in the wood itself and the surrounding soil structure (in the case of timber piles).

Decay type and severity vary considerably due to a vast difference in environmental conditions. Because wood is a hygroscopic material, it is affected by changes in the relative humidity or water potential of the surrounding environment (Eaton et al., 1993). The presence of water in wood is an essential requirement for fungal colonization and decay to occur. Wood which is kept dry is safe from decay, but as soon as a moisture content of 20% or more is attained, it becomes susceptible to attack by fungi (Eaton, et al. 1993). Temperature variations also contribute to the growth of fungal decay while certain fungi are also known to respond to light because of their phototropic behavior.

### **7.2.1.1 Brown Rot**

One of the most common forms of fungal decay is known as brown rot (red rot). Brown-rot decay is characterized by the wood's reddish brown to dark brown appearance and softened texture to some depth when wet. At late stages of decay and when dry, the wood commonly shows deep-cross-cracking due to shrinkage caused by loss of wood cell wall carbohydrates (carbon source) and shows longitudinal cracking (Eaton et al., 1993). The depth and size of cracking varies as fungal and wood species vary accordingly. Brown rot most often occurs as an internal form of decay while external surfaces appear sound due to surface drying of the timber. Under higher humidity the outer surfaces often show signs of decay.

### **7.2.1.2 White Rot**

In the early stages, white rotted wood may show darkened and brown tinges and streaking. In the more advanced stages, white rot decay is characterized by its lightened bleached appearance. The cuboidal cracking associated with brown rot does not occur but the surface does become softened while shrinkage occurs only in the late stages of decay (Eaton et al., 1993). In most cases, the white-rotted wood becomes rather fibrous along the grain and tends to attack hardwoods rather than softwoods.

### **7.2.1.3 Soft Rot**

Soft rot wood can be identified by the soft and considerably darkened surface while beneath the surface the wood is sound. When dried, the rotted surface shows fine shallow longitudinal and cross-cracking. Decay normally begins at the surface and propagates in the cross-section as the surfaces are eroded by environmental conditions. (e.g., fast moving water). In some cases, the wood will appear to be moderately sound but when broken it produces "carrot" short fractures (Eaton et al., 1993). Soft rot is a

major cause of decay in treated wood products exposed in all but anaerobic environments where moisture is present.

### **7.2.2 Bacterial Decay**

Bacterial decay occurs in wood that is exposed to wet and moist environments. Though it has been identified as a decay mechanism, their role as agents of decay is not as prominent as those of the fungi. Decay occurs due to the capability of the bacteria to break down the wood's cell walls. Three different types of decay micromorphology attributed to bacterial attack have been described: tunneling, cavitation and erosion decay (Eaton et al., 1993). Decay by bacterial attack is characterized by a softened surface in affected areas of the wood and loss of fiber strength. Surface layers have a spongy texture while decay in most cases progresses inward from the outer regions.

### **7.2.3 Marine Borer Attack of Wood**

Because timber piles are one of the most commonly used sub-structures in bridge construction, in many cases they are subject to attack by marine boring animals. There are two main groups of marine boring animals, the molluscs and the crustaceans. These agents of deterioration can cause very severe damage in a relatively short period of time.

#### **7.2.3.1 Teredinids (Shipworms)**

One of the most common borers found in marine environments is the teredinids, more commonly known as shipworms. These small worm-like animals have a body with two shells or valves at the anterior end of the animal which enable it to bore into wood, forming tunnels. The animal will remain in this tunnel for its entire life span while tending to avoid intruding into bordering tunnels as they grow and remove the wood. The animal does not re-emerge from the wood but will continue to bore alongside others within the timber until the wood is more or less destroyed and begins to fragment and

break up (Eaton et al., 1993). In warm waters, some species can grow up to one to two meters in length.

#### **7.2.3.2 Limnoria**

Crustaceans differ from molluscs in appearance, their mobility, and their mode of burrowing. Adults have segmented bodies and legs which allow them to move throughout the timber. Thus the crustaceans can move to fresh wood, whereas the molluscan wood borers only grow into the wood, enlarging the burrow or tunnel as they mature. Limnoria are the most commonly found crustacean agents of decay. Limnoria create an extensive network of long narrow tunnels at or just below the surface of the wood. Limnoria decay is often characterized by the respiration pits or regularly spaced holes at the surface. The tunnels are approximately 1-3 mm in diameter.

### **7.3 Simulation and Evaluation of Internal Defects**

Damaged timber pilings are abundant in bridge applications. Piles with varying damage properties are easily obtainable, but due to the complex geometry of the damage, it is difficult to accurately measure the intact portion of the cross-sectional area of a pile. As a result, the development of an accurate relationship between damage quantity and wave propagation properties is not easily obtainable. Therefore, attempts were made to simulate damage in the laboratory utilizing a drill press developed at North Carolina State University. In this manner, the percentage of remaining cross-section could be easily determined and correlated with measured stress wave properties

#### **7.3.1 Experimental Setup and Drilling Process**

Four CCA southern yellow pine timber pilings were obtained from the North Carolina Department of Transportation. Each was approximately 40 feet in length with diameters ranging from 10 to 14 inches. For ease of testing, the piles were cut into 10 foot sections

before evaluation began. All piles were obtained at air dry moisture contents of ranging from approximately 15 to 45%.

Various intact sections of the timber pilings were tested using the bending wave technique as described in Chapter 2. Sections of piling were tested while simply supported in the laboratory. Wave properties were determined using SWAP at one foot intervals along the longitudinal axis of the pile.

A 1" heavy industrial drill accompanied by a 1" diameter auger wood boring bit was used to simulate internal damage on previously intact sections. Beginning from the exposed face of the piling, holes were drilled along the longitudinal axis of the pile using a drill press developed specifically for this application. Because many of the bits used for drilling were broken due to misalignment, and due to the extreme force necessary to drive a bit of this size, a drill press utilizing a pulley-drive system was developed. The drill press can be seen in Figure 7.1.

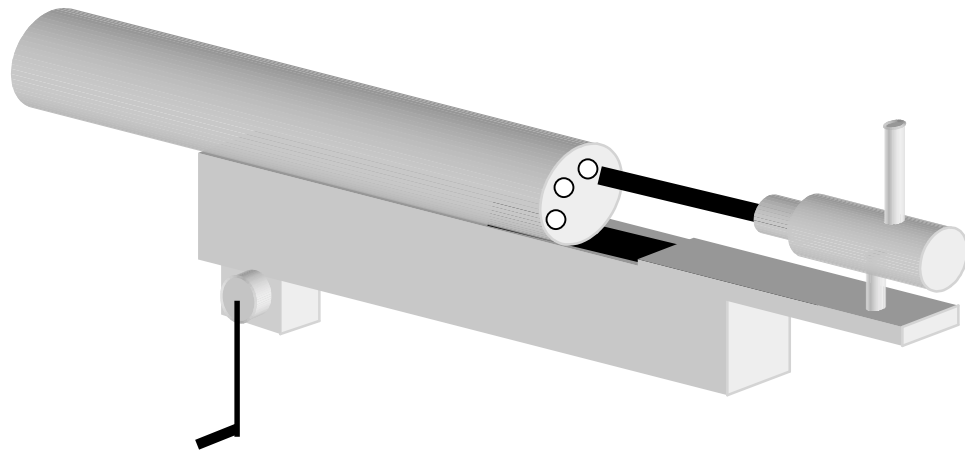


**Figure 7.1** Drill press with timber pile for laboratory damage simulation.

In reality, damage is not uniform across the entire length between sensor locations. Much of the damage in field piles is local and may not contribute a significant loss of cross-sectional area. These local areas of damage reduce the volume, in turn possibly affecting the wave propagation properties. To account for this during experimentation, the depth of penetration and percentage removal varied. Using the bending wave technique, the wave propagation properties were then measured at specific intervals of damage. Energy was imparted to the pile using both the modified hammer and the WSM-99.

Wave propagation properties can be directly related to the material properties and conditions of the medium through which the wave is passing. During previous experimentation, properties obtained from the frequency domain were unreliable when measured for intact sections. Small variations in the internal structure of wood have a dramatic effect on properties as such. Because damage creates a significant loss of cross-section in the pile, it was of interest to determine if large variations (due to deterioration) had significant influence on properties measured in the frequency domain from which relationships could be developed. Parameters considered for evaluation during the course of damage were: phase velocity, attenuation ratio, dominant frequency, centroid frequency, and area under the frequency spectrum plot. A detailed description of these parameters is given in Chapter 3.

### **7.3.2 Condition Assessment Using The Frequency Domain**

As previously stated, because of their dispersive nature, stress waves are composed of many frequencies traveling at their own individual velocities. This phenomenon is illustrated by the frequency magnitude spectrum plot for a stress wave. These plots indicate specific frequencies embedded in a waveform and their corresponding magnitudes. The frequencies which compose a stress wave are dependent on the material properties of the medium through which it passes. Variations in the cross-sectional

properties will cause variations in the composition of the stress wave that influence the composition of the frequency-magnitude plots.

Properties obtained from the frequency domain provide a much more sensitive measure of the material properties than those properties obtained from the time domain. As a result, information obtained from the frequency spectrum magnitude plots in conjunction with wave velocity and LC values were to be used for condition assessment (specifically the centroid frequency and attenuation ratio parameters).

#### **7.3.2.1 Effect of Damage on the Centroid and Dominant Frequency**

Previous research (Qian, 1997) indicated that the centroid frequency, determined from the area under the FFT plot, tended to shift as a function of the remaining cross-sectional area. Higher frequencies (5000-10000 Hz) contained within stress waves resulting from damaged portions of wood specimens were lower in magnitude than those of intact sections. As a result, a decrease in the measured centroid frequency was suspected to indicate deterioration in the cross-section. Figure 7.2 is a plot of the measured centroid frequency of stress wave propagation as the remaining cross-sectional area of a timber pile varies. The centroid frequency variation as a function of the remaining cross-sectional area of a timber pile shows no specific trends.

Further investigation indicated that the dominant frequency was also an unreliable property for use in determining the remaining cross-sectional area. Figure 7.3 shows the dominant frequency measured as the remaining cross-section decreases. Results again show a variation that can be attributed to the unreliability of the frequency information. Variations occur due to the sensitivity of the frequency spectrum plot resulting from various discontinuities in the medium and the corresponding direction of wave propagation relative to their position in the cross-section.

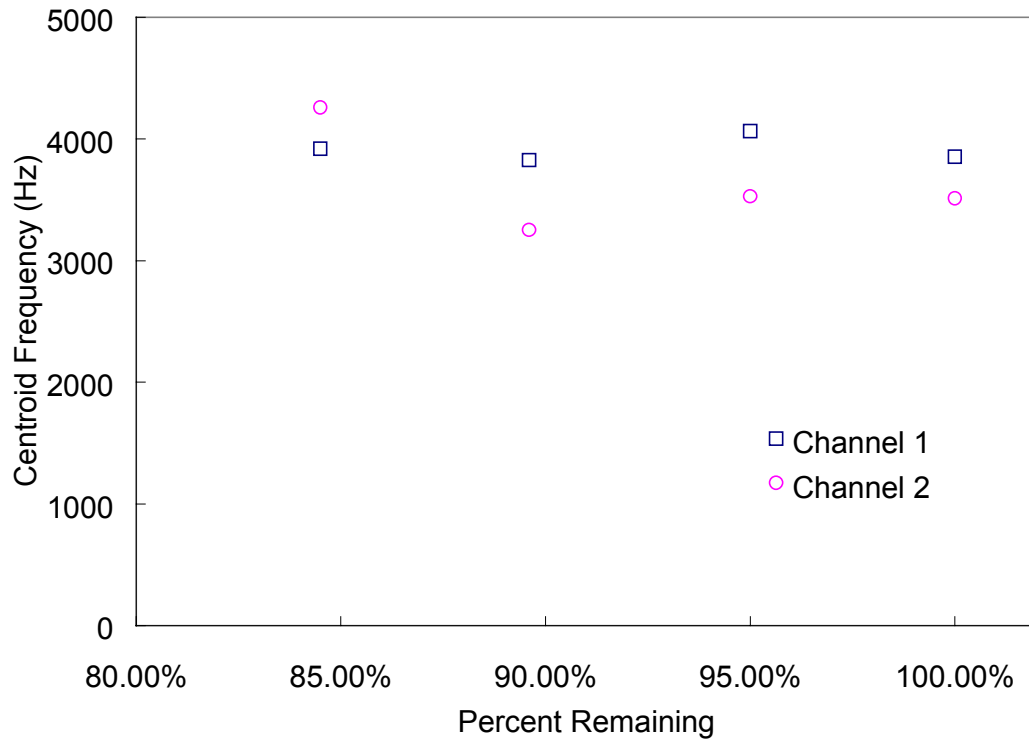


**Figure 7.2** The centroid frequency measured using the bending wave technique for wave propagation through a timber pile section with varying degrees of damage.

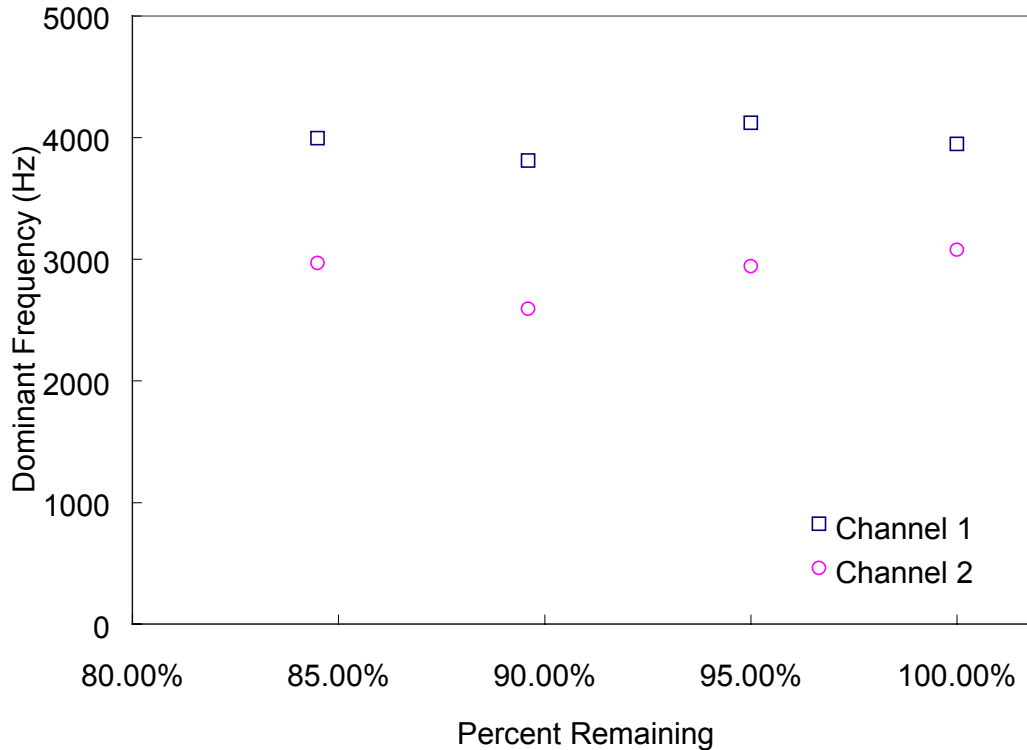


**Figure 7.3** The dominant frequency measured using the bending wave technique for wave propagation through a timber pile section with varying degrees of damage.

### 7.3.2.2 Effect of Damage on the Attenuation Ratio

The attenuation ratio (AR) of a stress wave, also determined from the frequency domain, is a measure of the wave's capability to travel through specific media. The magnitude of the frequencies present in the stress wave will dissipate as the wave passes through the medium. In theory, the magnitude of the FFT plot (area under the curve) will progressively decrease as the wave moves away from the impact location. Therefore, the AR will be based on a range from zero to one.

Previous research (Qian, 1997) had also shown the AR was a function of the remaining sound area. Because damage present in the pile impedes the attenuation of

the stress wave, the greater the damage is, the lower the AR. Figure 7.4 shows the attenuation ratio as the damage increases for a typical pile cross-section.

The AR was unpredictable and no specific trend was identified during the course of experimentation. The frequency spectrum created upon impact is very sensitive to the surface conditions, internal conditions, and impact variations (i.e., angle of impact and magnitude) and is unpredictable. As a result, the AR determined from such plots will include the effect of these variations, producing an unreliable relationship between stress wave propagation properties and material properties.

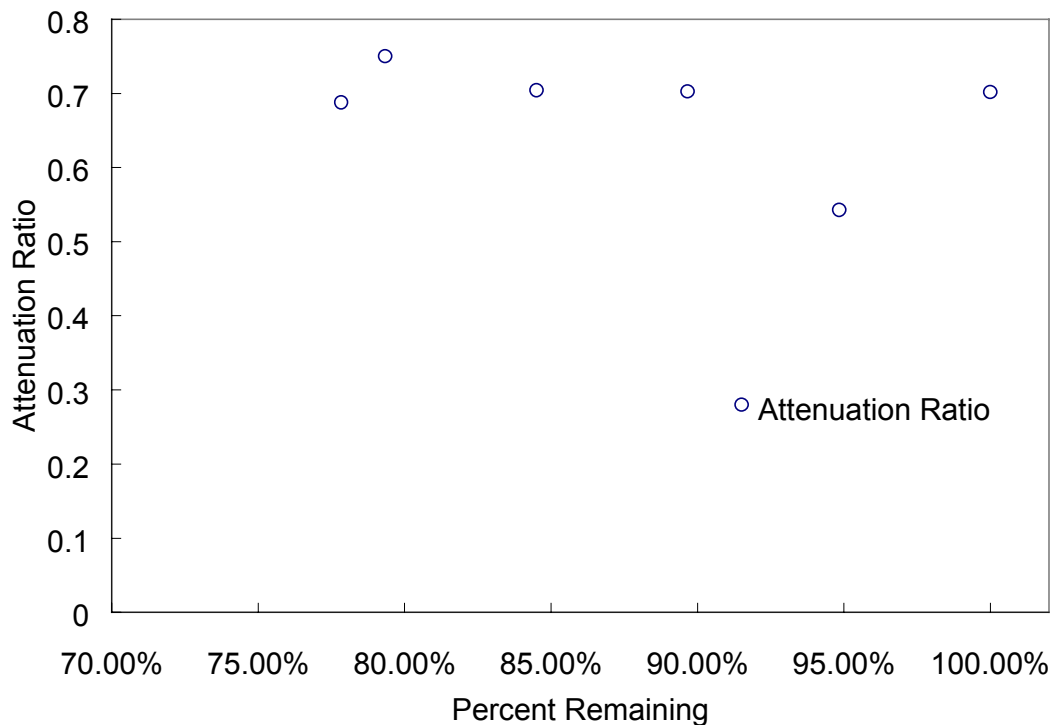


**Figure 7.4** Attenuation ratio versus damage for a typical pile section obtained using the bending wave technique.

### 7.3.3 Condition Assessment Using the Time Domain.

The most promising property used for assessing the remaining pile cross-section was the wave propagation speed or phase velocity (the speed of a specific frequency embedded in the waveform). Previous research (Chen, 1995 and Qian, 1997) had shown specific trends between wave speed and damage in timber piles. Wave speeds measured for damaged portions of timber piles at varying liquid contents can be seen in Figure 7.5. Results indicate a strong relationship between the remaining cross-sectional area and the phase velocity. As the cross-section was removed, the wave speed decreases in a linear fashion on the order of 100 ft/s per 5% reduction.

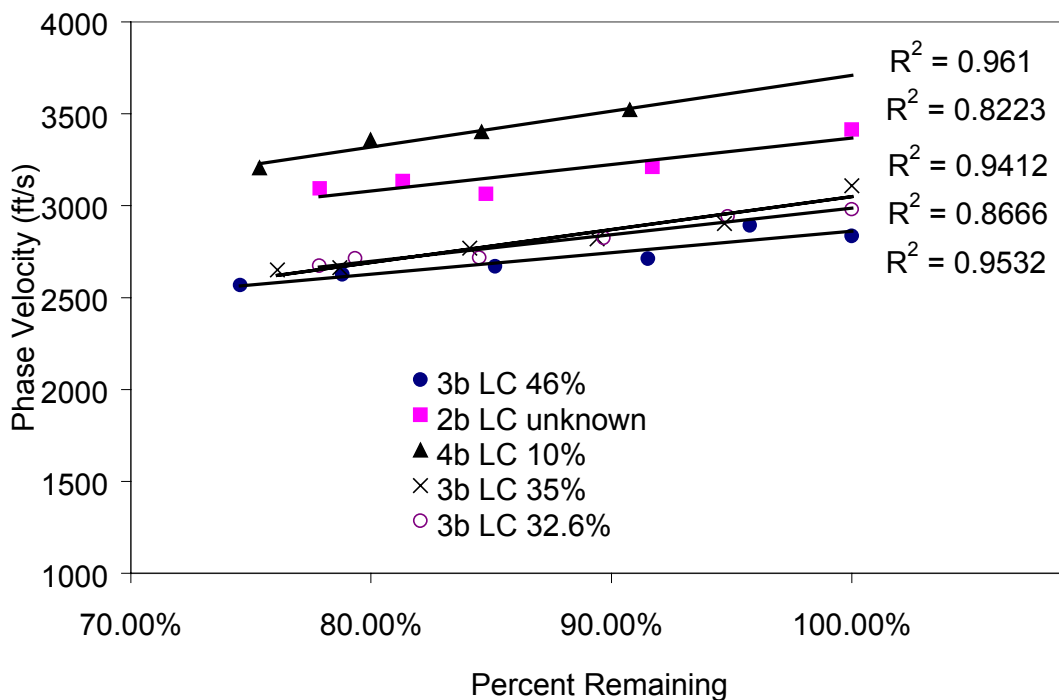


**Figure 7.5** Phase velocity as damage increases for pile sections with varying liquid content values.

Based on the findings from Figure 7.5, the phase velocity ( $V_{ph}$ ) as a function of the liquid content (LC) and the remaining cross-sectional area (RCSA) can be expressed in the following form:

$$V_{ph} = A + f(LC) * (RCSA) \quad (7.1)$$

where,

$RCSA$  = remaining cross-sectional area (%).

$V_{ph}$  = phase velocity (ft/s).

$f(LC)$  = slope of the damage trend (varies with LC).

$A$  = coefficient

In Figure 7.5, as the liquid content increases, the amount of reduction in phase velocity as a function of damage tends to decrease, i.e., the slope of the trend line decreases. Figure 7.6 (on the following page) illustrates this phenomenon. The slope of the trend,  $f(LC)$ , that relates damage to phase velocity becomes smaller as the liquid content of the specimen increases. In other words, in piles with higher liquid contents, the phase velocity reduction due to the amount of deterioration (or reduction in cross-section) is not as large as those measured for drier specimens. As a result, when the liquid content of the specimen becomes great, the measurable effect of damage on the wave propagation speed will become negligible. This relationship can be expressed in the following form (see Figure 7.6):

$$f(LC) = Ce^{-D(LC)} \quad (7.2)$$

where,

$C, D$  = coefficients

$LC$  = liquid content (%)

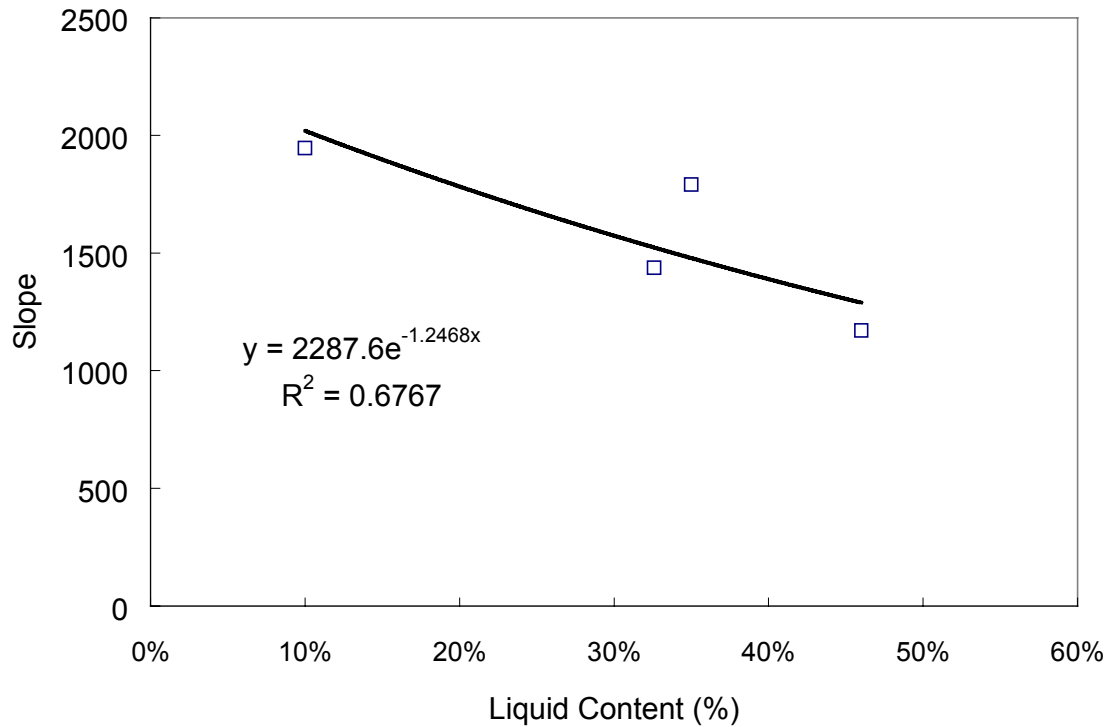


**Figure 7.6** Damage trends shown in Figure 7.5 as liquid contents of specimens vary.

Hence, upon substituting eqn. (7.2) into eqn. (7.1), the relationship between the  $V_{ph}$ ,  $LC$ , and the  $RCSA$  can be expressed in the following form:

$$V_{ph} = A + Ce^{-D(LC)} * (RCSA) \quad (7.3)$$

Assuming  $A$  is a constant, the value of  $C$  and  $D$  can be found from non-linear regression analysis. Various values of  $A$  were investigated to determine the regression curve which yielded the greatest  $R^2$ . The resulting equation relating  $V_{ph}$  to the remaining cross-sectional area for various liquid contents is given by:

$$V_{ph} = 1600 + 2373e^{-1.4687(LC)} * (RCSA) \quad (7.4)$$

Figure 7.7 shows the predicted RCSA using eqn. (7.4) versus the measured RCSA in the laboratory. Based on the line of equality, eqn. (7.4) adequately predicts the RCSA for our sample population. The predicted value is conservative in 58% of cases while the maximum difference between predicted and the actual value is  $\pm 11\%$ . Using this relationship, a trial chart can be developed to predict the remaining cross-sectional area of timber pilings (based on lab findings). The chart is shown in Figure 7.8. Each line represents a different moisture content (shown in increments of 10%). Knowing the LC of the specimen, and measured phase velocity across a specimen (determined using the bending wave technique), the RCSA can be found.

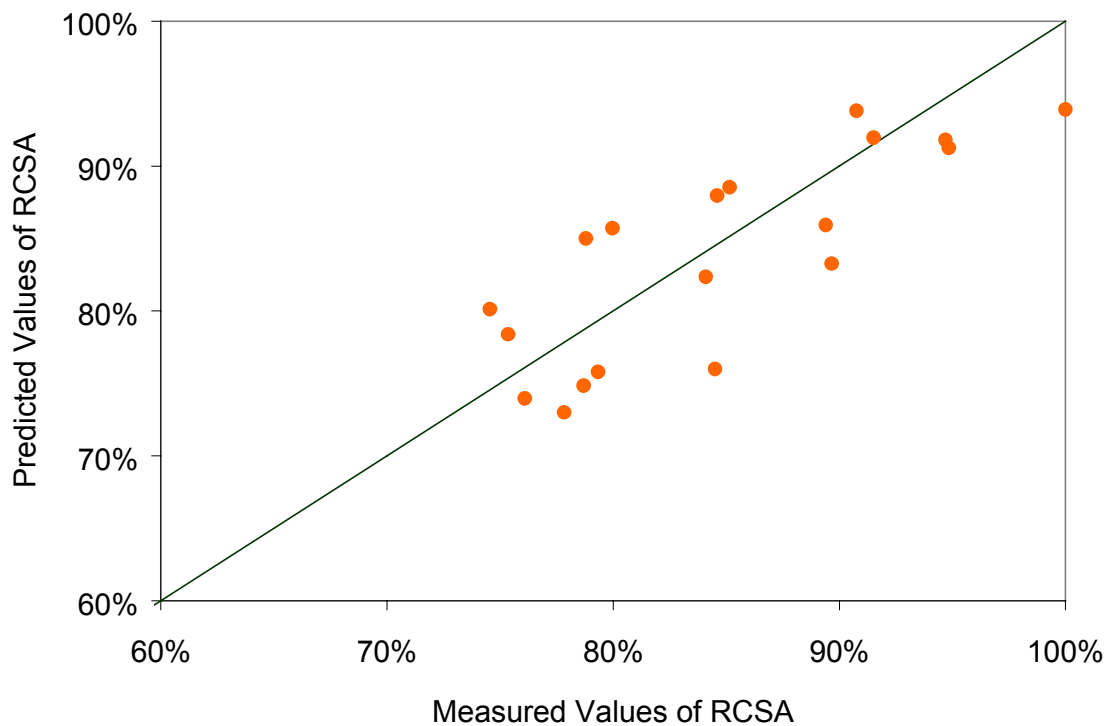


**Figure 7.7** Average measured RCSA versus predicted value based on Equation 7.4.

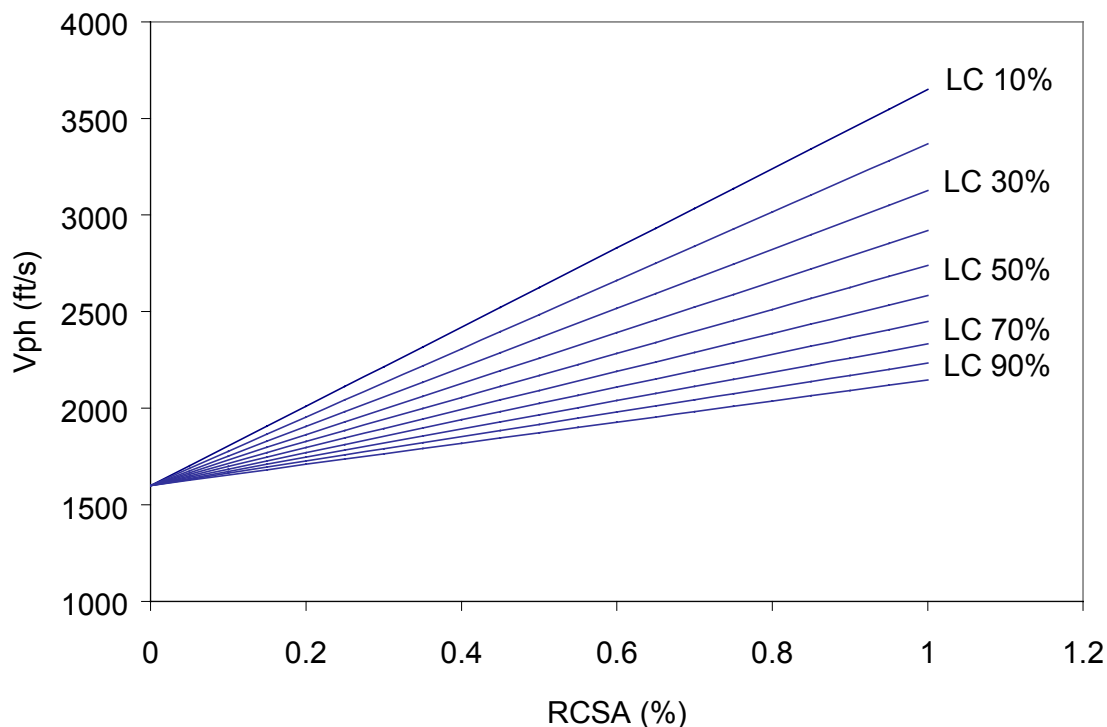


**Figure 7.8** Condition Evaluation Chart Developed Using Laboratory Data.

## 7.4 Summary

Condition assessment using the frequency domain is unreliable. Structural and surface variations inherent in timber result in inaccurate properties obtained from the frequency domain. Therefore, it is not recommended to use such parameters in evaluating the condition of timber pilings. Conversely, strong relationships were illustrated from parameters obtained from the time domain. As the degree of internal damage increases, the phase velocity measured decreases correspondingly in a linear fashion. Using the basic relationship provided herein from Equation 7.4, one can attempt to predict the remaining sound area of a timber pile.

## Chapter 8

# Investigation of Installed Timber Piles

### 8.1 Experimental Design

The experimental design for this research required piles with various cross-sections (i.e., intact and damaged) and that each specimen would be tested under various conditions (i.e., in-situ and extracted). Stress wave tests were performed on twenty-two installed timber piles. All specimens were obtained from the NCDOT. A table of relevant information for each pile is shown in Appendix A. All specimens were a part of the structural support of bridges on rural roadways in North Carolina. Pile condition was dictated by the method from which it was obtained from the NCDOT. The majority of intact specimens were obtained in the Spring of 1998 from reconstruction projects of the Bridge Maintenance Unit. In these cases, the entire structure was being replaced. This replacement was not instigated by specific pile damage, but the overall age and condition of the entire structure. Most damaged sections however, were obtained from DOT prompt action requests. These requests stem from the two-year inspection cycle of highway bridges. DOT crews inspect all state bridges every two years to ensure adequate maintenance and performance of these structures. This inspection covers all aspects of a highway bridge. Based on their observations, inspectors may determine that a pile needs to be replaced immediately to ensure the safety of the structure and its users.

Stress wave tests were performed on installed timber piles under the following three conditions:

- In-situ (IS)
- Extracted-wet (EW)
- Extracted-dry (ED)

### **8.1.1 In-situ Testing**

Testing was performed on all specimens while in service. The boundary conditions of an in-situ pile can be thought of as “fixed-fixed.” This is because the top of the pile is embedded in the concrete of the bridge deck structure and the bottom is embedded in the ground. Cores were obtained from every location and the corresponding liquid content was determined.

### **8.1.2 Extracted-wet Testing**

Immediately following removal from the structure, extracted-wet tests were performed on extracted piles. Once the bridge deck was removed, piles were cut at ground level and lifted to the approaching roadway surface for subsequent testing. Piles were simply supported during the course of these stress wave tests. The extraction process is illustrated in Figure 8.1. No cores were taken under these circumstances because it was assumed that the change in moisture content would be insignificant between the time of extraction and the collection of data. Stress wave data was coupled with the corresponding LC from in-situ tests. A typical day of extracted-wet testing is illustrated in Figure 8.2.



**Figure 8.1** Extraction of installed timber piles.



**Figure 8.2** Field testing of piles in the extracted-wet condition.

### **8.1.3 Extracted-dry Testing**

The third and final condition of testing is the extracted-dry condition. Extracted piles were transported to the Bridge Maintenance yard in Raleigh upon completion of extracted-wet testing. Stress wave tests were performed on piles after they were either air or kiln-dried. A photograph of the typical test setup is shown in Figure 8.3. The goal of the third and final condition of testing was to obtain stress wave data that represented the same locations with the same damage, but with different moisture content information. The target LC of this final condition was 10-15%.



**Figure 8.3** Extracted-dry Testing with the Wood Spring Mechanism.

### **8.1.3.1 Kiln Drying**

Piles were stored at the BMU site for over eight months when it was determined that air-drying of piles was too time consuming. An experiment was conducted on pile Q to examine the feasibility of drying the piles in a kiln operated by the Forest Products Laboratory at North Carolina State University. The goal of this experiment was to determine if the piles would suffer damage as a result of the accelerated drying process. Pile Q was dried for about a month using a typical drying schedule for wood poles. The pile was cut into pieces and photographs were taken of each section before, during and

after the drying process. No significant damage was noticed as a result of this experiment and it was determined that the kiln could be used to decrease pile drying time.

Six piles were kiln dried for four weeks using the same standard schedule for wood poles. The kiln and the piles of the first and only kiln batch are shown in Figure 8.4. Upon removal from the kiln, stress wave tests were performed on these specimens. Cores were obtained and LC determined. Table 8.1 compares the in-situ to the post-kiln LC (extracted-dry value). At the conclusion of the kiln drying of the first batch of piles, it was realized that it would be extremely difficult to bring every position on every pile to the target LC of 10-15%. The table shows that location 1 of pile U (designated "U1") lost an insignificant amount of liquid in four weeks of kiln drying. There are two possible reasons for this phenomenon. The first is that the pile may have reached its driest state but the presence of a significant amount of creosote provided the high liquid content. Another possible explanation is that the pile simply needed more time in the kiln.

It was decided that extracted-dry tests would be performed on the piles stored at the BMU "as is." In other words, since the target LC value was determined to be unobtainable, stress wave tests would be performed and cores would be taken. The stress wave data and corresponding LC values would be considered that of the extracted-dry condition although the target value had not been reached. It was assumed however that due to the length of storage, the tested locations of each pile had to have decreased. This assumption proved to be correct upon the measurement of the liquid contents of piles not placed in the kiln. The difference in LC between in-situ and extracted-dry measurements for air-dried piles ranged from 5 to 90 percent.



**Figure 8.4** Piles loaded in kiln for drying.

**Table 8.1** Comparison of liquid content for kiln dried piles.

PILE/LOCATION	IN-SITU LC (%)	POST-KILN LC (%)
N1	46.96	32.44
N2	69.59	45.19
N3	N/A	44.68
R1	29.66	18.3
R2	28.48	21.9
R3	38.75	10.9
S1	51.3	9.67
S2	73.71	8.02
S3	95.25	11.4
S4	94.8	17.48
T1	17.76	8.44
T2	20.79	8.85
T3	63.42	11.2
T4	87.42	8.89
U1	51.12	50.79
U2	70.43	53.84
U3	80.9	55.55
W1	35.58	28.9
W2	56.72	39.9
W3	73.92	47.7

## 8.2 Cutting of Pile Sections

Extracted piles were cut into 6 in. sections upon completion of extracted-dry testing. Of the twenty-two piles obtained from the field, 8 contained damage. Damage varied widely from pile to pile. In some cases (Pile AA for example) only a small portion (one foot length) of the pile was damaged while in others (e.g. Pile CC), the entire length of pile was missing a portion of cross-sectional area. An average Remaining Cross-Sectional Area (RCSA) was determined for each test location using the methods described in the next section. Figure 8.5 shows a worker from the Wake County BMU cutting an extracted pile into sections.



**Figure 8.5** Cutting of Extracted Piles

### **8.3 Determination of Remaining Cross-sectional Area**

Average RCSA values were computed using Sigma Scan 4.0. This software package has a variety of imaging tools. Sigma Scan can perform a variety of calculations and manipulations on photographs in standard computer image formats. The photographs of pile sections were scanned into a computer where the damaged portions could be highlighted by the user and automatically calculated. The measuring tape appearing in each photograph provided a scale for software calibration. For each one foot section tested, the RCSA was determined for the top, middle and bottom, and then an average value was computed. These values were coupled with the corresponding LC and phase

velocity for that section. The first column of Table 8.2 indicates the damaged sections (pile/test location) and second column provides the corresponding RCSA.

A few samples of scanned images containing pile cross-sections are given here for observation. Figure 8.6 depicts a pile section that contributed to the RCSA calculation of CC4. The external voids evident in the photograph make the calculation of RCSA very simple. The user simply outlines the sound area (within Sigma Scan) and calculates the percentage of remaining area based on the actual diameter of the pile.

**Table 8.2** Remaining cross-sectional area of damaged extracted field piles.

PILE/TEST LOCATION	REMAINING CROSS SECTIONAL AREA (%)
CC1	92.30
CC2	90.80
CC3	88.80
CC4	86.62
CC5	68.55
CC6	41.48
CC7	36.83
S1	51.60
S2	44.40
S3	45.40
O2	75.03
O3	78.33
EE2	51.45
EE3	56.00
EE4	56.85
P2	48.00
P3	84.28
BB7	90.60
BB8	91.17
AA8	81.25
DD2	91.45



**Figure 8.6** Damaged portion of pile CC.



**Figure 8.7** Damaged section of pile EE.

A similar situation is illustrated in Figure 8.7. This section contributed to the calculation of RCSA for pile EE, location 2. This damage consists of internal voids which closely resemble the type of damage simulated in the laboratory (see Chapter 7).

The calculation of the RCSA is not always this simple. Evidence of this is illustrated in Figure 8.8. The damage in this section is more intricate than the damage shown in the two previous figures. Although voids are obviously present, other portions of the section are in the process of decay. The presence of decaying wood makes the calculation of remaining cross-sectional area more difficult. User discretion is more critical in these sections where judgement of which areas are functional and which are not is extremely

crucial. Discoloration of the wood and texture changes were used as indicators of damage in these situations.



**Figure 8.8** Damaged section of Pile O.

## 8.4 Test Results

All stress wave parameters are calculated using the methods described in the previous sections. These values are associated with the location on the pile from which they were obtained. Liquid content is determined from a core sample using the HMA. The result is

that each location (test setup) within the piles tested is associated with the calculated stress wave parameters and a specific liquid content. Also, liquid contents and stress wave parameters will vary depending on the condition in which the pile was tested (i.e., position 1 on pile G in the in-situ vs. extracted-dry condition).

### 8.4.1 Frequency Information

A plot of attenuation ratio versus liquid content for intact field piles is shown in Figure 8.9. This data was obtained using the modified hammer.

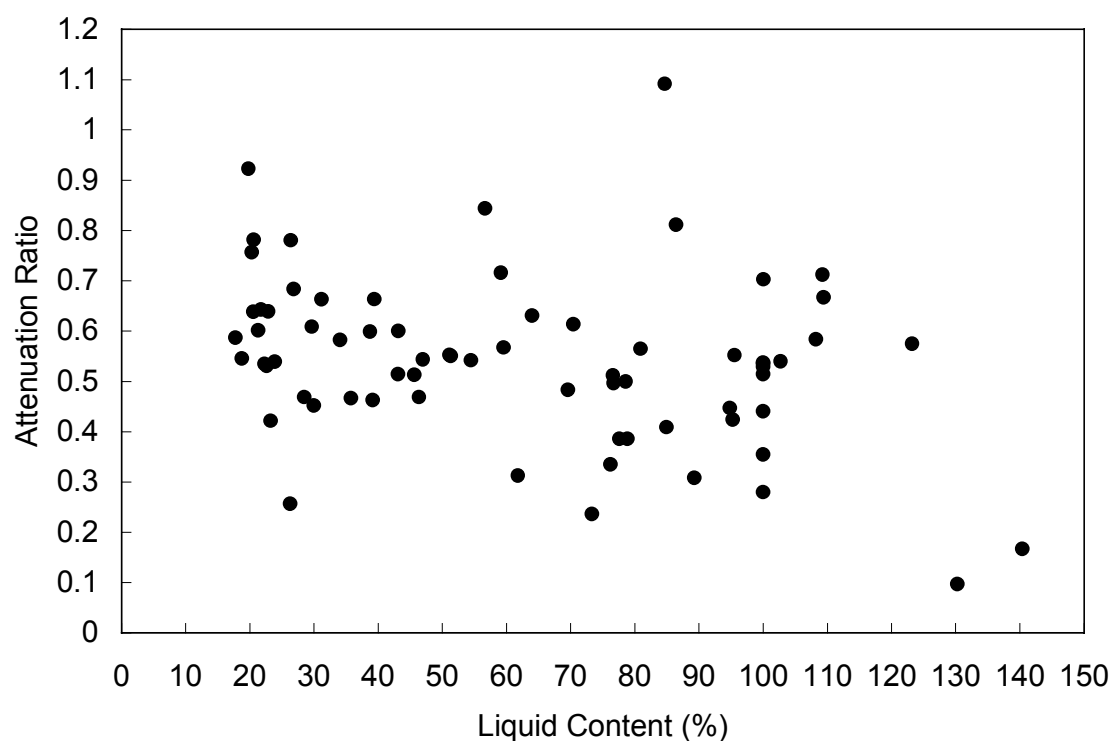


**Figure 8.9** Attenuation ratio vs. liquid content for intact field piles

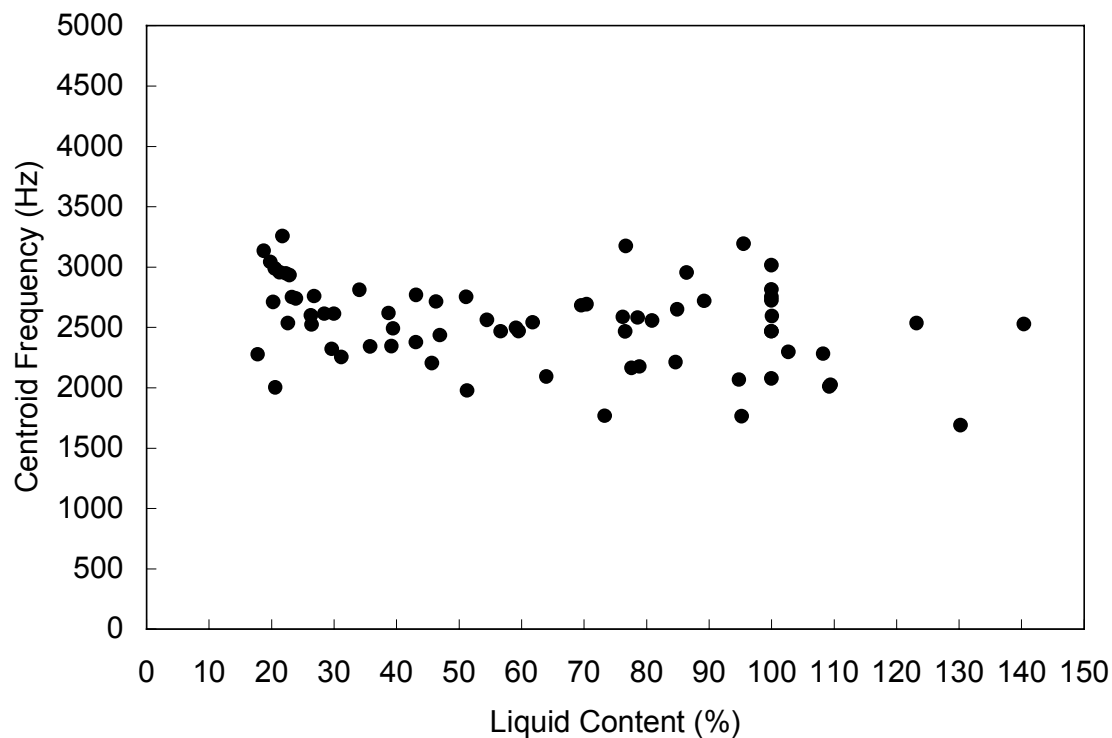


**Figure 8.10** Centroid frequency vs. liquid content for intact field piles.

Shown in Figure 8.10 is a plot of centroid frequency versus liquid content. The data in this graph were obtained from intact field piles using the modified hammer.

Shown in Figure 8.11 is a plot of dominant frequency vs. liquid content. Again, the modified hammer was used during in-situ testing to obtain these data points. No significant trends can be found in any one of these three plots. It was apparent from this information that frequency parameters are not appropriate for the condition evaluation of timber piles.

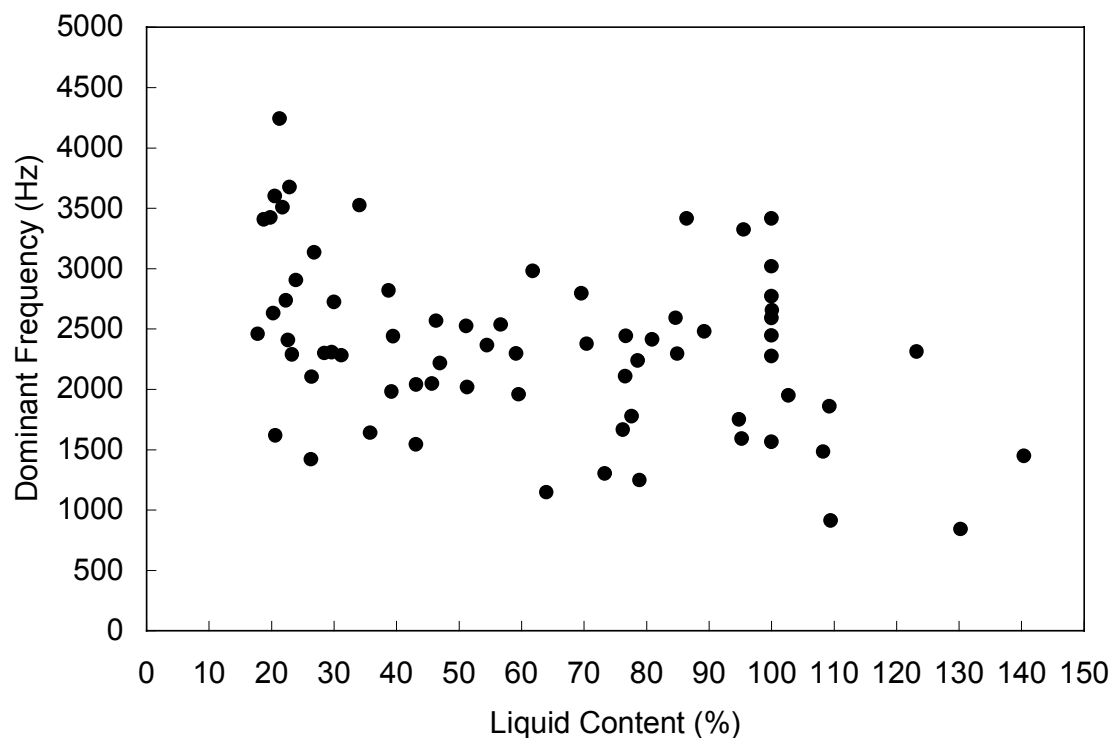


**Figure 8.11** Dominant frequency vs. liquid content for intact field piles.

This conclusion is an interesting one due to the nature of parameters involved. Frequency parameters are very specifically defined and there is no chance for error if the correct equations and methods are used. Compared to phase velocity determination, frequency parameters are much more straightforward to obtain. Phase velocity calculations are dependent on both the judgement and experience of the user during the process of choosing the correct peaks.

## **8.4.2 Phase Velocity Information**

Based on the information obtained from laboratory testing, it was hypothesized that phase velocity had the potential to be a strong indicator of pile condition. The results presented in this section will show that this is true with installed timber piles as well.

### **8.4.2.1 Impact Device**

The modified hammer was used throughout the course of this research because it was known to be an effective device. A standard procedure presented to the NCDOT, however, required a more standardized mechanism. The requirements of this device were as follows:

- minimize impact-to-impact variation
- minimize operator-to-operator variation
- reproduce the signals created by the modified hammer

This problem was undertaken in the laboratory at NCSU. Upon completion of a comparison of three devices (Modified Hammer (MH), Wood Spring Mechanism (WSM) and steel ball), it was concluded that the WSM would be an effective standard impact device for the stress wave method. With the above goals met, it was decided that the WSM would be the standard impact device recommended to the NCDOT for condition evaluation of timber piles.

During the development of the standard impact device, the wood spring was utilized in the field along with the modified hammer for comparison. Although final relationships, recommendations and procedures are limited to the use of the wood spring device, results from both hammers are presented here.

#### 8.4.2.2 Selection of Standard Kernel

At the start of the analysis process, four standard kernel values were selected to facilitate the automatic calculation of phase velocity using AUTOSWAP. These four values (1500, 2000, 2500, 3000 Hz) represented the most common values observed in the analysis. When all results had been tabulated, 2500 Hz undoubtedly produced the best trends and all results presented herein utilize this frequency for the kernel.

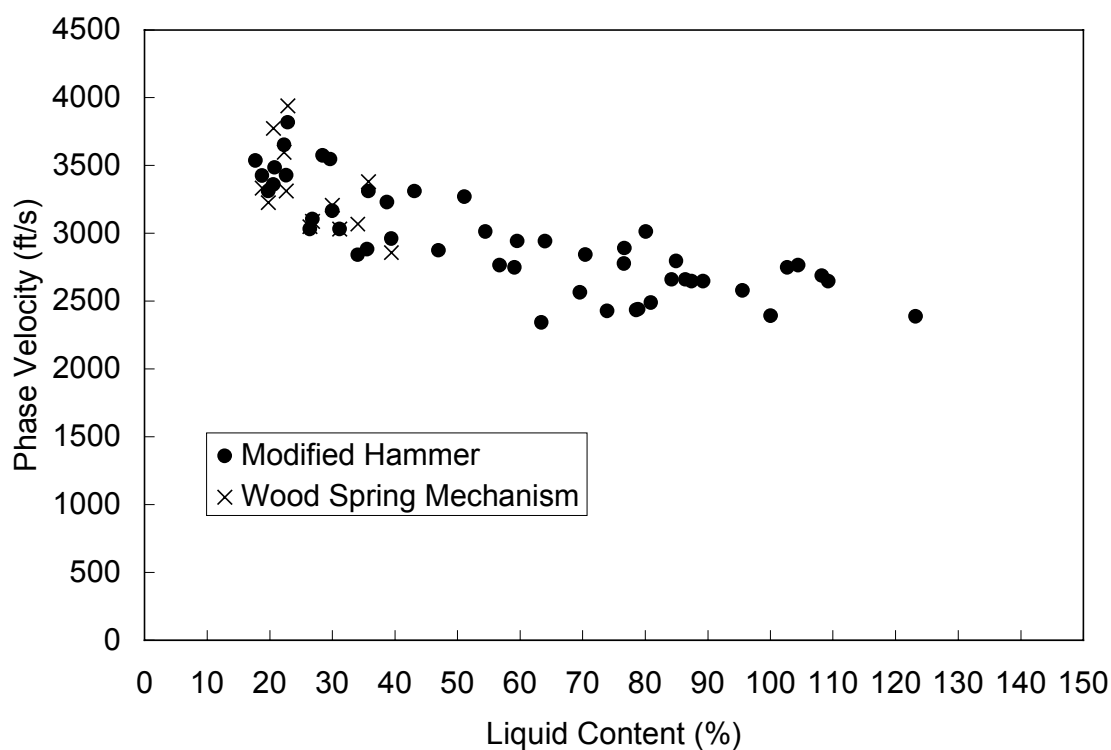


**Figure 8.12** Phase velocity vs. liquid content for intact sections in the in-situ condition.

#### **8.4.2.3 In-situ Results**

In-situ data were collected over a two year period from rural bridges in central and eastern North Carolina. Liquid contents were obtained by obtaining a core in the field and running them in the HMA as the procedure dictates. Figure 8.12 shows a plot of phase velocity versus liquid content of intact piles for the MH and WSM. A trend is apparent in both figures. As liquid content increases, phase velocity decreases, which confirms the results of previous research. No damaged piles are included in this plot, and therefore, the isolation of the liquid content is maximized. The range of liquid contents is a testimony to the various conditions in the field. The WSM data nicely overlap the MH data, confirming the conclusions presented in Chapter 4.

#### **8.4.2.4 Extracted-wet Results**

Extracted-wet data was collected immediately following pile extraction. Cores were not obtained during this phase of testing, and the stress wave data was associated with the corresponding liquid content from in-situ tests. A plot of phase velocity vs. liquid content for intact sections in the extracted-wet condition is shown in Figure 8.13. Again, a definite trend exists between phase velocity and liquid content. There is a significant overlap of the data from both impact devices.

#### **8.4.2.5 Extracted-dry Results**

Stress wave data were collected from the field piles after either kiln or air-drying. Cores were taken after each test in order to determine each LC. Methods of testing were similar to those in the two previous conditions of testing except for the number of sides of the pile on which data was collected.

As discussed in Chapter 5, the natural variability of wood introduces another variable worthy of consideration. To reduce the affects of natural variation of wood, it was decided that three sides of the pile would be tested. Three phase velocities are obtained for each test location, and average is computed. This value is then coupled with the

appropriate LC for analysis. By testing three sides of the pile and computing an average, a decrease in the randomness of the data is expected.

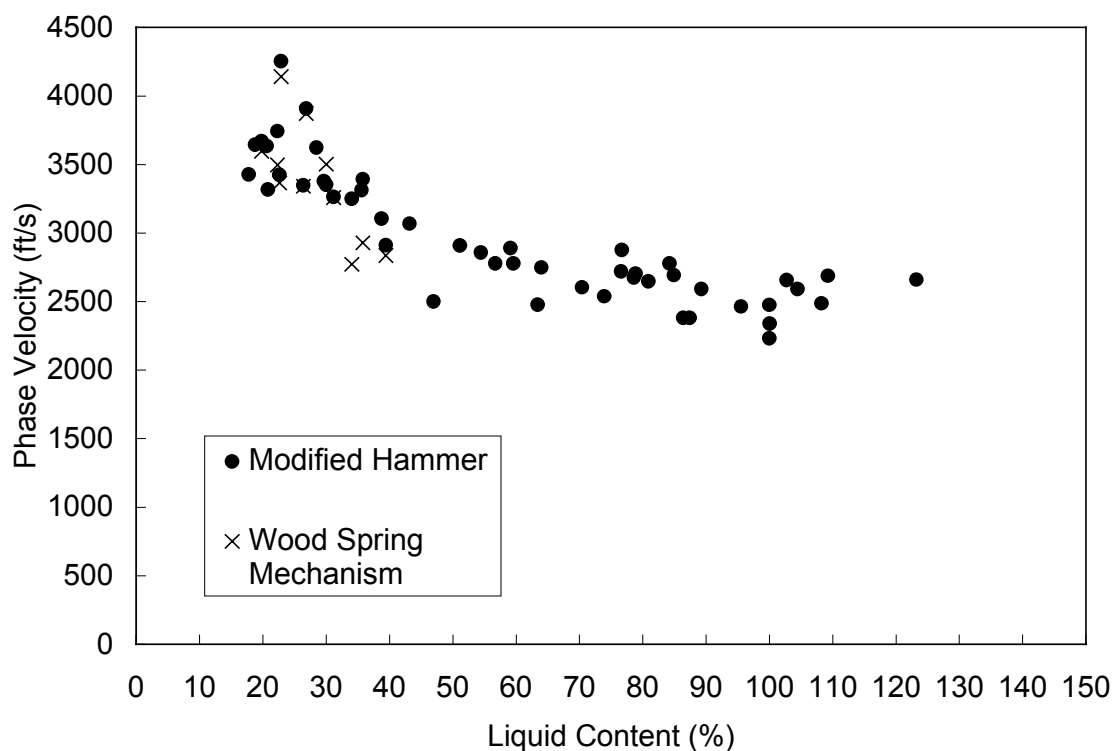


**Figure 8.13** Phase velocity vs. liquid content for intact sections in the extracted-wet condition.

A plot of phase velocity vs. liquid content for intact piles in the extracted-dry condition is shown in Figure 8.14. In general, the LC values are lower than those of the first two conditions due to the drying processes imposed on this condition. The same trend is evident and the overlap of the both devices is consistent.

Upon the comparison of the phase velocity results from the three conditions of testing two definite conclusions can be made:

- The WSM duplicates the results of the MH reasonably well;
- As liquid content increases there is a corresponding decrease in phase velocity

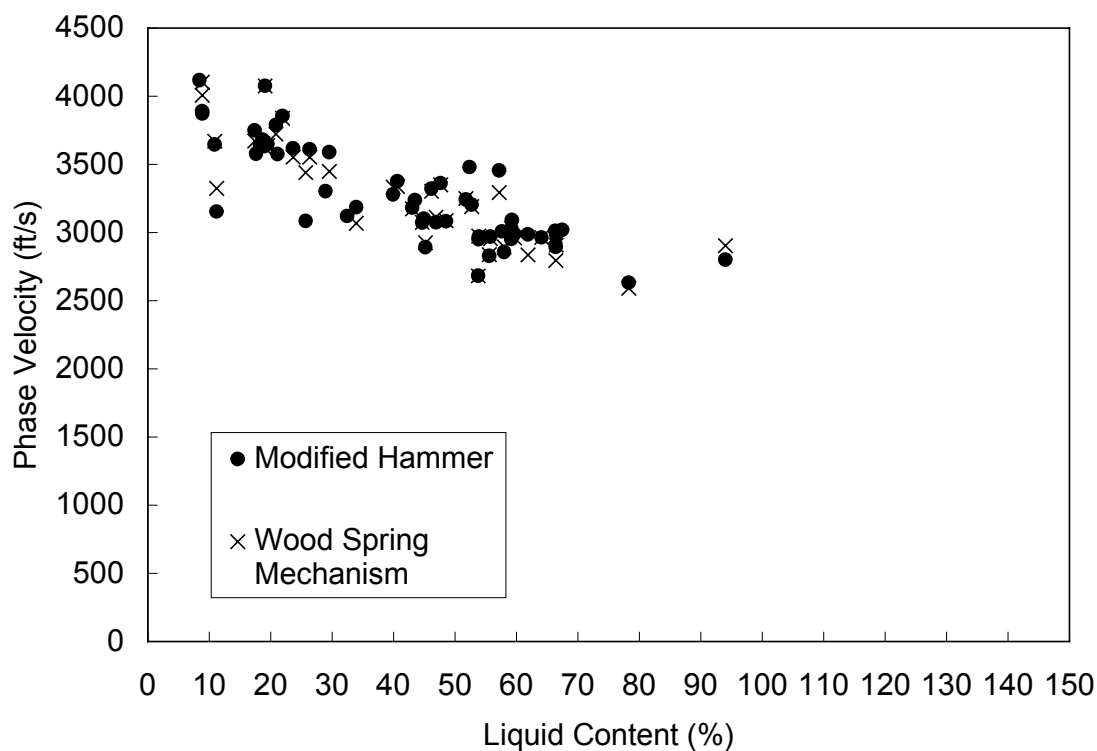


**Figure 8.14** Phase velocity vs. liquid content for intact sections in the extracted-dry condition.

#### 8.4.2.6 Effect of Boundary Conditions

To formulate the final relationship between phase velocity and liquid content for intact sections, the effect of boundary condition must be determined. It is hypothesized

that the effects are very small since the test methods are of a local nature. The boundary conditions of the pile in an in-situ test are different from those of both extracted testing conditions. A plot of phase velocity vs. liquid content for the modified hammer is shown in Figure 8.15. The goal of this comparison is to show that the affect of boundary condition is very small. Data from the modified hammer is used to answer this question because more MH data exist than those of the WSM, and the answer to this question should be independent of device used. These two particular testing conditions have been chosen because an individual core was obtained after each test.

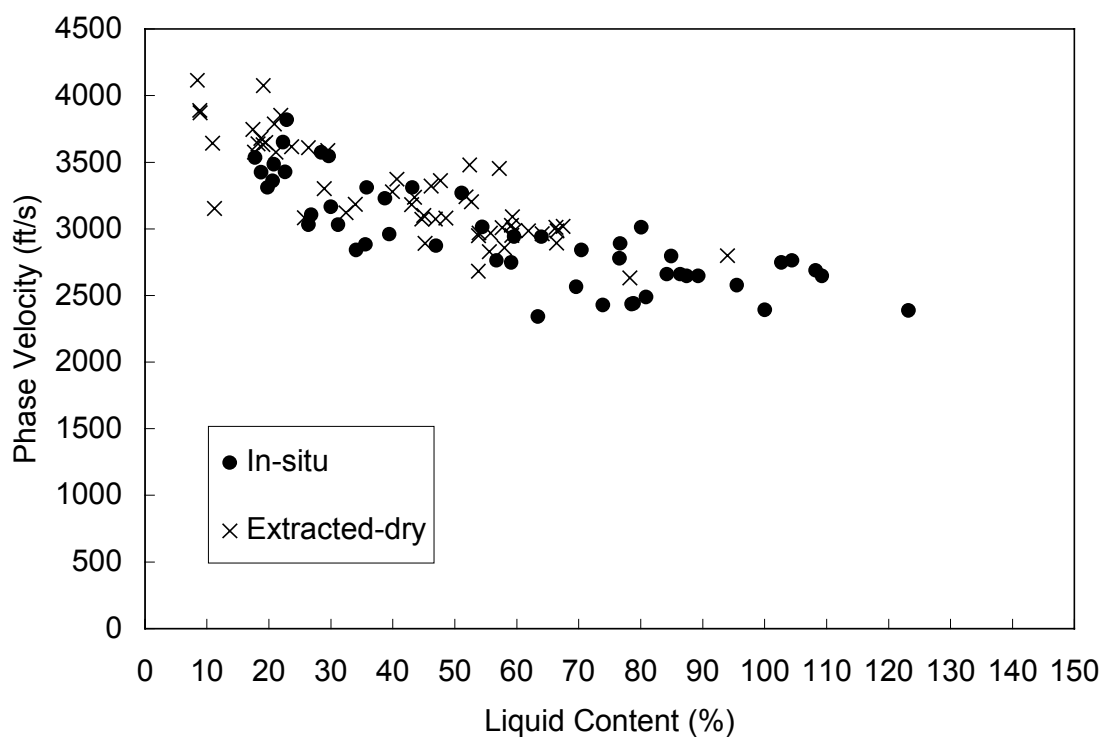


**Figure 8.15** Phase velocity vs. liquid content for in-situ and extracted-dry conditions using the modified hammer.

A consistent overlap of the data is seen in the above figure. This is an indication that all other variables aside, the effect of boundary condition is not very profound. A statistical approach to this proof is the performance of an Appropriate Likelihood Ratio Test; other wise known as an F-Test for multiple nonlinear regression (Monahan, 1999 and Mendenhall et al., 1999). This method compares the variation of a number of parameters and indicates whether the number of variables can be reduced. In this case the variation of the parameters for each condition (full model: individual in-situ and extracted-dry data sets) is compared to the variation of the data when they are combined into one model (reduced model). The computed F-statistic for this case was 4.07. This value was less than the critical F-statistic of 4.79, showing that except in one percent of cases, the parameters reduce to one group and the reduced model is justified. This test was also performed for the intact data obtained with the wood spring device. Results were similar in that the variables were shown to be capable of reduction in all but one percent of cases.

This conclusion allows the formulation of the relationship of phase velocity to liquid content for intact piles using data from the three conditions of testing with reasonable confidence.

#### **8.4.2.7 Number of Lines and Data Files to be Considered for Each Test Location**

Due to the uncertainties associated with the natural variability of wood it was decided that three lines would be tested and 5 data files would be obtained for each test location. For the procedure to be practically implemented, it must be as efficient as possible. The necessity for three testing lines and five data files was examined. Figure 8.16 shows a plot of average phase velocity using 5 files versus average phase velocity using 2 files. Upon the observation of this figure, it is obvious that using 2 files as opposed to 5 files will yield very similar phase velocity information. Considering time saving and precision of phase velocity measurement, the collection of two files is therefore recommended in the final procedure.

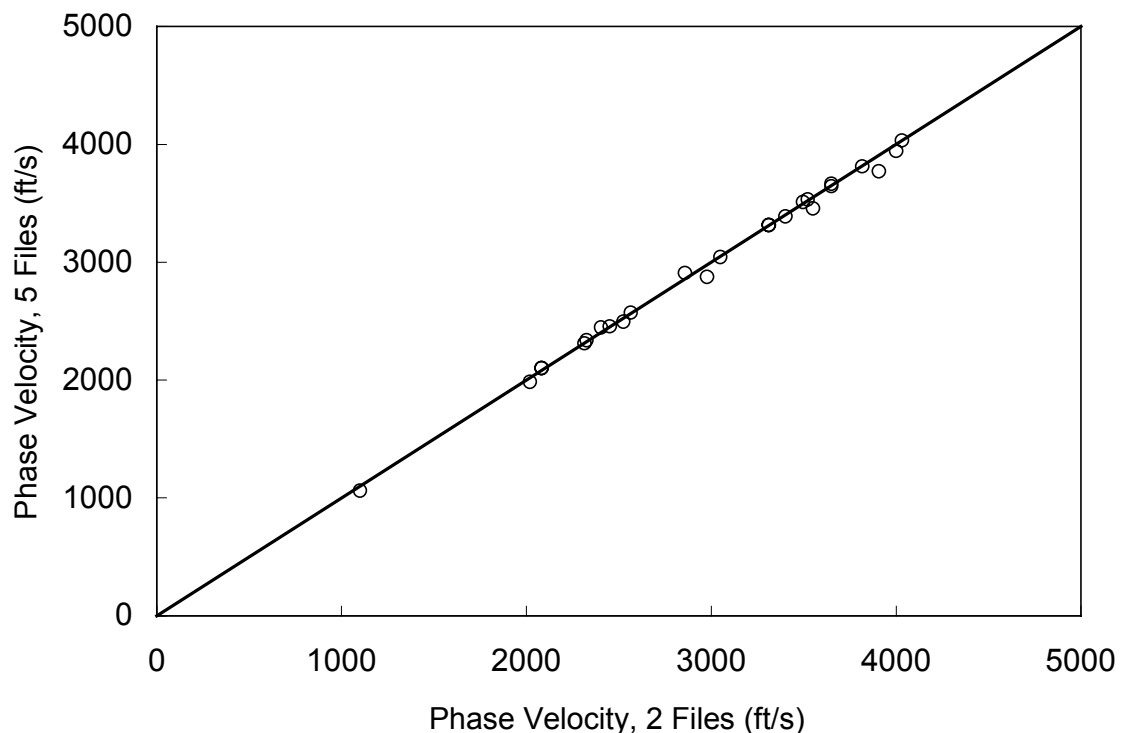


**Figure 8.16** Average phase velocity of 5 files vs. 2 files

Although 2 files have shown to be adequate for phase velocity information, the number of lines needs to be determined. Figure 8.17 shows a plot of the predicted remaining cross sectional area computed using 5 files and 3 lines versus 2 files and 1 line. The predicted remaining cross-sectional area has been calculated using the relationship developed in Section 8.4.2.9. The majority of data points in this figure are located close to the line of equality. This indicates that in most cases, there is a small difference between the predicted RCSA using 5 files and 3 lines and 2 files and 1 line. There are three points which stand out as having a significantly lower prediction using 5 files and 3

lines of testing. This effect is minimal, however, since this occurs only in 9% of cases. The final recommendation for the procedure is to test only one line.

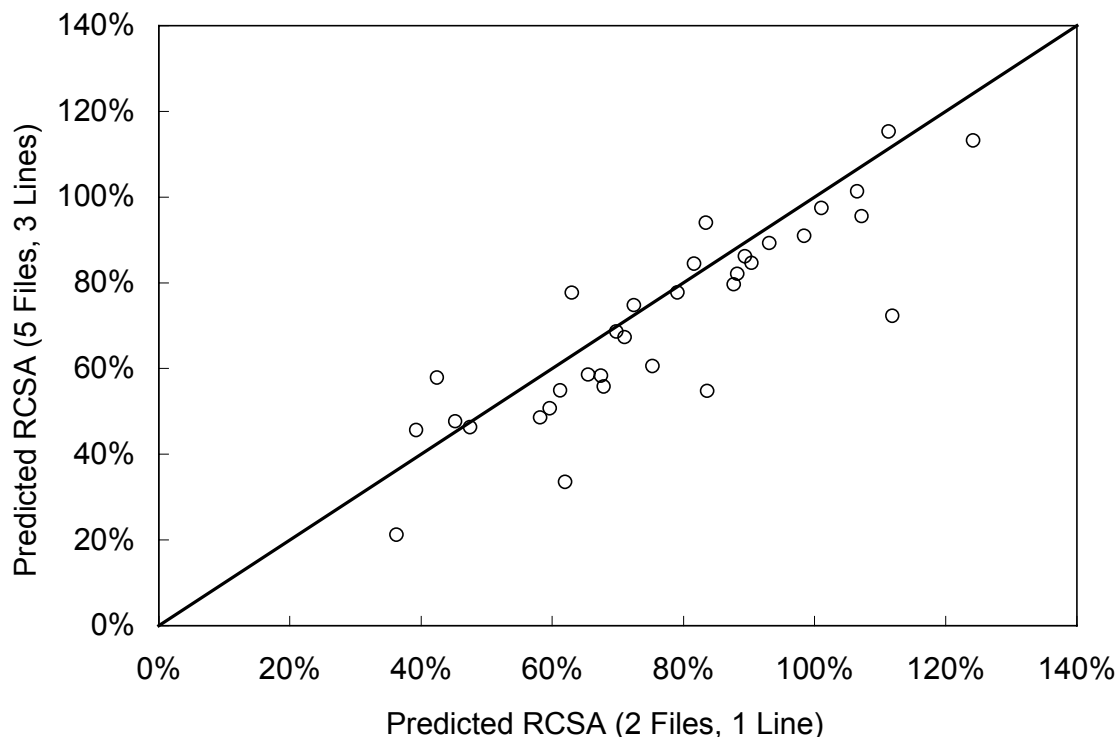


**Figure 8.17** Predicted RCSA for 5 files and 3 lines vs. 2 files and 1 line.

The results presented in this subsection are very important from a practical standpoint. The time (and hence cost) savings achieved by testing only one line as opposed to three and collecting only two files as opposed to five are significant. Based on the final recommendation of this section, the test time can be decreased by 40-60%.

#### 8.4.2.8 Relationship between Phase Velocity and Liquid Content

All phase velocity data collected during the course of this study and obtained using the WSM are shown in Figure 8.18. The phase velocities presented in the remaining section of this chapter consist of 2 files from 1 line of testing.

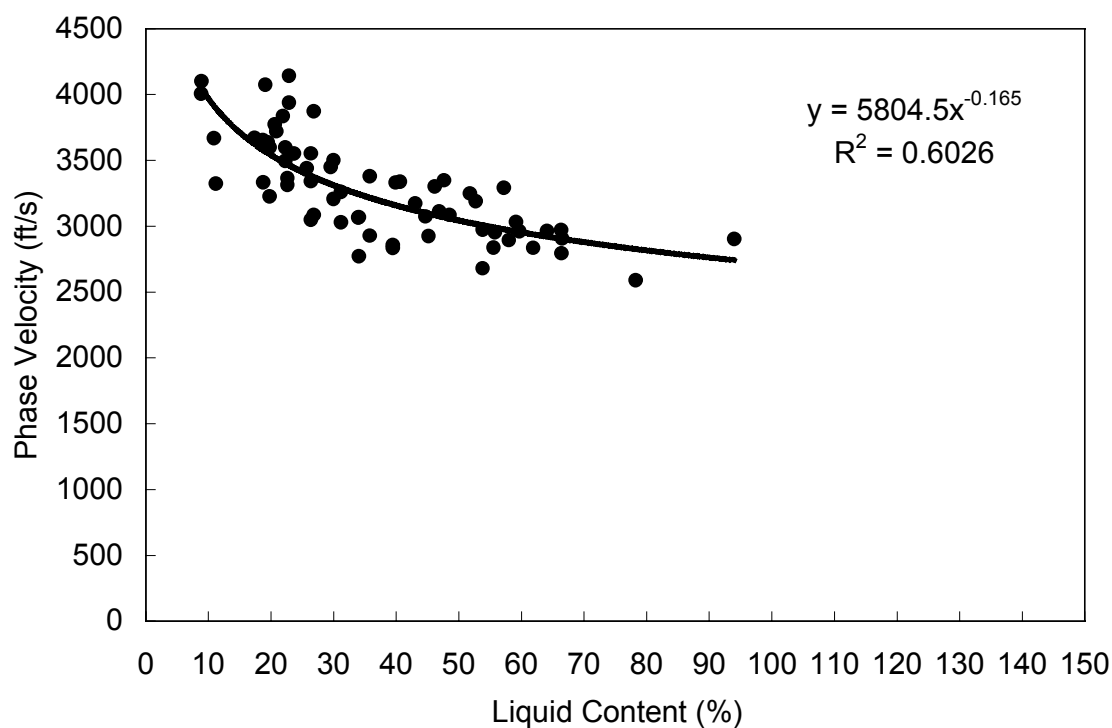


**Figure 8.18** Phase velocity vs. liquid content for WSM data.

A non-linear regression curve is shown in Figure 8.18. The data shown in this figure were obtained from intact sections. The relationship obtained using nonlinear regression is as follows:

$$V_{ph} = 5804.5(LC)^{-0.165} \quad (8.2)$$

where,

$V_{ph}$  = Phase Velocity (ft/s)

$LC$  = Liquid Content (%)

As a preliminary check to the relationship developed in the next section, intact and damaged data were plotted on the same graph. The goal was to determine if the data could indicate if a pile was damaged before proceeding a step further to the prediction of the remaining cross-sectional area. A plot of intact and damaged data along with 95% confidence interval line for the intact relationship is shown in Figure 8.19. The damaged pile data has also been classified into two categories: internal and external damage.

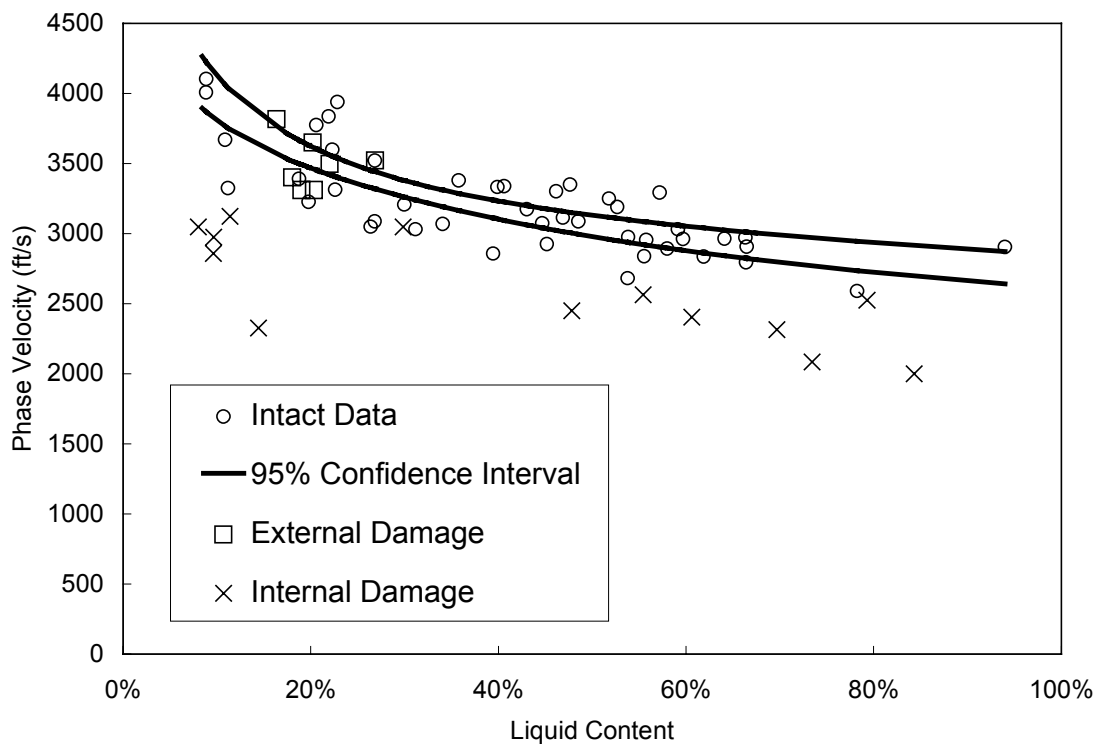


**Figure 8.19** Phase velocity vs. Liquid Content with Intact Relationship 95 % Confidence Intervals.

Clear trends are evident upon observation of Figure 8.19. There is a definite dividing line between the damaged and intact pile data. Although the externally damaged points are located within the intact confidence interval, these piles would not have to be tested using the final procedure because the extent of the damage could be seen upon visual inspection.

#### 8.4.2.9 Formulation of Condition Analysis Charts

A chart for condition evaluation of timber piles has been developed using field data collected during the course of this research. This chart was then compared to a similar relationship developed with laboratory data (Chapter 7). The methods utilized in formation of the model are described below.

In Figure 7.5, the graph of the controlled damage in the laboratory clearly shows that the slope of each trend-line is dependant on the liquid content. Plotting trend-line slope versus liquid content, the following relationship was determined:

$$S = 2287.6e^{-1.2468*LC} \quad (8.3)$$

where,

S = slope of trend-line for phase velocity versus RCSA relationship

LC = liquid content associated with trend-line

From Figure 4.3, the following general equation can be written:

$$V_{ph} = A + RCSA(B) \quad (8.4)$$

where,

$V_{ph}$  = phase velocity (ft/s)

A = y intercept

B = constant

Substituting the form of Equation 8.3 in for B in Equation 8.4 yields:

$$V_{ph} = A + RCSA * (C * e^{d(LC)}) \quad (8.5)$$

where,

$V_{ph}$  = phase velocity (ft/s)

A = y intercept

RCSA = remaining cross-sectional area (%)

C = coefficient

D = coefficient

LC = liquid content

Unknowns A, C, and D can be determined based on field data. It can be theorized that the y intercept (A) will be zero when the RCSA is zero. In other words, when there is no remaining cross-sectional area, the phase velocity is zero. This hypothesis was tested and it was determined that the value of A = 1477. Equation 8.3 can be rearranged into the following form:

$$LN((V_{ph} - a) / RCSA) = d(LC) + LN(c) \quad (8.6)$$

In this equation,  $V_{ph}$  and RCSA are known. Trial values of A were between 1000 and 1900. For each guess of A,  $LN((V_{ph} - A)/RCSA)$  versus LC was plotted. An  $R^2$

value was determined for each corresponding A value and plotted in Figure 8.20. The resulting linear relationship for Equation 8.6 is shown in Figure 8.21.

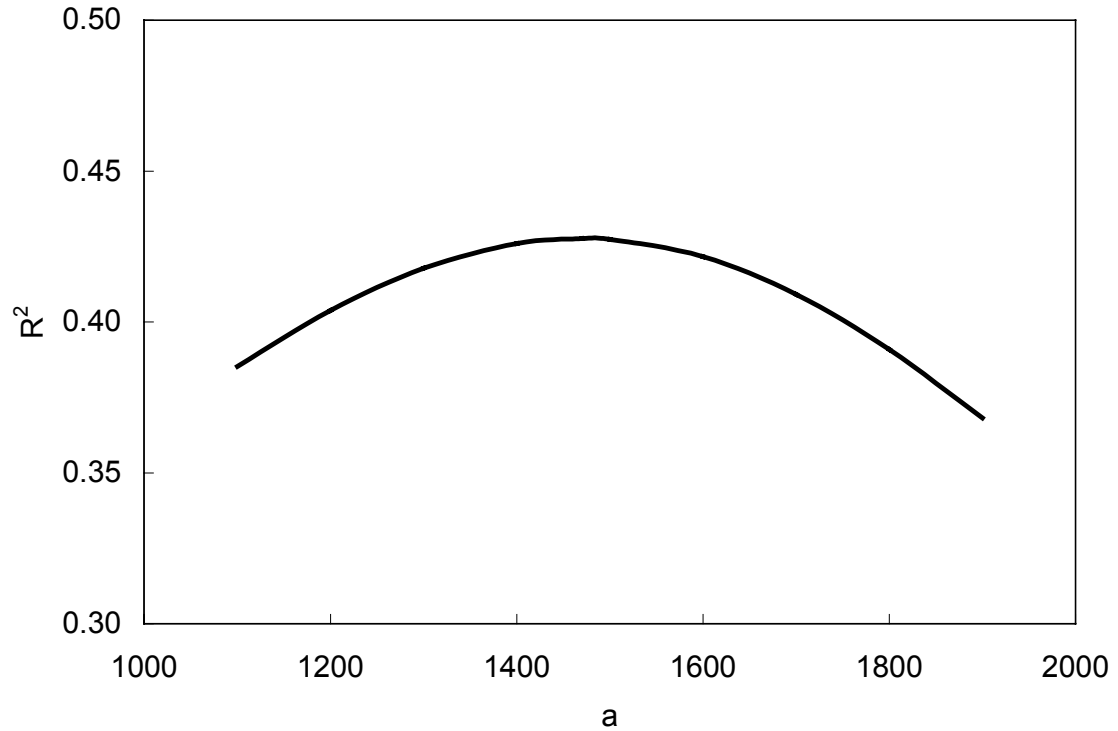


**Figure 8.20** Plot of  $R^2$  vs. A.

The maximum value of  $R^2$  was determined to be 0.4173 using an A value of 1477.

The linear regression analysis for the data in Figure 8.21 results in the following relationship:

$$LN((Vph - a) / RCSA) = -0.8294(LC) + 7.7714 \quad (8.7)$$

Coefficients C and D are determined by equating the right-hand sides of Equations 8.6 and 8.7:

$$-0.8294(LC) + 7.7714 = d(LC) + LN(c) \quad (8.8)$$

The coefficients C and D have values of 2371.8 and  $-0.8294$ , respectively.

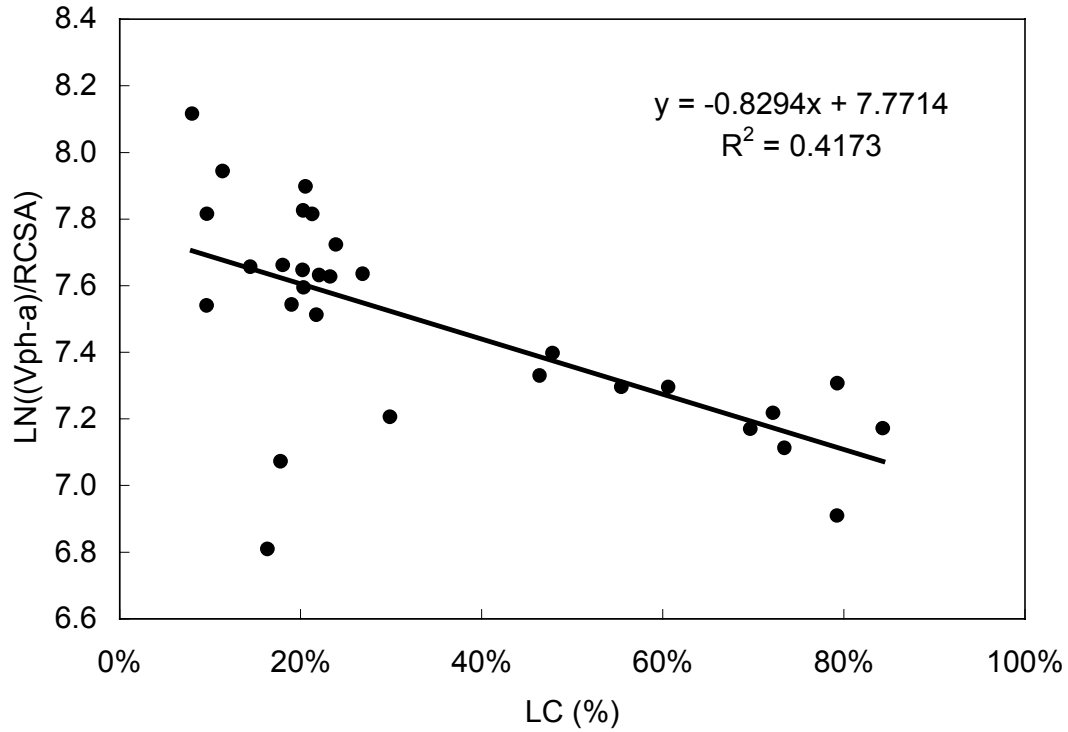


**Figure 8.21**  $\text{LN}((V_{ph} - A)/RCSA)$  vs.  $LC$ .

The final relationship for condition evaluation of piles can be expressed as:

$$V_{ph} = 1477 + RCSA * 2371.8 * e^{-0.8294 * LC} \quad (8.9)$$

Since phase velocity and liquid content are measurable quantities, it is more convenient to express the condition evaluation relationship in the following form:

$$RCSA = \frac{V_{ph} - 1477}{2371.8 * e^{-0.8294 * LC}} \quad (8.10)$$

where,

$V_{ph}$  = phase velocity (ft/s)

LC = liquid content

The resulting timber pile condition evaluation chart is illustrated in Figure 8.22. Trend-lines have been shown for liquid contents between 10 and 100% in 10 percent intervals. The performance of this chart is evaluated in Figure 8.23. This figure shows a plot of predicted RCSA versus measured RCSA.

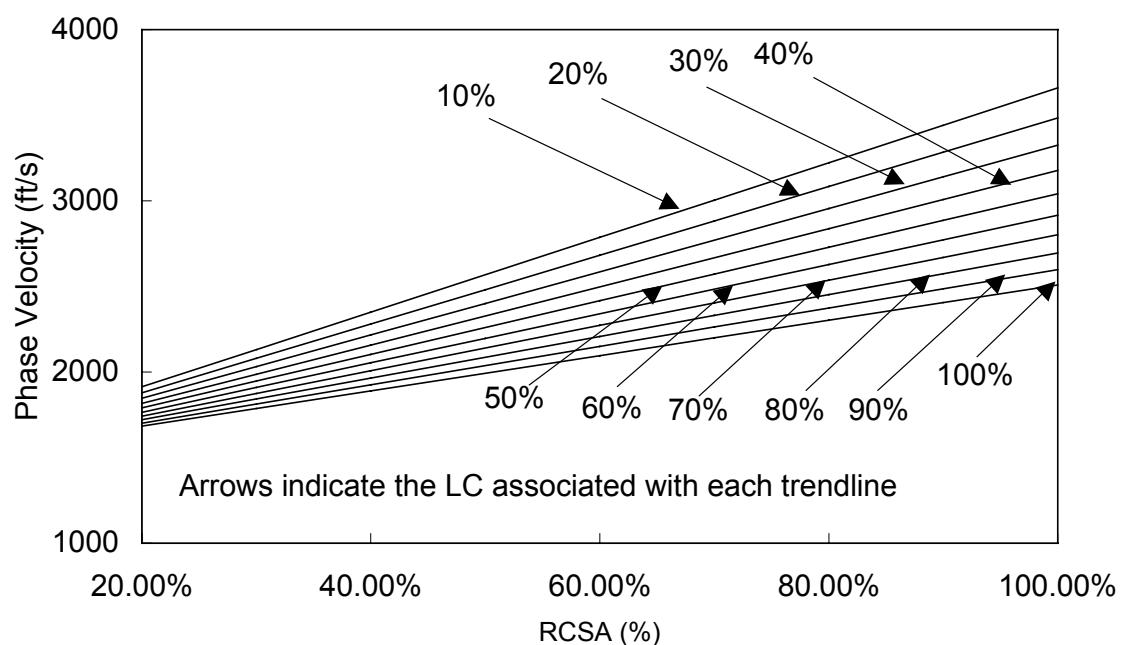


**Figure 8.22** The condition evaluation chart.

A similar approach was used in the determination of a condition evaluation chart for laboratory data. The final equation for determination of remaining cross-sectional area is expressed as:

$$RCSA = \frac{Vph - 1600}{2373 * e^{-1.4687 * LC}} \quad (8.11)$$

It was desirable to determine which relationship had better accuracy in predicting timber pile condition. Shown in Figure 8.24 is a plot of predicted RCSA versus measured RCSA using the laboratory relationship for the analysis of field data.

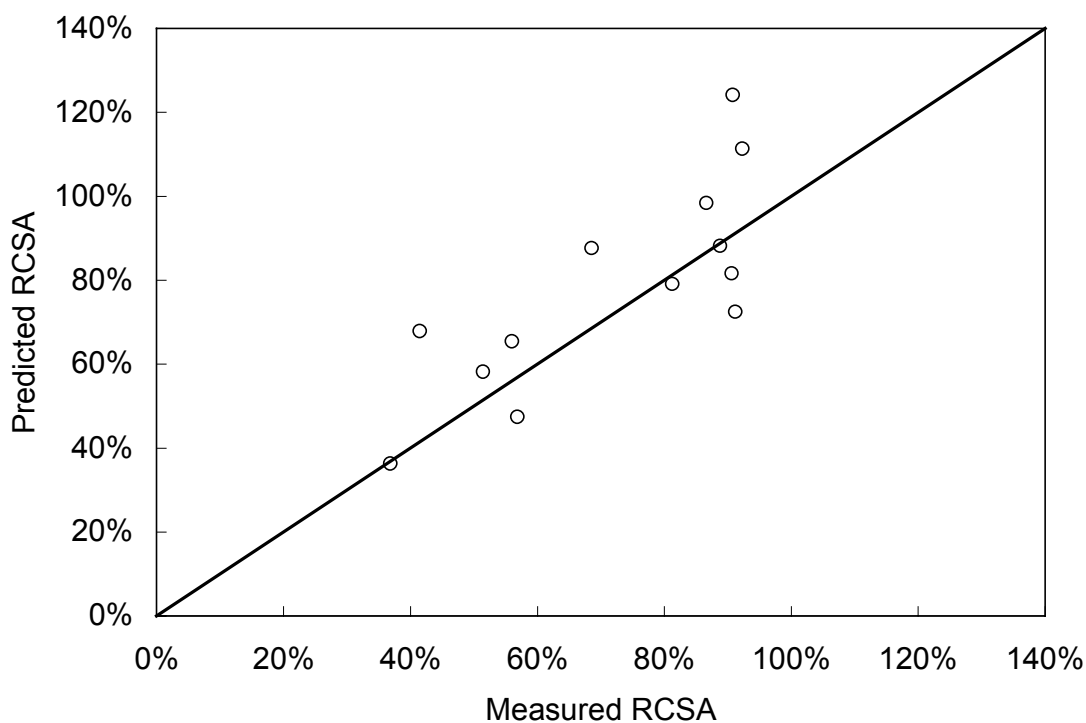


**Figure 8.23** Predicted RCSA vs. measured RCSA.

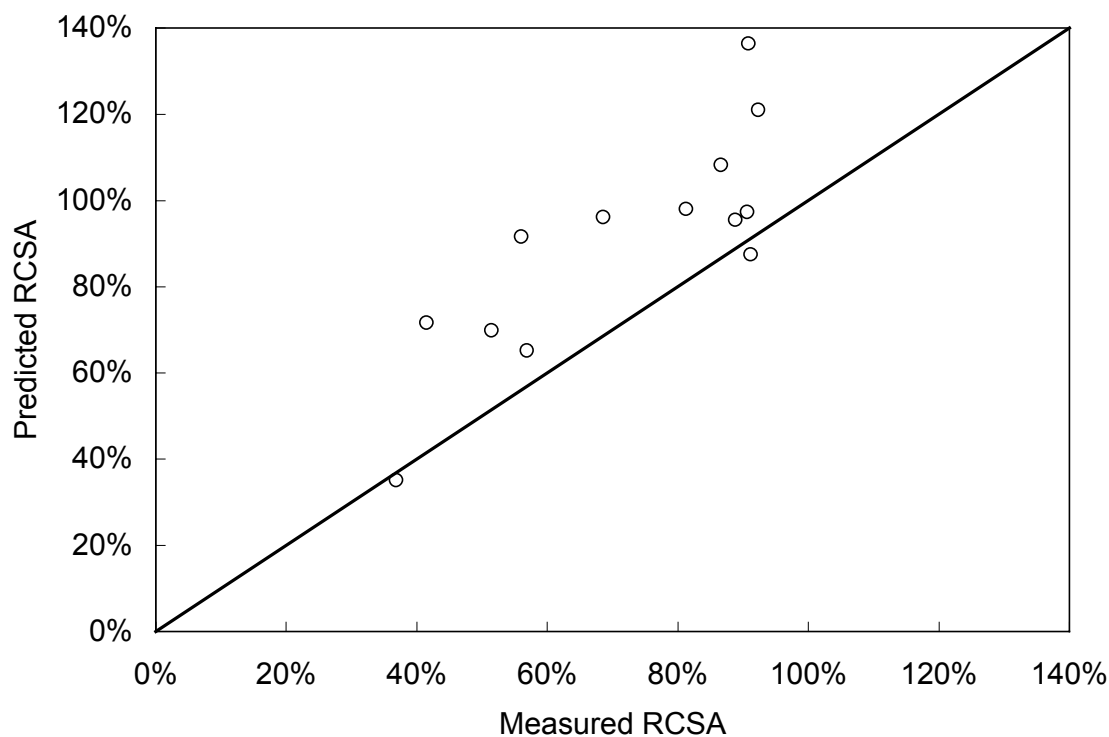


**Figure 8.24** Predicted RCSA vs. measured RCSA using the relationship developed in the laboratory.

The error associated with both condition evaluation relationships is summarized in Table 8.3. This table emphasizes a number of observations apparent upon comparison of Figures 8.23 and 8.24. The SSE value for the field relationship is less than the value for the laboratory relationship indicating that the field model generally produces a better prediction of RCSA. This conclusion is apparent in the preceding plots. Theoretically, all points should fall on the Line of Equality (LOE). In reality it is desirable for the points to fall on or below the LOE, indicating that when the procedure is incorrect, it is at least conservative. The points in Figure 8.23 fall on or around the line of equality while

many data points in Figure 8.24 fall above the LOE. The SE value for the lab relationship is six times that of the field relationship, indicating the laboratory relationship's tendency for overestimation of RCSA. The range of error is also apparent from the numbers in the table. The error of the field relationship ranges from -17.28% to 34.53% compared to -3.66% to 46.65% for the laboratory relationship. In other words, the laboratory relationship not only overestimates in most cases, but also has a greater magnitude of error in general.

**Table 8.3** Summary of errors associated with condition evaluation relationships.

	SSE <sup>1</sup>	MINIMUM ERROR	MAXIMUM ERROR	% OF CONSERVATIVE CASES
Field Relationship	1.09	-0.1728	0.3453	30.8
Laboratory Relationship	2.41	-0.0366	0.4565	15.4

Notes: 1 SSE is the sum of squared error ((predicted RCSA– measured RCSA)<sup>2</sup>).

## Chapter 9

### Conclusions

This research was performed to develop a database relating properties of stress wave propagation in timber to physical properties of timber pilings. The bending wave technique was used to measure wave propagation properties in the time and frequency domains in both laboratory and field specimens.

The development of a standard impact device for use in the bending wave technique that provides adequate and repeatable frequency content for analysis is essential. Because the technician performing the bending wave technique will vary, an impact device which reduces operator-to-operator variations is necessary. It is also important to produce consistent impacts to ensure adequate information can be obtained regularly. Of the various devices tested, the WSM-99 provides the most desirable impact. Variability due to operator inconsistency is reduced. The frequency content of waveforms produced from impacts made with the WSM-99 is in the desired range for condition assessment, 2000 to 3000 Hz. Stress wave properties measured from resulting impacts provides information that can detect a reduction in the cross-sectional area.

Variations in the internal structure of the pile influence wave propagation properties. These anomalies occur in the form of cracks, knots, pitch pockets, and growth rings. Because they introduce discontinuities in the medium, variations in measured stress wave properties will occur. Properties obtained from the frequency domain are sensitive to these discontinuities and therefore are unreliable in assessing the condition of timber pilings. The time domain is less sensitive to these variations and also provide more accurate information.

Variations in the condition of the contact surface between the impact device and the pile have a significant effect on wave propagation properties. These variations and their influence on properties measured in the time domain (more specifically, the phase velocity) can be reduced by obtaining repetitive measurements at each position along the length of the pile. Multiple surfaces have been considered in both laboratory and field stress wave testing. Although an average phase velocity of three circumferential positions might reduce occasional random errors, one position is recommended as part of the final procedure. This decision was made in light of significant cost and time savings.

The liquid content (LC) affects the wave propagation speed through timber. As the LC increases, the phase velocity decreases. Field and laboratory data confirm previous research done by both Chen (1995) and Qian (1997). A relationship between liquid content and phase velocity was identified for both CCA (laboratory) and creosote (field) treated piles.

The bending wave technique was utilized in the collection field of data from twenty-two installed timber pilings in North Carolina. Data obtained during the course of this research represents a wide range of pile and testing conditions. Out of twenty-two piles tested, eight were determined to contain damage. This information was used to create a chart for the condition evaluation of timber piles. Similar methods were utilized in a study of timber piles in the laboratory. A comparison of the accuracy for the final condition evaluation relationships for both field and laboratory has been performed.

Analysis of field data has produced a number of interesting findings. Frequency information appears to be inadequate for the condition assessment of timber piles. The natural variability of wood (cracks, checks and knots) as well as the presence of damage may introduce too many discontinuities for frequency information to be reliable. No trends were found in the frequency domain. Phase velocity information seems to be less sensitive to the variability of wood. A relationship was determined between phase velocity and liquid content for intact sections.

A framework for the condition assessment of timber piles has been developed. This tool has been defined as the condition evaluation chart. Phase velocity and liquid content information determined from the field can be combined with this tool to predict the remaining cross-sectional area of timber piles. The field relationship was found to be conservative in 30.8% of cases compared to 15.4% for the laboratory model. The range of error for laboratory relationship was also greater than that of the field model. SSE values for field and laboratory models were 1.09 and 2.41, respectively.

Future research in this area should focus on a number of topics. The chart for condition evaluation should not be thought of as the answer to all problems. Upon the completion of testing of additional installed timber piles, the relationship should be reevaluated and modified if necessary. A larger database could only add to the effectiveness of this method.

Additional research might also focus on compression tests of field and laboratory specimens to determine a correlation between them. Remaining cross-sectional area is very difficult to quantify in most field specimens obtained during this study. The significant difference in the characteristics of damage between laboratory and field piles makes the formation and verification of the chart extremely difficult.

Diameter corrections have not been included in the results contained herein. Previous research conducted by Chen (1995) has indicated the effect of diameter. Results from Murphy (1999) however were inconclusive. Although the diameter effect is thought to be far less significant than the affects of the factors discussed in Chapter 4, this correction would add to the accuracy of the method.

## List of References

- [1] Bendat, J.S. and A.G. Piersol. *Engineering Applications of Correlation and Spectral Analysis*. John Wiley & Sons, New York, 1970.
- [2] Bray, D.E. and McBride. *Nondestructive Testing Techniques*. John Wiley & Sons, Inc., 1992.
- [3] Brungraber, R., R. Gutkowski, W. Kindya, and R. McWilliams. "Timber Bridges: Part of the Solution for Rural America." *Transportation Research Record 1106, Fourth International Conference on Low Volume Roads*. Transportation Research Board, 1987.
- [4] Cartz, Louis, *Nondestructive Testing*. ASM International, Materials Park, OH, 1995.
- [5] Chen, Shunyi. "Condition Assessment of Installed Timber Piles and Comparison of Transform Techniques Using Stress Wave Method." *Ph.D. Dissertation*. North Carolina State University, Department of Civil Engineering, Raleigh, NC, 1995.
- [6] Degarmo, E.P., J.T.Black, and R.A. Kohser. *Materials and Processes in Manufacturing*. Macmillan, New York, 1988.

- [7] Donato, Paul J. "Development of Testing and Analysis Techniques for the Nondestructive Evaluation of Installed Timber Piles Using Stress Waves." *MS Thesis*. North Carolina State University, Department of Civil Engineering, Raleigh, NC, 1999.
- [8] Douglas, R.A., J.L. Eddy, and H.E. Wahls. On Transforms and the Dispersion Computations Used for Evaluating Layer Properties. *Nondestructive Testing of Pavements and Backcalculation of Moduli*, ASTM STP 1026. Baltimore, MD, 1989.
- [9] Eaton, R.A. and M.D.C. Hale. *Wood: Decay, Pests, and Protection*. Chapman & Hall, London, 1993.
- [10] Graff, K.F. *Wave Motion in Elastic Solids*. Ohio State University Press, 1975.
- [11] Holt, James Darrin. "Comparing the Fourier Phase and Short Kernel Methods for Finding the Overall Lengths of Installed Timber Piles." *Ph.D. Dissertation*. North Carolina State University, Department of Civil Engineering, Raleigh, NC, 1994.
- [12] Katzke, Evan D. "Nondestructive Evaluation of Asphalt Pavement Surface Layers Using Stress Wave Testing." *M.S. Thesis*. North Carolina State University, Department of Civil Engineering, Raleigh, NC, 1997.
- [13] Kim, Y.R., B. Kasal, S. Chen, and S.R. Auger. "Condition Assessment of an Underwater Timber Gate Using Dispersive Wave Propagation Analysis." *Proceedings of the 5<sup>th</sup> World Conference on Timber Engineering*. Lausanne, Switzerland, August 1998.

- [14] Kolsky, H. *Stress Waves in Solids*. Dover Publications, New York, NY, 1963.
- [15] Murphy, C.M. "Laboratory Evaluation of Stress Wave Propagation Properties in Timber Pilings Using the Bending Wave Technique." *MS Thesis*. North Carolina State University, Department of Civil Engineering, Raleigh, NC, 1999.
- [16] Pellerin, R.F., J.A. Lavider, R.J. Ross, R.H. Falk. "Nondestructive Evaluation of Timber Bridges." *Proceedings from the International Society for Optical Engineering, Nondestructive Evaluation of Material and Composites*. December, 1996.
- [17] Qian, Yu. "Nondestructive Evaluation of Structural Condition of Timber Piles Using Stress Wave Techniques." *M.S. Thesis*. North Carolina State University, Department of Civil Engineering, Raleigh, NC, 1997.
- [18] Ramirez, Robert W. *The FFT Fundamentals and Concepts*. Prentice Hall PTR, Englewood Cliffs, New Jersey, 1985.
- [19] Richart, F.E., J.R. Hall, and R.D. Woods. *Vibrations of Soils and Foundations*. Prentice Hall Inc., 1970.
- [20] Ross R.J., R.C. DeGroot, and W.J. Nelson. "Technique for Nondestructive Evaluation of Biologically Degraded Wood." *Experimental Techniques, The Society for Experimental Mechanics, Inc.* September/October, 1994.
- [21] Ross, R.J. and R.F. Pellerin,. "Nondestructive Testing for Assessing Wood Members in Structures: A Review." *Technical Report, United States*

*Department of Agriculture, Forest Service.* Forest Products Laboratory, 1994. General Technical Report FPL-GTR-70.

- [22] Ross, R.J., J.C. Ward, , and A. TenWolde. “Stress Wave Nondestructive Evaluation of Wetwood.” *Forest Products Journal*, Vol. 44, No. 7/8, 1994.
- [23] Ross, R.J., R.C. Degroot, W.J. Nelson, and R.K. Lebow. “The Relationship Between Stress Wave Transmission Characteristics and the Compressive Strength of Biologically Degraded Wood.” *Forest Products Journal*, Vol. 47, No.5, 1997.
- [24] Ross, R.J. and R.F. Pellerin. “NDE of Green Material with Stress Waves: Preliminary Results Using Dimension Lumber.” *Forest Products Journal*, Vol. 41 No. 6, 1991.
- [25] Ross, R.J., K.A. McDonald, and L.A. Soltis. “NDE of Historic Structures-USS Constitution.” *Proceedings from The International Society for Optical Engineering, Nondestructive Evaluation of Material and Composites.* December, 1996.
- [26] Wiggins, Lin. “Re: Timber Pile Data.” E-mail correspondence with the author, 1999.

# **NONDESTRUCTIVE EVALUATION OF THE STRUCTURAL CONDITION OF TIMBER PILES**

Project: HWY 98-5

## **Volume 2 of 2**

A Final Report Submitted to the  
North Carolina Department of Transportation  
*(FHWA/NC/2000-004)*

by

Y. Richard Kim, Ph.D., P.E.  
S. Ranji Ranjithan, Ph.D.  
Paul J. Donato  
Chris M. Murphy

Department of Civil Engineering  
North Carolina State University

May 2000

**Technical Report Documentation Page**

<b>1. Report No.</b> FHWA/NC/2000-004	<b>2. Government Accession No.</b>	<b>3. Recipient's Catalog No.</b>	
<b>4. Title and Subtitle</b> Nondestructive Evaluation of the Structural Condition of Timber Piles (Volume 2 of 2)		<b>5. Report Date</b> May 2000	
		<b>6. Performing Organization Code</b>	
<b>7. Author(s)</b> Y. Richard Kim, S. Ranji Ranjithan, Paul J. Donato, Chris M. Murphy		<b>8. Performing Organization Report No.</b>	
<b>9. Performing Organization Name and Address</b> Center for Transportation Engineering Studies Box 7908 Mann Hall North Carolina State University Raleigh, NC 27695-7908		<b>10. Work Unit No. (TRAIS)</b>	
		<b>11. Contract or Grant No.</b>	
<b>12. Sponsoring Agency Name and Address</b> North Carolina Department of Transportation Raleigh, NC 27699-1549  Federal Highway Administration 400 Seventh Street, SW Washington, DC 20590		<b>13. Type of Report and Period Covered</b> Final Report July 1998 – December 1999	
		<b>14. Sponsoring Agency Code</b> HWY-98-5	
<b>15. Supplementary Notes</b>			
<b>16. Abstract</b> <p>Condition evaluation of timber piles is currently based on traditional methods of visual inspection and sounding. Unfortunately, this method is vague and in many cases relies on interpretation of information and not on measurable parameters. Because nondestructive evaluation (NDE) using stress waves provides a fast and relatively inexpensive way of predicting the condition of in-service structural systems, these techniques have become an increasingly common tool for field evaluation of structural components. In this research, the bending wave technique has been used to measure wave propagation parameters for installed timber piles. Both laboratory and in-situ piles were tested in various conditions (i.e., liquid content and damage degree). The results were used to formulate analysis and testing procedures for quantitatively determining the condition of timber piles.</p> <p>In this research, a high correlation between stress wave parameters and the condition of timber was found. Stress wave properties measured in the time domain, more specifically the phase velocities, are effective indicators of the remaining sound cross-sectional area of timber pilings. Properties of stress wave propagation obtained from the frequency domain are unreliable and are sensitive to natural structural variations of timber. A strong relationship was observed between the phase velocities and liquid contents for intact sections. Controlled laboratory data from damaged pile sections were used in conjunction with information obtained from field specimens to develop a condition prediction model. In predicting the remaining cross-sectional area of field specimens, the prediction model yielded conservative results in 30% of the cases. A qualitative reject/accept criterion was also developed that distinguishes between intact and damaged pile sections.</p> <p>A field testing procedure evolved during the course of this research. The testing methods (that are utilized to obtain appropriate stress wave properties used to predict pile condition) as well as analysis procedures are presented. Additional testing of installed timber piles will allow for the improvement of the current analysis procedures and methods.</p>			
<b>17. Key Words</b> Timber pile Nondestructive evaluation Bending wave Remaining sound area		<b>18. Distribution Statement</b> No restrictions.	
<b>19. Security Classif. (of this report)</b> Unclassified	<b>20. Security Classif. (of this page)</b> Unclassified	<b>21. No. of Pages</b> 82	<b>22. Price</b>

## **DISCLAIMER**

The contents of this report reflect the views of the author(s) and not necessarily the views of the University. The authors are responsible for the facts and the accuracy of the data presented herein. The contents do not necessarily reflect the official views or policies of the North Carolina Department of Transportation nor the Federal Highway Administration at the time of publication. This report does not constitute a standard, specification, or regulation.

## **Abstract**

Condition evaluation of timber piles is currently based on traditional methods of visual inspection and sounding. Unfortunately, this method is vague and in many cases relies on interpretation of information and not on measurable parameters. Because nondestructive evaluation (NDE) using stress waves provides a fast and relatively inexpensive way of predicting the condition of in-service structural systems, these techniques have become an increasingly common tool for field evaluation of structural components. In this research, the bending wave technique has been used to measure wave propagation parameters for installed timber piles. Both laboratory and in-situ piles were tested in various conditions (i.e., liquid content and damage degree). The results were used to formulate analysis and testing procedures for quantitatively determining the condition of timber piles.

In this research, a high correlation between stress wave parameters and the condition of timber was found. Stress wave properties measured in the time domain, more specifically the phase velocities, are effective indicators of the remaining sound cross-sectional area of timber pilings. Properties of stress wave propagation obtained from the frequency domain are unreliable and are sensitive to natural structural variations of timber. A strong relationship was observed between the phase velocities and liquid contents for intact sections. Controlled laboratory data from damaged pile sections were used in conjunction with information obtained from field specimens to develop a condition prediction model. In predicting the remaining cross-sectional area of field specimens, the prediction model yielded conservative results in 30% of the cases. A qualitative reject/accept criterion was also developed that distinguishes between intact and damaged pile sections.

A field testing procedure evolved during the course of this research. The testing methods (that are utilized to obtain appropriate stress wave properties used to predict pile condition) as well as analysis procedures are presented. Additional testing of installed timber piles will allow for the improvement of the current analysis procedures and methods.

# Table of Contents

<b>List of Tables .....</b>	<b>v</b>
<b>List of Figures.....</b>	<b>vi</b>
<b>1. Introduction.....</b>	<b>1</b>
1.1 Motive for Procedure.....	1
1.2 Background.....	2
1.2.1 History of Nondestructive Evaluation.....	2
1.2.2 Definition: Nondestructive Evaluation.....	3
1.2.3 The Stress Wave Method.....	4
<b>2. Basic Principles of the Test Method.....</b>	<b>6</b>
2.1 Overview.....	6
2.1.1 The Bending Wave Testing Procedure.....	6
2.1.2 Energy Source (Impact Device).....	7
2.1.3 Sensors.....	8
2.1.4 Signal Acquisition.....	9
2.1.5 Signal Processing Tools.....	9
2.2 Stress Wave Parameters Used for Condition Assessment.....	10
2.2.1 Wave Speed and Phase Velocity.....	11
2.2.2 Determining the Wave Speed.....	11
<b>3. Stress Wave Analysis Program.....</b>	<b>16</b>
<b>4. Field Testing Procedure.....</b>	<b>25</b>
4.1 The Bridge Inspection Report.....	27
4.2 Recording Bridge Location.....	27

4.3	Pile Identification.....	28
4.4	Taking Pictures of Piles.....	28
4.5	Recording Pile Dimensions.....	28
4.6	Sketching the Pile and Bent.....	29
4.7	Rating a Pile.....	29
4.8	Pile Preparation.....	30
4.8.1	Snapping the Lines.....	30
4.8.2	Determining Sensor Locations.....	30
4.9	Equipment Setup.....	31
4.10	Stress Wave Testing.....	32
4.10.1	Data File Identification.....	32
4.10.2	Oscilloscope Settings.....	34
4.10.3	Collecting Data.....	35
4.11	Coring of Each Location.....	39
4.12	Drying of the Cores.....	40
4.13	Final Notes.....	40
<b>5.</b>	<b>Condition Evaluation.....</b>	<b>41</b>
5.1	Condition Evaluation Procedure.....	41
5.2	Analysis Examples.....	44
5.2.1	Pile AA, Chatham County Bridge #47 (Intact).....	44
5.2.2	Pile S, Warren County Bridge #64 (Damaged).....	51
5.2.3	Bridge #10, Chatham County (Field Demonstration to NCDOT).....	57
5.3	Summary.....	59
	<b>List of References.....</b>	<b>60</b>

<b>Appendix A: Reference Information for the Field Testing</b>	
<b>Procedure.....</b>	<b>61</b>
A.1 Typical Pile Information Sheet.....	61
A.2 Equipment Required for Testing.....	63
A.3 HMA Settings.....	64
<b>Appendix B: Laptop Setup Instructions.....</b>	<b>65</b>
B.1 Installation of SWAP Software.....	65
B.2 Installation of PCMCIA-GPIB Card.....	66

## List of Tables

5.1	Summary of information for AA1.....	51
5.2	Summary of information for S1.....	57
5.3	Phase Velocities for Bridge #10, Chatham County.....	58
5.4	Guidelines for obtaining a liquid content.....	59
A.1	Equipment used for stress wave procedure.....	63
A.2	Basic HMA settings.....	64

## List of Figures

1.1	Schematic diagram of basic test setup.....	4
1.2	Equipment used for stress wave tests.....	5
2.1	Field bending wave testing configuration.....	8
2.2	Typical raw signal obtained from the bending wave test.....	10
2.3	Typical raw signal obtained from the bending wave testing procedure.....	12
2.4	FFT plot for typical raw signal using the bending wave technique.....	13
2.5	SKM plot for typical raw signal shown in Figure 2.3 using the SWAP.....	14
3.1	The main menu of SWAP.....	17
3.2	Input file name screen.....	18
3.3	Raw data plot.....	18
3.4	FFT parameter screen.....	19
3.5	FFT calculation and plot module.....	21
3.6	Two channel FFT plot.....	21
3.7	SKM parameter screen.....	23
3.8	SKM calculation and plot module.....	23
3.9	SKM plot.....	24
4.1	Schematic of equipment setup.....	31
4.2	Example of high quality raw data.....	36
4.3	Example of poor quality raw data.....	38
4.4	Example of poor quality raw data.....	38
4.5	Schematic diagram of sensor, impact and coring locations.....	39
5.1	Phase velocity versus liquid content plot for qualitative indication of pile condition.....	42
5.2	Raw signal for first file collected at AA1.....	44
5.3	Raw signal for second file collected at AA1.....	45
5.4	Magnitude versus frequency plot of aaw11.....	46
5.5	Magnitude versus frequency plot of aaw12.....	47

5.6	SKM plot for aaw11.....	48
5.7	SKM plot for aaw12.....	48
5.8	Qualitative plot of phase velocity versus liquid content with AA1.....	50
5.9	The raw signal for s11.....	52
5.10	The raw signal for s12.....	52
5.11	The FFT plot for s11.....	53
5.12	The FFT plot for s12.....	53
5.13	The SKM plot for s11.....	54
5.14	The SKM plot for s12.....	55
5.15	S1 data plotted on the qualitative chart.....	56

# Chapter 1

## Introduction

Timber piles are a very common means of supporting a variety of structures. Factors such as ease of installation, strength, and low cost promote the use of timber piles use in bridges and piers. They have also been used extensively in the support of beach homes and mountain cottages (Holt et al., 1994a). The state of North Carolina maintains approximately 17,262 bridges, 2,964 of which are supported wholly or in part by timber pilings (Wiggins, 1999).

One problem with this versatile building material is its vulnerability to decay over time. This degradation comes in a number of forms. Rot, fungi and wood boring insects combined with a harsh environment lead to loss of strength and remaining cross-sectional area (or volume). Maintenance of bridges and other structures containing timber pilings requires the periodic evaluation of their condition to ensure public safety.

### 1.1 Motive for Procedure

Visual inspection, sounding and coring are the current methods of timber pile condition evaluation used by the North Carolina Department of Transportation. These practices do not give an adequate indication of pile condition. A need has developed for a method that produces more quantitative results. A nondestructive testing procedure for the determination of timber pile condition has become necessary.

A number of individuals have conducted research on the Nondestructive Evaluation (NDE) of timber piles. Stress waves (longitudinal or bending) and ultrasonic are among the most common methods used. Initial research focused on longitudinal stress waves. These tests however, are limited due to the inaccessibility of the pile top.

Chen (1995a) studied the feasibility of bending wave tests (with side impact). Qian (1997) performed additional research on this method.

The purpose of this research was to develop a nondestructive testing procedure for the condition evaluation of timber piles. This includes the evaluation of methods for in-situ moisture content determination and the development of relationships between stress wave parameters, moisture content and damage using laboratory and field data.

## **1.2 Background**

### **1.2.1 History of Nondestructive Evaluation**

The need for quality assurance in the testing of materials has been around since at least 400 BC. Ancient Athenian law contained strict guidelines concerning counterfeit currency. In ancient Greece, coins suspected of being counterfeiting were subject to the test of the touchstone (Varoufakis, 1996). The rubbing of a suspect coin would be compared to that of coins known to be official currency. These simple tests served as a tool to enforce the laws of antiquity and can be considered one of the first known uses of nondestructive evaluation.

Visual inspection is the most common form of nondestructive test. Some believe that the majority of material defects can be detected by eye. Visual inspection, however, does not yield quantitative results. Today, most applications desire more information, such as the size of flaw or the exact location of a defect or void, which visual inspection could not provide especially when defects are internal.

In recent years, NDE has developed into a very broad and complex field, which utilizes the latest technology to solve a variety of difficult problems. Listed below are some of the most common uses of NDE:

- Quality control and monitoring of processes
- Characterization of material properties
- Measurement of geometric characteristics

- Detection of internal or external imperfections

Today, NDE serves as a vital tool for maintenance and quality assurance in a wide variety of fields. Applications exist in all aspects of engineering including the nuclear, mechanical, and aerospace industries and in the evaluation of civil infrastructure.

### **1.2.2 Definition: Nondestructive Evaluation**

Non-destructive evaluation is the science of identifying the physical and mechanical properties of a piece of material without altering its end-use capabilities and using this information to make decisions regarding appropriate applications (Ross et al., 1998). Listed below are the typical steps pertaining to the performance of an established NDE procedure:

1. Experiments
2. Analysis
3. Conclusions
4. Determination of Appropriate Action

Experiments are performed on an object using one of many NDE methods, some of which are discussed in the next section. Data are obtained and processed according to the requirements of the testing procedure. Through signal processing raw data, obtained from the laboratory or field, are transformed into more useful information. These transformations are obtained using techniques which have been proven over the years (refer to Chapter 2). Many signal processing methods exist and they vary depending on the procedure and the experience of the NDE technician. The resulting information, allows a technician to make conclusions about the condition of the object in question. In the final step, a decision on the appropriate action to be taken is made (i.e., process adjustment, component replacement, etc.).

### 1.2.3 The Stress Wave Method

The stress wave method consists of the following key steps: an impact, data collection and analysis. An impact is made perpendicular to the pile's longitudinal axis. As the waves travel down the length of the pile, the sensors mounted to the pile surface record particle motion. This information is observed through an oscilloscope and is collected on a personal computer. A schematic diagram of the basic test setup is shown in Figure 1.1.

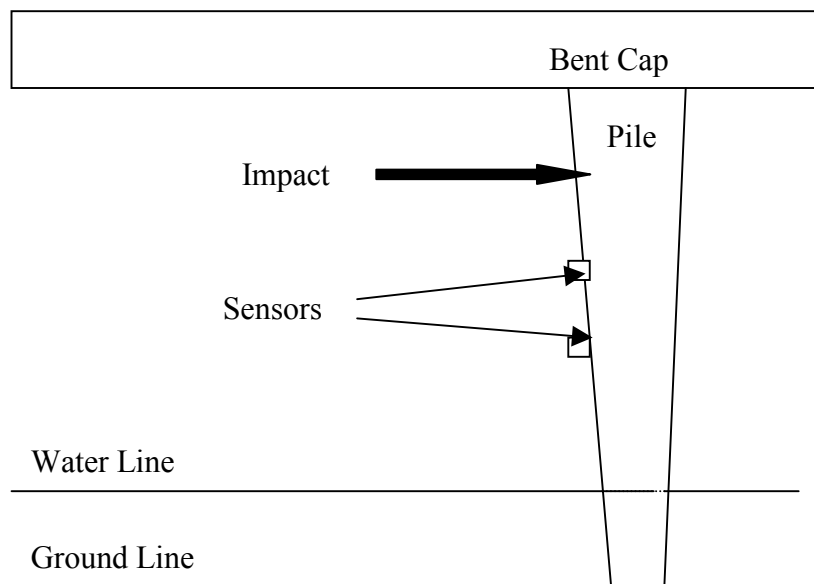


**Figure 1.1** Schematic Diagram of Basic Test Setup

The equipment used in these tests consists of the following:

- Impact Device
- Sensors
- Signal Conditioner
- Tektronix Oscilloscope

- Personal Computer

A photograph of the basic equipment used during the course of this research is shown in Figure 1.2.



**Figure 1.2** Equipment used for stress wave tests.

## **Chapter 2**

### **Basic Principles of the Test Method**

#### **2.1 Overview**

The bending stress wave technique is similar to the longitudinal technique described by Ross et al. (1997). A stress wave is induced by an impact made on the pile's surface. This creates a stress wave field consisting of, but not limited to: shear, compression (longitudinal), surface (Rayleigh), and flexural waves. Wave propagation is detected by a linear array of sensors attached along the longitudinal axis of the pile. The particle displacements detected by the sensors are then converted to voltages and displayed as digitized signals on an oscilloscope. Signal processing tools are then used to determine information necessary to evaluate the condition of the medium.

This technique does not distinguish between types of waves. Although bending waves are thought to contain the most energy, raw data from a stress wave test contains information from a combination of several mechanical inputs to the accelerometers by the various components of the structure (Douglas et al., 1989). Many studies, however, have determined relationships between material properties and stress wave parameters using similar test methods. This has led to the conclusion that at least one wave, most likely the flexural component, is dominant in the signal.

##### **2.1.1 The Bending Wave Testing Procedure**

An impact is made perpendicular to the surface of the pile, inducing a stress field that propagates radially outward from the point of origin. Depending on the frequency composition required for evaluation, the impact is made with the appropriate impact mechanisms. In this research, different devices were utilized with varying material

properties. Through experimentation, it was found that wood was the most desirable material for creating an impact, most likely due to the matching impedance of the materials.

Sensors were attached to the timber pile through a magnetic head that is coupled to one-inch roofing nails. In this research, piezoelectric accelerometers were used to measure the particle accelerations along the wave front. Four accelerometers were attached in a linear fashion at one-foot intervals along the longitudinal axis of the pile. As the disturbance propagates through the medium (induced by the impact device), the resulting particle motion is captured using a digital oscilloscope. The sensors measure the particle acceleration. The oscilloscope reads the voltage changes from each sensor as the wave front passes and plots them as a function of time. The raw signal is transferred and stored on a computer. Signal processing tools developed at North Carolina State University are then used to determine spectral information and wave propagation speeds. A diagram of the testing procedure used in the field is given in Figure 2.1.

### **2.1.2 Energy Source (Impact Device)**

One of the critical aspects in successfully using the bending wave technique for condition assessment is creating a proper impact. Most importantly, the impact must create a signal containing the frequency range of interest. For this research, the frequency range used was approximately 2000 to 3000 Hz. Also, operators using this technique have rarely any formal training in the use and interpretation of stress wave information. Therefore, it is particularly important to provide an impact that not only provides adequate spectral information but also relies minimally on user discretion. This will reduce random errors due to the impact-to-impact variations and operator-to-operator variations. The appropriate impact can be supplied using the WSM-00 or WSM-99 devices.

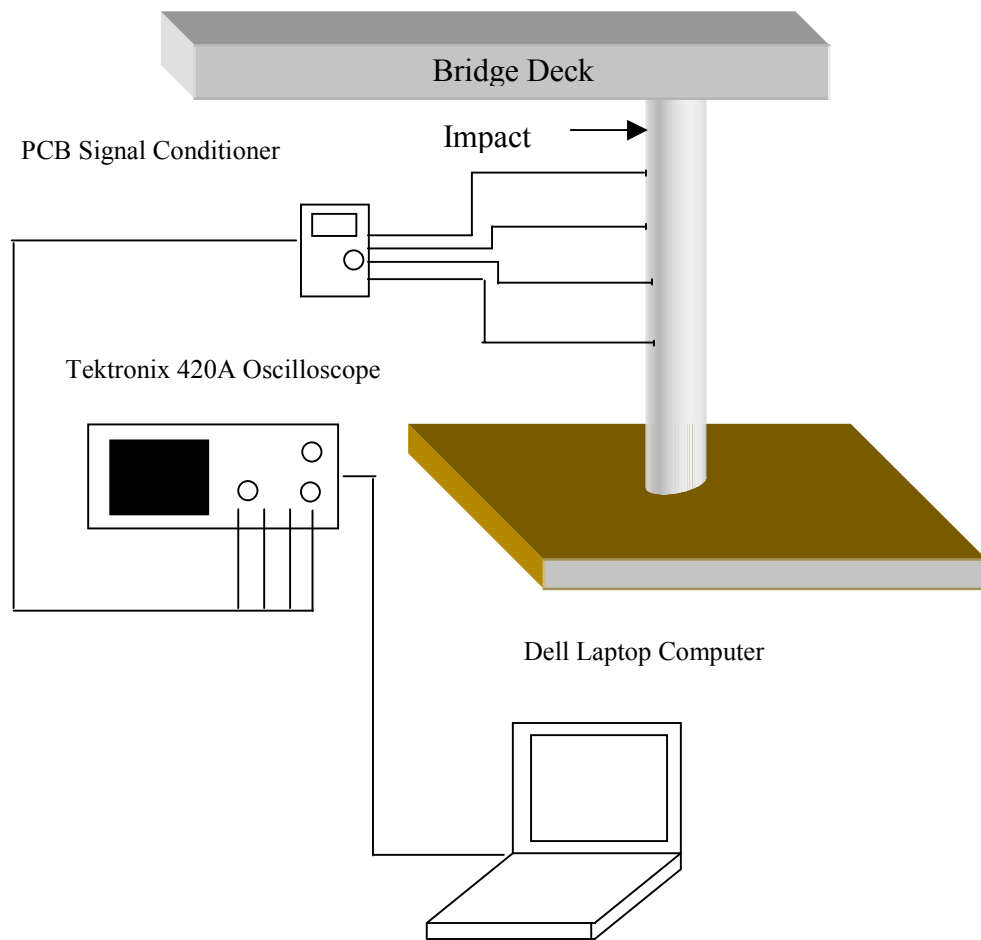


**Figure 2.1** Field bending wave testing configuration

### 2.1.3 Sensors

Upon disturbing the medium by an impact to its surface, a wavefront will propagate radially outward in all directions, inducing particle motion. The particle motion results from shearing action of adjacent particles as the wavefront passes. For this research, PCB model 303A02 piezoelectric accelerometers were used to measure the particle accelerations at the pile surface. The measured particle acceleration is then converted to voltage and stored on a digital oscilloscope. A laptop computer is used to collect the data from the oscilloscope.

Sensors are attached in a linear fashion along the longitudinal axis of the pile. The accelerometers have magnetic heads that allow coupling to the pile surface with the use of standard roofing nails. Roofing nails have a large diameter head that provides sufficient area to mount the gages. The nails should be driven in such a manner that the head does not touch the surface of the pile. The accelerometers were connected to a PCB Piezotronics ICP power supply, model 482A05. The power supply was then connected to an oscilloscope using standard coaxial cable.

#### **2.1.4 Signal Acquisition**

When measuring particle displacements, the time base is used to generate a time axis for an amplitude history that will completely describe the waveform. The oscilloscope uses a ramp voltage to drive an electron beam at a constant rate across the face of a CRT (cathode ray tube). The measurement of the signal drives the pen or CRT trace in a direction normal to the time-base drive, which results in a time history of amplitude variation (Ramirez, 1985). The time base is partitioned into equal intervals, normally reported in milliseconds. A typical bending wave is shown in Figure 2.2.

It is of particular importance to collect a sufficient number of points to fully describe the waveform. If the time window is too short, an incomplete picture of the waveform will be displayed from which few conclusions regarding wave shape and type can be discerned. The sampling rate can be adjusted to vary the time window using the horizontal scaling function. Vertical scaling of the waveform can also be performed to enhance signal clarity. For this research, a Tektronix 420 digital oscilloscope was used.

#### **2.1.5 Signal Processing Tools**

Once a signal is obtained, it must undergo signal processing to determine spectral information that characterizes the waveform. The Stress Wave Analysis Program (SWAP) contains features that can be utilized to determine necessary wave propagation parameters. SWAP is a program written in Visual Basic that has the capability of data acquisition and signal processing. SWAP has built-in utilities that perform frequency-

domain analysis using the FFT for the calculation of frequency parameters and time-domain analysis for the construction of the dispersion field using either SKM or Fourier Phase Methods. SWAP also has the capability of graphically presenting the information to ensure data is presented in a convenient and organized manner. The features and uses of SWAP will be described in Chapter 3.

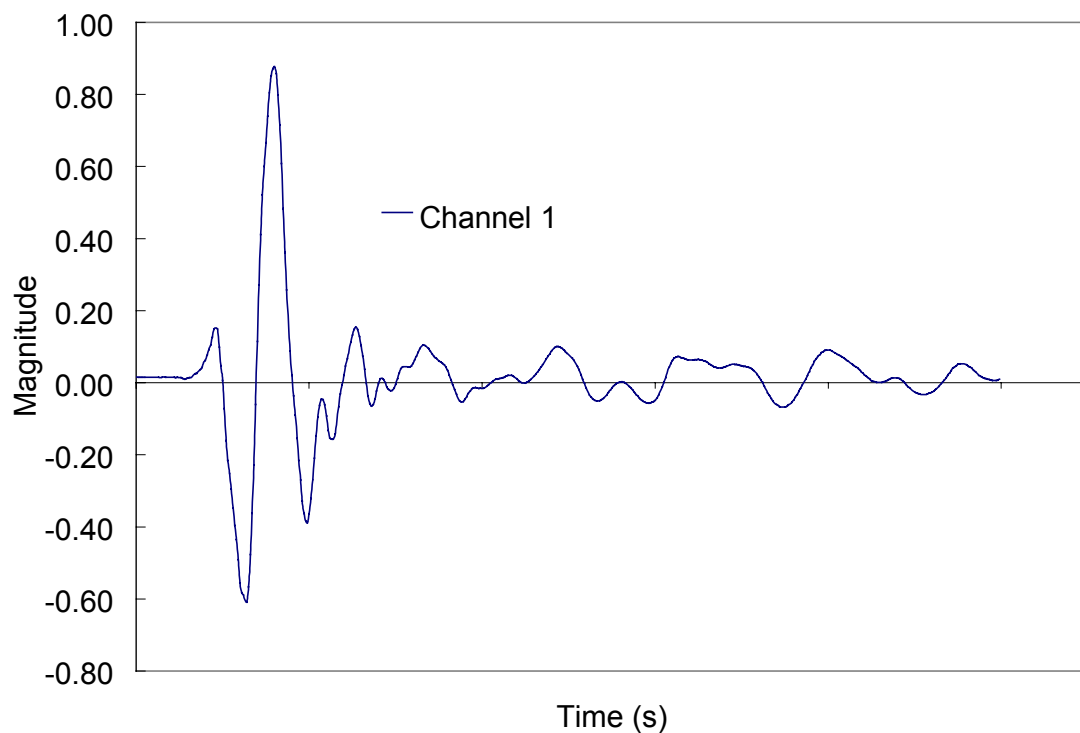


**Figure 2.2** Typical raw signal obtained from the bending wave test.

## **2.2 Stress Wave Parameters Used for Condition Assessment**

As stress waves propagate through the medium, their characteristics reflect the material properties of the medium through which they are passing. These parameters are

used as evaluation tools in non-destructive testing procedures. Terms that are important in the characterization of material properties are described below.

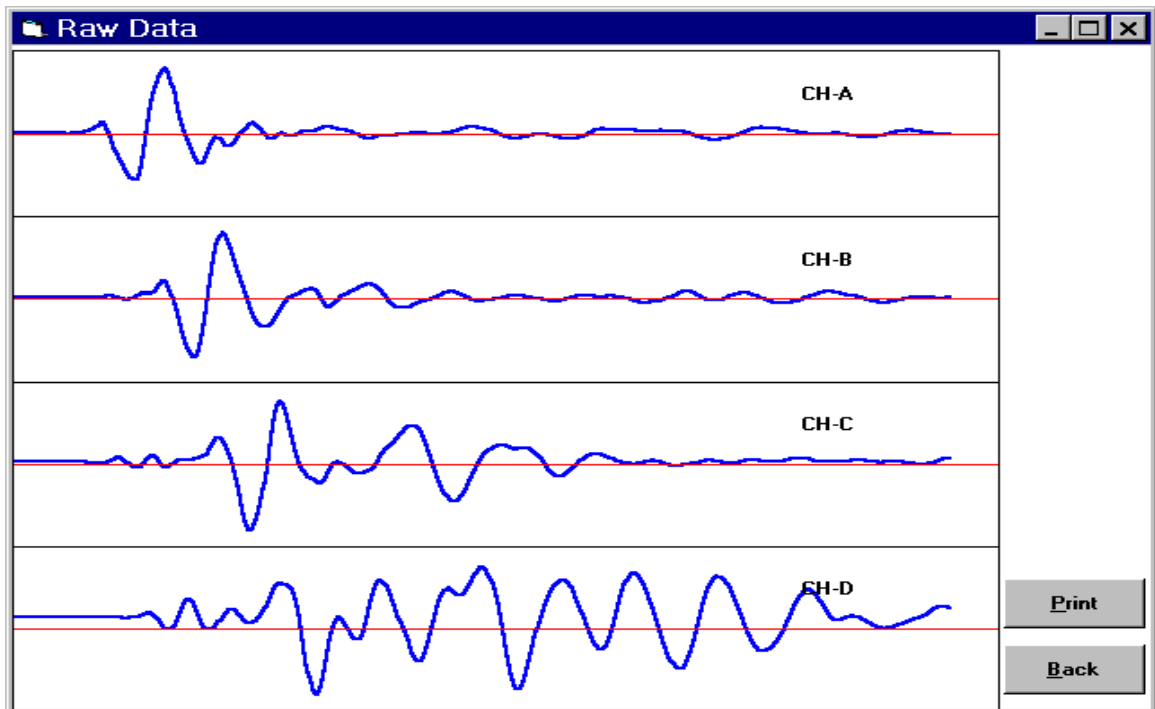
### **2.2.1 Wave Speed and Phase Velocity**

Throughout this document, wave speed and phase velocity have been used to describe the speed of transmission of elastic wave propagation through a specific medium. It is important to distinguish the difference between them. The wave speed is the speed of the elastic wave propagating through the medium. As discussed previously, a stress wave is composed of many frequencies, traveling at their own specific velocities. Using signal processing techniques, an attempt is made to isolate frequencies that are the greatest in magnitude using the FFT and SKM. The phase velocity is the speed at which a specific frequency contained within the stress wave is traveling. Therefore, for a single stress wave there exists one wave speed, while there are many phase velocities depending upon the frequency of interest.

### **2.2.2 Determining the Wave Speed**

Because many frequencies are embedded in a single waveform, it is difficult to obtain a theoretical value for the wave speed. Inclusions and discontinuities in the timber also inhibit the path of the waveform, influencing wave propagation speeds. The wave speed must be determined experimentally.

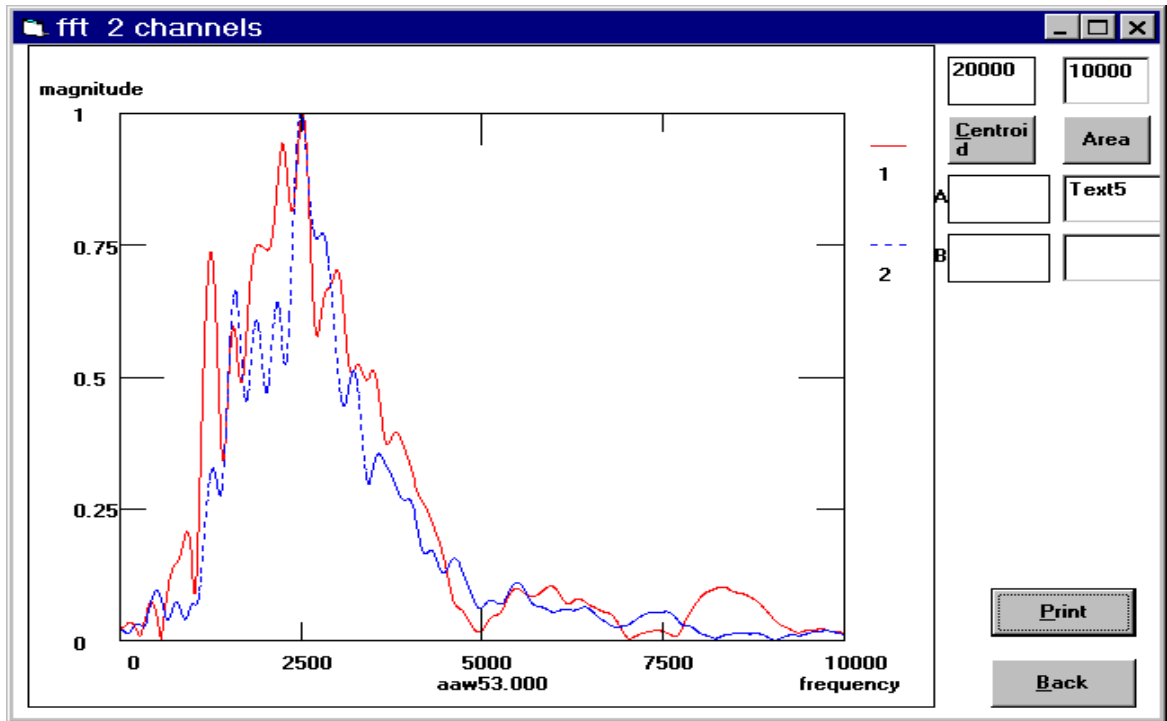
A typical waveform is measured using the bending wave technique as described in Section 2.1.1. The resulting waveform is then stored on a computer as a time versus amplitude record, which is processed at a later time using SWAP. Figure 2.3 shows a typical raw waveform displayed using the SWAP.



**Figure 2.3** Typical raw signal obtained from the bending wave testing procedure.

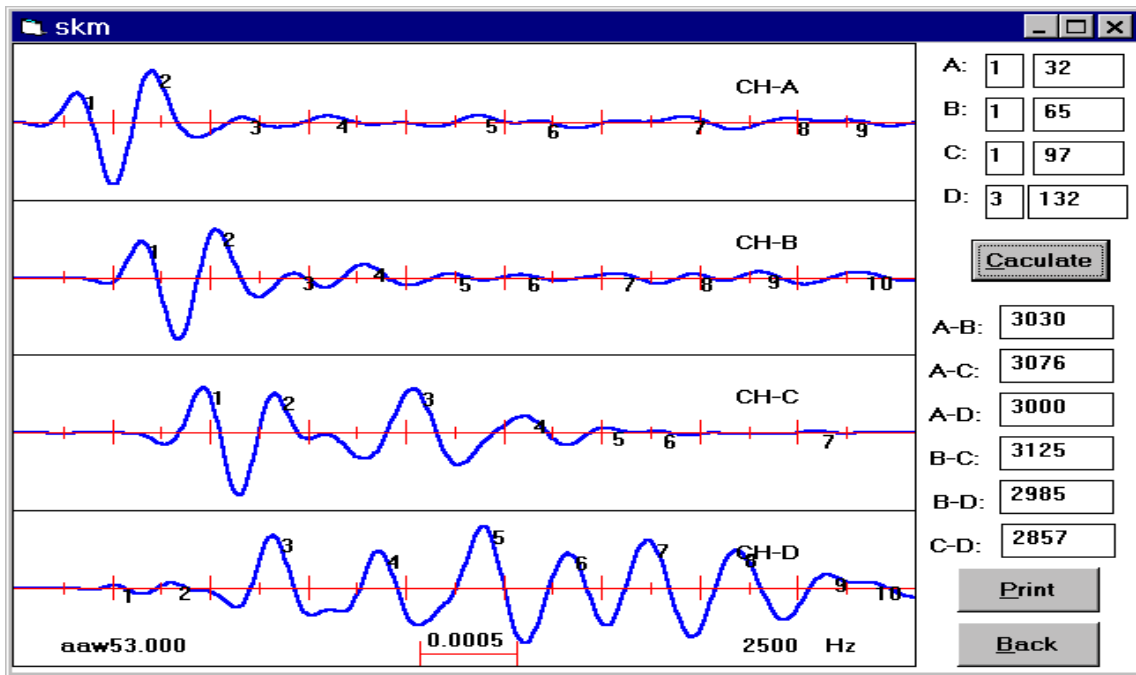
CH-A through CH-D represent the corresponding measured waveform detected at each sensor location. Figure 2.4 is the Fast Fourier Transform (FFT) plot for the signal shown in Figure 2.3. The plot illustrates the frequencies that compose the waveform and the corresponding magnitudes. From Figure 2.4, the dominant frequency, i.e., the frequency with the greatest magnitude embedded in the waveform, is approximately 2500 Hz. This is the frequency that is used as the “kernel” in the Short Kernel Method (SKM).

Figure 2.5 shows the SKM plot of the time records obtained for the signal measured in Figure 2.3 using a 1 cycle 2500 Hz kernel for each channel. The SKM has acted as a “sieve” in that it extracted the 2500 Hz component from the signal and displayed its approximate location on the time records of each channel. A large amplitude in each channel corresponds to how well the kernel is aligned with the raw signal.



**Figure 2.4** FFT plot for typical raw signal using the bending wave technique.

To calculate the phase velocity, one can use the first positive peak labeled 1 in Figure 2.5. In theory, the raw signal will maintain its form while appearing at each sensor location at different times, first appearing at the sensor location closest to the impact, then at the next furthest sensor, and so on, until sampling is terminated. Corresponding peaks in each channel indicate when the waveform passed that location. In the raw signal (Figure 2.3), corresponding peaks are difficult to detect in CH-C and CH-D. However, with the use of the SKM, the corresponding peaks can be determined.



**Figure 2.5** SKM plot for typical raw signal shown in Figure 2.3 using the SWAP.

In Figure 2.5, after signal processing using the SKM, one can see the peak labeled 1 in CH-C corresponds to the peak labeled 3 in CH-D. Finally, knowing the distance between sensors, and the time (as recorded in the amplitude-time record for each channel), the wave speed can be determined using the following equation:

$$V_{ph} = \frac{D}{n \times \Delta t}$$

where,

$V_{ph}$  = phase velocity of a specific frequency contained within the waveform (ft/s).

$D$  = distance between accelerometers (ft).

$n$  = the number of data points between peaks.

$\Delta t$  = the time interval between data points obtained from the oscilloscope.

For the waveform shown in Figure 2.5, the phase velocity determined using a 2500 Hz kernel is 3030 ft/s. In other words, this is the velocity of the 2500 Hz wave as it travels from the first to the second sensor (CH A to CH B).

## Chapter 3

### Stress Wave Analysis Program

Analysis software for stress wave testing has evolved over the years through the research and experience of the Stress Wave Analysis Group (SWAG) headed by Dr. Y. R. Kim at North Carolina State University. *As of the writing of this document, analysis software was not yet completed and therefore certain functions shown on the screen menus are not described here because their use was being investigated.* Functions pertinent to the conclusions of this document are thoroughly described in the sections below.

The Stress Wave Analysis Program (SWAP) is a program written in Visual Basic (version 4.0) for the acquisition and processing of test data. A graphical interface provides a convenient working environment for data collection, analysis and data presentation. SWAP has the ability to perform frequency-based analysis using the Fast Fourier Transform (FFT) and time domain analysis using the Short Kernel Method (SKM).

FFT functions can be used to calculate attenuation ratios and centroid and dominant frequencies. Phase velocities can be obtained using the SKM module. Figure 3.1 shows the main menu containing all of the features of SWAP. The functions of the keys shown in Figure 3.1 are described below under bold-faced headings that represent the names of the respective button.

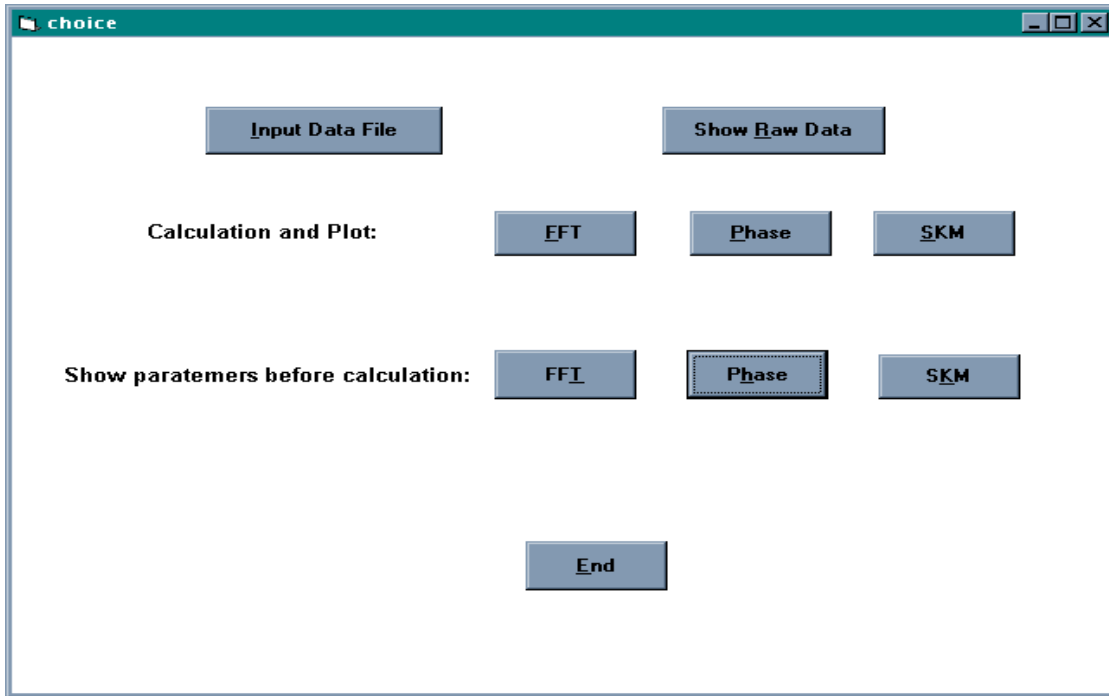


**Figure 3.1** The main menu of SWAP.

**Input Data File:** Enter file name for data collection or analysis. This screen is shown in Figure 3.2. The first step in the utilization of SWAP is to indicate the data file to be analyzed or collected. The program will fail if a data file name is not typed into the field shown in Figure 3.2. If a file already exists, input the name and click first on the “Ok” button. To return to the main module for analysis press “Back.” To collect data from the oscilloscope, input the desired file name and click on “Collect Data.” The program will download raw data from the Tektronix oscilloscope and retrigger the device. In other words, when raw data is collected, the SWAP automatically prompts the oscilloscope to be prepared for another collection. If data are not collected because the quality is poor, the oscilloscope trigger button will have to be pressed manually for the signal from the next impact to be received.

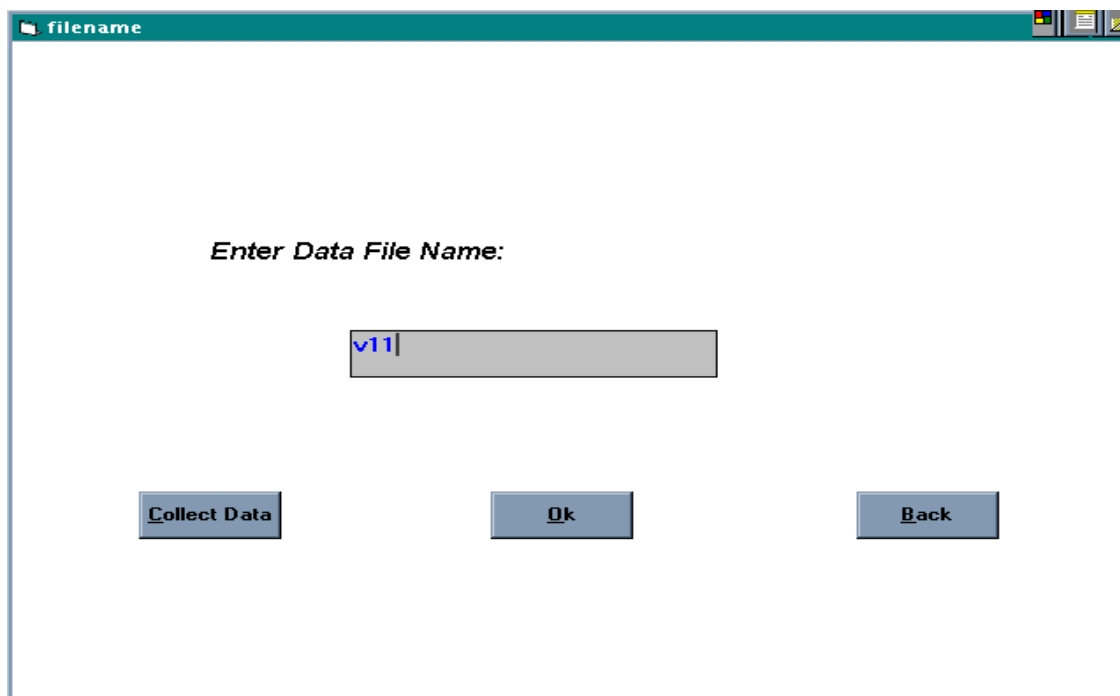


Figure 3.2 Input file name screen.

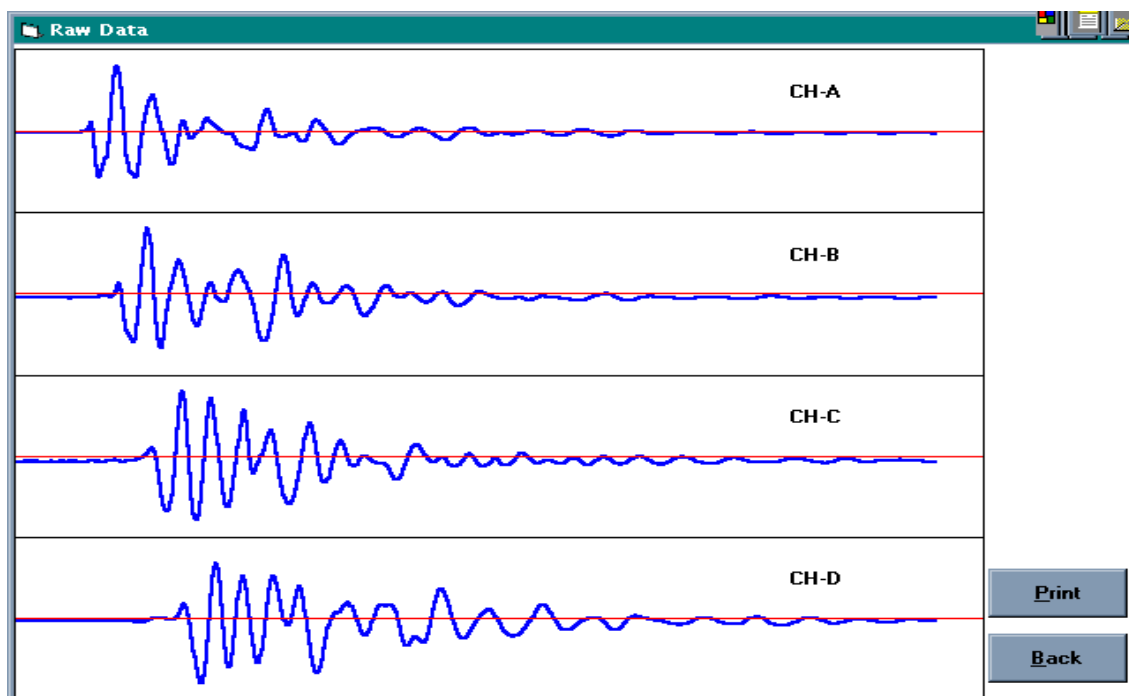


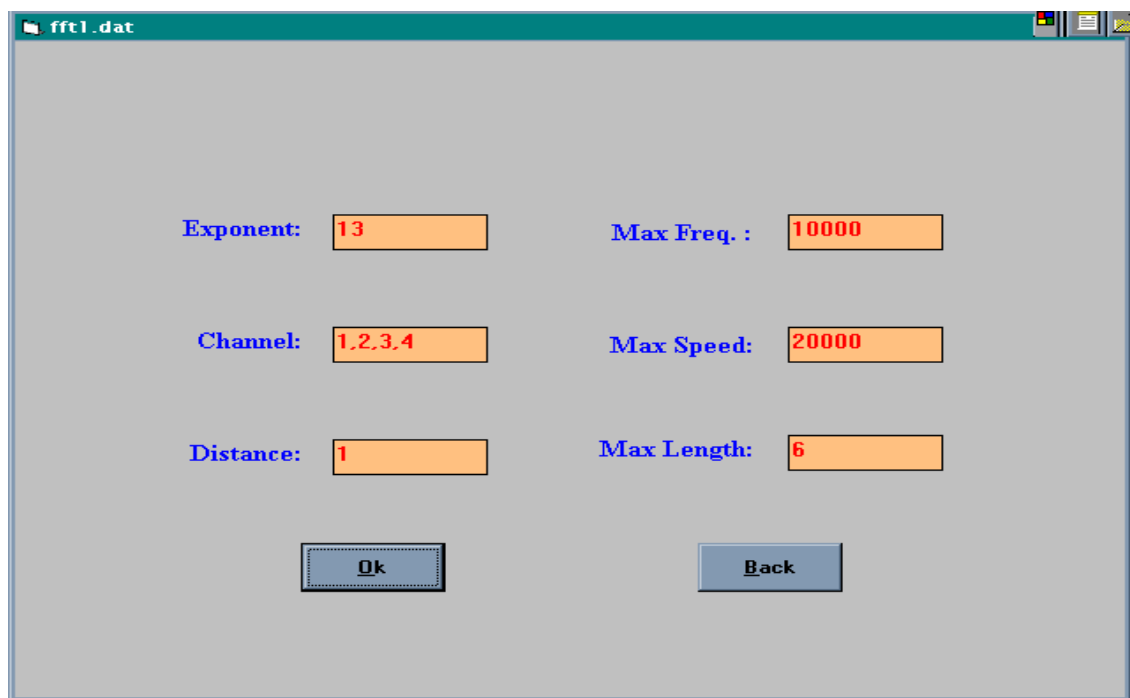
Figure 3.3 Raw data plot.

**Show Raw Data:** Shows data in its original form. See Figure 3.3 for raw data screen. This plot should be an exact copy of what is shown on the oscilloscope screen.

**FFT (show parameters before calculation):** The FFT parameter screen is shown in Figure 3.4. A list of the parameters is shown below. The number listed in parentheses is the required value and for the purposes of this procedure they should remain unchanged.

- maximum frequency (10,000) – maximum frequency in plotted frequency spectrum
- channels (1,2,3,4) – channels to be displayed in spectrum plot
- exponent (13) – exponent of value “13” for proper FFT operation
- distance (1) – standard one foot sensor spacing

A click on the “Ok” button in this module will bring up the FFT calculation and plot module. Clicking the “Back” button will lead to the FFT parameter screen.



The screenshot shows a window titled "fft1.dat" with a grey background. It contains six input fields arranged in two columns. The left column has "Exponent:" with value "13", "Channel:" with value "1,2,3,4", and "Distance:" with value "1". The right column has "Max Freq.:" with value "10000", "Max Speed:" with value "20000", and "Max Length:" with value "6". At the bottom, there are two buttons: "Ok" on the left and "Back" on the right.

Exponent:	13	Max Freq.:	10000
Channel:	1,2,3,4	Max Speed:	20000
Distance:	1	Max Length:	6

Ok Back

**Figure 3.4** FFT parameter screen.

**FFT (calculation and plot):** The FFT calculation and plot screen is shown in Figure 3.5. A click on “Ok” will run the FFT analysis and a status bar on the bottom of the Windows 95/98 desktop will indicate when calculations have been completed. The message “finished - fft” will appear next to an MSDOS icon. Upon completion, there are three choices for FFT plot format.

- Plot A – Plot of single channel. Enter desired channel number.
- Plot A\*B – Plot of two channels. Enter desired channel numbers (usually 1 and 2).
- Plot 4ch – Plot all four channels.

An example of the two-channel plot is shown in Figure 3.6. A click on one of the above buttons prior to the completion of calculations will cause an error and the program will shut down. Centroid frequency and area information can be obtained by clicking on the appropriate buttons.

To print any screens from the stress wave analysis program, the screen contents must be copied to the clipboard and pasted into Word or similar software. The print functions of SWAP were rendered inoperable upon the upgrade to Windows 95. The steps for printing are described below:

- Minimize or close all applications except for SWAP.
- Obtain the desired screen or graph.
- Place mouse icon on the SWAP screen.
- Simultaneously press the “Alt” and “Print Screen” buttons on the keyboard.
- Paste the item into a Word (or equivalent) document and size accordingly.

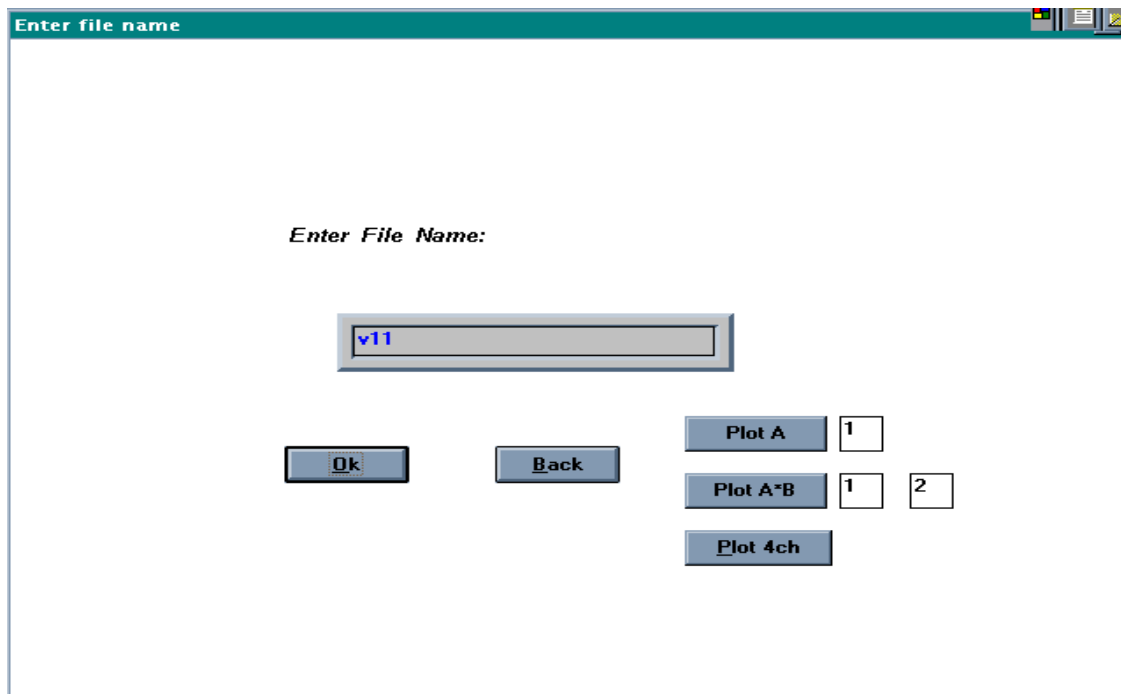


Figure 3.5 FFT calculation and plot module.

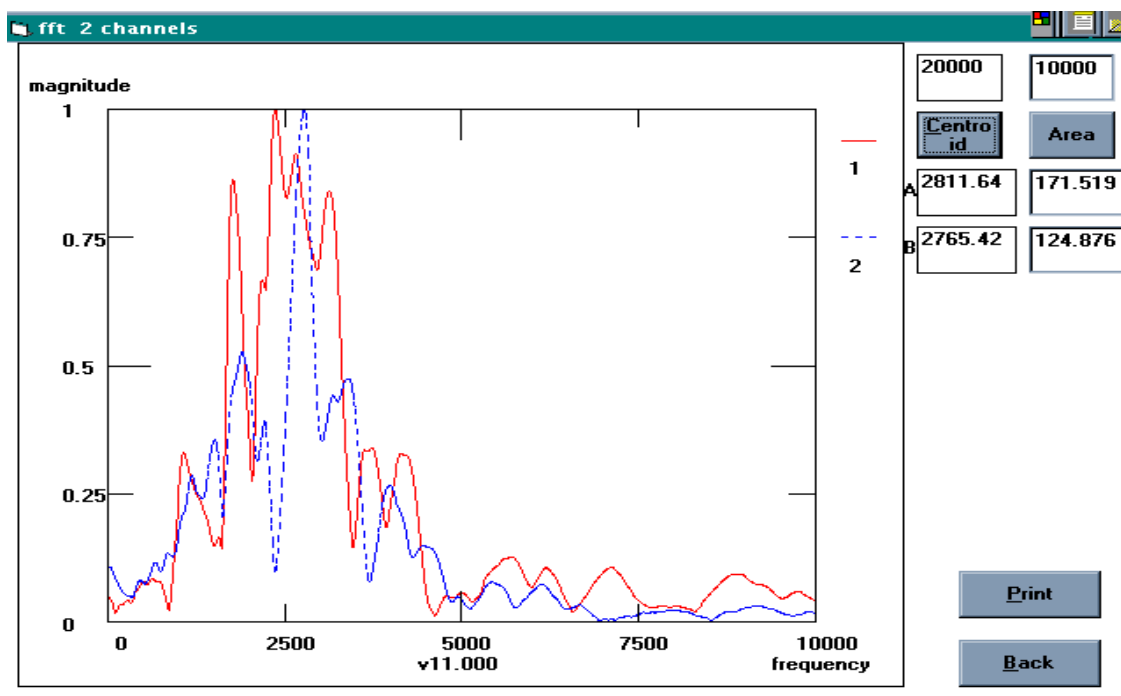


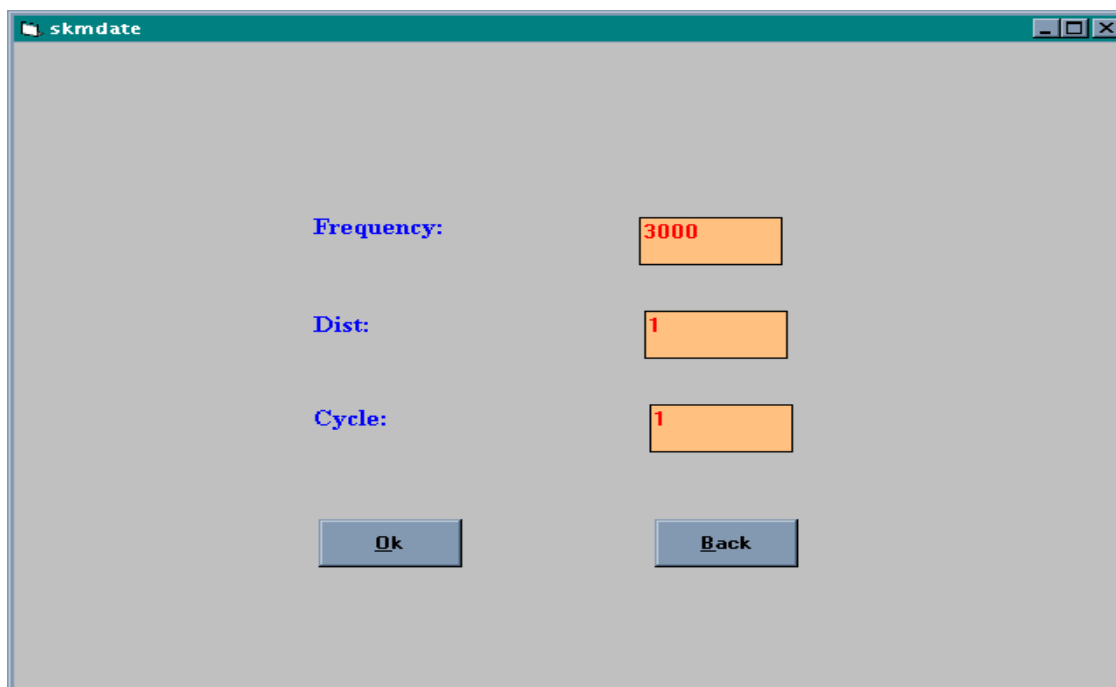
Figure 3.6 Two channel FFT plot.

**SKM (show parameters before calculation):** The SKM parameter screen is shown in Figure 3.7. Listed below are the SKM parameters, definitions and typical values. Typical values appear in parenthesis (these values should remain unchanged).

- frequency (2500) – This is the kernel used to calculate the time domain plot of a specific phase in the raw signal. 2500 Hz is the standard kernel used for this procedure.
- dist (1) – This is the distance or sensor spacing, which is set at the standard one foot.
- cycle (1) – The number of cycles or wavelengths of the kernel. One cycle has been set as a standard.

A click on the “Ok” calls the SKM calculation and plot module. Clicking “Back” will bring up the main menu.

**SKM (calculation and plot):** The SKM calculation and plot module are shown in Figure 3.8. A click on “Ok” will run the SKM calculations and a status bar will appear on the bottom of the desktop. When the message reads “Finished – skm4,” it is then permissible to proceed to the actual plot screen. When the “plot” button is selected, a screen similar to that shown in Figure 3.9 will appear.



skmdate

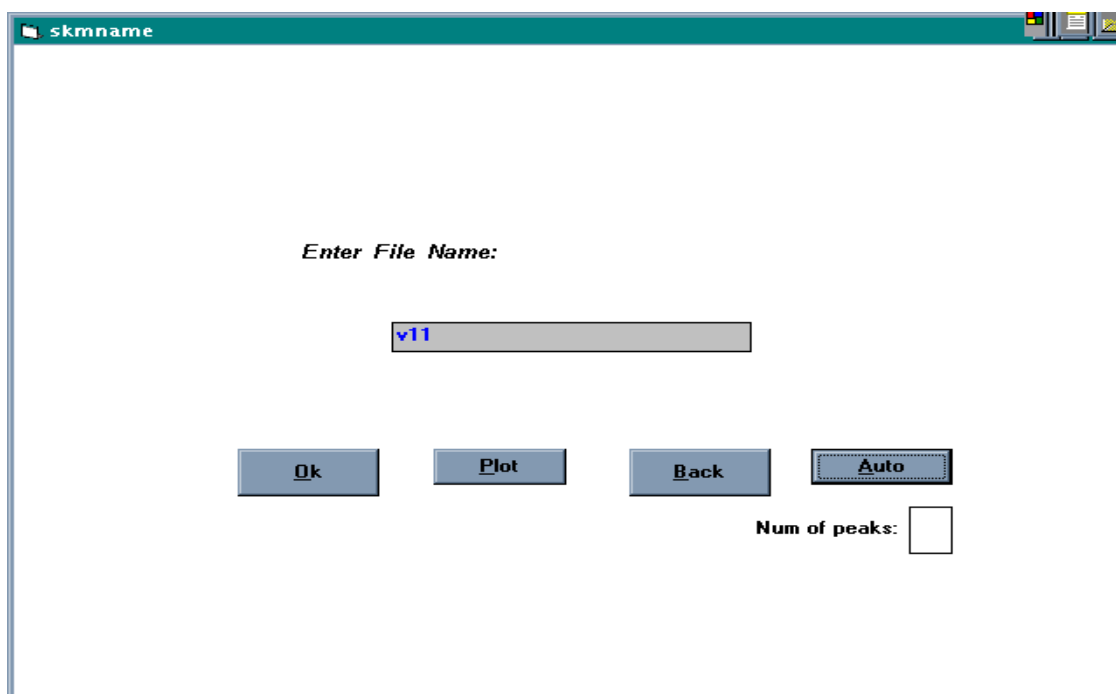
Frequency: 3000

Dist: 1

Cycle: 1

Ok Back

Figure 3.7 SKM parameter screen.



skmname

Enter File Name:

v11

Ok Plot Back Auto

Num of peaks:

Figure 3.8 SKM calculation and plot module.

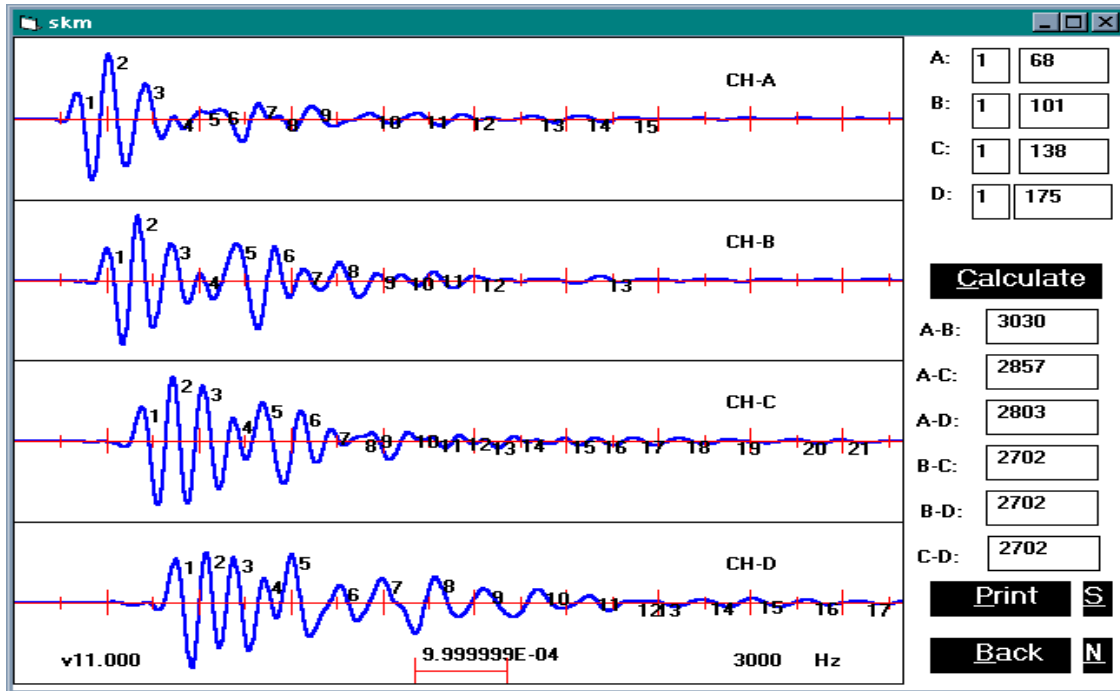


Figure 3.9 SKM plot.

SWAP is very useful in stress wave applications. The graphical interface makes it easy to use and understand. Unfortunately not all of the bugs have been eliminated from the program at this time. Most errors will shut down the program. Some of the most common causes of error are listed below:

- Trying to plot the FFT or SKM before the calculations have been finished
- Attempting to perform analysis on a file that does not exist.
- Placing the wrong type of character in a field. In other words, putting a letter where a number is supposed to appear and vice versa.
- Using a button or function not mentioned in this chapter. These functions were still being evaluated at the time of this writing and they should be ignored.

## Chapter 4

# Field Testing Procedure

The procedure presented in this chapter was developed as a result of the field testing of 22 timber piles. Field testing of timber piles requires the completion of a number of tasks to obtain all necessary information required for successful NDE. At least two technicians are needed to execute this procedure; one person impacting the pile and the other to adjust the scope and collect data. Listed below are general steps (in the order they should be performed) for the preparation, performance and completion of field inspection of timber piles using the bending wave method. Details of each setup are described in the subsequent sections.

1. Read the bridge inspection report.
2. Record the bridge location and other information.
3. Identify the piles to be tested.
4. Take pictures of piles to be tested.
5. Record the pile's dimensions.
6. Sketch the pile and the bent to which the pile belongs.
7. Rate a pile by sounding and appearance.
8. Pile preparation.
9. Equipment setup.
10. Performance of bending wave tests.
11. Core the tested locations.
12. Dry the Cores in the Halogen Moisture Analyzer.

The tools and equipment utilized in this procedure are fairly standard. It most important is that all of the necessary information is properly obtained. A list of the tools and equipment necessary is shown below:

**Computer Equipment:**

Laptop personal computer equipped with SWAP and AUTOSWAP software

Tektronix oscilloscope, Model TDS 420

National Instruments connecting cable (connects laptop to oscilloscope)

Four PCB sensors with magnetic tips (optional waterproofing and cable length at user's discretion)

PCB signal conditioner

Four PCB cables (connects signal conditioner to the oscilloscope)

**Tools:**

1. Tape measure
2. Chalk line (to make a straight line for sensor attachment)
3. 1" galvanized roofing nails (used to mount sensors)
4. Carpenter's hammer (place roofing nails)
5. Plastic sandwich bags with zipper (storage of cores)
6. Permanent marker (to label bags with cores)
7. Coring device
8. Large nails (to start hole for coring)
9. Double headed nail (to unclog coring device)
10. Spray paint (mark pile after testing)
11. WSM-99 (standard impact device)
12. Modified hammer (impact device)
13. Extension cord
14. Surge protector

15. Gas generator

**Miscellaneous:**

1. Bridge inspection report
2. Pile information sheets
3. Index cards
4. Waders (if necessary)

## **4.1 The Bridge Inspection Report**

Prior to on-site inspection, a full evaluation of the present site conditions should be made from the bridge inspection report. This document has information pertaining to the super-structure such as (but not limited to): materials, location, photographs and previous inspection conditions. This will give the field technicians an idea of what type of conditions to expect (i.e., deep water, traffic, etc.).

## **4.2 Recording Bridge Location**

A pile data sheet, similar to that shown in the Appendix A, should be used to record the following information: bridge number, county, date, type of bridge, number of bents, treatment type and locations of piles being tested. This information will be useful to those individuals not present during field testing.

A brief description of the bridge should include water levels (if applicable) and orientation (i.e., whether the piles considered for testing are on the east, west, north, or south side of the roadway). Any other information thought to be pertinent for future evaluation should be recorded as well.

### **4.3 Pile Identification**

Inspection teams of the NCDOT use visual observation, sounding and coring to estimate a pile's integrity. Once a pile's integrity is suspect, a more detailed analysis will be performed using the bending wave technique. The locations of piles to be tested are identified by inspection teams. Inspection teams should label suspect piles with spray paint, chalk or an equivalent method. Great care should be taken in identifying the appropriate piles for testing.

### **1.4 Taking Pictures of Piles**

Having photographs of a test specimen is invaluable. Photographs assist in identifying piles by visual markings and may reveal information that was overlooked during on-site evaluation. Pictures should first focus on the entire bent and then the specific piles to be tested. Make sure to capture the entire exposed length, and if external damage is present, photographs should be taken of these specific areas. A system of identification will be required in the photographs so as to identify what is being shown. Index cards can be tacked or nailed to piles containing some information on what is being photographed. In the case of external damage, a ruler or tape measure should also appear in the photograph to indicate scale. Pile identification, bent, and bridge number are among the information to be presented on the cards.

### **1.5 Recording Pile Dimensions**

Take measurements of the pile's exposed length. The exposed length should be measured from the bent to the water (if any) or ground. If water is present, the depth of the water should be measured as well. In the case of deep water, the assistance of a scuba diver is required for recording dimensions and testing. The location and dimensions of diagonal bracing and bolts should be noted as well.

## 4.6 Sketching the Pile and Bent

A sketch of a pile should be made using recorded dimensions and on-site visual observations. The bent cap should be included in the drawing along with bracing, bolt locations, and any external damage. Sensor locations should be included as well. This schematic diagram along with the measured pile dimensions and sensor locations will be used later during the computational analysis phase of the procedure to obtain a complete picture of the test specimen. This schematic diagram should later be coupled with the measured pile dimensions for a complete picture of the test specimen. A pile information sheet should be used to record all important information.

## 1.7 Rating a Pile

Visual inspection of a pile is very important and quite simple. Note any apparent visual flaws along the exposed length of the pile including: cracking, rot, construction damage, and any other possible physical defects. External damage may be evident, and in some cases it may be severe. If damage is visible, dimensions and location should be noted.

Another method of inspection is sounding. This consists of impacting the pile with a mallet or hammer. Sounding is a skill that takes time and experience to develop. It is critical in determining sensor locations. Tap the pile along its exposed length and listen for hollow sounding sections. The entire circumference and exposed length should be checked. Sensors should not be mounted in areas of severe cracking, rot or external damage. This practice will lead to data that yield incomprehensible results.

Note any findings from these two methods on the pile data sheet. These data may be useful during the analysis phase.

## **4.8 Pile Preparation**

### **4.8.1 Snapping the Lines**

Sounding and visual inspection are very important in deciding where to place the line of sensors. After visual inspection and sounding have been completed, a line must be snapped with a chalk line. Sensors will be placed on this line where the test is to be conducted. Again, it must be stressed that this line must not be placed along sections of severe cracking, rot or external damage. The natural variability of wood has an influence on stress wave data. The idea is to obtain data from best line possible so that one inadequate surface does not influence the final outcome of the analysis.

### **4.8.2 Determining Sensor Locations**

A tape measure should be used to determine the sensor locations. The standard sensor spacing is one foot. Nails are attached to each line in one foot increments. Sensors are attached to the 1" galvanized roofing nails using their magnetic base. These nails were chosen based on the similarity in the diameters of the nail head and the magnetic heads of the sensors. The sensors record the accelerations of a pile after it has been impacted.

Sensors should be located as close to the ground as possible. Place a nail on all three lines (in the same horizontal location) one inch from the ground or river bottom. Again, scuba divers may be necessary to assist in sensor attachment and impact creation in case of deep water. Since a chalk line cannot be snapped underwater, a tape measure should be held in line with it while the nails are mounted. Nails should be placed on the pile so that approximately  $\frac{1}{4}$ " of the nail is still exposed. This bottom nail will become the reference position for the rest of the sensor locations. Starting from this nail, place a nail every foot along the pile on all three lines. The spacing should be exactly one foot as this distance is used in the calculation of phase velocity in the analysis software. Close attention should be paid to the condition of the nails. Since the nails are not made for this purpose, the quality of the head is often substandard. Only nails with flat circular heads should be chosen for sensor attachment. The top two feet of the exposed length should

remain free of nails. This is to leave room for the use of the standard impact device. The impact for setup 1 will occur one foot from the bent and the first sensor will be located two feet from the bent. The location and number of setups should be recorded on the pile information sheet. A setup is a data set corresponding to a specific one foot length of pile. Setup one for example would be the uppermost test setup on a given pile. Once all of the nails are in place, the computer equipment and sensors can be connected.

## 4.9 Equipment Setup

Equipment setup for this test is relatively simple. A list of the necessary equipment with model numbers and company names and contact information is given in Appendix A. A schematic diagram of the basic equipment connections is shown in Figure 4.1.

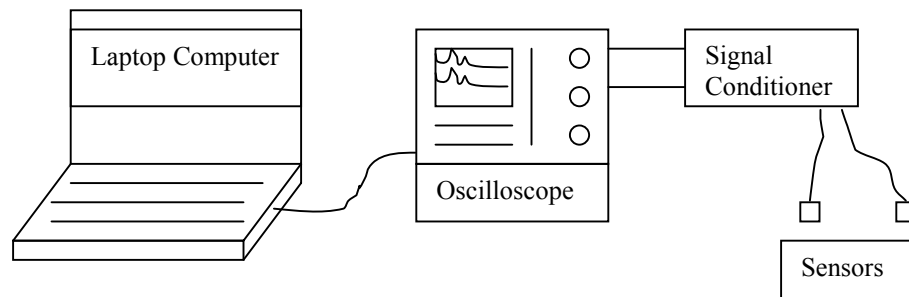


**Figure 4.1** Schematic of equipment setup.

First, connect the oscilloscope to the laptop computer using the National Instrument connecting cable. The cable should be plugged into the GPIB card in the

laptop and the GPIB port in the back of the scope. This connection allows SWAP to communicate with the scope and collect the data.

The 2 ft. PCB cables can then be used to connect the signal conditioner to the oscilloscope. Care should be taken when connecting these cables because of the small space to work with around the connectors on the signal conditioner. Ensure that the cables are securely attached. Also, ensure that all the connectors are in the proper place (i.e., cable in socket 1 on the scope is in socket 1 on the signal conditioner).

Next, the PCB sensors can be connected to the signal conditioner. The sensors consist of long PCB cables with a connector on one end and an accelerometer on the other. Waterproof sensors and cables should be utilized when appropriate. It helps to use some colored tape to coordinate the sensor and cable attachment. Colored tape can be wrapped around the cables to eliminate any confusion during setup and testing. A standard color could be used for each channel (i.e., green for channel 1, red for channel 2, etc.).

Finally, plug in the computer, scope and signal conditioner into the surge protector. The surge protector should be connected to the gas generator via a heavy-duty extension cord. It helps to place the generator as far away as the extension cord will allow so that the amount of noise and exhaust experienced by the technicians is minimized. Once all of the devices are powered up and working properly, testing can begin.

## **4.10 Stress Wave Testing**

Click on the SWAP icon on the laptop to bring up the Stress Wave Analysis Program. This program can collect and analyze data as discussed in Chapter 3.

### **4.10.1 Data File Identification**

Type in the code to enter the main command window. Click on “Input Data File” and enter the file name of the first data set to be collected. It is important to devise an

efficient system of naming files so as to eliminate confusion. An example of the identification system for this research project is described below. Other more convenient systems may be implemented with testing and analysis experience.

**Filename:** ccw23

**cc = pile ID**

The length of the filename has to be no more than 8 characters so it is not possible to include all relevant information (pile number, bent number, bridge number, county, etc.) This relevant information will be included on the pile information sheet along with the pile ID.

**w = type of impact device**

The impact device letter is one of two letters. A “w” signifies the use of the wood spring device and an “m” indicates the modified hammer. Hammer usage will depend on signal quality.

**2 = setup number**

There can be any number of setups on a pile depending on its length. Obviously longer piles will have more setups. The number two corresponds to the second setup from the top of the pile. Remember that a setup describes a specific foot of pile length in which sensor one is mounted on the top and sensor two is mounted on the bottom. The value of this number will vary depending on the number of setups.

**3 = file number**

It was found necessary to collect and analyze more than one data file per setup due to the natural difficulty in obtaining high quality and consistent signals. Two files were chosen as the standard number of files to collect. The value of this number will range between 1 and 2.

### 4.10.2 Oscilloscope Settings

The basic settings of the oscilloscope are saved for each successive use. These settings include, but are not limited to: trigger levels and edge sources, acquisition modes, horizontal and vertical scales and display settings. Some of these settings need to be adjusted constantly throughout testing to obtain proper data while others will remain the same for the lifetime of this procedure. Details regarding the specific applications, settings and controls of the oscilloscope can be found in the Tektronix® owner's manual.

The scope will recall the setup used on the previous test allowing the fundamental acquisition settings to be in place when it is turned on. The scope also has a memory which can recall a factory or user defined setup. Settings obtained from the Appendix and the procedure's first use should be stored in the memory as user defined. If accidental changes occur, the proper settings can be recalled at the touch of a button from the setup menu.

The horizontal and zoom menus will be constantly adjusted during the collection of data. Changes to the horizontal menu will include the record length and the sensitivities of the various channels. Accelerations of the pile are measured and recorded through the sensors and scope by voltage level. A higher voltage setting indicates a greater force of impact and a decreased sensitivity. A lower voltage indicates a weaker impact and an increased sensitivity. The voltages should first be adjusted in the zoom-off mode. In this mode all of the signals are shown on the same horizontal line. Upon experience, a technician will obtain the knowledge and instinct necessary to quickly adjust the levels to those which facilitate the collection of good data.

Typically in the zoom-off mode, the voltage for the first channel is set at 500 millivolts (mv). The remaining channels are usually set at 200 or 100 mv. These settings are not standard, however, and actual values will depend on the condition of the pile and the impact force and quality. Some piles are more sensitive than others and higher voltages will be required. It takes a significant amount of experience to be able to adjust

the scopes setting quickly and efficiently to obtain adequate signals. Time and patience cannot be taken for granted.

The signals in the zoom-off mode should not go off of the screen. This will cause data to be cut off, which will create problems in analysis. Maximum amplitudes of these signals should be around three-quarters of their maximum allowed value. This problem will be evident in the zoom-on mode as well. In this mode, wave peaks will be flat-lined instead of curved.

The zoom-on mode depicts the signals as they will be collected in the laptop. This mode allows the user to see the signals on separate horizontal axes. It is in this mode where the operator will study the quality of signals and decide to collect. Signal quality is extremely important to the success of this procedure. Poor signal quality will yield substandard results. The analysis phase will lead either to the wrong conclusion or no conclusions at all.

### **4.10.3 Collecting Data**

Starting with the first setup, signals can be created with the standard impact device. The two impact devices, WSM-00 and WSM-99, are very easy to use. The creation of an impact is simple. In the case of the WSM-99, the degree to which the hammer is raised will depend on the signal quality. The impact of the WSM-00 can be adjusted by changing the location of the trigger along the cylinder spring. Both devices must be held firmly to the pile surface. Two hands are required for the WSM-99 while only one is necessary for the WSM-00. After several impacts, one will obtain a feel for the adjustments required on the scope and the force of impact required to obtain quality data. The hammer of the impact device must hit the pile approximately one foot from the first sensor. This allows the signal attenuation at sensor 1 to be relatively consistent. Slight adjustments to the device position will be necessary to obtain quality data. Surface conditions have an influence on the data and the impacted area should be scraped clean of debris, tar, creosote and any other objects which would inhibit the clean contact of the hammer with the pile surface. Scraping can be performed with the claw end of a

carpenter's hammer or any equivalent device. This cleaning process should be repeated every time the sensors are moved to the next setup.

Two data files are required for each setup. Careful attention is needed when naming files to eliminate any confusion. The software will not show a message indicating a file is being overwritten. The only assurance that the data represents what it was intended to depends on the diligence of the laptop and scope operator. Save the best quality files possible for each setup. It can take between 20 and 40 impacts to obtain the best two signals. On any given setup, the signal quality will usually improve over time as the surface of the pile deforms to the hammer shape.

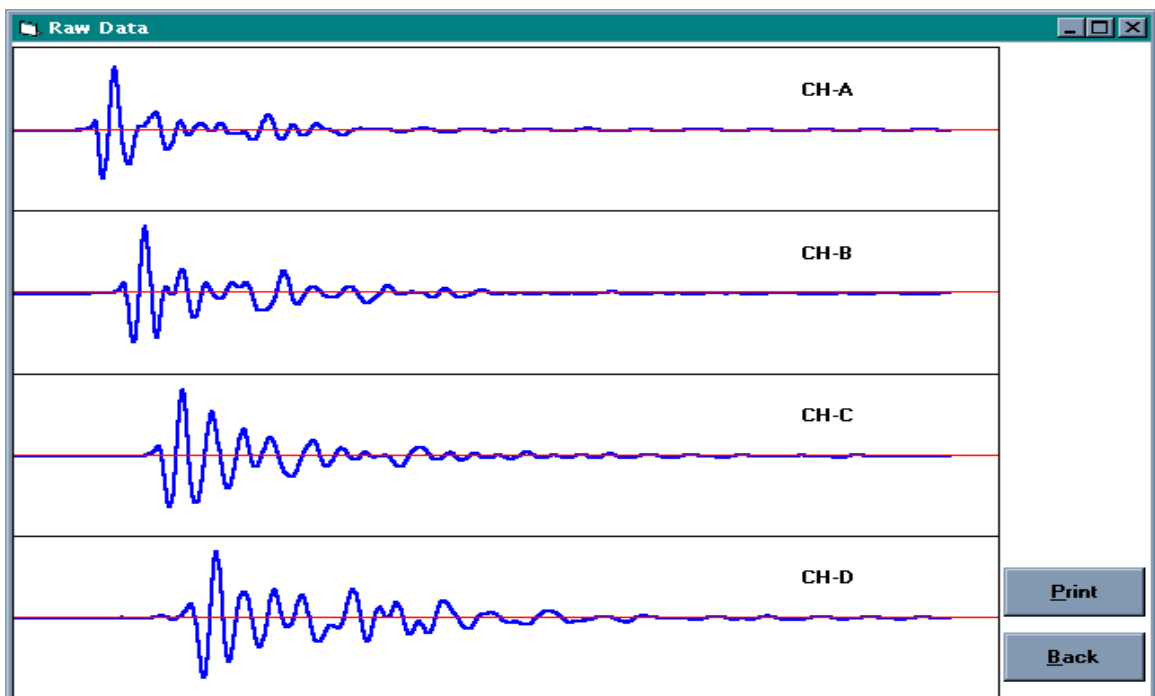


**Figure 4.2** Example of high quality raw data.

Signal quality is one of the most important aspects of this procedure. If the signal quality is inadequate, then analysis will not yield useful results. Due to the number of signal types experienced during the course of this research project, it would be impossible to show every case and explain them effectively. For the purposes of this document, basic guidelines are given and examples of extreme cases are shown. The two most important aspects of signal quality are the presence of patterns and complete peaks and troughs in the first part of the signal. A plot of high-quality raw data is shown in Figure 4.2.

In this signal, the peaks and troughs of each channel are clearly defined and a definite pattern is present. As expected, sensor one registers the signal first and sensor four receives it last. This behavior should be expected due the way the sensors are mounted. The pattern shown in Figure 4.2 reflects the fact that the first sensor is closest to the impact and the remaining sensors record the signal as the wave travels down the length of the pile. Analysis of data of this quality will lead to reliable results.

A sample of poor raw data is shown in Figures 4.3 and 4.4. The signal in Figure 4.3 is obviously of lower quality than that of the previous figure. The peaks of channel one are not smooth and uniform. The largest peak is actually skewed to the left. Also the large trough of channel one seems to be flat-lined which indicates that the settings were too sensitive and the reading is off of the screen. Problems are evident in Figure 4.4 as well. No definite patterns are visible in this figure. The amplitudes of the signal are too small indicating that the scope was not set to be sufficiently sensitive.

Once the technicians are comfortable with the data they have collected, the sensors can be removed from the pile and the computer equipment shut down and packed up. It is also advised to check the hard disk of the computer to make sure all of the desired data file have been properly saved.

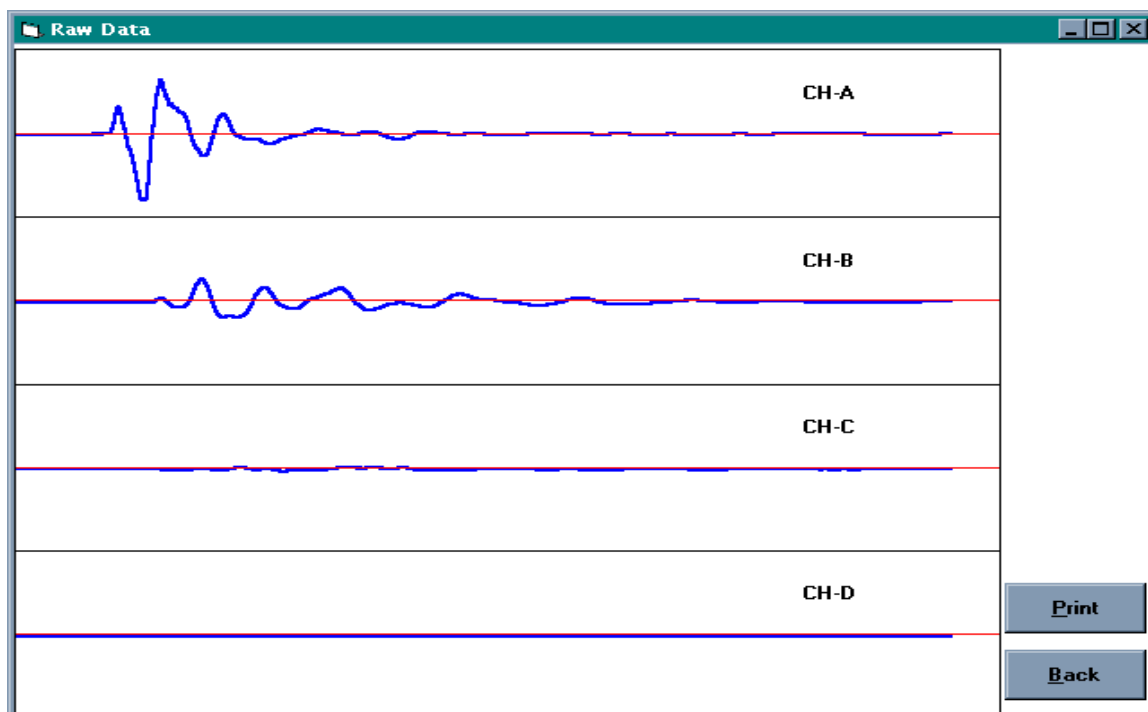


Figure 4.3 Example of poor quality raw data.

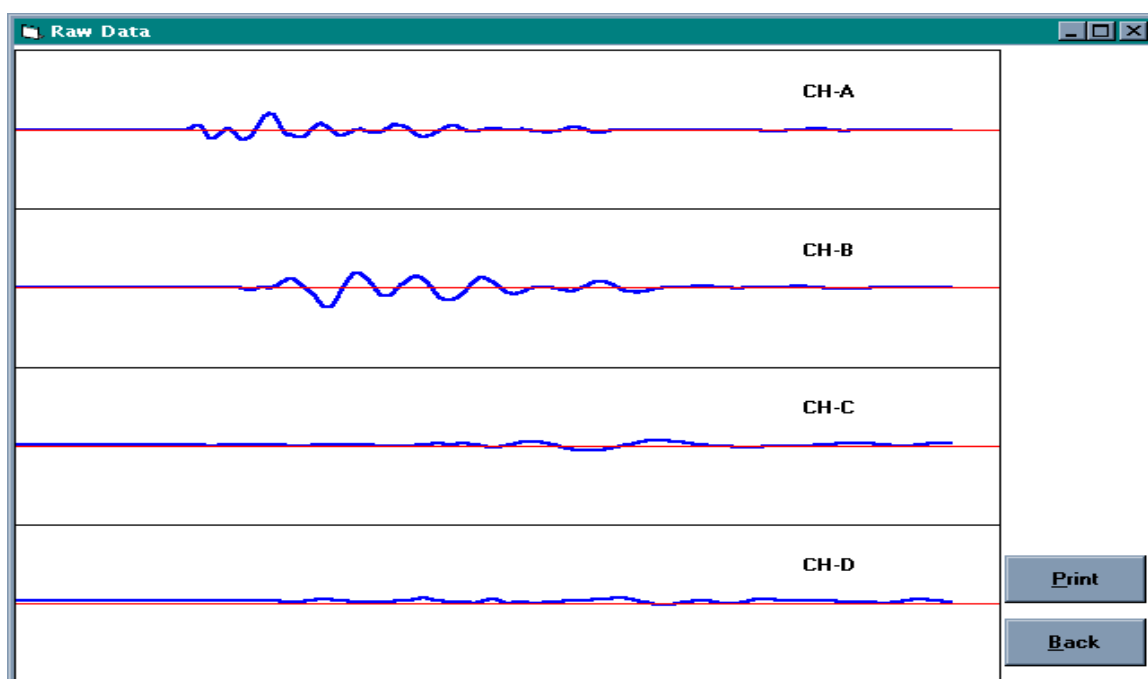


Figure 4.4 Example of poor quality raw data.

## 4.11 Coring of Each Location

To obtain liquid content information for in-situ piles, each setup must be cored. This task is performed using a standard wood coring device. A core should be obtained mid-height between the nails where sensors one and two were located in each setup. A core needs to be obtained for each stress wave test setup (i.e., the number of cores will be equal to the number of setups). A schematic diagram explaining the locations of sensors, impacts and cores is shown in Figure 4.5.

Each cored location should be marked with a small hole created with a hammer and nail. These “starter holes” facilitate the performance of the coring process. The coring device should be bored into the pile until it has penetrated the entire diameter of the pile. The extraction rod can then be inserted to obtain the core sample.

Core samples should be placed in a plastic Ziploc® sandwich bag. These bags should be labeled with a permanent marker so the source of the core is known. All excess air should be removed from the bag before it is sealed with the core inside.

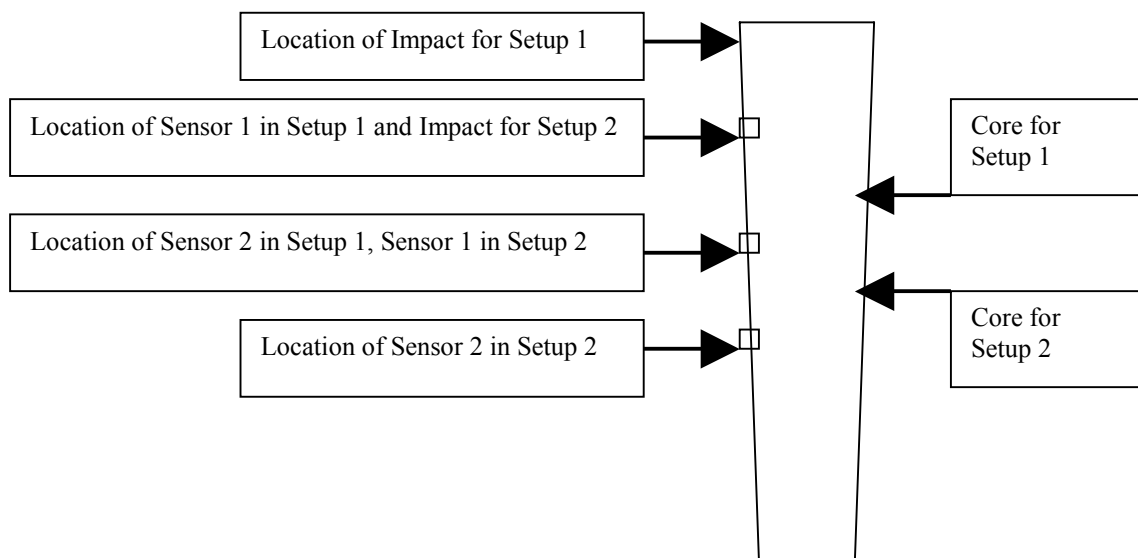


**Figure 4.5** Schematic diagram of sensor, impact and coring locations.

## 4.12 Drying of the Cores

The drying of the cores is performed in the Halogen Moisture Analyzer (HMA). The method for drying cores has been obtained from laboratory studies. Settings for the Mettler-Toledo Halogen Moisture Analyzer are shown in Appendix A.

The settings outlined in the appendix should be followed along with the basic guidelines given by Mettler-Toledo®. The basic steps are summarized below:

1. Adjust the HMA so it is level on the table or countertop
2. Turn the unit on
3. Open the sample door and place a sample tray inside
4. Tare the device
5. Reopen the sample door and place the core on the tray
6. Press the start button and wait for the unit to signal that the test is over
7. Tabulate the results

It is important to identify each LC value with its corresponding test setup so that it can be paired with the appropriate phase velocity value.

## 4.13 Final Notes

Communication and patience is required of both technicians during these tests. It takes a considerable amount of time to find the right location and impact. The tedious and repetitive nature of this method may affect the attitudes of those conducting the work. When frustration develops it shows in the data. This should be expected but it can be overcome with the proper patience and communication between the collector and impact device operator. It also helps when roles are reversed every so often to relieve some of the monotony of the procedure.

# Chapter 5

## Condition Evaluation

### 5.1 Condition Evaluation Procedure

The condition evaluation procedure consists of combining all of the information obtained from a pile through stress wave testing and determining the appropriate course of action. The basic steps in this process are identified below:

1. Perform tests on a pile in the field (according to Chapter 4)
2. Dry cores in the HMA and obtain LC values
3. Perform analysis on stress wave data using SWAP
4. Combine analysis results with visual observations, sounding and other considerations specific to the specimen
5. Determine appropriate action

Pile specimens can be obtained from NCDOT bridge inspection teams. Once these pilings have been identified, the field procedure can be performed in accordance with the steps described in Chapter 4. The field testing procedure will yield a variety of information including: stress wave data, photographs of pile sections, notes on visual inspection and sounding, schematic drawings of the test setup, and wood core samples.

In the laboratory, the cores should be dried in the HMA according to the procedure outlined in Section 4.12 and Appendix A. The drying of the cores should take priority once field-testing is completed so that the most efficient and accurate liquid content value is obtained as efficiently as possible from the samples. It is not advisable to bring the HMA into the field because of the need for a level surface and time

constraints. Care should be taken to avoid leaving the samples in plastic bags for longer than necessary or areas of extreme temperatures.

The raw data should be analyzed in SWAP once in-situ testing has been completed. Since two data files will be collected from each location, there will be two phase velocities to calculate using the SKM. Each location consists of a 1-foot section of pile as indicated in Chapter 4. Once the phase velocity has been calculated for the two files obtained from a given location, an average phase velocity should be computed. This average phase velocity should then be coupled with the corresponding liquid content obtained from the HMA.

An average phase velocity and liquid content are now available for each 1-foot of pile length. This information should first be plotted on the graph shown in Figure 5.1.

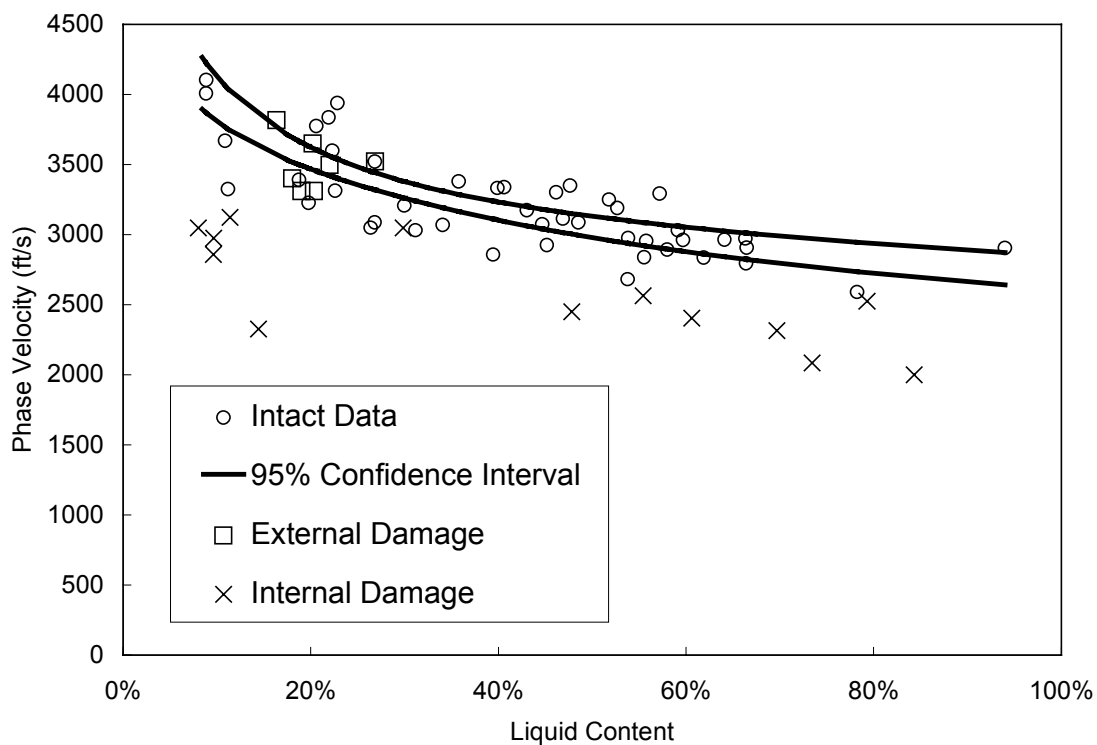


**Figure 5.1** Phase velocity versus liquid content plot for qualitative indication of pile condition.

Although this method will not yield quantitative results, it will give a reasonable indication of pile condition in reference to damaged and intact data collected during the course of this study. It is a method to quickly reject or accept pile condition.

The next step in the condition evaluation process is the calculation of remaining cross-sectional area. Knowing the average phase velocity and liquid content for a given section, the RCSA can be predicted using Equation 5.1.

$$RCSA = \frac{V_{ph} - 1477}{2371.8 * e^{-0.8294 * LC}} \quad (5.1)$$

where,

$V_{ph}$  = the average phase velocity of the test location under consideration (ft/s)

$LC$  = liquid content of the core specimen obtained from the test location using the HMA device (percentage expressed as a decimal value)

$RCSA$  = remaining cross-sectional area (percentage expressed as a decimal value)

The final step in condition evaluation is the determination of appropriate action. An engineer should make a decision based on all of the information obtained during the course of pile testing and analysis. In other words, the decision should be made based on the information provided by the qualitative plot (Figure 5.1), the RCSA relationship (Equation 5.1), and the variety of other information obtained during the testing phase (photographs, visual inspection and sounding). Judgement should also take into consideration any relevant safety factors, expected service life and general condition of the structure under consideration. The usage and location of the structure may also be important in the decision making process.

## 5.2 Analysis Examples

A few examples of data analysis are presented in this section. The data presented in this section were collected from installed timber piles tested during the course of this study. Examples of both intact and damaged sections have been used.

### 5.2.1 Pile AA, Chatham County Bridge #147 (Intact)

Pile AA was tested in-situ on August 28, 1998. This pile was part of a very large one-lane steel truss bridge structure. This particular pile was located inland, away from the creek which passed beneath the bridge. The exposed length was 9.67 feet. The length of the specimen allowed for 8 test setups designated AA1 through AA8. The data was obtained using the WSM-99 device. Upon extraction, AA8 was determined to have a RCSA of 81.25%. All other locations (AA1-AA7) were intact. For simplicity only location 1 is considered here. Figures 5.2 and 5.3 show the raw signal as displayed in SWAP for the two stress wave data files collected from location 1.

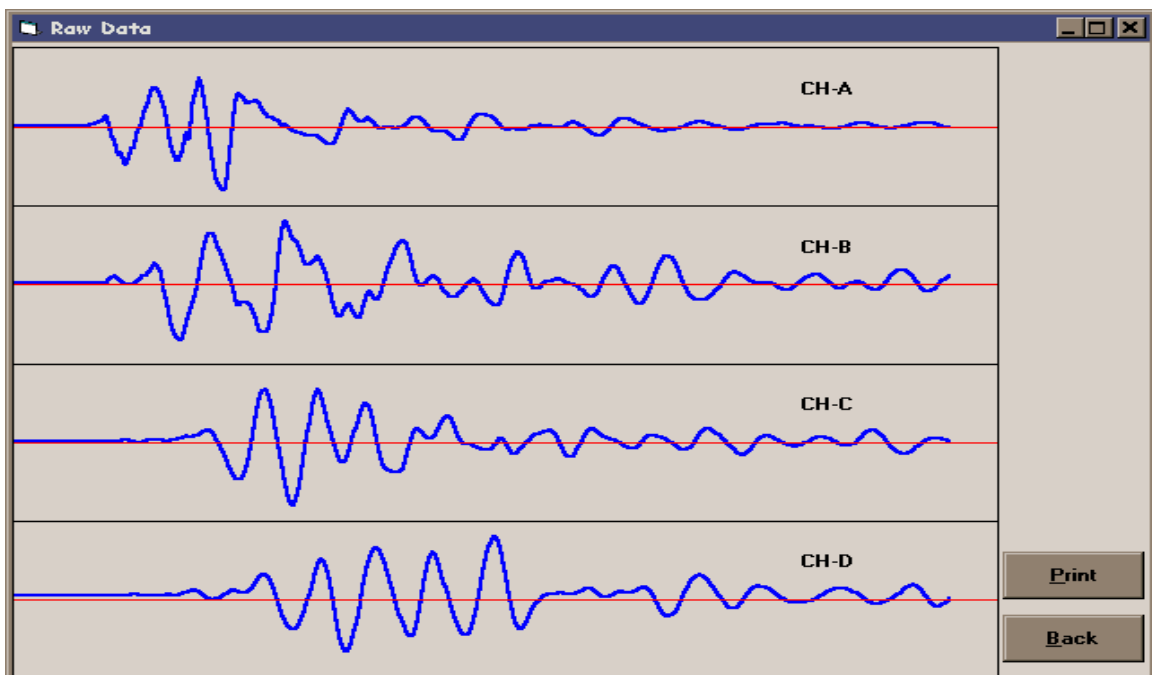


**Figure 5.2** Raw signal for first file collected at AA1.

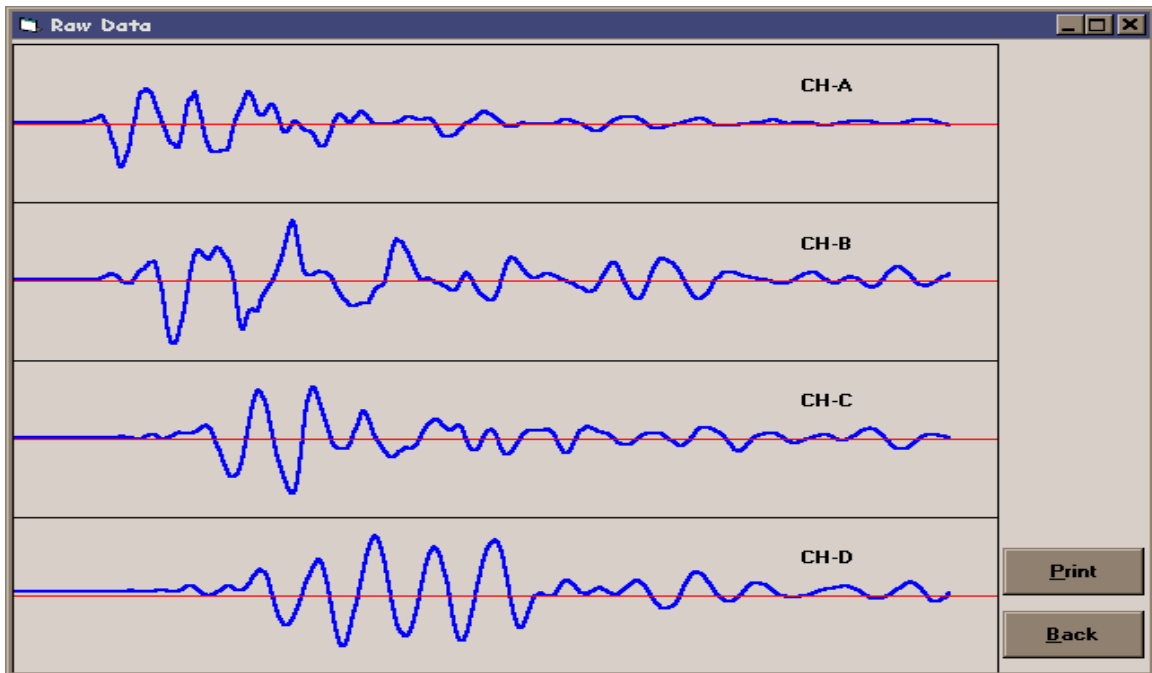


**Figure 5.3** Raw signal for second file collected at AA1.

Figures 5.2 and 5.3 show raw signal with mediocre quality. Although peaks and patterns are evident, the overall signal is not as smooth as one would want. It should be noted that because this pile was located away from the creek, the liquid content values were relatively low. The experience of the research team showed that high quality signals were more easily obtainable in piles with high liquid content values.

Figures 5.4 and 5.5 show the magnitude versus frequency plots for location 1 obtained using the FFT capabilities of SWAP. Note that the file names appear in the figures. The data files were named according to the following convention:

Filename: aaw11

**aa** – pile name designated by the testing team. These letters correspond to the more lengthy information on the pile information sheet (pile, bridge, county).

**w** – indicates that the WSM-99 device was used.

1 - Test location (1 corresponds to the location closest to the concrete bent)

1 – File number (1 corresponds to the first data file collected)

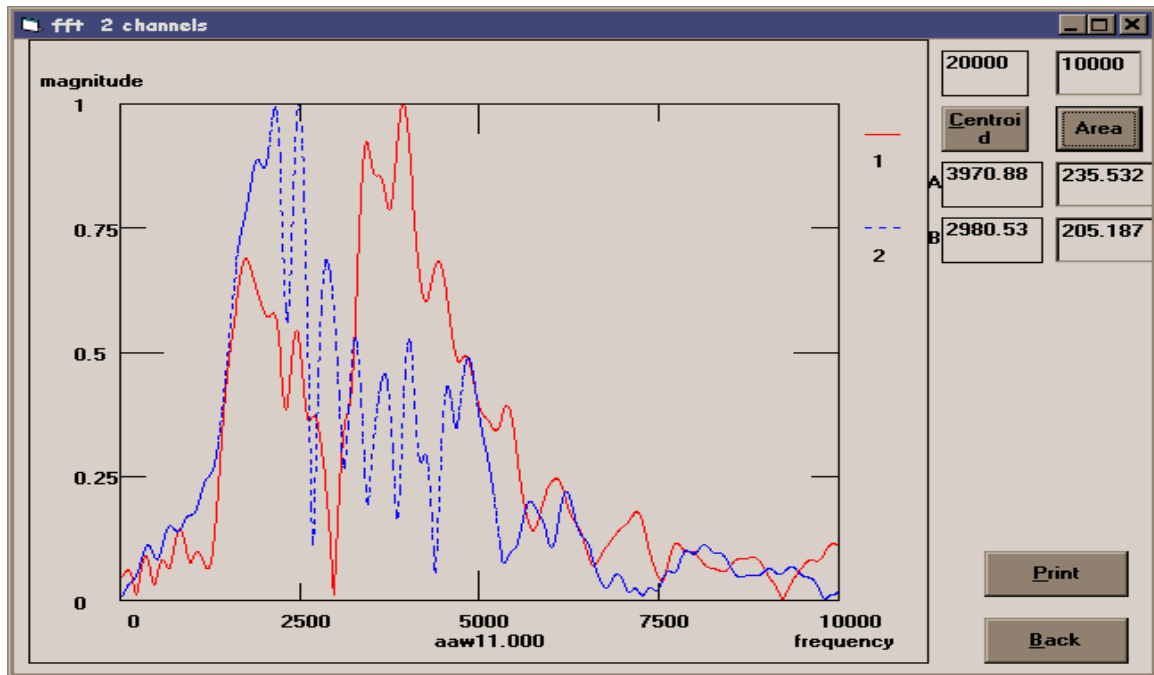


**Figure 5.4** Magnitude versus frequency plot of aaw11.

In both of these plots, it is evident that the majority of the frequency content exists between 1300 and 5000 Hz. The purpose of these plots is not for qualitative purposes. These plots are just used to make sure that the majority of the frequency content is at least centered around 2500 Hz. This is true in both of these cases although it may be more prominent in other data sets.

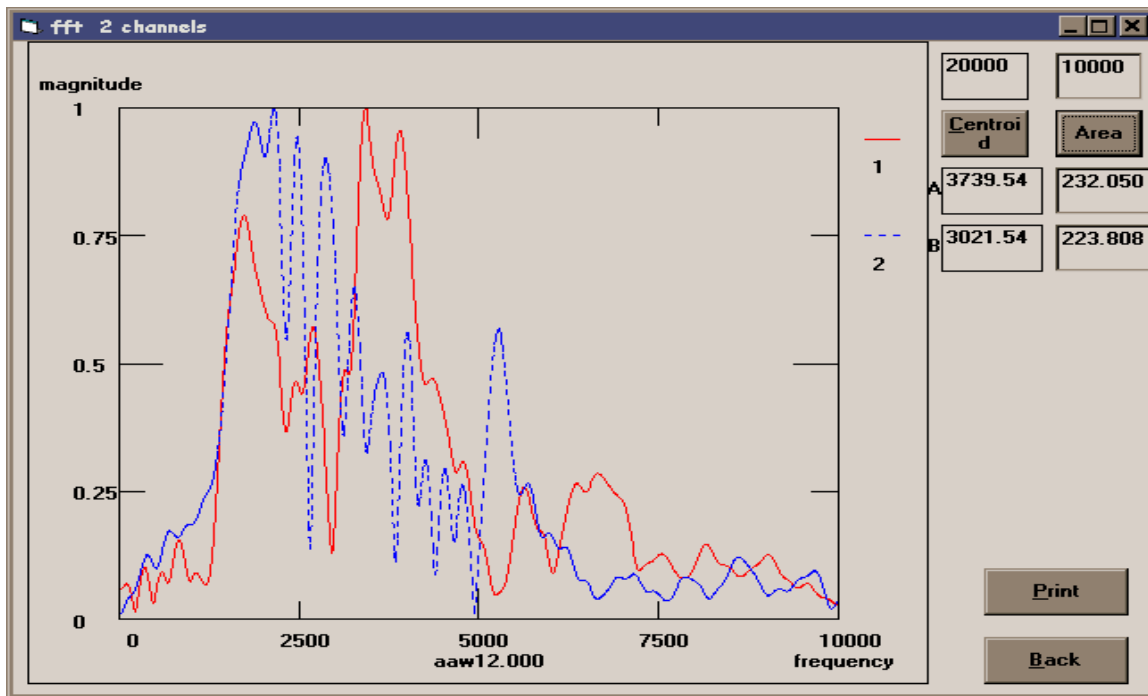


**Figure 5.5** Magnitude versus frequency plot for aaw12.

In most cases, the process of looking at the magnitude frequency plot can be avoided. The use of the standard 2500 Hz kernel has developed over the course of this research project. Based on the standard impact and the common properties of most timber piles, the frequency content is usually centered around this value. Confirming the location of the energy by using the FFT is useful in determining the validity of the SKM results. Since the SKM acts as a sieve to filter out a specific frequency, the best results are obtained when that frequency contains a large percentage of the energy present in the signal.

The SKM plots (using the 2500 Hz kernel) for aaw11 and aaw12 are shown in Figures 5.6 and 5.7, respectively. The peaks have been selected and the phase velocities are shown to the right of each screen. The phase velocities are determined to be 3448 and 3333 ft/s for data files 1 and 2, respectively.

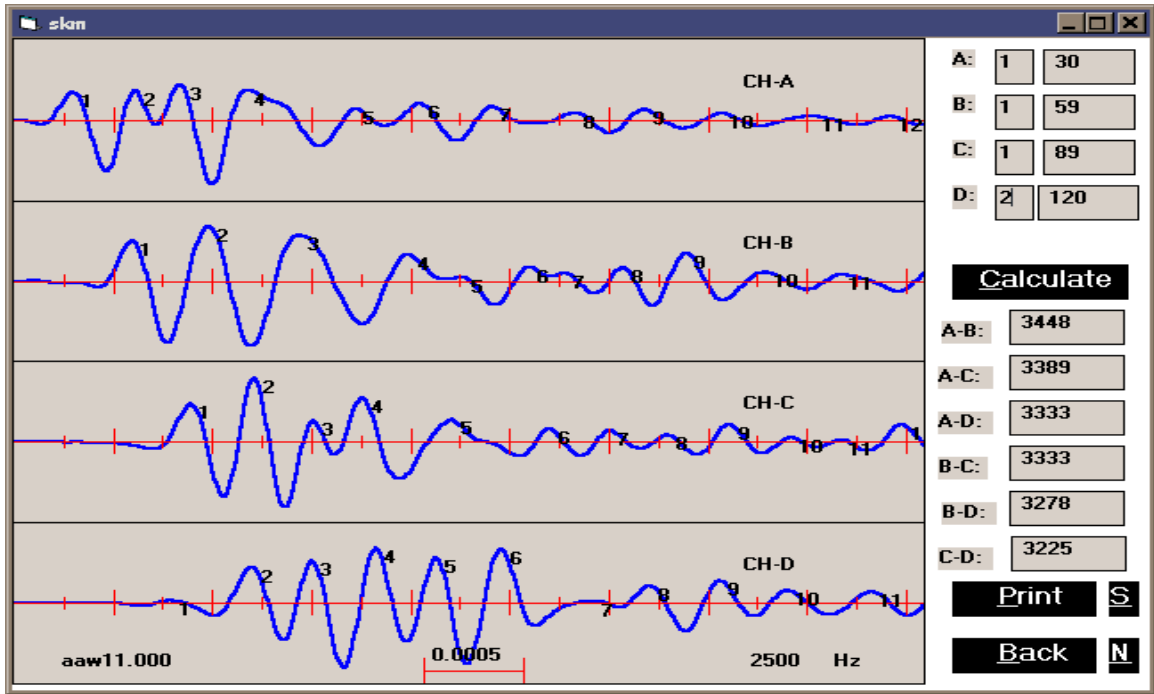


Figure 5.6 SKM plot for aaw11.

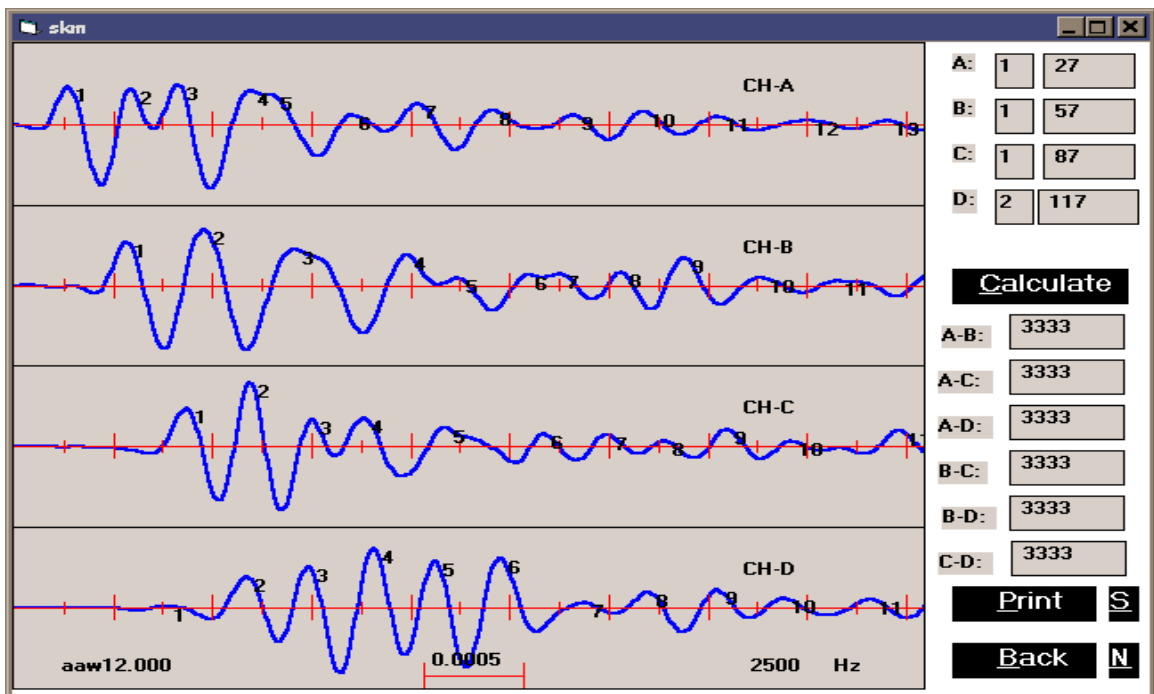


Figure 5.7 SKM plot for aaw12.

The ability to properly select waves peaks for phase velocity calculation is obtained with experience. In both of the cases shown above, the first peak of channels one and two were selected. The information obtained from the stress wave test corresponds to the 1 foot length of pile between sensors one and two. Ideally, the wave shown on the first line marked CH-A should closely resemble that shown on second line marked CH-B. The difference between these two waves is a shift on the time axis. This shift exists because the wave is received by the sensors which closest to the impact first. In other words, the farther away a sensor is from the impact, the longer it will take for the signal to be received. Pattern recognition is the key to successful selection of corresponding wave peaks in phase velocity calculation. The shapes of the signals in channels one and two should closely resemble one another with the only difference being the shift in the time axis. In Figures 5.6 and 5.7, the first wave (crest and trough) is very similar in channels one and two. This similarity leads to the confidence in selecting peak 1 in both channels in data files aaw11 and aaw12.

Now that phase velocities have been obtained, an average should be computed. The average phase velocity of location one on pile AA is calculated to be 3391 ft/s. It should be noted that the core from location 1 yielded a liquid content value of 18.78%. As indicated in Section 5.1, the first step is to plot the data from AA1 against the intact and damaged data obtained during this study. Figure 5.8 shows the data from AA1 as indicated by the solid circle symbol.

It can be seen that the data from AA1 fall just below the lower bound 95% confidence limit. This point is also in the region of the intact data. Although AA1 resides close to the externally damaged pile data, it should be noted that no external damage was visually evident on AA1 during in-situ tests. Qualitatively, this location appears to be intact but we need to proceed to the next step and calculate the RCSA.

The predicted RCSA of AA1 using Equation 5.1 is 94%. The measured RCSA was found to be 100%. This prediction, although lower than 100%, should be viewed in light of the other information obtained during the course of testing and analysis. Table

5.1 summarizes the information required to make a sound decision regarding the condition of AA1 (pile AA, position 1).

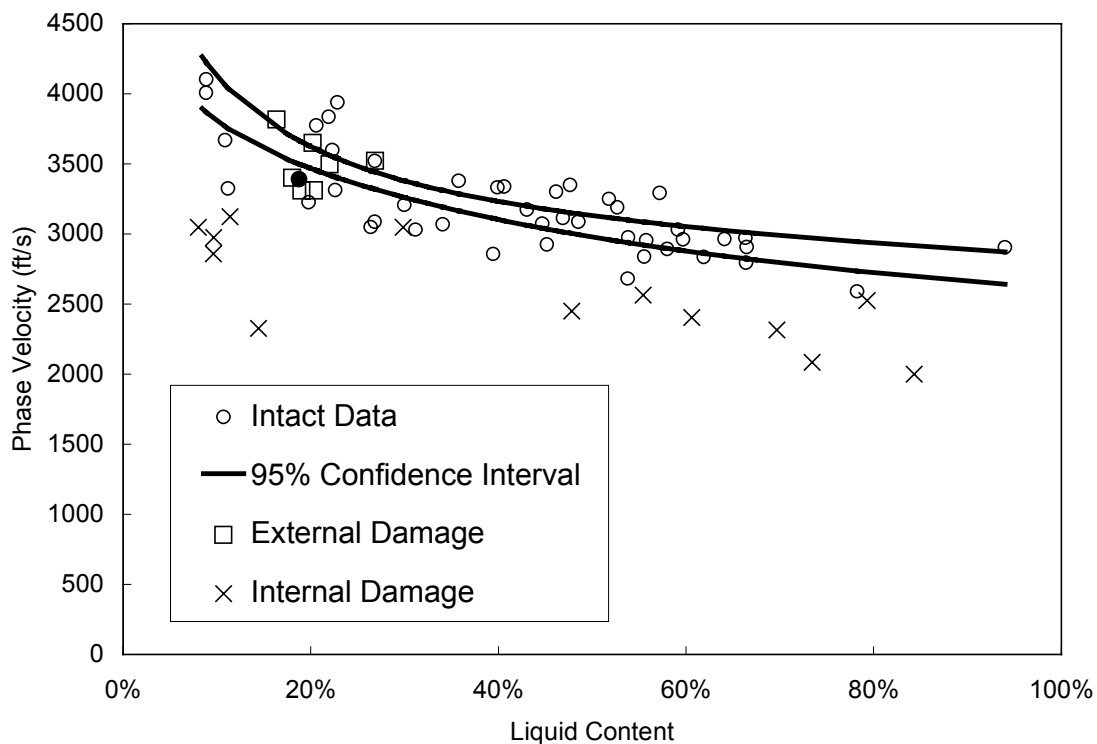


**Figure 5.8** Qualitative plot of phase velocity versus liquid content with AA1.

The research team is of the opinion that this pile should be considered intact. This opinion, however, could be considered biased because location AA1 is known to be intact. The distance of the pile from the creek is a big factor. Decay usually occurs in piles that have a wet/dry transition zone along the exposed length, which pile AA does not have. It is up to the engineer performing analysis to consider this data as well as other information pertinent to the specific pile and/or bridge in order to make a decision regarding replacement.

**Table 5.1** Summary of information for AA1.

ITEM	COMMENT
Visual Inspection	No external damage
Sounding	Appeared solid
Average Phase Velocity	3391 ft/s
Liquid Content	18.78%
Qualitative Analysis	Within intact region, near 95% confidence lower bound
Quantitative Analysis	Predicted RCSCA = 94%
Additional Comments	Pile located 40 feet from river bed which explains the low MC value. Wet dry transition zone probably underground. Full core obtained.

### 5.2.2 Pile S, Warren County Bridge #64 (Damaged)

In-situ stress wave tests were performed on pile S on April 26, 1998. This pile was located in 1 foot of water in a small river. No external damage was reported. The 5.83 foot length of the pile allowed for 4 test setups. This section will consider the first setup known as S1. Again, this is the setup closest to the concrete bent. Figures 5.9 and 5.10 show the raw signals collected at the location under consideration.

Upon observation of the raw signals in Figures 5.9 and 5.10, it is obvious that the signal quality is not as high as that of AA1 (previous section). The wave signal is jagged and diminishes very quickly. A smooth raw signal will decrease the difficulty associated with the selection of peaks. The quality of these signals are an indication that the pile may contain damage. In general, the presence of damage has been shown to decrease signal quality.

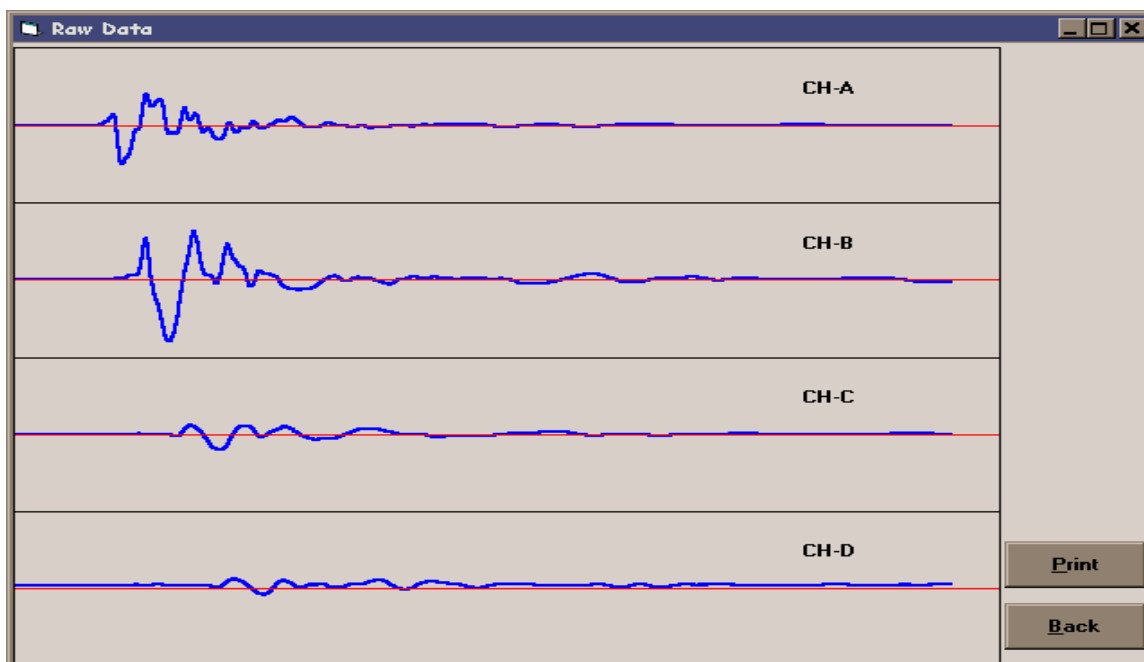


**Figure 5.9** The raw signal for s11.

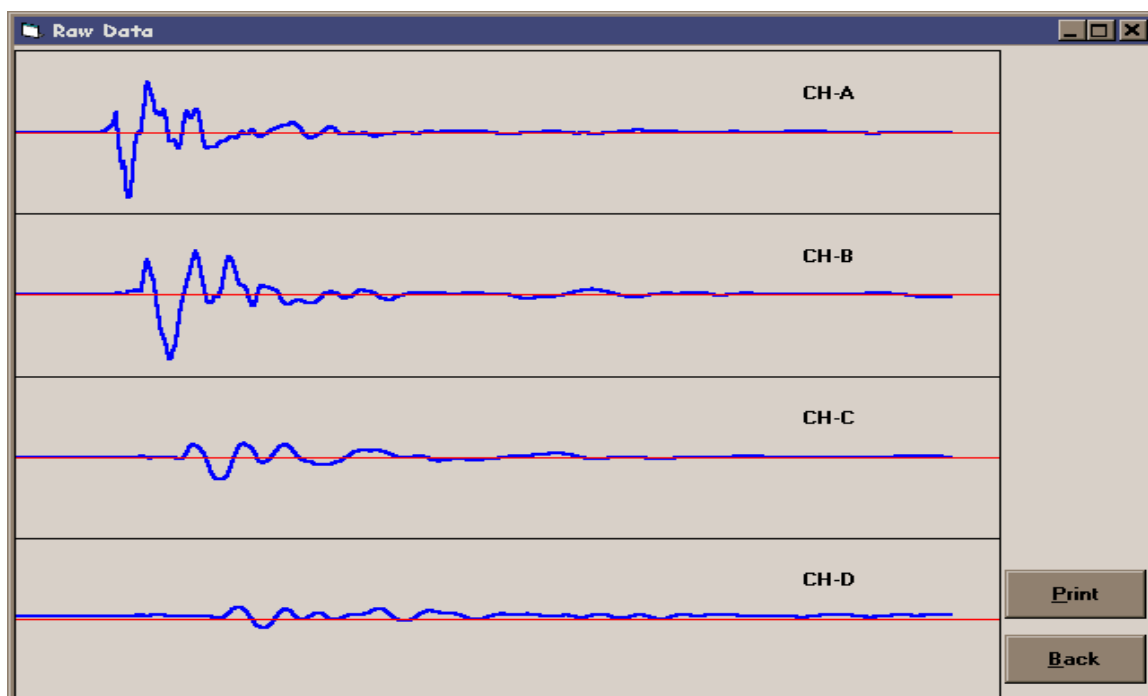


**Figure 5.10** The raw signal for s12.

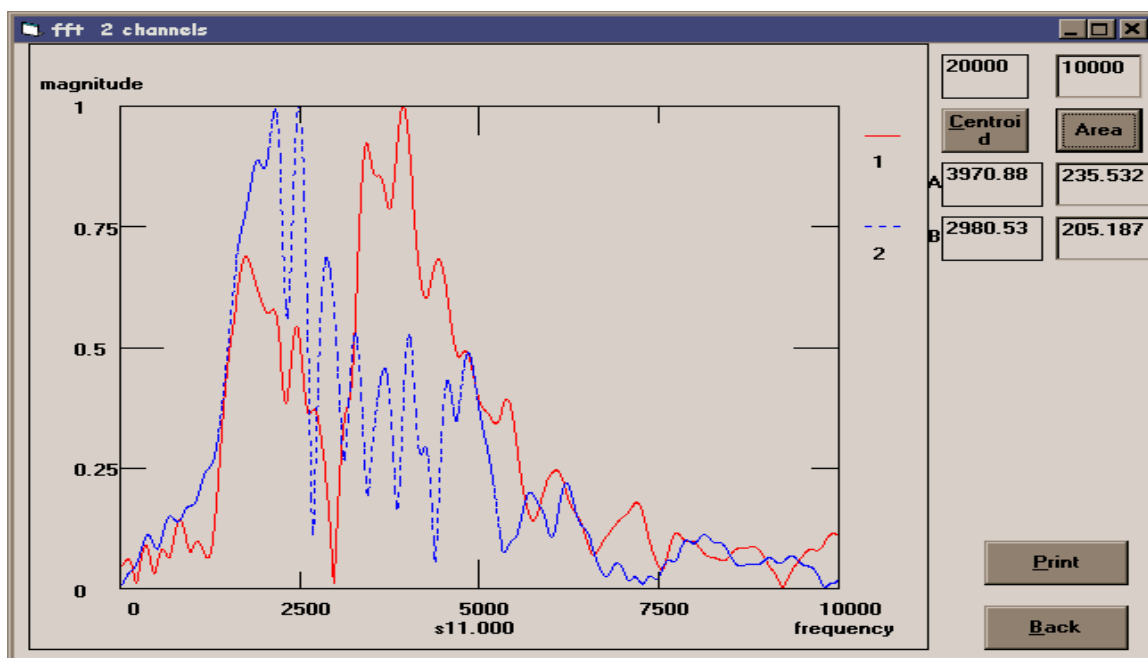


Figure 5.11 The FFT plot for s11.

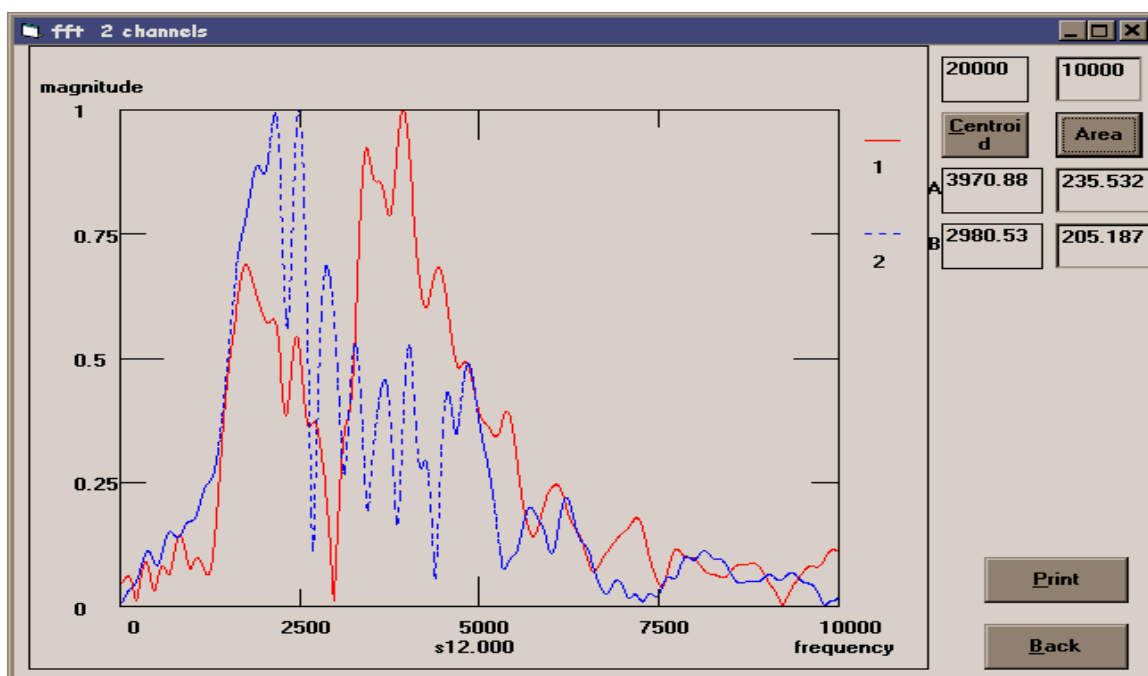


Figure 5.12 The FFT plot for s12.

Figures 5.11 and 5.12 show the FFT plots associated with the raw signals obtained from S1. Again, these graphs are presented to confirm that the energy in the signal is close to the 2500 Hz frequency.

The two FFT plots for S1 resemble those for AA1. The frequency content is centered around 2500 Hz. The fact that the highest magnitude does not occur at the 2500 Hz frequency is not critical.

Figures 5.13 and 5.14 show the SKM plots for both files collected at S1. Again the standard kernel of 2500 Hz has been used. This kernel must remain at 2500 Hz because the qualitative and quantitative relationships presented in this chapter have been developed on the basis of this frequency.

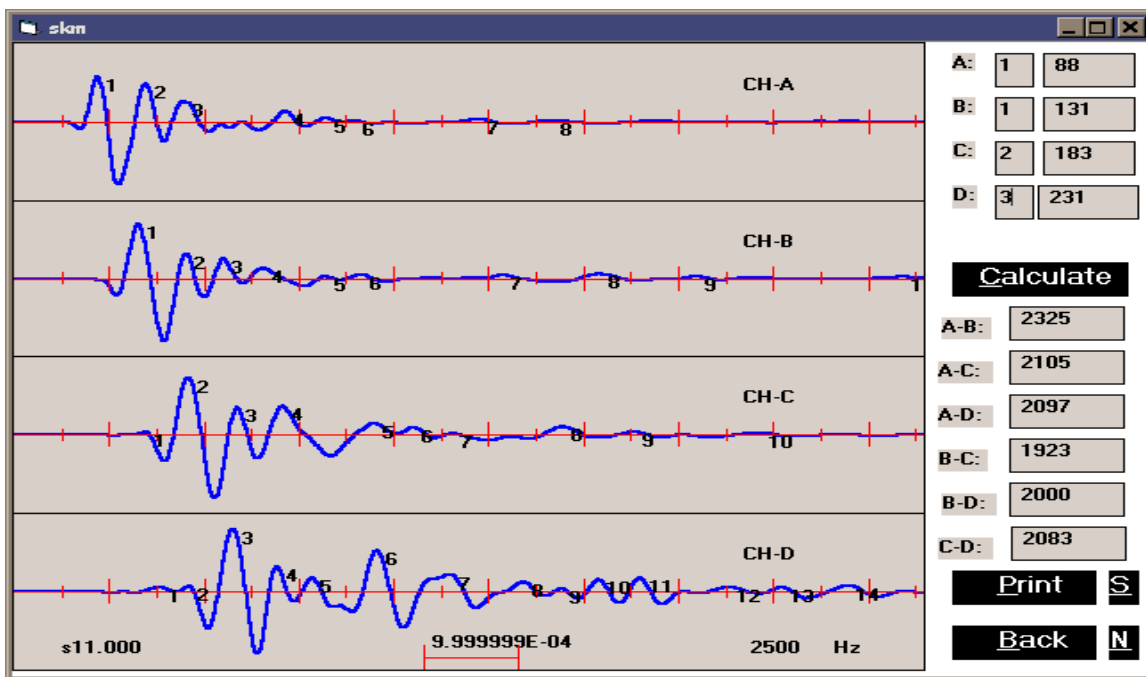
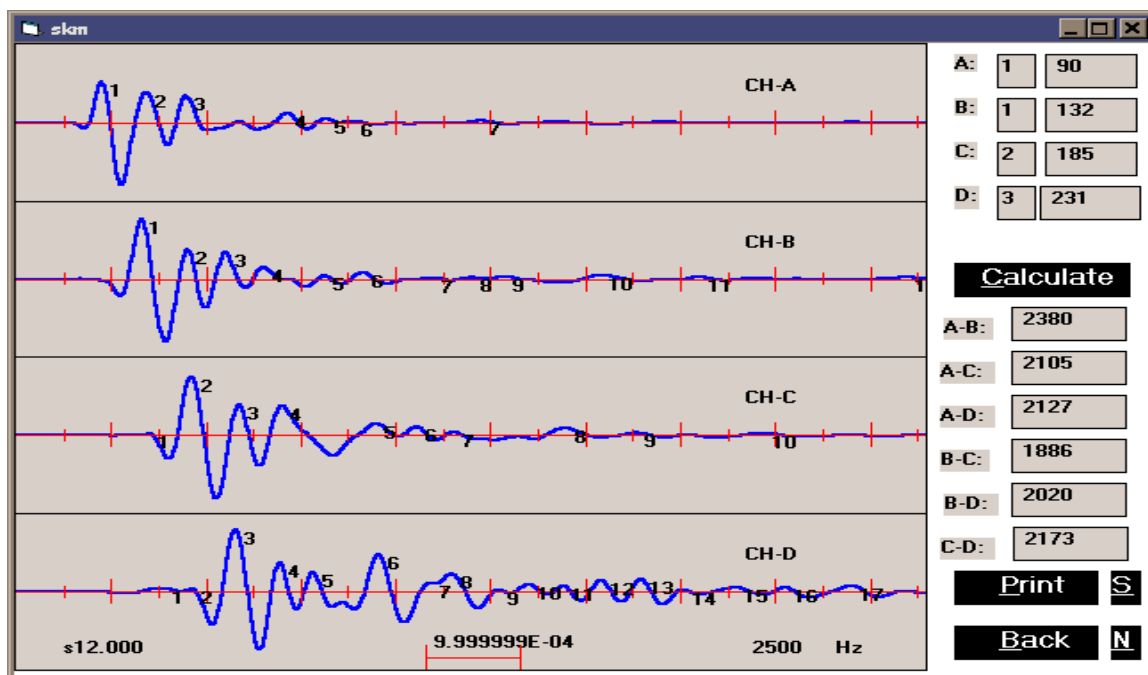


Figure 5.13 The SKM plot for s11.



**Figure 5.14** The SKM plot for s12.

The phase velocities for s11 and s12 were determined to be 2325 and 2380 ft/s, respectively. The average phase velocity for location S1 is 2353 ft/s. The liquid content was determined from the HMA to be 9.67%. Figure 5.15 shows the data obtained from S1 on the qualitative plot of phase velocity versus liquid content. The S1 datum is indicated by the black triangle. The datum from S1 resides in the lower half of the figure along with other data points from damaged piles. This data point is also below the 95% lower bound confidence interval.

The RCSA using Equation 5.1 was predicted to be 41.7%. After extraction and cutting of the pile section, the measured RCSA was found to be 51.6%. In this case, the model under-predicts the RCSA. Table 5.2 summarizes the findings for S1.

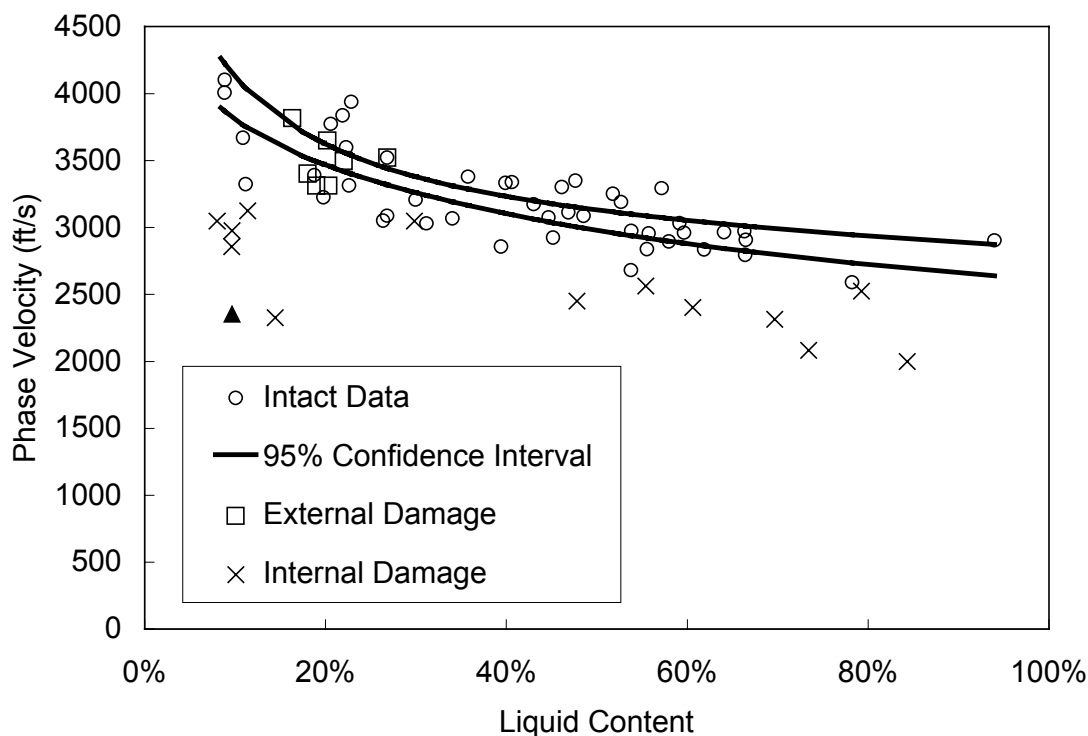


**Figure 5.15** S1 data plotted on the qualitative chart.

Using the information presented in the Table 5.2, the DOT engineer must make a decision on the appropriate action for a timber pile. The preceding examples are simplified in that they only consider the information from one setup on the corresponding pile specimen. In reality, the amount of phase velocity and liquid content information obtained would depend on the number of test setups. For example, eight test setups would yield eight corresponding average phase velocities and liquid content values. All of the information and results would have to be compiled and presented for a decision to be made.

**Table 5.2** Summary of information for S1.

ITEM	COMMENT
Visual Inspection	No visual damage
Sounding	Borderline hollow
Average Phase Velocity	2391 ft/s
Liquid Content	9.67%
Qualitative Analysis	Way below the 95% confidence interval
Quantitative Analysis	Predicted RCSCA = 41.7%
Additional Comments	Low phase velocity and low liquid content are suspect. Missing some core material.

### 5.2.3 Bridge #10, Chatham County (Field Demonstration to NCDOT)

Two piles were tested from Bridge #10 in Chatham County as part of a demonstration to the NCDOT. The research team performed an in-situ test on Monday, December 20, 1999. The two specimens utilized for this demonstration were piles 4 and 5 from Bent 2. Visual observations and sounding indicated that pile 5 was intact and pile 4 was damaged. There was a large hole (2"x7"x2") on the southern face of pile 4.

Phase velocities were obtained from the top and bottom of both piles. Only the liquid content at the bottom of pile 4 was obtained. Phase velocity information was calculated by taking an average of 2 files from each test location. As required, data were obtained using only one linear array of sensors (one test line). Table 5.3 gives a summary of the phase velocity information.

**Table 5.3** Phase Velocities for Bridge #10, Chatham County

PILE/TEST LOCATION	PHASE VELOCITY (FT/S)
5top	3012
5bottom	2809
4top	2446
4bottom	1947

The reject-accept criteria presented in Figure 5.15 is the most useful tool for determining timber pile condition. This graph can be utilized in the field to make a decision on whether or not to take a core value. Although the procedure outlined in Chapter 4 instructs the technician to take a core at every location where stress wave data are obtained, we can examine the data from piles 4 and 5 and determine certain coring guidelines. Taking a core and obtaining the liquid content in some cases is absolutely necessary. This is when the phase velocity information lies in the transition zone between intact and damaged piles. Certain phase velocities are so high that regardless of liquid content, the pile can be determined to be intact. This assumption is made based on the results in Figure 5.15. The same is true for phase velocities that are extremely low.

Pile 4 is a good example of the phase velocity being on the low side. The bottom of pile 4 (known to be damaged) had an average phase velocity of 1947 ft/s. There are no intact pile data points in Figure 5.15 which fall anywhere near that value of phase velocity, regardless of liquid content. This indicates that the pile is damaged and that obtaining a core would be useless. Since this pile has to be removed, there is no need to even consider the results at the top of the section.

Pile 5 illustrates phase velocities that lie in the transition zone. The average phase velocities of the top and bottom of pile 5 were determined to be 3012 ft/s and 2809 ft/s, respectively. These data points reside in the transition zone because depending on liquid content, previous data has been determined to be both intact and damaged (i.e., damaged at lower LC and intact at higher LC). Data points that lie in the transition zone should be

supported by a liquid content value. The guidelines for determining if a liquid content value should be obtained are presented in Table 5.4.

**Table 5.4** Guidelines for obtaining a liquid content

PHASE VELOCITY RANGE	ACTION
$3400 < V_{ph}$	Intact pile
$2600 < V_{ph} < 3400$	Take core, determine liquid content
$V_{ph} < 2600$	Damaged pile

As in the previous two sections, if liquid content is determined the RCSA can be calculated. The guidelines presented in Table 5.4 should be considered in addition to other information (as shown in Tables 5.1 and 5.2) obtained from in-situ testing.

### 5.3 Summary

The condition evaluation procedure is a relatively simple operation. The key to the success of the stress wave method lies in the steps presented in Chapter 4. If the data obtained from the field are of a poor quality, analysis will not yield any useful results. A major goal in designing this procedure was to make it sufficiently practical for use by the NCDOT. The examples presented in this section demonstrate this.

## List of References

Chen, S. (1995a). "Condition Assessment of Installed Timber Piles and Comparison of Three Transform Techniques Using Stress Wave Methods," Ph.D. Dissertation, North Carolina State University, Raleigh, NC.

Douglas, R. A., Eddy, J. L., Wahls, H. E., (1989). "On Transforms and the Dispersion Computations Used for Evaluating Layer Properties," *Nondestructive Testing of Pavements and Back Calculation of Moduli*, Edited by A.J. Bush and G.Y. Baladi, ASTM STP 1062, ASTM, Philadelphia, PA.

Holt, J. D., Douglas, R. A., (1994a). "A Field Test Procedure for Finding the Overall Lengths of Installed Timber Piles Using Dispersive Wave Propagation Methods," Technical Report to the UNC Institute for Transportation and Research Education.

Qian, Y. (1997). "Nondestructive Evaluation of Structural Condition of Timber Piles," Master Thesis, North Carolina State University, Raleigh, NC.

Ramirez, R. W., (1980). *The FFT: Fundamentals and Concepts*, Prentice-Hall, Inc., NJ.

Ross, R. J., DeGroot, R. C., Nelson, W. J., Lebow, P. K., (1997). "The Relationship between Stress Wave Transmission Characteristics and the Compressive Strength of Biologically Degraded Wood," *Forest Products Journal*, Vol. 47, No. 5, USDA Forest Service, Madison, WS.

Varoufakis, George J. (1996). "Non-destructive Tests of Attic Silver Coins in Antiquity," In *Non-Destructive Testing*, D.V. Hemelrijck and A. Anastassopoulos, editors, A. Abalkema Publishers, Brookfield, Vt.

Wiggins, C. O. "Lin" (1999). Personal communication with the research team.

# Appendix A: Reference Information for the Field Testing Procedure

## A.1 Typical Pile Information Sheet

A typical pile information sheet is shown below. The dimensions, sensor locations, pile ID and file names are invaluable pieces of information for the analysis phase of the procedure.

### Pile Data Sheet

Bridge # \_\_\_\_\_ County \_\_\_\_\_ Bent # \_\_\_\_\_ Pile # \_\_\_\_\_

Pile ID \_\_\_\_\_ Date \_\_\_\_\_ Treatment \_\_\_\_\_

Schematic of Pile:

**(Include all dimensions, setup and core locations)**

## **Pile Data Sheet (Continued)**

General Observations (external damage, severe cracking, sounding results, etc.):

File Names and Setup Information:

Miscellaneous Notes:

## A.2 Equipment Required for Testing

**Table A.1:** Equipment used for stress wave procedure.

ITEM	MODEL	COMPANY	WEBSITE	PHONE
Oscilloscope	TDS 420 A (equipped with a GPIB socket)	Tektronix®	<a href="http://www.tek.com">http://www.tek.com</a>	(800) 545-2712
Sensors	W353B16	PCB Piezotronics, Inc.	<a href="http://www.pcb.com">http://www.pcb.com</a>	(716) 684-0001
Cables	power supply to sensor-003P10 power supply to scope-012A03	“	“	“
Signal Conditioner (Power supply)	482A03	“	“	“
Laptop	n/a	Any IBM compatible PC	N/a	N/a
Software (SWAP)	n/a	Dr. Y. R. Kim	<a href="http://www4.ncsu.edu/~kim/">http://www4.ncsu.edu/~kim/</a>	(919) 515-7758
Halogen Moisture Analyzer	HR73 HMA	Mettler-Toledo	<a href="http://www.mt.com">http://www.mt.com</a>	(800) METTLER
PCMCIA Card, connection cable	PCMCIA-GPIB #777156-02	National Instruments™	<a href="http://www.ni.com">http://www.ni.com</a>	(512) 794-0100

## A.3 HMA Settings

**Table A.2:** Basic HMA Settings

HMA FUNCTION	SETTING	DESCRIPTION
Drying capability of substance	-5	Indicates slow drying substance
Method Temperature Adjustment	Icon: 	Temperature brought to desired setting as soon as test is started.
Method of MC Calculation	Icon: 0 to -1000	Calculates MC based on dry weight
Temperature	150° C	-
Time	45 minutes or less	The machine will shutoff automatically although occasionally it continues indefinitely. No significant change was recognized after 45 minutes.

# Appendix B: Laptop Setup Instructions

## B.1 Installation of SWAP Software

The purpose of this section is to provide the steps involved in the installation of the data collection and analysis software (SWAP) on an IBM compatible laptop computer. Floppy disks have been provided with this report. The required files are listed below.

### Program Files:

1. Project1.exe
2. fft.exe
3. fft.a
4. fft.b
5. fft.c
6. fft.d
7. fft1.dat
8. skm4.exe
9. skm.dat

### Library Files:

1. threed16.ocx

The library files listed above will already exist on many machines. Their existence depends on the age of the computer, the operating system and the type of software the machine contains.

The steps in the installation of SWAP are outlined below:

1. Create a folder in the **C** drive of the computer called “**swap.**”
2. Copy the **program files** into this folder.
3. Copy the library file into the existing folder called **C:windows/system** (if they already exist there is no need to rewrite them).
4. Create a shortcut for **project1.exe** and drag it to the desktop, rename the shortcut “**SWAP**”.
5. Click on the SWAP shortcut and open the program.
6. Follow the instructions of Chapter 3 for program use.

**Important note: When data are collected, they reside in the SWAP folder on the C drive. Data must remain in this folder for SWAP to recognize the data and open the files. If files are moved to another folder, SWAP will not be able to find the files.**

Swap can also be used on a computer for analysis only. In this case, no PCMCIA-GPIB card is required because a connection to a scope is not necessary. To use SWAP for analysis only, follow the steps in Section B.1 only (i.e., steps in the next section are not required).

## **B.2 Installation of PCMCIA-GPIB Card**

The purpose of the PCMCIA card is to allow the laptop computer to communicate with the Tektronix oscilloscope. A connection cable (laptop to scope) and installation software are included with the purchase of a new PCMCIA-GPIB card from National Instruments. The basic steps of card installation are described below. Refer to the instructions included with the card for more detailed information.

1. Install the PCMCIA-GPIB card in one of the slots in the laptop computer.

2. Turn on the computer.
3. Install the card software using the disk included with the purchase of the card (the computer often recognizes the card without the installation of the included software so this step may not be necessary).
4. Connect the cable to the card.
5. Connect the cable to the GPIB socket in the back of the oscilloscope.
6. When the oscilloscope is turned on and the SWAP is ready, a signal can be collected.